Kiggavik Project

Environmental Impact Statement

Tier 3 Technical Appendix 5J

Tailings Characterization and Management

December 2011

TABLE OF CONTENTS

LIST OF TABLES

LIST OF FIGURES

LIST OF ATTACHMENTS

1 INTRODUCTION

1.1 OVERVIEW

The Kiggavik Project is a proposed uranium ore mining and milling operation located in the Kivalliq region of Nunavut approximately 80 km west of the community of Baker Lake (Figure 1.1-1).

This document is a Technical Appendix to Volume 5, Aquatic Environment, of the Kiggavik Environmental Impact Statement (EIS). Information relevant to tailings characterization, assessment and management is presented in this Technical Appendix.

The Kiggavik Project includes four open pit mines and one underground mine. The Main Zone, Centre Zone and East Zone Pits are near each other and the Andrew Lake Pit and End Grid Underground Mine are located about 15 km to the southwest (Figure 1.1-2). With respect to tailings management, which is the focus of this Technical Appendix, the main facilities will include the Kiggavik mill and three mined-out open pits converted into Tailings Management Facilities (TMF) (Figure 1.1-3).

Tailings management encompasses all aspects of tailings preparation, delivery and disposal. This document provides a detailed discussion of the proposed design, operation and decommissioning of the tailings management system at Kiggavik. Additionally, predicted operational and long-term effects, mitigative measures, and contingency measures related to tailings management are presented. The assessment of potential long-term impact of tailings through the groundwater pathway is based on information presented in the Technical Appendix 5B “Geology and Hydrogeology Baseline”, Technical Appendix 5D “Groundwater Flow Model” and Technical Appendix 4D “Baker Lake Long Term Climate Scenario”. Detailed information relevant to mine rock is presented in the Technical Appendix 5F “Mine Rock Characterization and Management”.

1.2 PURPOSE AND SCOPE

This purpose of this report is to document tailings data and tailings modelling results and to describe the proposed tailings management plan for the Kiggavik Project and the measures proposed to prevent and /or mitigate the potentially adverse effects of tailings on the receiving environment.

The scope of this document is to:

- Characterize the physical and geochemical properties of the materials, as they relate to the long-term management of mill tailings;
- Assess the various options for long term management of tailings;
- Choose the preferred option to propose in the mine plan submission;
- Describe the measures taken for design and construction of the preferred option; and
- Describe the measures to monitor and provide assurance that the management option performs as required to safeguard human and environment health and safety during operations and long-term closure of the tailings management facility.

This report is organized as follows:

- Section 1 describes the general contents of the document and how it is organized;
- Section 2 reviews tailings disposal alternatives;
- Section 3 describes the proposed tailings management facilities for the Kiggavik Project;
- Section 4 describes the assessment methodology and predictions of thermal behaviour of tailings during and after deposition, both under current climate and climate change conditions;
- Section 5 describes the assessment methodology and predictions of tailings consolidation during and after deposition;
- Section 6 describes the assessment methodology and predictions of geochemical behaviour of tailings during and after deposition;
- Section 7 describes the assessment methodology and predictions of potential long-term environmental effects related to tailings management;
- Section 8 presents the proposed monitoring and follow-up programs;
- Section 9 presents a summary of key results; and
- Section 10 presents references cited in this report.

This report was prepared by AREVA, Mahoney Geochemical Consulting Newmans Geotechnique and SRK Consulting.

2 REVIEW OF TAILINGS DISPOSAL PRACTICES

2.1 INTRODUCTION

The following options for the disposal of tailings were reviewed:

- Above Ground Disposal;
- In Lake Disposal; and
- In-Pit Disposal

2.2 ABOVE GROUND DISPOSAL

Above ground disposal of mine waste and mill tailings from uranium operations has been commonly used in the Canadian mining industry in northern environments. These facilities require that the base and impoundment materials be of sufficiently low permeability to reduce seepage to an environmentally acceptable level.

Above ground facilities are constructed to take advantage of natural topographic features that will form part or all of the containment structure for the waste materials. Commonly, a number of engineered structures, such as dams, are constructed to augment the natural features to form a tailings containment structure. The dams are constructed using natural materials to ensure longevity; however, as they are water bearing structures they require continuing inspection and maintenance, which is a significant drawback in an isolated project.

Following milling operations, the tailings area is drained and the entire tailings surface is covered with a soil cap made of local till and a protective rock layer to prevent erosion and mechanical degradation of the cover material.

To prevent freezing of the tailings and/or ice lens formation in a cold environment and prevent dust migration and radon gas/gamma radiation release, a pond has to be maintained over the entire tailings surface. During operation, it can be difficult to maintain a sufficiently deep pond on the entire tailings surface. Total water coverage is problematic with an above ground facility as the deposition of tailings is usually carried out using spigots located on the TMF rim, creating a dry beach along the impoundment edges, or by a barge that moves around the pond to spread the tailings subaqueously.

While it would be feasible when the TMF is well below capacity, near the end of the project the dam rim will need to be significantly higher than the placed height of tailings to allow for pond depth and necessary freeboard, requiring considerable volumes of extra material to build the dams. These higher dams would produce a much larger disturbed area for borrow materials

and larger constructed footprint, but also be significantly more geotechnically challenging for long term stability.

2.3 IN-LAKE DISPOSAL

Disposal of tailings solids and waste rock directly into an existing lake is carried out in Canadian mining and has been shown to be the most effective means for protection of the environment under certain circumstances. In-lake disposal is subject to assessment by the Department of Fisheries and Oceans (DFO) to determine the potential impact on the aquatic systems involved. This assessment is carried out under an amendment to Schedule II of the *Metal Mining Effluent Regulations* of the *Fisheries Act*, with DFO as the Responsible Agency, and Environment Canada as the Responsible Enforcement Agency.

Impacts of the addition of tailings, defined as a deleterious substance, and the potential for destruction of fish habitat requires an assessment of the potential impacts and/or habitat restoration or compensation under the Fisheries Act.

In-lake disposal in a relatively flat area may have operating issues with providing enough storage capacity or maintaining a sufficiently deep pond if the topography does not allow for natural barrier of sufficient depth as in a steep valley system.

2.4 IN-PIT DISPOSAL

In-pit disposal entails direct placement of tailings in slurry or paste form into an open pit. A number of construction options ranging from a pit designed solely for ore extraction, to a modified ore pit to enhance TMF operation to a purpose built pit can be utilized.

Disposal of tailings in a mined pit at the end of mining offers the opportunity to reduce footprint on the site and the ability to cover and minimize the exposure of the partially mineralised wall rock of the pit to metal leaching and/or acid rock drainage processes. However; the primary benefit is the elimination of an engineered surface tailings facility; thereby removing potential long-term infrastructure such as water retaining dams.

Since the tailings are deposited below ground surface, they are less susceptible to natural degradation processes such as erosion, frost, seismic activities, etc. Consequently, the need for long-term maintenance and institutional control can be minimized (CNSC, 2011).

This tailings management method is currently being used at most uranium mills in Saskatchewan.

2.4.1 Natural Surround versus Pervious Surround Alternatives

The key design issue associated with in-pit disposal of tailings concerns the method of long-term hydraulic isolation of the tailings within the TMF from the natural groundwater flow system. Two fundamental design alternatives have been considered and implemented in Saskatchewan to date: natural surround with subaqueous tailings deposition and pervious surround with subaerial tailings deposition.

Pervious surround involves placing a pervious material around the perimeter of deposited tailings to promote groundwater flow around the tailings mass rather than through the tailings mass, thereby limiting contaminant release from the tailings. With the pervious surround, tailings are deposited subaerially, exposing tailings at the surface. The pervious surround concept was incorporated into the design of the Rabbit Lake TMF in Northern Saskatchewan.

The natural surround concept accommodates subaqueous tailings deposition from a barge, which promotes more uniform tailings placement, decreased tailings segregation, and eliminates zones of frozen tailings when compared to subaerial deposition required by the pervious surround system. Frozen layers in the tailings mass may impede consolidation of the tailings, resulting in lower tailings densities and higher hydraulic conductivity. The advantages of the natural surround system all contribute to producing a low hydraulic conductivity tailings mass. The natural surround concept was incorporated into the design of the JEB TMF. The hydraulic conductivity contrast between the consolidated tailings and the surrounding rock is a minimum of two orders of magnitude in the case of the JEB TMF, resulting in diffusion being the dominant contaminant release mechanism.

The natural surround subaqueous system is also advantageous from a radiation protection perspective. The underwater placement of tailings virtually eliminates dust and very significantly lowers exposures to radon and gamma fields, thus protecting workers and wildlife from radiation exposure.

2.4.2 Pit Engineering Options

Drainage

The rate of consolidation of tailings is a direct function of the tailings hydraulic properties, as well as the drainage state on surface and at the base of the pit. In order to facilitate more rapid consolidation it can be beneficial to install a bottom drain, which allows the flow path for dissipation of excess pore water pressure to be both to the surface and to the base of the pit. In order for a bottom drain to function in an optimal state, it must allow for a reduction in excess pore water pressure to zero, the same condition that would exist at the surface.

In the JEB TMF, an underdrain filter of sand and rock was installed at the base of the pit to promote drainage of tailings pore water, further accelerating tailings consolidation. Water flows

through the underdrain sump, which is connected to a dewatering drift and raise. Pumping water from this system minimizes the outward migration of tailings pore water from the TMF during the operational and decommissioning periods, thereby maintaining hydraulic containment.

The efficiency of the underdrain option is dependant on the permeability of the drain. To be efficient the drain needs to remain sufficiently permeable over time; that is the potential for permeability reduction factors such as chemical precipitation, sand plugging or freezing needs to be low. In permafrost conditions any underdrain installed with a pumping system in host rock risks freeze off. Possible options to implement a drainage system in a permafrost environment would include a bottom drain pumping / extraction system located in the centre of the thawed tailings and/or vertical drains installed through the tailings.

Pit Liners

The benefit of constructing a liner to minimize the release of contaminants from the tailings mass was evaluated as part of the initial JEB TMF design. The following pit liner alternatives were considered:

- a full pit liner;
- sump liner only; and,
- no liner.

Computer modelling determined that a full liner, if constructed with a very low permeability, similar to tailings mass, would be slightly more effective than a no liner design in minimizing diffusive contaminant flux to the surroundings (COGEMA 1997). However maintaining proper construction QA/QC for a low permeability liner was determined to be very difficult, if not technically impossible, in a flooded pit condition, especially during winter conditions. Consequently, a full pit liner was not considered further.

A sump liner was also determined to have an insignificant effect on reducing contaminant flux, as only a minor component (approximately 4%) of the total contaminant flux was determined to migrate through the area of the sump. A liner was also found to interfere with movement of this groundwater, thereby reducing the effectiveness of the hydraulic containment of the facility during operations. For these reasons a liner was not considered in the original design.

For the Kiggavik Main Zone TMF a liner installed at the bottom of the pit is considered to be a possible option to further isolate the tailings from the sub-permafrost aquifer and to account for the potential impact of climate change on permafrost. With respect to the JEB environment the Kiggavik Main Zone environment also presents specific features that would increase the efficiency of a bottom pit liner. This includes limited groundwater inflows under dewatering conditions due to the low hydraulic conductivity of the surrounding rock mass, including the sub-

permafrost aquifer. As a result the liner would be installed under relatively dry conditions allowing for proper construction QA/QC.

There are a number of potential liner materials available for a TMF. These include: i) synthetic flexible membrane liner (FML) such as polyvinyl chloride, polyethylene and butyl rubber; ii) admixed materials such as asphalt, concrete, and soil asphalt; iii) compacted native materials such as till and crushed sandstone and iv) native soil/rock material potentially amended with bentonite. There are advantages and disadvantages for each of the liner type materials; Table 2.4-1 presents a comparison of the potential options.

Some FMLs are susceptible to wrinkles, laceration, abrasion and puncture, and prone to cracking or distorting during adverse weather conditions during installation. One of the major concerns in using synthetic membrane liners is field seaming during installation. The locations of bad seams or leaks are difficult to identify. The FML option is usually high cost as the cost of construction quality assurance of the FML is typically comparable to the cost of the geomembrane liner (Danilek and Laine 2001). Admixed materials such as asphalt or concrete are also expensive and do not offer a low permeability liner.

Compacted native soil liners have the longest record of successful performance based on thousands of years of uses and inherent characteristics of soils (Kays 1977). Where suitable native materials are available, the use of native soil as a liner material is preferable. If necessary, the hydraulic conductivity of the native materials can be lowered using an amendment material such as bentonite. In comparison with the synthetic FML, the bentonite amended soil would have the following major advantages; i) self-sealing capabilities, ii) material inertness to degradation and leaching, iii) low permeability nature of the amended material, and iv) less complicated to construct (Liao 1989).

A bentonite amended soil liner installed on the floor of the Main Zone pit would be a reasonable TMF engineering option for the deepest part the Kiggavik Main Zone TMF.

Table 2.4-1 Comparison of Potential Liner Options

Liner Options	Advantage	Disadvantage
Flexible Membrane Liner	• Contain a wide range of waste fluids. • High resistance to chemical and bacterial deterioration. • Very low hydraulic conductivity if there is no leak through the liner.	• Major concern is field seaming during installation. • Prone to puncture if not properly protected. • For stage construction, the quality of seam for expansion will be difficult. • Operation pond will require operating procedure and frequent inspection to ensure no puncture. • Usually high cost. • Expensive field QA to produce high confidence of the final product.
Admixed Materials	• Universal availability and versatility of materials.	• High cost • Do not offer very low permeability. • Structure subject to cracking. • Difficult to provided good seal between liner portions constructed at different stages.
Compacted native material such as till and sandstone	• Use local materials which can be amended as necessary. • Hydraulic conductivity can be lowered using amendment material such as bentonite. • Easy to construct, superior seal between liner portions constructed at different stages. • Material inertness to degradation and leaching. • Long history of success. • High performance system. • Provide good buffer for retardation of solute contaminant.	• Material must be processed-till must be screened to remover large size cobble and rocks, or sandstone must be crushed to produce enough fine content. • Potential effects of wetting-drying, and freeze-thaw cycles. • For bentonite amended material, mixing/blending and method co compaction are critical.

2.5 COVER

Two major design alternatives have been traditionally considered to cover tailings during decommissioning of a tailings management facility; either a dry cover design or a pond above the tailings.

Dry Cover

A typical dry cover is constructed over the tailings to prevent dust migration and physical access to the material. Ultimately the dry cover is built above local ground surface and graded to shed precipitation and blend into the existing topography. The cover can be constructed using mine rock to produce an erosion barrier over the tailings, with a top layer of overburden to provide a vegetation medium. If deemed necessary the cover can be designed as an infiltration and/or oxygen barrier.

Pond

As an alternative to the dry cover, the tailings can be covered at closure using mine rock to produce an erosion barrier and/or a layer of overburden added to form a substrate for aquatic habitat. A pond is then allowed to flood. For instance as consolidation occurs in the underlying tailings a depression is formed that fills with direct precipitation, surface runoff, and in some circumstances groundwater inflow. The pond/lake can be integrated into the existing drainage system to promote flow through the lake.

An evaluation of the two cover options was conducted as part of the decommissioning planning of the JEB TMF. This evaluation determined that placement of a soil cover would result in additional tailings consolidation and thus lower decommissioned hydraulic conductivity of the tailings mass. For this reason the backfilled pit decommissioning option was selected over the pond option as the preferred design option.

2.6 EXAMPLES OF TAILINGS MANAGEMENT IN PERMAFROST REGIONS

Diavik

A composite cover of 0.5 m of silty sand till overlain by 3 m of clean mine rock has been proposed. It is predicted that the active layer will extend partly into the silty sand. Oxidation of the tailings will be prevented firstly by the upper zone of the silty sand being fully saturated and secondly by the fact that the lower part of the silty sand and the tailings will be in permafrost.

Nanisivik

The Nanisivik Mine was developed to produce zinc and lead mineral concentrates. The mine was put into production in 1976 and closed in 2002.

Nanisivik initially discharged the tailings under water within an existing lake. After the lake was filled, tailings were discharged in a surface cell constructed above the original lake by means of progressive upstream dyke construction. The dyke was constructed on top of a shale causeway fill, underlain by tailings, overburden consisting of silt sediments and sandy till and finally, dolomite and shale bedrock. Two thermocouples installed through the causeway showed the underlying stratigraphy was frozen to at least 11 m. The dyke design consists of upstream construction of about 4 m wide zone of sand and gravel sized shale material obtained by ripping exposed shale bedrock. With the exception of the first lift, which was 3m high, the dyke was raised in 2 m lifts until it reached the target elevation.

The cold temperatures measured within the tailings illustrate the relatively rapid cooling of the tailings. The temperature readings show that in about 4 to 5 years of tailings placement, the tailings temperature at greater depths were between -5°C to -7°C. The relatively quick cooling and development of permafrost in tailings not covered with water was demonstrated at several locations.

To select a cover design with the smallest thaw depth for the surface tailings, five test pads were constructed. The effect of cover layering, compaction, saturation and colour of the surface layer was studied. The thaw depth was monitored for a period of 8 years. Overall the cover design that has been proposed includes one meter of shale (sandy gravel sizes) covered with 0.25 m of esker sand and gravel. Permafrost is anticipated to stay within the cover.

Raglan

Raglan Mine is a nickel-copper operation that started production in 1997. It is located in northern Quebec, about 80 km southeast of Hudson Strait.

The mine is located above the tree line in the continuous permafrost region. It has a barren landscape that is influenced by being at a relatively high elevation (600m). The region is characterized by a landscape of mounds of broken rock and shallow valleys with modest slopes.

Encapsulation of the tailings in permafrost was selected as the best site closure option as the tailings can generate net acidity and runoff enriched in metals in above freezing temperatures if exposed to air and moisture. The preparation and storage of the tailings involves filter pressing of the tailings to a filter cake consistency. The process plant produces tailings consisting of sandy silt particle sizes. The tailings are pumped into plate filter presses, where excess water is removed to produce a filter cake with a moisture content between 18% and 20%. The tailings are trucked to the stack where they are dumped, spread and compacted to form a mound. At closure the tailings will be covered with 1.2 m of crushed sandy esker material that is expected

to retain some moisture and followed by 1.2 m mine rock surface zone for erosion protection. The cover is expected to maintain the tailings permanently encapsulated in permafrost.

The tailings site was chosen to be a small plateau to prevent surface water flowing towards the tailings stack and to avoid eliminating a potential mineral source. The final tailings stack will occupy an area of about 76 ha. It is about 2 km from the process plant. A perimeter ditch surrounds the stack and collects all surface drainage during the stack operation and directs it to a collection pond from which it is pumped to a water treatment plant. Overburden at the stack consists of relatively thin layers, of about 1m, of either ablation or lodgement till. The tills consist of a bony matrix of boulders, cobbles and gravel with a silty sand matrix. Underlying the overburden is a combination of volcanic rocks and mafic to ultramafic intrusives.

Lupin

Lupin Mine is a gold property that was developed by underground mining. The mine is located on the west shore of Contwoyto Lake, approximately 285 km southeast of Kugluktuk, Nunavut. The mine opened in 1982.

Lupin started its operation by depositing the tailings in a large surface tailings containment area (TCA) developed about 5km south of the plant. The TCA was created by the construction of four small dams and two divider dykes. A paste backfill plant was then constructed to pump some of the tailings underground and provide additional safety for underground mining. This also reduced the volume of tailings deposited on the surface. Progressive reclamation was started in 1995 with the placement of an esker sand cover over the tailings. In 2002 the operator proposed a partially saturated esker cover (saturated zone cover) as a closure plan for the reactive tailings at Lupin.

Rankin

The Rankin Inlet mine was a nickel-copper mine that operated between 1957 and 1962 (Meldrum et al 2001). This operation produced 297,000t of tailings that were discharged into three tailings ponds and scattered on the surface in an area between Rankin Inlet community and Hudson Bay. Because of low ground elevation and the proximity to Hudson Bay, the tailings were periodically flooded by seawater. This resulted in the tailings pore water becoming saline with a maximum salinity of 52 ppt. The ore contained a Ni-Cu platinum group of elements bearing sulphide mineralization. Petrographic examination showed the tailings contained 5-20% pyrrhotite that would make the tailings highly reactive. The pyrrhotite and minor amounts of pyrite, chalocopyrite and pentlandite caused the tailings to be classified as reactive sulphide tailings.

The existing tailings were a concern to the community for over 30 years after closure because tailings deposited above the high-tide dried and were spread across the vicinity through wind erosion and surface waters drained from the ponds. Surface tailings deposits caused metals to

be introduced into the sea. Due to environmental concerns, reclamation work was done between 1992 and 1994.

The reclamation consisted of treating the contaminated water in the three tailings ponds and pumping out the water from the Deep Pond. A temporary dyke with a crest elevation of 5 m was constructed to protect the tailings from high tides. The maximum high tide at Rankin Inlet is about 4 m. About 48,000 m^3 of surface tailings were removed from high ground and deposited within 1 m of sand and gravel esker to encapsulate the tailings in permafrost (Erickson 1995). The elevation of the top of the cover varies between 4.2 and 4.8 m above sea level. It is assumed that the active layer would stay within.

Rankin Inlet is located in the continuous permafrost region with a MAAT between -7 and -8°C and an average active layer thickness of 1.5m in till and gravel. There was a concern about the effectiveness of the permafrost encapsulation concept because of unfrozen pore water caused by the salinity of the pore water and the potential for heat generation through sulphide oxidation. Field and laboratory-testing programs were started in 1997 to determine the effect of the salinity and sulphide oxidation on the effectiveness of permafrost encapsulation (Meldrum 1998 and Meldrum et al 2001)

.

3 PROPOSED TAILINGS MANAGEMENT

3.1 CONCEPT

3.1.1 Design Considerations

Choosing the preferred option for the disposal of tailings involves a process that looks at the criteria for protection of health, safety and environment during the TMF operational period and after decommissioning and the economics of the option as it relates to the proposed mine plan.

General design criteria

The primary criteria considered in evaluating the alternatives include the following:

- Technical Feasibility. Key factors include chemical and hydraulic containment, the use of proven technology, and reliability.

- Operational Feasibility. Key factors include radiation protection, safety, operational efficiency, and ability to monitor and control.

- Environmental Considerations. Key environmental considerations include source term control, hydraulic containment, impact to the receiving environment, and ability to monitor. Public acceptability is considered to be included in consideration of environmental impacts.

- Cost and Management Considerations. Key factors include construction, operation and maintenance costs, construction and operation schedules, staffing, and overall project management implications.

Performance during the operational period

The key design criteria for protection of health, safety and environment during the TMF operational period include the following:

- Mill process optimization. The objective of this design criterion is to produce thickened tailings with low pore water concentrations of key potential constituents of concern.

- Secondary containment. The objective is to ensure that secondary containment is applied to all pipelines used for pumping of reclaim water and tailings associated with the operation of the TMF.

- Radon Gas and Gamma Radiation Control. The objective is to ensure that radiation protection measures are enhanced by design.

- Cold temperatures management. Based on experience at other tailings management facilities operated in northern Canada, and specifically at sites operated by AREVA in northern Saskatchewan, it is recognized that the design and operation of a TMF in arctic conditions has unique specificities to take into account due to cold temperatures. The major issues are related to the freezing of tailings during transport and emplacement. For instance tailings lines are prone to freezing if blockages occur. Also there is an increased potential dust migration due to "freeze drying" of exposed surface tailings and ice lenses can form within the tailings reducing the ability to dewater tailings and increasing time required for full consolidation.

Long-term performance

The key design criteria for protection of health, safety and environment after decommissioning of the TMF include the following:

- Long-term, secure containment and isolation of the TMF.

- Surface stabilization of the tailings and prevention of wind and water erosion and transport

- Control of contaminants release over the long-term

- Aesthetically pleasing landscape that meets the final land-use requirements of the stakeholders

The long-term environmental performance of the decommissioned facility depends upon the rate of release of potential contaminants to the receiving environment. The rate of contaminant loading to the receiving environment will ultimately be governed by the concentrations of soluble contaminants within the tailings mass (i.e., tailings pore water), the mechanisms for contaminant release from the tailings to the surrounding groundwater system, and transport of contaminants within the groundwater pathway to the receiving environment.

3.1.2 Overview

The proposed tailings management plan for the Kiggavik Project has been designed according to the following principles:

- To avoid interaction between tailings and natural water bodies;
- To maximize the use of mine workings for long-term management of tailings;
- To ensure the long-term protection of Kiggavik's terrestrial, aquatic and human environment.

Historically, non-uranium northern mines in the continuous permafrost zone have benefited from the presence of permafrost conditions around the area of tailings management. The continuous permafrost in the ground provides a hydraulic barrier, which prevents the migration of potential contaminants from the tailings facility into the environment. Above ground tailings impoundments were engineered to allow the permafrost to aggrade into the tailings, thereby creating a stabilized mass, encapsulated by frozen conditions. It is now considered possible that climate change will threaten the integrity of tailings management structures that rely on maintaining present temperatures and permafrost conditions for stability and integrity.

The proposed tailings management approach for the Kiggavik Project is modelled after AREVA's McClean Lake operation in northern Saskatchewan and is based on the "in-pit tailings management facility" concept, which represents the approach accepted by the regulatory agencies at uranium mills currently operating in northern Saskatchewan.

In-pit disposal of tailings in the mined pits is considered to be the best tailings management option at Kiggavik for minimizing the potential operating and closure impacts to the receiving environment. In-pit disposal will also reduce the footprint of the tailings management facility (TMF), and provide the most secure, long-term facility for the tailings at the Kiggavik site.

The preferred option for tailings management at the Kiggavik site is summarized in Figure 3.1-1. The preferred option consists of producing thickened tailings that will be neutralized and treated to control uranium, radium-226 and metal concentrations. Tailings will be deposited subaqueously within the mined out pits. Subaqueous placement of tailings will prevent freezing of the tailings and enhance radiation protection.

The natural surround concept will be used. At closure the tailings will be covered using mine rock to enhance consolidation and prevent wind and water erosion. A final cover of overburden will be added for revegetation.

Tailings will be deposited in three open pits at the Kiggavik site. Based on the current mine schedule, tailings will be deposited into the East Zone Pit, followed by the Centre Zone and Main Zone pits. The East Zone Pit is sized to store tailings from the milling of the East Zone,

Centre Zone and initial Main Zone ore, until such time as the Centre Zone Pit is ready to accept tailings. Similarly the Centre Zone Pit is sized to store tailings from the milling of the Main Zone ore. The Main Zone pit is sized more traditionally to optimize resource extraction. The Main Zone pit is the largest of the three open-pits mined at Kiggavik. As such it is also proposed to use the Main Zone pit for long-term management of Type 3 mine rock resulting from open-pit mining of the Kiggavik deposits.

3.2 TAILINGS PREPARATION

Barren streams

In the Kiggavik mill, the following barren streams will be received in the Tailings Neutralization Feed Tank:

- Pulp Residue from the RIP Circuit
- Waste regenerant from the Resin Regeneration Circuit
- Sand filter filtrate from the Uranium Precipitation Circuit
- Water Treatment Plant (WTP) sludge
- Discharge from the area Sump & Pump

Neutralization and Thickening Processes

In the treatment process, lime ($Ca(OH)_2$), ferric sulphate ($Fe_2(SO_4)_3$) and barium chloride ($BaCl_2$) will be utilized to promote the removal of metals and radium from the discharge water. These reagents will be contained in tanks in the reagent area of the plant and pumped to the tailings preparation circuit.

- Lime ($Ca(OH)_2$) will be added to the first Tailings Neutralization Tank to adjust the pH of the slurry to 4.0 and will be also added to the remaining two Tailings Neutralization Tanks to maintain a slurry discharge pH of between 7.0 and 8.0.
- Barium Chloride ($BaCl_2$) will be added to the 2nd Tailings Neutralization tank to reduce radium in solution.
- Ferric Sulphate ($Fe_2(SO_4)_3$) will be added to the flash mixed tank if necessary . Ferric Sulphate can also be added to the 2nd Tailings Neutralization Tank in the event that the 1st tank is bypassed.

There will be 3 Tailings Neutralization Tanks operating in series. The Feed Tank will discharge by gravity to the 1st agitated Tailings Neutralization Tank. The 1st tank and piping will be arranged to allow bypassing of each tank for maintenance with minimum disruption to the operation of the circuit. Process air can be added to the bottom of the Tailings Neutralization Tanks, if required, to ensure that contaminants are in their oxidized state.

The last Tailings Neutralization Tank will discharges to the high rate Tailings Neutralization Thickener where Flocculant "A" will be added to the feed pipe and/or feed well to settle the solids. Tailings Thickener Underflow Pumps will transfer the thickened underflow at a nominal average of 38% (w/w) solids to the TMF for long term disposal of the solids. The thickener overflow will discharge to the Tailings Overflow Tank from where it will be pumped by Discharge Pumps to either the Water Treatment Plant or the TMF.

A relatively comparable process has been proven to be successful at AREVA's McClean Lake operation in reducing trace metals concentrations in tailings pore water. Based upon a review of Kiggavik laboratory test data and coupled with a series of geochemical models it is anticipated that the proposed neutralization process for the Kiggavik mill tailings will produce stable tailings with long-term uranium and trace metal concentrations of less than 1 mg/L.

3.3 TMF PREPARATION

Open pits rock slope designs

The Kiggavik open pits that will be converted into TMFs will be excavated in generally competent to very competent rocks which exhibit brittle rock characteristics. The othoquartzites and the granitic intrusive in particular are very strong rocks. The metasediments are not of the same strength, but are still very competent with respect to providing a stable wall for an open pit. The only low strength materials are the altered rocks associated with the mineralization and thus will generally be removed as ore. The stability of slopes excavated under these conditions will therefore be primarily controlled by the orientations, spacing, persistence and strength of the discontinuities that exist within the rock mass.

Interpretations of outcrop mapping and oriented core data suggest that the major controlling structural systems in the vicinity of the open pits are very consistent. A stereographic study of the kinematics of failure was conducted for a range of proposed slope orientations to identify discontinuities oriented such that they could give rise to slope failure. The kinematics of failure study showed that the most likely potential mode of failure are planes and wedges. Information on horizontal and sub-vertical joint spacing suggests that block shapes with potential toppling are not likely. Rather, blocks will occur, and ravel rather than topple. This type of failure is likely to be confined to near surface, bench scale instability in some walls of the pits. The potential for small scale wedge and planar type failures has also been identified but is again likely to be confined to bench scale. The conclusion of the kinematic study is that slopes of 50º to 55º could

be mined however the requirement for safety berms to contain bench scale failure will determine the inter-ramp slope geometry.

Pit Floor Heave

Pressure readings taken from vibrating wire piezometers installed in the proposed Main Zone pit location in 2009 indicate that groundwater is present at a significant pressure under the zone of permafrost. As the pits are excavated, this groundwater pressure should remain relatively unchanged, while the rock above the permafrost interface will be reduced. This may lead to pit floor heave. If pit floor heave is anticipated vertical pressure relief drains will be installed in the pit floor as the pit excavation progresses, with preference for a ring of drains on a geotechnical bench at a suitable elevation above the base of permafrost. These will depressurize the pit floor, and reduce the potential for heave. Water from the drain holes will be collected within the pit sumps and removed from the pit as part of the water management program.

Monitoring During Mining

The ongoing development of the pit will require an observational approach. With this method, which is common practice in the mining industry, the initial pit excavations are monitored and the pit slope designs are modified on an ongoing basis throughout the life of the pit. It is expected that revisions will be made based on further review and mapping and stability performance monitoring, as mining exposes subsurface geology in the proposed pit.

A pit slope monitoring program will be established early in the life of the pits. The monitoring program is intended to both confirm the assumptions made regarding the structural and geologic models and to detect unexpected conditions in sufficient time that remedial measures can be adopted. This program should include both pit mapping to confirm the engineering geology model upon which the designs are based, as well as monitoring to detect any movement in the slopes.

The program will be conducted largely by the mine geotechnical staff; with periodic reviews by an experienced rock slope design engineer. The monitoring program will include aspects relating to the following:

- Geologic Mapping - in order to confirm the geological model on which the current slope designs are based and assess the potential for slope steepening, routine geologic mapping will be carried out as the slopes are excavated.

- Slope Monitoring - regular visual inspections of the bench faces and the crest areas will be conducted for early evidence of slope instability. Occurrences of tension cracks behind the slope crest are indicators of movements and the beginning of instability in the slopes. Instrumentation will also be installed around the perimeter of each pit to monitor slope movement as the excavation progresses.

Structural measurements will be collected over the full depth of the pits.

Drainage

A base drain has not been incorporated into the Kiggavik TMFs design.

Incorporation of a drainage system within the pits in a permafrost environment poses operational challenges. The efficiency of the underdrain option is dependent on the permeability of the drain. To be efficient, the drain needs to remain sufficiently permeable over time; that is the potential for permeability reduction factors such as chemical precipitation, sand plugging or freezing needs to be low. In permafrost conditions any underdrain installed with a pumping system in host rock risks freeze off.

The main constraints pertain to continued operation of the drain in the event the permafrost re-establishes itself either at the location of the drain or along any point where the drainage water is extracted to surface - such as via the pit side walls or piping internal to the pit. Long term maintenance of the mechanical equipment making up any portion of the drainage system is also challenging due to the potential for freeze up and the limited, if not inaccessible location of the equipment (e.g., beneath the pits). The depths of the pit are such that the pump system would have to be installed at depth (e.g., a suction system from surface cannot draw from the pit depth due to cavitation) and this makes access all but impossible if they should become frozen in. While elaborate systems to maintain piping from freezing are possible, such as heat tracing, the ability to rely on access for maintenance is not there. As such, the pits should be designed to rely on consolidation by drainage to surface as discussed below.

Pit Liner

The benefit of constructing a low permeability pit liner to minimize the release of contaminants from the tailings mass into the local groundwater system was discussed in Section 2.4-2.

At this stage it is considered that a pit liner will not be necessary given the low hydraulic conductivity of both the tailings and the surrounding rock mass. However it is recognized that such a liner installed on the floor of the deepest part of Main Zone pit might be a reasonable TMF engineering option reinforcing the isolation of the tailings from the sub-permafrost aquifer, especially if borehole mining activities are used to extract mineralization extending further in depth beneath the Main Zone open pit bottom.

3.4 TAILINGS PIPELINE

The Tailings Neutralization thickener underflow will be pumped to one of three TMFs which will be mined out open pits, located south of the mill (Centre, East, and Main). Initially, only the East Pit will be available to receive tailings when the mill first begins operation.

Tailings will be pumped from the Tailings Neutralization circuit through a dual contained High Density Polyethylene (HDPE) pipe to the pump house, located south of the purpose built pit (PBP), and then directed towards the TMF. The pipe will be a 300 mm dual contained, insulated, with a leak detection system and about 2 km in length. To prevent freezing, the pipe will also be equipped with an electric heat tracing system.

The pipeline will run along a trestle and then along the ground. In order to avoid thawing of the permafrost the pipeline will be supported by a bed of engineered fill. At road crossings the pipeline will go underneath the road through larger HDPE pipe. The pipeline will discharge through a tremie at a barge on the TMF. The barge will be movable to aid in the even deposition of tailings. It is anticipated that an alternative to the barge, allowing for increased operational flexibility, will be proposed at the time of licensing application.

Table 3.4-1 identifies the preliminary design criteria for the tailings pipeline. The rheology of the slurry was assumed to have properties similar to Bingham fluid. The yield stress and Bingham viscosity were determined by experience and through current literature in similar mining in northern Canada.

Table 3.4-1 Preliminary Slurry Pipeline Design Criteria

Parameters	Units	Values
Liquid Density	kg/m^3	1,000
Fines Particle Density	kg/m^3	2,600
Coarse Particle Density	kg/m^3	2,600
Slurry Mixture Density	kg/m^3	1,310
Percent Fines	%	15
Percent Solids	%	38
Pipe Roughness	-	0.015
Slurry Yield Stress	Pa	25
Bingham Viscosity	Pa.s	0.030
Pipe Length	m	2,180
Pipe Diameter	mm	300
Maximum Diameter of Suspended Solids	µm	>75
Nominal Flow Rate	m^3/hr	300
Nominal Pressure	kPa	1400

3.5 TAILINGS THICKENER OVERFLOW PIPELINE

The Tailings Thickener overflow, which may periodically be in excess of the Kiggavik water treatment plant capacity, will travel by pipeline from the mill to the TMF. The flow will be pumped through the pump house to the barge, or alternative, in the TMF. The pipeline will be supported with the same system as the tailings line. The pipeline will be an HDPE dual contained pipe with insulation, heat trace and leak detection. The preliminary design criteria are given in Table 3.5-1.

Table 3.5-1 Preliminary Tailings Thickener Overflow Pipeline Design Criteria

Parameters	Units	Values
Liquid Density	kg/m^3	1,000
Viscosity	mPa.s	0.030
Pipe Roughness	mm	0.0015
Pipe Length	m	1,275
Pipe Diameter	mm	200
Flow Rate	m^3/day	672
Pressure	kPa	640

3.6 BENEFIT OF THE WATER COVER

Thermal analysis of tailings deposition was modeled in a series of staged models which considered the change in elevation of tailings over time as well as the alternating placement of tailings in winter and summer seasons. The modeling shows that over time, in the absence of mitigation measures, layers of frozen and unfrozen tailings could develop within the pit TMF. This result is supported by observation of an existing in pit TMF in northern Saskatchewan which has less severe winter climate conditions. Based on these analytical and observed findings, deposition of tailings with the possibility of their freezing and affecting consolidation is deemed important to avoid.

Sub-aqueous deposition of tailings is one possible means to prevent the freezing of tailings during winter deposition. A water cover holds high latent heat which must be removed prior to temperatures at the base of the water dropping below zero Celsius - which would indicate possible freezing of tailings at that location. Analysis was carried out to determine the minimum depth of water cover to maintain in place on a year round basis such that the temperature at the base of the water cover does not drop below the freezing point (see Section 4.4). Model results show that with a 5 m deep water cover in place, the base temperature is buffered from the climate at surface and maintains a year round temperature of approximately 3°C, which corresponds with observed under ice lake temperature values in arctic environments.

Based on this analytical result and on observed arctic lake temperature profiles, it was concluded that a 5 m deep water cover would be maintained throughout deposition and early consolidation. Once significant consolidation is observed then the water cover would be replaced with a rock surcharge load and eventually a final cover system.

3.7 TAILINGS DEPOSITION AND RECLAIM SYSTEM

Overview

The tailings will be routed to a deposition system, which will be used to deposit the tailings subaqueously, using the tremie technique, under the surface of the TMF pond. The tailings will be deposited subaqueously near the surface of the previously deposited tailings on the bottom of the pond. As the tailings level builds up, the TMF water level and deposition pipe will be raised to maintain the proper tremie depth. To prevent freezing the pond will contain at least five metres of water cover.

Cold temperature operating conditions

During cold temperature conditions, when a layer of ice covers the pond, special operating considerations will be required. An ice-free condition will be maintained for the barge, or alternative, by pumping water through a distribution header around the perimeter of the barge. The washdown pump located on the barge will provide a dual function as a de-icing pump. The pump will distribute pond water from an internal sump in the barge through the header pipe with sufficient circulation to maintain an ice-free condition around the barge.

Reclaim

Reclaim from the TMF will be pumped to the water treatment plant for treatment. The reclaim pumps will be located on the opposite site of the deposition system to prevent disruptions to reclaim collection from tailings discharge. Each TMF will have 2 reclaim pumps installed, one in operation with a second standby pump. Reclaim water may be pumped from more than one pit at a time, dependent on the pumping needs. The reclaim waters will be pumped to a tank in the reclaim pumphouse via a dual-contained, insulated, and heat-traced HDPE pipeline. The reclaim tank discharge will be pumped to the water treatment plant via a dual-contained, insulated and heat-traced HDPE pipeline. The pumping rates from each TMF will be controlled to maintain the minimum water cover in each TMF, and to provide a consistent flow to the water treatment plant that is within the plant design capabilities.

3.8 QUANTITIES

Approximately 11.5 million tonnes of tailings solids are expected to be generated from processing of existing Kiggavik Project ore sources based on the expected mill production

schedule. For design purposes the containment volume was conservatively based on an average solids content of 40% (by weight) translating to a low dry density of 0.533 tonnes/m^3 while the average solids content of the tailings in pit is predicted to increase from 40 % to 70%. Under this conservative assumption the containment requirement was estimated at 22 million m^3, approximately.

3.9 DECOMMISSIONING

3.9.1 Concept

Closure of the TMF facilities will be implemented as a progressive closure program as tailings deposition and consolidation occur. For instance closure of the East Zone TMF will likely be implemented during operation while the Main Zone TMF will likely be closed and decommissioned upon termination of the milling operation. Closure activities will be conducted with the objectives of:

- stabilizing the surface of the tailings and prevent wind and water erosion;
- controlling the release of contaminants over the long-term; and,
- developing sustainable landform comparable with local topography

For East Zone and Centre Zone TMFs the conceptual decommissioning plan consists of fully back filling the TMFs above the tailings mass with Type 2 mine rock and installing a compacted till cover. Figure 3.9-1 summarizes the decommissioning concept for East Zone and Centre Zone TMFs.

Based on existing resources and milling schedule, the Main Zone TMF would only be partially filled with tailings upon termination of the milling activities. However it is considered likely that additional resource will be found over the life of the project and that the Main Zone TMF will eventually be fully filled with tailings. Therefore, the base case for the decommissioning of Main Zone assumes that Main Zone TMF will be fully filled with tailings in a manner similar to East Zone and Centre Zone TMFs. The conceptual decommissioning plan consists of fully backfilling the TMF above the tailings mass with first Type 3 mine rock then Type 2 mine rock and installing a compacted till cover. The Type 3 mine rock is expected to be associated with some acid generation and/or metal leaching potential and/or uranium solid content greater than 250 ppm U.

In the unlikely case where no additional resource would be found over the life of the project Main Zone TMF would be partially filled with tailings. In that case the conceptual decommissioning plan consists of fully backfilling Main Zone TMF above the tailings mass with first Type 3 mine rock then Type 2 mine rock and installing a compacted till cover. As an

alternative, the TMF would be only partially backfilled with mine rock then a compacted till cover would be installed, above which a pond would be allowed to develop.

Figure 3.9-2 summarizes the base case decommissioning concept for the Main Zone TMF.

3.9.2 Decommissioning Stages

A four stage progressive decommissioning plan is envisaged for the Kiggavik TMFs, commencing during operation. Centre and East Zone TMFs are expected to consolidate within an approximately 10-year period. A water cover would be maintained to prevent freezing of the tailings surface and allow expulsion of consolidation water.

Stage 1

Placement of tailings will be controlled to achieve a level to slightly mounded tailings surface. At the same time, the water cover will be progressively reduced to achieve a uniform water cover of sufficient depth to facilitate tailings placement. The surface water pond will be pumped through the treatment plant and any sludge recovered will be discharged to the TMF. When the tailings have been levelled and distributed, and the water cover reduced, placement of the soil and rock cover will commence.

Stage 2

Experience in Northern Saskatchewan has demonstrated that waste rock can be placed directly on the tailings surface if care is exercised. The surface of the tailings can be expected to be unconsolidated and relatively soft, allowing the rock fill to sink into the tailings and displace them. This is an undesirable effect since continued placement will cause a wave of unconsolidated tailings to run ahead of the rock fill. To prevent this, it is proposed that a 2-m layer of sand fill, approximately, will be placed over the tailings surface to act as a support filter. A 2-m thick layer of rock will be placed over the sand layer. If there is standing water over the sand support layer, the rock will be placed in a uniform layer onto the ice cover during the winter. The rock will settle uniformly onto the sand surface during the following summer thaw.

A leachate collection system will also be constructed during the summer thaw to allow consolidation flows related to pore fluid seepage to be recovered and treated. The leachate collection system will consist of simple corrugated metal wells installed in a granular blanket within the fill material. HDPE pipe would be considered due to its resistance to corrosion and ability to accommodate large differential movement. Temperature and pore pressure sensors will be installed within the tailings to allow pore water pressure dissipation and temperature to be monitored during and after cover construction.

Stage 3

When the temperature sensors indicate that the tailings are thawed, the third stage of cover placement will commence. The third stage of decommissioning will consist of placement of a Type 2 mine rock cover. Using the mine fleet sufficient rock will be placed in a mounded configuration to accommodate this amount of consolidation settlement. Consolidation will expel pore fluid, which will be collected in the leachate collection system at the surface of the tailings. All water from the leachate collection system will be treated before discharge and any recovered sludges disposed of by burial in a designated area on the upgradient side of the TMF.

With ongoing settlement, recontouring of the Stage 3 rock cover will be performed as required to maintain a well drained surface.

Stage 4

When pore pressure monitoring indicates that consolidation is complete (following Stage 3 cover placement), the final cover will be placed and revegetated. The final cover for the TMF will consist of clean waste rock with a compacted till cover. The tailings would be covered in one season to prevent freezing. At the same time, the water treatment plant sludge disposal area will be decommissioned, covered using a till material cover, and revegetated.

Main Zone

Experience gained during decommissioning of the East Zone and Centre Zone TMFs will benefit the decommissioning of Main Zone TMF. Decommissioning of the Main Zone TMF will be similar to the closure tasks for East Zone and Centre Zone TMFs; however, in addition to a Type 2 rock cover, any Type 3 mine rock stockpiled on surface during mining in the Kiggavik site will be disposed of into the TMF on top of the tailings.

3.10 WATER MANAGEMENT

Water management requirements will be largely based on the total volumes and rates of expulsion of water from tailings during consolidation. The total amount of water that can be expected to be released in the TMFs by the consolidating tailings is in the order of 13.1 million cubic meters. Additional water to consider for water management purposes would include any precipitation (snow or rain) or surface water that runs into the pits. This is nominal relative to the tailings expulsion water.

During operation tailings pond water will be pumped to either the water treatment plant or the process water tank for recycling through the mill processes. The objective of the pumping system will be to ensure that the tailings pond is maintained at a relatively stable level and that the elevation of water in the tailings pond is maintained below the active zone. A minimum of 5m of free water will be maintained on the tailings surface during subaqueous deposition of the tailings).

4 THERMAL BEHAVIOUR

4.1 INTRODUCTION

The objective of this part of the assessment is to evaluate through mathematical modelling the thermal behaviour of the Kiggavik TMF, during operation and after decommissioning, taking into consideration the potential for climate change.

Deposition of uranium tailings in mined out open pits in Northern Saskatchewan (e.g., Key Lake Mine, Rabbit Lake Mine, McClean Lake Mine) has revealed that, in the absence of preventive measures, there is a high likelihood that tailings deposited on surface during winter months will freeze into layers ("ice lenses") that subsequently do not thaw in the following summer season. The implication of forming these ice lenses is that they become a blockage for dissipation of excess pore water pressure and consolidation. Therefore the assessment of tailings thermal behaviour during the operating period focuses on the thermal conditions associated with the potential formation of ice lenses within the tailings mass.

Climate change is also a significant concern in all arctic regions due to the potential for disturbing the delicate heat balance required for the existence of permafrost. Climate change models suggest that there will be alternate cooling and warming trends over the next few hundred years (see Technical Appendix 4D "Baker Lake Long Term Climate Scenario").

For the purpose of this assessment a warming trend of 5°C over the next 100 years has been considered, including a warming trend of 3°C over the next 30 years. This period should encompass the life of mine plus closure period. Figure 4.1-1 shows the two assumed warming trends that are applied in the subsequent analysis. Existing data indicates that the mean annual temperature is between -6 and -7 °C and given that permafrost depth is sensitive to this value, both values are used in this study as the starting temperature from which climate warming is assumed. This section of the assessment presents thermal analyses somewhat similar as those carried out in the past (see for instance; EBA 1990, Nixon 1989, Nixon and Holl 1998) but with more details regarding pit geometry, mine plan deposition sequence, material properties, and boundary conditions.

4.2 THERMAL PROPERTIES

4.2.1 Thermal Conductivity

Thermal property testing was conducted on host rock sampled in the Main Zone area. The measured thermal conductivity and volumetric heat capacity for all samples are listed in full in Table 4.2-1.

Table 4.2-1 Thermal Conductivity of Kiggavik Host Rock

Site	Hole / depth	Total porosity (%)	Dry density (g/cc)	SG (calc)	Thermal conductivity (W/m*deg. K)	Specific Heat (MJ/m^3*deg. K)	Thermal conductivity (kJ/day/m/C)	Vol. Heat Capacity (kJ/m3/C)
Kiggavik Main Zone	MZ-07-03 / 236.0 m	0.29	2.596	2.60	3.446	2.126	297.73	2126
	MZ-08-02 / 255.0 m	0.74	2.765	2.79	2.330	2.218	201.31	2218
	MZ-08-04 / 142.2 m	0.49	2.581	2.59	3.386	2.011	292.55	2011
	MZ-08-04 / 170.3 m	1.83	2.567	2.61	3.385	1.952	292.46	1952
	MZ-09-1A / 215.5 m	0.29	2.665	2.67	3.456	1.854	298.60	1854
	MZ-09-1A / 216.3 m	0.39	2.602	2.61	3.203	1.745	276.74	1745
	MZ-09-1A / 246.6 m	13.94	2.242	2.60	3.576	1.618	308.97	1618
	MZ-09-1A / 257.0 m	8.53	2.400	2.62	2.909	1.804	251.34	1804
	MZ-09-1A / 300.5 m	0.48	2.597	2.61	3.578	1.635	309.14	1635
	MZ-09-03 / 227.0 m	0.31	2.634	2.64	3.342	1.505	288.75	1505
	MZ-09-03 / 236.0 m	0.42	2.608	2.62	3.226	1.586	278.73	1586
	MZ-09-03 / 240.2 m	0.98	2.560	2.58	3.584	1.506	309.66	1506
	MZ-09-03 / 247.8 m	0.41	2.602	2.61	3.109	1.913	268.62	1913
	MZ-09-04 / 239.0 m	0.52	2.609	2.62	3.913	1.450	338.08	1450
	MZ-09-04 / 240.1 m	0.85	2.611	2.63	3.914	1.733	338.17	1733
	MZ-09-04 / 241.5 m	0.60	2.618	2.63	3.925	1.856	339.12	1856
	LG88-329 / 72.5 m	0.47	2.628	2.64	2.995	1.953	258.77	1953
	LG88-352 / 36.6 m	0.89	2.587	2.61	3.453	1.797	298.34	1797
Mill Site	RMI09-02 / 19.0 m	13.51	2.299	2.66	2.262	1.883	195.44	1883
	RMI09-02 / 23.5 m	0.40	2.592	2.60	3.147	1.917	271.90	1917

The table reports an average thermal conductivity of 3.35 W/m/°C which is equivalent to 289 kJ/day/m/°C with a standard deviation of 36.5 kJ/day/m/°C. The average reported heat capacity is 1750 kJ/m^3/°C with a standard deviation of 236 kJ/m^3/°C. These values are for the host rock with a very low reported total porosity of 0.5%. The porosity is equal to the volume of water in the sample should the sample be fully saturated. These values are strongly dependent on rock mineral composition, in particular quartz content, and they can be used along with standard thermal property calculation procedures to develop the appropriate thermal values for the same rock type but under a wider range of water contents - such as would exist for the tailings when re-deposited back in the pit.

Figure 4.2-1 shows thermal properties of the tailings under fully frozen and fully thawed conditions over a range of likely saturated water contents. The measured values were used to back-calculate the likely quartz content and mineral specific heat capacity and then those values were applied to a range of water contents and void ratios as may be experienced by the tailings. This is considered as a very accurate method of developing thermal model input properties. It should be noted that as opposed to hydraulic properties, which can vary many orders of magnitude, thermal properties can only double in value, approximately, across the same soil / rock types.

In addition to the tailings, two other material types are considered in the thermal model: the host rock in which the pit is excavated and the waste rock material placed on top of the final tailing lift in order to enhance consolidation and protect the exposed tailings surface. Figures 4.2-2 and 4.2-3 show the thermal properties of these material types under fully frozen and fully thawed conditions over a range of likely saturated water contents.

The actual value applied in the thermal models depends on the material type and whether the analysis is short or long term (e.g., during mining or over several hundred years post-mining). There are short term values that apply to high void ratio (e.g., water content) depositional stages and there are long term, lower void ratio consolidated values, which apply to analyses that consider extended time periods and freeze-back of permafrost over several hundred years.

While Figures 4.2-1 to 4.2-3 show the fully frozen and thawed values, there is a transition between the two states as the water in the material freezes and that this transition is a function of soil particle size and salt induced freezing point depression (see Section 4.2.2). The actual functions applied in the thermal model are on Figure 4.2-4 for the tailings and waste rock (i.e., surcharge load material). The host granite rock is assumed to have very minimal water content (on bulk) and therefore all water was assumed to change phase and release latent heat instantly at zero degrees Celsius. The calculation of the freezing point depression of the tailings is given in Section 4.2-2.

While the thermal functions presented on Figure 4.2-4 are based on measured values they can be verified against actual measured field conditions at Kiggavik. The current depth of permafrost at Kiggavik is about 220m below surface and this position is governed by three factors: the geothermal heat flux below, the mean annual ground surface temperature, and the thermal conductivity of the rock. It has been well established all over the world that the geothermal heat flux ranges between 5.2 and 6.9 milli-Watts / m^2. Ground temperature profiling at the Main Zone area shows that the temperature gradient suggests a mean annual surface temperature that ranges between -6°C and -7°C as shown (reference). If these two boundary conditions are applied in a thermal model of undisturbed granitic rock, the permafrost depth will be computed to be at a depth of 220m if the thermal conductivity is 274 kJ/day/m/°C, a value very close to the laboratory reported average of 289 kJ/day/m/°C. The difference between the calibrated value of 274 kJ/day/m/°C and the measured average of 289 kJ/day/m/°C is less than half the standard deviation of all measured values (e.g. 36.5 kJ/day/m/°C as reported above). In summary, the confidence in thermal property values applied in the model is high. There is sufficient data for thermal gradients in the host rock at Kiggavik to calibrate the rock material properties and model boundary conditions.

4.2.2 Freezing Point Depression

Freezing point depression is a phenomenon by which water in porous materials does not freeze at 0°C. There are two main mechanisms that contribute to lowering the freezing point below zero. First, capillary forces in porous material develop surface tensions between water, ice and soil particles and this tension must be overcome by reducing the temperature in order to change

phase. Secondly, dissolved ions in the pore water, such as the addition of salts, can further reduce the freezing point depression. The influence of dissolved ions on the freezing point depression is computed using the equation

$$\nabla T = K_f * C_m * i$$

Where:

K_f = freezing point depression constant (°C*L/mol)

C_m = molar concentration (mol/L)

i = Van't Hoff factor (= 2 for most dissolved salts in water).

Table 4.2-2 shows that the ion related freezing point depression at JEB is very limited, at about 0.18 degrees. Given that the Kiggavik tailings properties are not expected to be significantly different from the JEB tailings properties it is reasonable to use the JEB data to simulate the Kiggavik tailings thermal behaviour. The freezing point depression is also a function of capillarity and this effect is illustrated in Figure 4.2-5. This figure is based on observed data from Rabbit Lake tailings as well as the computed ion related freezing point depression for JEB tailings.

Table 4.2-2 Ion Related Freezing Point Depression

Ion Type	Molecular Weight (g/Mol)	Concentration (mg/L)	Molar Concentration (mol/L)
Ca^{2+}	40.08	546.59	0.0136
Mg^{2+}	24.31	114.60	0.0047
Na^{+}	22.99	126.48	0.0055
K^{+}	39.10	33.08	0.0008
Si^{4+}	28.00	6.26	0.0002
$HCO3^{-}$	61.00	130.97	0.0021
$CO3^{2-}$	60.01	10.00	0.0002
Cl^{-}	35.00	55.27	0.0016
OH^{-}	17.01	1.00	0.0001
SO_4^{2-}	94.00	1899.77	0.0202
			0.0491
		Freeze depression Constant (°C * L/mol)	1.858
		Van't Hoff Factor	2
		Freeze depression temperature (°C)	0.18

NOTE: This computed freezing point depression is that due to dissolved ions. There is additional freezing point depression due to the capillary nature of freezing water in porous materials. Both mechanisms contribute to the over-all freezing point depression.

4.3 MODEL DEVELOPMENT

4.3.1 Introduction

The prediction of the thermal behaviour of deposited tailings is dependent on many parameters and assumptions, including surface boundary conditions, warming trends, soil properties, salt contents and freezing point depression.

Thermal modeling of tailings deposition and near term afterwards was carried out using two industry accepted, commercial software programs. TEMP/W is a finite element two-dimensional model developed by Geo-Slope International Ltd that considers steady state or transient heat transfer by conduction with an option for convection (e.g., heat flow in moving water). The model allows for construction sequences to be considered, which means the model domain and boundary conditions are allowed to change with time and space. In addition the COMSOL model was used for three-dimensional thermal modeling. COMSOL is an advanced multi-physics model distributed by the COMSOL Group and is capable of considering latent heat of phase change in porous materials along with conduction and convection. Given identical inputs, both models will give identical outputs. The advantage of using one over the other is related to geometrical differences and tailings deposition sequencing.

4.3.2 Initial and Boundary Conditions

The permafrost at the Kiggavik site has stabilized over time to extend to a depth of about 220 m to 240 m (see Technical Appendix 5B “Geology and Hydrogeology Baseline”). Stabilized permafrost exists because there is a balance between the geo-thermal heat flux at depth and the yearly mean ground surface temperature. In other words, the cooling effect of the sub-freezing ground surface temperature exactly balances the heat effect from the earth’s core. The East Zone and Centre Zone pits are planned to be mined to a depth of 85 and 104m respectively, which will result in its deepest elevation being about 110 m above the permafrost base. The Main Zone Pit is planned to be mined to a depth of approximately 245 m, which will result in the pit floor being below the base of the permafrost. Therefore, there is a potential difference in long term thermal regime between the two types of TMF. The modeling program considered the different pit geometry in terms of depth as well as the proximity of each pit to the other in the event the larger Main Zone pit thermal regime has an influence on the others over the long term.

Monitoring of temperatures near surface in the Kiggavik area has shown that the surface yearly average temperature is about -6 to -7°C. This observation combined with the measured depth of the permafrost was used to calibrate the host rock material properties and also evaluate the thermal state prior to tailings deposition (i.e., initial conditions for the models). Figure 4.3-1 shows the region being modelled with the three pit geometries and locations. Note that the Main Zone pit is assumed conical shaped in the model which is a little different than the

probable field case. However, the volume of the pit (and therefore the heat added by the warm tailings) is representative of the field case.

The results shown in the figure are the long term pre-mining state and they indicate that the boundary conditions applied to generate these computed initial conditions match the in-situ measured case. The model base and surface boundary conditions are also presented on this figure for the two assumed ground surface temperature case that are considered. This model result is the existing undisturbed condition and therefore is used as the starting condition for all transient tailings deposition models and climate change permafrost erosion / re-establishment models. For the climate warming scenarios considered, the functions shown in Figure 4.1-1 were applied in lieu of the constant temperature applied to generate the in-situ result.

4.4 PREVENTION OF ICE LENS FORMATION

4.4.1 Objective

In order to restrict the development of ice lenses on the surface of the tailings at Kiggavik, subaqueous deposition of the tailings is proposed. Subaqueous deposition of tailings involves placement beneath a free water surface such that the water is deep enough, on a year round basis, to maintain temperatures at the top of the tailings greater than the freezing point. In this way, the tailings are unable to develop alternating frozen and thawed layers over the yearly climate cycle. This procedure has been successfully applied at the JEB facility at McClean Lake.

The purpose of this component of the assessment was to determine, for the climatic conditions at Kiggavik, what depth of free water is necessary to ensure that the surface of the tailings does not freeze. The analysis was run for 365 days using a temperature boundary function which reflected temperatures ranging from +10°C to -25°C. This function is based on measured data reported in the Technical Appendix 5B “Geology & Hydrogeology Baseline”.

4.4.2 Profile Description

A one-dimensional profile of the Kiggavik tailings pit was developed to create a simplified thermal analysis. The purpose was to investigate how deep a water layer would need to be maintained on the tailings surface to ensure that temperatures at the tailings surface remained above freezing. The depth of water was varied at 1m, 3m, 5m and 7m. The general profile itself remained unchanged and is shown as Figure 4.4-1.

4.4.3 Material properties and boundary conditions

The material properties used for the simplified thermal analyses included a granitic host rock, tailings and a water layer. The material properties of tailings and rock are provided in Section 4.2. The boundary conditions applied to the bottom of the model are the same as those

described in above for the in situ case with an assumed ground surface temperature of -6°C. The surface boundary condition applied to the free water surface is shown in Figure 4.4-2.

4.4.4 Results

Water Layer – 1 m

As shown in Figure 4.4-3 when a water layer of 1m is maintained on the surface of the tailings the temperature at the surface of the tailings decreases below zero during a typical year. This result indicates that ice lenses would penetrate into the tailings under these conditions.

Water Layer – 3 m

When the water layer is maintained at 3 m deep, the temperature at the tailings surface remains above zero (0°C) as shown in Figure 4.4-4. This result indicates that a water depth of at least 3m would be required to ensure that ice lenses do not develop within the tailings.

Looking at the temperature profile in the water layer over time indicates that approximately 1.5 m of ice develops during the winter freeze as shown in Figure 4.4-5. This result is consistent with the results of studies on depth of ice in lake water in Northern Canada (Dyck, 2007). The good agreement between modeled and field observations also serves to confirm the selection and application of the surface model boundary conditions for all thermal analyses carried out.

Water Layer – 5 m and 7 m

Given that 3 m of free water is sufficient to maintain a temperature above freezing in the underlying tailings, increasing the depth of water serves as additional assurance that the surface of the tailings will remain unfrozen during winter freeze as shown in Figure 4.4-6.

These results show that the maximum thickness of ice in the water layer is predicted to be approximately 1.5 m, which means that the tailings surface will experience temperatures above freezing throughout the year if a sufficient water cover is in place. To provide additional assurance that ice lenses will not develop in the tailings, it is proposed that approximately 5m of free water be maintained on the tailings surface at Kiggavik during subaqueous deposition of the tailings. All subsequent thermal and consolidation modeling are carried out with the assumption that the tailings will be deposited subaqueously under a minimum 5 m of free water.

4.5 THERMAL BEHAVIOUR DURING AND AFTER DEPOSITION

Transient modelling of tailings deposition was carried out with the objective of answering the following questions:

- Will the subaqueous placement actually prevent the tailings from freezing?
- Will the base or sides of the tailings freeze, which may prevent a bottom drain mechanism from working?
- Will the permafrost around, within, and below the pit be permanently degraded or will it come back over time?

Tailings deposition under transient conditions was simulated using the initial conditions discussed previously. Successive stages were then simulated with the results of the previous stage used as the initial condition of the next stage (Figure 4.5-1). New lifts of tailings were assigned an assumed deposition temperature of 10°C. This value is likely low but is conservative when considering the freeze-back potential of tailings during the deposition process. At each stage of the analysis a water cover of 5 m was applied to the tailings surface, in order to confirm the lack of development of frozen tailings layers. The rationale for the 5 m was presented in the previous section. This transient depositional sequence modeling was only applied to the Centre Zone pit in order to illustrate the process of preventing ice layers as well as to closely inspect the interaction between the tailings and the pit wall and permafrost. The conclusions from the Centre Zone pit would apply equally to the other pits as the zone of interest is not the entire pit but the tailings / pit wall contact.

4.5.1 Deposition and Tailings / Pit Wall Thermal Interaction

Figures 4.5-2 shows the thermal state at key intervals during and after deposition in the Centre Zone Pit. These figures confirm that the water cover acts as a thermal barrier to limit freezing during winter deposition. The latent heat stored in the water is released when it is cooled which delays and limits the depth of frost penetration in the tailings surface.

Figures 4.5-2 also shows that permafrost near the surface and at the sides of the pit freezes back into the tailings. The lateral freeze back is due to the large heat sink in the surrounding permafrost, which can remove any heat introduced by the warmer tailings. This freeze back on the sides may limit the successful operation of an under-drain mechanism that passes through the sides of the pit and any interruption in the pumping may result in freeze up of drain pipes which could prove very difficult to unplug.

4.5.2 Long Term Tailings - Permafrost Interaction

Over the long term, in the absence of climate change, the bulk of the warmer tailings mass form a single, thawed zone within the pit which has enough heat within it to break through the permafrost below the centre of the any of the three pits. The sequence of images in Figure 4.5-3 shows the progression of thawing into the walls of all three pits and below. Over time, they also show the mechanism by which the permafrost starts to re-establish itself top-down from the surface of the tailings. This top-down freezing would only happen once the final earth cover is placed on the consolidated tailings - e.g., once the water cover is removed (recall the water cover prevents freezing down from surface). As such, the elapsed times shown in these images are approximately from the time of closure onwards.

Close inspection of the sequence of images shows that for the two smaller pits, there are instances in time early on where there are two ice zones along a vertical profile. Moving down from surface, there is permafrost re-establishing on surface, there is then a zone of thawed tailings, beneath which is a zone of permafrost. Over time, this lower zone of permafrost is thawed by the combination of tailings and geothermal heat. Over the very long term, however, the permafrost moving downward from surface reaches its original position at 220m (in the absence of any climate warming trend).

Figures 4.5-4 to 4.5-6 present a more accurate position of surface down permafrost growth (as well as early on sub-pit thawing) over time for each pit. In the absence of climate warming, the permafrost is re-established fully at a depth of 220m by 2000 years. In the Main Zone, it is not quite fully established by this time and it appears it will take much longer than the time scales modeled. Also note that in the Main Zone the excavation is deeper than the initial permafrost so there is no existing ice beneath the base of the pit early on after closure. Finally, when reviewing these figures keep in mind the pit depths. The Main Zone is 245m deep, the Centre Zone 104m deep, and the East Zone 85m deep. The black line in the images shows the pit depth for reference.

4.6 POTENTIAL IMPACT OF CLIMATE CHANGE

4.6.1 Assumptions

The boundary conditions applied to the models for the climate warming analyses were presented above in Section 4.1. Two warming trends for the mean annual ground surface temperature were considered: warming from -7 to -2 °C or warming from -6 to -1 °C. Analyses were carried out for a natural ground case (e.g., with no pits) as well as for all the pits. In these analyses, the East Zone and Centre Zone pits were assumed to be full of tailings with a rock surcharge above and no water cover. The Main Zone configuration consisted of three options: full of tailings with a cover system, half full of tailings with a cover system constructed at depth and open to atmosphere above, and finally an empty pit with no tailings but full of water.

4.6.2 Results

4.6.2.1 Potential Impact on Natural Permafrost

Figure 4.6-1 shows the anticipated depth of permafrost predicted over 2000 years for the two assumed warming trends. The initial permafrost is -220m but this increases to approximately -100m for the case 2 trend (e.g. -7 to -2 °C) or -45m for the warmer trend (e.g., -6 to -1 °C). The model results meet with expectations from a qualitative perspective. Given no change in geothermal heat for either case, then the depth of permafrost is controlled solely by the mean annual surface temperature.

4.6.3 East Zone Warming Trends

Figure 4.6-2 shows the permafrost status with depth and time in the East Zone pit for the two assumed warming trends. In both cases, and as shown previously for the no warming case, there is a zone of ice beneath the pit that slowly melts during the initial post closure period. After this time, all of the newly forming permafrost is driven by downward growth from surface in response to cold mean annual ground surface temperatures. These figures show that for either warming trend the permafrost freezes down from surface to a depth lower than its new long term anticipated depth. It reaches a maximum depth of between 125 and 170 m after about 500 years (for the two warming trends) and then the bottom position of permafrost rises in elevation towards its natural surrounding value of either -45m or -100m as reported above. For the case 1 warming, the permafrost establishes itself above the pit base elevation of -85m which means there will be thawed tailings in the bit bottom indefinitely. For the case 2 warming, the permafrost eventually establishes itself below the bit bottom depth.

4.6.4 Centre Zone Warming Trends

Figures 4.6-3 shows the permafrost status with depth and time for the Centre Zone pit for the two warming cases. The Centre Zone pit has a significantly larger base area and as such, there is much more heat transfer downwards to the permafrost below. As a result, the permafrost growing downwards from surface does not extend to below the pit base as it does in East Zone. Here, once the ground below the pit thaws, the only ice growth is a long slow re-establishment of permafrost from the surface downwards to the long term natural anticipated depths of -45 or -100m for each warming case respectively. For this pit, and for both warming cases, the permafrost will establish itself above the base of the pit.

4.6.5 Main Zone Warming Trends

Figures 4.6-4 and 4.6-5 show the Main Zone permafrost status for the case where the pit is full of tailings or where it is half full with a cover and air above in the upper half. There are no permafrost trends to report for the case where the pit has a lake in it as for this case; the permafrost cannot establish and a talik results. The reason for prevention of permafrost in this case is much the same as that given to justify use of a water cover during tailings placement in order to prevent frozen tailings layers from developing and inhibiting consolidation.

4.6.6 Combined Effects

The question may be raised whether the thermal response of the Main Zone TMF will have an impact on the other two TMFs. This can be addressed by considering the three zones together in a 3D model. The assumption is made that the East and Centre Zone TMF's are full of tailings at closure. The final configuration of the Main Zone TMF considers three options. For the case where the Main Zone pit is full of tailings, the long term permafrost state re-establishes at more or less a consistent depth across the site depending on the assumed climate warming

conditions. Those results are presented above. For the case where the Main Zone TMF is full of water and a talik forms beneath the pit, there is a different long term permafrost regime as shown in Figure 4.6-6. For the case where Main Zone is water filled, the long term mean annual temperature of the lake water is assumed to be 2.5°C. Lakes in lower latitudes with distinct winter seasons exhibit year round temperatures of approximately 4°C which corresponds to the temperature at which water is most dense. This phenomenon results in continual mixing of water resulting in the most dense water settling in over most of the depth of the lakes. In arctic climates, the mean annual lake temperature can drop to lower than 4°C due to the lower mean annual air temperatures and less energy input. In this study, the exact lake temperature in the TMF is not so important. As the figure shows, even for the lower temperature water, a clear talik is formed. In terms of the influence of the Main Zone talik on the other TMF's it appears from this result that the Main Zone is far enough away from the Centre Zone to adversely impact the re-establishment of permafrost at Centre Zone.

4.6.7 Freeze Back Details in Covers

The previous freeze back discussions consider the long term ground temperature profiles in each pit as part of the site wide response to climate condition. This section considers freeze back at a smaller scale in the cover systems installed on the TMF's over top of the consolidated tailings.

Figure 4.5-3 shows a 3D view of the pits after 20 years of freeze back post cover placement. It can be seen that there is a large unfrozen zone within the tailings but that near surface there is re-establishment of a frozen zone. The details of the progress of freeze back are presented in Figure 4.6-7. The graph is from a 1D model set up with very small element sizes to capture the exact depths of freezing over time in a cover material 10 m thick sitting above tailings. In this example, the climate warming trend of -6 °C to -1 °C was applied as a surface boundary. Even with this boundary condition the fact that there is a mean annual air temperature that is below zero within the first year results in the onset of a frozen barrier at the surface of the cover.

The results show that the heat stored in the tailings at the time of cover placement does not significantly slow freeze down. The model used 6°C as the temperature of in situ tailings which is slightly above the expected long term temperature of 4°C (related to maximum density of water) that will result from the tailings being deposited under water. The model suggests that once the water cover is removed, the waste rock will cool and freeze across at surface - therefore sealing in any liquid water filled pores and creating a barrier to either downward or upward flow. This process is expected to occur over a very short period of time (i.e., one winter).

5 GEOTECHNICAL BEHAVIOUR AND CONSOLIDATION

5.1 INTRODUCTION

The objective of this part of the assessment is to evaluate through mathematical modelling the consolidation behaviour of tailings in the Kiggavik TMFs, during operation and after decommissioning. Results of the thermal modeling studies presented previously suggest that the tailings will not freeze if they are deposited subaqueously under a sufficiently thick (~ 5 m) water cover. Moving forward on this basis, the consolidation modeling presentation in this section was carried out under the assumption that the tailings mass will be thawed. The consolidation modeling was carried out to estimate the final elevations of tailings in the TMFs, the quantity of the seepage from the tailings as a result of consolidation and the final tailings geotechnical properties.

5.2 GEOTECHNICAL PROPERTIES

Geotechnical properties of tailings that are of primary interest for predicting the post-decommissioning effects include the density and hydraulic conductivity. The relationship between applied load and tailings density, or void ratio, is used to predict the volume that tailings will occupy within the decommissioned TMF. The relationship between tailings hydraulic conductivity and void ratio, or effective stress is used to predict the final hydraulic conductivity of consolidated tailings within the decommissioned TMF.

Testing was conducted on laboratory produced tailings from the various ores to be processed at the Kiggavik mill (Ginger CEBTP, 2009 and 2011). Tests included consolidation and permeability tests. Laboratory data was cross-referenced with field data from measurements at the AREVA McClean Lake JEB tailings management facility and the results were used to develop likely field properties at Kiggavik.

5.2.1 Granulometry

The grain size distributions of the laboratory produced Kiggavik tailings are presented in Figure 5.2-1. Silt and clay sizes in the tailings range between 74% and 82%. D_{10} (effective grain size) ranges between 2.8 µm and 2.95 µm, D_{30} (grain size such that 30% of the grains are smaller than this size) ranges from 7.5 µm and 9.3 µm, and D_{60} varies from 26 µm to 38 µm.

5.2.2 Hydraulic Conductivity

Kiggavik Laboratory data

Compressibility tests were carried out in oedometric cells which were filled by gravity, due to liquid nature of the tailings slurry. Tests were conducted on five different laboratory produced tailings samples under increasing loads, from 5 kPa to 1253 kPa. The solids content of the samples (solid percentage, by weight) before applying the loading sequence ranged from 33.9% to 52.8%. The solids content of the samples at the end of the consolidation experiment, at 1253 kPa, ranged from 72.1% to 79.2%. The hydraulic conductivity of the tailings samples was measured at each loading increment from 44 kPa to 317 kPa.

Table 5.2-1 summarized the consolidation test results.

Table 5.2-1 Summary of Consolidation Testing

Pressure (kPa)	Void Ratio	Hydraulic Conductivity (m/s)
5	1.96 to 4.65	Not measured
44	1.23 to 1.84	1.07×10^{-8} to 6.26×10^{-8}
83	1.12 to 1.68	4.20×10^{-8} (one measure)
161	1.04 to 1.51	4.11×10^{-9} to 2.53×10^{-8}
317	0.94 to 1.30	2.41×10^{-9} to 6.26×10^{-8}
629	0.83 to 1.09	Not measured
1253	0.72 to 1.15	No measured

JEB TMF data

The JEB TMF data is shown on Figure 5.2-2. The range observed in the JEB pit is due to two phenomenon: segregation of coarse and fine during deposition and decrease in conductivity within each of the coarse and fine zones due to increase in effective stress as part of consolidation. Within the fine zones the conductivity ranges between 1×10^{-6} m/s and 1×10^{-8} m/s at the time of deposition and then the range drops by two orders of magnitude as the effective stress increases with depth and consolidation. Within the coarse zone at JEB, the conductivity of the newly deposited tails ranges between 1×10^{-7} m/s and 2×10^{-5} m/s and then it too drops by two orders of magnitude as consolidation and pit depth increases. Based on these ranges, and as observed in Figure 5.2-2, there is an overlap between coarse and fine zones that is likely due to the actual mixing of coarse and fine as part of the complex deposition process.

The laboratory testing cannot fully capture the complex segregation between coarse and fine zone. The CEBTP conductivity values were reported as a function of effective stress as measured during consolidation testing. The reported values ranged between $2x10^{-9}$ m/s and $6x10^{-8}$ m/s at an effective stress of about 317 kPa which lie within the range of field reported values from JEB. Although the CEBTP test data did not cover a wide range of stress conditions the ranges tested do agree with JEB, with gives some assurance that the JEB data is likely a valid representative source of information.

For the purpose of this assessment it is considered that field data should be given more weighting in any assessment of conductivity properties because it considers the influence of the depositional process on the overall conductivity, whereby the laboratory data only considers the artificially induced change in conductivity due to increasing effective stresses. The field data shows the in-situ tailings conductivity ranging approximately between 2.0×10^{-5} m/s and 2.0×10^{-9} m/s, with an approximate median of 2.0×10^{-7} m/s. When determining the conductivity value to use in the analysis it is important to not use an average value as this would likely result in a much higher overall conductivity. This is due to the fact the range of values are typically on a logarithmic scale. If the values were averaged, the high conductivity values would skew the result and the computed consolidation would occur much faster than in reality. To account for this distribution of hydraulic conductivity values the median value of the fine zone JEB conductivity was applied as the base case conductivity and then this was decreased two more orders of magnitude as the effective stress increased. In this way, the computed consolidation values take into account the longer time for pore water pressure dissipation in fine zones and overall, they would tend to be on the conservative side.

Sensitivity Analysis

In applying an assumed median conductivity function to the entire tailings mass no consideration is given to the fact there might be segregation between coarse and fine zones. However in the pit a fine zone will take longer to dissipate its trapped pore water compared to the coarse zone. If the fine zone is surrounded by a coarse zone then the flow path length for this water to move will be much shorter than if the trapped water has to migrate always to surface. While part of this process is accounted for by using a median conductivity value, an attempt was made to more accurately capture the process of preferential flow paths in coarse zones. The corresponding analysis is presented in Attachment A where random distributions of tailings hydraulic conductivities within the pit are compared to median conductivity of the over-all pit in terms of impacts on water dissipation durations and volumes. Results of the analysis suggest that the likely in-pit consolidation is expected to behave as if the overall conductivity is somewhat higher than the assumed median value. In other words, the presence of randomly applied coarse zones is expected to provide some preferential flow paths that will enhance dissipation of excess pore pressures.

5.2.3 Consolidation Parameters

The Kiggavik laboratory and JEB field soil property data were compared and a “design” basis set of model input relationships were developed. These relationships are shown in Figure 5.2-3 and Figure 5.2-4. Figure 5.2-3 shows that the void ratio drops from a placement value of about 3.5 (at zero stress) to about 1.0 at an effective stress of 1000 kPa. The design basis consolidation curve is slightly higher than the measured laboratory values to better reflect the observations from the existing JEB TMF which take into account the complex deposition and heterogeneity in the field, relative to the laboratory. The design value is also slightly conservative in that it errs on the fine grained tailings response as opposed to the rapid consolidation of the coarse grained tailings.

Figure 5.2-4 shows the design basis conductivity functions applied in the modeling plus the JEB TMF observed and laboratory measured values. The range of conductivity for the design basis is determined from the values measured at JEB TMF, taking into consideration the potential for preferential flow paths resulting in some increase of the mean value. In general, the range applied in the modeling is felt to be conservative when the overall consolidation performance is considered.

5.3 MODEL DEVELOPMENT

5.3.1 Numerical Model

Consolidation modeling was carried out with the FS CONSOL non-linear finite strain software package (GWP Software Inc, Edmonton, Canada). The software theory is described in more detail by others (Golder, 2005) and it has been applied successfully at other in pit tailings facilities (McClean Lake, JEB facility, AREVA, 2005). In general, the FS CONSOL model considers conservation of linear momentum and equilibrium of solid and pore water; conservation of mass, and conservation of pore water mass. As part of this study, the software results from FS CONSOL were compared for quality control with those of SIGMA/W (Geo-Slope International Ltd, Calgary) with good agreement. The SIGMA/W software is a general purpose finite element code and is used worldwide in geotechnical practice. SIGMA/W solves consolidation by fully coupling deformation and pore water pressure response according to the theory of elasticity and conservation of mass.

A brief overview of the theory for consolidation of saturated medium is presented in Attachment B.

5.3.2 Boundary and Initial Conditions

The consolidation of the deposited tailings was analyzed assuming tailings deposited in a thickened slurry form at a solid content of approximately 40%.

The three pit geometries used in the FSCONSOL model are shown in Figure 5.3-1. These geometries are considered to be reasonable simplifications of the actual TMFs. The three TMFs are simulated by a conical shape, which matches relatively well the actual East Zone and Centre Zone geometry. Main Zone TMF may be more similar to two intersecting cones in reality however, it is simulated by a conical shape with an equivalent diameter and volume.

The FSCONSOL model requires the user to input the TMF shape as a series of lifts with each lift having a depth and average cross-sectional area. Typically, the lifts get a larger surface area as the TMF increases in height. Each lift is then filled according to the rate of deposition. As lower lifts fill up, the deposited tailings spread over and fill the larger cross-section lifts above. In this way, the pit is eventually filled with tailings. The FS CONSOL model requires a tailings dry mass deposition rate as a function of time as well as the initial solids content, surface and base hydraulic boundary conditions. The different rates of deposition for each TMF are shown in Figure 5.3-2. The top boundary condition in all scenarios was set as a 5 m free water surface, which agrees with the findings of the thermal analysis and the discussion on mitigating ice lens formation within the tailings. The bottom boundary condition was set either as a no-flow case or a zero excess pore water pressure case, to simulate a bottom drain.

As tailings deposition progresses, previously deposited tailings consolidate due to the additional surcharge. The models were solved for as long as necessary in order to capture the dissipation of excess pore water pressures and settlement during operation. The models were also used to simulate consolidation associated with the conceptual decommissioning scenarios.

5.4 CONSOLIDATION RESULTS

Results of consolidation modeling for the various pits and for the best judgement range of hydraulic conductivity of the tailings are presented in the following sections. For each case, the tailings height (including current settlement), average % solids, volume of water expulsed, and remaining in-pit volume were calculated over time. The impact of a bottom drain during operation and the impact of the mine rock cover during decommissioning were also evaluated. Time in all cases is referenced to the start of tailings deposition in each pit.

5.4.1 East Zone TMF

Consolidation during deposition

The East Zone Pit was simulated as the shallowest of the three TMFs with a capacity to handle a total unconsolidated volume of just over 2.7 million cubic meters of tailings at a 40% solids content. The simulated tailings deposition schedule assumed that the tailings would be deposited over an approximate 1 year period. Figure 5.4-1 shows the consolidation results for East Zone TMF for two values of the initial hydraulic conductivity of the tailings. The effect of a bottom drain is also illustrated on this figure. Simulation results presented in Figure 5.4-1 include the tailings height, the average solids content and the consolidation flow. Based on the

model and pit geometry assumptions the tailings surface at the end of deposition and prior to full consolidation is estimated to be at a height ranging from 78 m to 70 m above the TMF floor (i.e., from 7m to 15 m below ground surface). The average solids content of the tailings in pit is predicted to increase from 40 % to 70% as shown in Figure 5.4-1. The end of consolidation of the exposed tailings surface is expected to be about 40m above the TMF floor. In reality, the site operations will likely be adjusted to capitalize on this available storage by diverting tailings destined for either the Centre or Main Zones such that the East Zone pit is eventually completely filled with consolidated tailings as part of the closure plan.

The volume of water expulsed from the tailings at the end of deposition is predicted to be about 1.38 million cubic meters of water. The rate of water expelled by the tailings is directly tied to the hydraulic conductivity of the tailings.

Addition of a bottom drain mechanism has an impact on the rate of consolidation as the drainage path changes from single drainage to surface, to double drainage both up and down. However, as discussed previously, there are complex logistical issues to overcome by having a bottom drain installed in a permafrost environment. Even though the base of the pit is likely to thaw over time, the thermal analysis shows that there is a likely freeze back from the side walls especially near surface which may complicate how the drainage water is removed from bottom of the pits. The closure planning is currently based on these results and the likely field consolidation rates are expected to lie between the high and low hydraulic conductivity cases with no drain included.

Most of the consolidation occurs after deposition and, regardless of conductivity, the tailings eventually settle to solids content of about 70%. This value is based on the mass - volume relationship of the tailings and the assumption that all of the excess pore water pressure will eventually dissipate. As such, the target end solids content is reasonably known now and the uncertainty is associated with how long it takes to get to that end value.

Figure 5.4-2 shows the simulated excess pore water pressure and hydraulic conductivity profiles at the end of depositions, following cover placement and after full consolidation for the East Zone Ksat=4 x 10^{-7}m/s case. The figures are not included for every case considered as the conclusions from each case would be repetitive The consolidation times can be determined from the series of images reported for the previous section. It is useful, however, to present these two figures as a confirmation that the modeled output matches with expectations given the input parameters. The simulated hydraulic conductivty profile of the consolidated tailings mass following cover placement ranges between 7 x10^{-8} m/s to 1.2 x 10^{-7} m/s which is a direct function of the effective stress versus conductivity input function. The model predicts that most of the residual pore water pressure will be dissipated after 7.6 years. However based on the series of figures presented above, the tailings are expected to consolidate fully between 4 and 8 years after start of deposition for all combinations of conductivity and drainage type considered.

5.4.2 Centre Zone TMF

The Centre Zone Pit was simulated as a relatively shallow TMF with a capacity to handle a total unconsolidated volume of just over 6.5 million cubic meters of tailings at a 40% solids content. Tailings deposition was assumed to occur over an approximate 2 year period. Figure 5.4-3 shows the consolidation results for Centre Zone TMF for two values of the initial hydraulic conductivity of the tailings. The effect of a bottom drain is also illustrated on this figure. Simulation results presented in Figure 5.4-3 include the tailings height, the average solids content and the consolidation flow. The tailings surface at the end of deposition and prior to full consolidation is estimated to be at a height ranging from 90 m to 75 m above the TMF floor (i.e., from 14 m to 29 m below ground surface). As with the East Zone TMF, the average solids content of the tailings in pit is predicted to increase from 40 % to 70%. The end of consolidation of the exposed tailings surface is expected to be about 50m above the TMF floor. In reality, the site operations will likely be adjusted to capitalize on this available storage by diverting tailings destined for either the Main Zones such that the Centre Zone pit is eventually completely filled with consolidated tailings as part of the closure plan.

Consolidation following cover-placement

The volume of water expulsed from the tailings at the end of deposition is predicted to be about 3.5 million cubic meters of water. The rate of water expelled by the tailings is directly tied to the hydraulic conductivity of the tailings.

Figure 5.4-4 shows the simulated excess pore water pressure and hydraulic conductivity profiles at the end of depositions, following cover placement and after full consolidation for the Centre Zone Ksat=4 x 10^{-7} m/s case. As with the East Zone results above, the figures are not included for every case considered as the conclusions from each case would be repetitive The simulated hydraulic conductivty profile of the consolidated tailings mass following cover placement ranges between 7 x 10^{-8} m/s to 1.2 x 10^{-7} m/s which is a direct function of the effective stress versus conductivity input function. The model predicts that most of the residual pore water pressure will be dissipated after 9.1 years. However, based on the series of figures presented above the tailings will consolidate fully between 4 and 13 years after start of deposition for all combinations of conductivity and drainage type considered.

5.4.3 Main Zone TMF

The Main Zone TMF was simulated as the largest of the TMFs with a capacity to handle a total unconsolidated volume of just over 31 million cubic meters of tailings at a 40% solids content. Tailing deposition was assumed to occur over an approximate 6 or more year period. Figure 5.4-5 shows the consolidation results for Main Zone TMF for two values of the initial hydraulic conductivity of the tailings. The effect of a bottom drain is also illustrated on this figure. Simulation results presented in Figure 5.4-5 include the tailings height, the average solids content and the consolidation flow. The tailings surface at the end of deposition and prior to full consolidation is estimated to be at a height ranging from 140 m to 120 m above the TMF floor

(i.e., from 100 m to 120 m below ground surface). As with the other TMFs, the average solids content of the tailings in pit is predicted to increase from 40% to 70%. The end of consolidation of the exposed tailings surface is expected to be about 80m above the TMF floor.

The volume of water expulsed from the tailings at the end of deposition is predicted to be about 8 million cubic meters of water. The rate of water expelled by the tailings is directly tied to the hydraulic conductivity of the tailings.

Consolidation following cover-placement

Figure 5.4-6 shows the simulated excess pore water pressure and hydraulic conductivity profiles at the end of depositions, following cover placement and after full consolidation for the Centre Zone Ksat=4 x 10^{-7} m/s case. As with the other TMF results above, the figures are not included for every case considered as the conclusions from each case would be repetitive The simulated hydraulic conductivty profile of the consolidated tailings mass following cover placement ranges between 7 x 10^{-8} m/s to 1.2 x 10^{-7} m/s which is a direct function of the effective stress versus conductivity input function. The model predicts that most of the residual pore water pressure will be dissipated after 16.5 years. However, based on the series of figures presented above the tailings will consolidate fully between 12 and 22 years after start of deposition for all combinations of conductivity and drainage type considered.

5.5 SUMMARY

Consolidation modeling was carried out for all three TMF's based on material input values derived from both laboratory testing and cross-reference to a similar facility at AREVA McClean Lake JEB TMF. The consolidation final density and tailings heights are based on material characteristics and can be predicted with good accuracy based on the assumption that all the excess pore-water pressure will dissipate. The uncertainty in consolidation modeling lies around estimating the bulk overall tailings hydraulic conductivity as a function of effective stress. The deposition process is complicated and results in segregation of fine and coarse particles which results in the development of preferential flow paths for dissipation of excess pressure. In this assessment attempts were made to understand the likely range of conductivity over the entire pit as well as to understand how some consideration could be given to account for preferential flow paths. Based on the various studies a range of saturated conductivity for the newly deposited tailings was found to be between 2.5 x 10^{-7} m/s and 4 x 10^{-7} m/s. These two values were used in all calculations involving prediction of consolidation rates.

The inclusion of a bottom drain system was accounted for in the modeling and, as anticipated, was found to make a difference on total consolidation durations. However, the logistics of installing a bottom drain system within a potentially frozen host rock are complex and it is considered more conservative to proceed on the basis that the drain is not present, or at least if present, has ceased to function over time.

The tailings were assumed to be deposited at a solids content of 40% and the theoretical maximum consolidation solids content is 70% in this case. The modeling was carried out to a point in time when the excess pore water pressures were completely dissipated and the maximum solids content reached. A summary of the time for full consolidation is presented in Table 5.5-1.

Table 5.5-1 Summary of Consolidation Results

TMF	End of Consolidation (fastest – in years)	End of Consolidation (Slowest – in years)	Water Expused (million cubic meters)
East	5	8	1.4
Centre	6	14	3.5
Main	14	22	8

6 GEOCHEMICAL BEHAVIOUR

6.1 INTRODUCTION

The tailings preparation circuits in the Kiggavik mill will be used to treat and neutralize tailings for the removal of soluble contaminants and to thicken the resulting tailings slurry prior to disposal. Following preparation processes, tailings will be pumped from the mill to the TMF for disposal. A series of tailings neutralization tests have been completed at AREVA SEPA Laboratory and SGS Canada (Lakefield Research) to evaluate the performance of the tailings preparation process proposed for the Kiggavik mill (see Section 3.2).

The laboratory testing program conducted by SGS Lakefield was designed to evaluate the performance of the process under normal operating conditions and to examine the impact of the neutralization parameters on the long-term concentrations of uranium and other metals in the treated tailings pore water. The SGS Lakefield testing programs are reviewed in the following sections. More Addition information is included in Attachments C. Laboratory results are presented and evaluated using various geochemical models.

6.2 INITIAL GEOCHEMICAL EVALUATION

A series of models were constructed using the programs PHREEQC (Parkhurst and Appelo, 1999) and Geochemist's Workbench (GWB) (Bethke, 2008, Bethke and Yeakel, 2010) to estimate uranium concentrations expected to be sent to the tailings management facility (TMF) from the tailings treatment circuit in the proposed Kiggavik mill.

There are several options to control uranium concentrations in tailings pore waters from the Kiggavik project. In general pH plays a strong role in determining uranium concentrations, whether that concentration is controlled by mineral equilibrium (mainly schoepite formation) or by surface complexation reactions. This pH dependency is primarily caused by the formation of uranyl carbonate complexes. Maintaining a proper pH in the tailings will be critical to keeping uranium concentrations low. The inclusion of a two-stage neutralization circuit will add flexibility in controlling uranium in the pore waters.

Mineral Equilibrium

Mineral equilibrium is probably the first and simplest approach in controlling the uranium concentrations. One of the simplest and therefore most likely solubility controls on uranyl is through the precipitation of schoepite [$UO_3 \cdot 2H_2O$, also represented as $UO_2(OH)_2 \cdot H_2O$] (Langmuir, 1997). Unlike many other uranium bearing phases, schoepite formation is not influenced by a limiting reagent.

At a pH of between 6.25 and 6.5 the concentration of uranium in solution is less than 1 mg/L if a stable crystalline schoepite is formed.

The presence of carbonate in solution can elevate the concentration of uranium through the formation of uranyl carbonate complexes. Controlling carbonate/bicarbonate alkalinity values is an important factor in maintaining low uranium concentrations. The alternative process is to control pH to values low enough that these uranium carbonate complexes are not the dominant form of uranium in solution. However these lower pH values (commonly around pH 7) may not be ideal for control of cations such as nickel, and zinc.

A treatment option involving the precipitation of carnotite (KUO_2VO_4) or tyuyamunite ($Ca(UO_2)_2(VO_4)_2$) may provide an alternative or (contingency) method to control uranium in pore water and the available literature suggests that this process could produce low concentration that may possibly be less than 0.1 mg/L.

Adsorption

Another process that can control uranium is adsorption onto mineral surfaces. Use of ferric sulfate to increase the amount of sorbent phase is an option, particularly if mineral precipitation kinetics hinder the formation of solid minerals. Surface complexation reactions occur between uranium (as uranyl) and ferrihydrite, which is often called hydrous ferric oxide (HFO). This process has been discussed in numerous books and papers (Mahoney et al. 2009a, 2009b, Langmuir, 1997, Merkel and Planer-Friedrich, 2008), and the method is commonly employed by water treatment facilities to remove various metals from water.

Target Uranium Concentration

The experimental work of Jang et al. (2006) suggests that a uranium concentration of approximately 1 mg/L could be attained through simple mineral precipitation. More sophisticated treatment options such as addition of ferric sulfate could in theory lower those concentrations to less than 1 mg/L and those concentrations could be stable over a wider range of pH values.

6.3 SGS LAKEFIELD TESTING

6.3.1 Laboratory Data

A series of neutralization tests were designed based upon an initial understanding of the proposed neutralization process and using data presented previously from the SEPA testing. The tests were designed to evaluate the removal of uranium, and other constituents of concern. The testing program was set up to represent the proposed neutralization circuit, with an option to add ferric sulphate to the barren streams following by neutralization at a pH of approximately 4 in one neutralization tank and then increasing the final pH to around 7 in a second tank.

In its initial conceptualization the laboratory testing program conducted by SGS Lakefield was designed to evaluate the addition of ferric sulphate to the barren stream to lower uranium and trace metals concentrations to levels below 1 mg/L, and to examine the impact of the final pH on the concentrations of uranium and other metals in the treated tailings pore water. A test matrix was prepared that consisted of four primary tests. The plan was to vary some of the starting conditions prior to the first step neutralization at pH of ~4.0. The variables under consideration included presence or absence of leach residue solids and increasing the Fe/U ratio, through ferric sulphate addition. Another goal of the program was to assess the influence of the final pH particularly on the concentration of uranium. To meet that objective, the testing matrix required that after neutralization at pH 4, the solutions be split into two separate aliquots and neutralized at pH values of 6.3 to 6.7 or 7.8 to 8.1. In subsequent tests (Tests 5, 6, and 7) a target pH of 7 was specified.

Four tests were initially designed:

- Test 1 used the final solution only (no solids),
- Test 2 used the solution with added ferric sulphate,
- Test 3 used solution and solids, and
- Test 4 included solution, solids and added ferric sulphate.

When the testing program was initially developed, Tests 2 and 4 assumed higher uranium concentrations and significantly lower total iron concentrations in the barren stream. The laboratory testing program at SGS Canada (Lakefield) demonstrated that the uranium recovery process using a resin-in-pulp (RIP) process would produce a solution with a final concentration of around 3 mg/L total uranium, and an iron concentration greater than 3,000 mg/L (a measured value of 3,970 mg/L). Based upon these values, and the initial geochemical modeling, which indicated that these solutions could, upon neutralization, produce satisfactorily low uranium concentrations without added ferric sulphate, it was decided to postpone Tests 2 and 4 until the results of Tests 1 and 3 became available. Based upon the low concentrations of uranium obtained in Tests 1 and 3 it was decided that addition of more ferric sulphate to the treatment process was not required, and so Tests 2 and 4 were cancelled.

Additional tests have been designed as part of the aging test program. These tests have been given the designation Test 5, 6 and 7. Based upon an initial review of the Tests 1 and 3 results, and because of the apparent increase in uranium concentrations with increasing pH it was decided that a pH of 7 would provide reasonable final pH value. Tests 5, 6 and 7 were prepared to provide that information at a pH of approximately 7.

- Test 5 was primarily prepared for tailings for addition geotechnical evaluations, and

- Tests 6 and 7 and were designed to provide addition confirmation of the Test 1 and 3 results, and to provide longer aging tests.

Details related to the design of these tests are provided in Attachment C with Tables 2 to 8 (within Attachment C) providing a summary of the concentrations obtained through the SGS Lakefield laboratory test program. It should be noted that the aging test program is still on-going and is expected to continue during several months and served as a basis to the Tailing Optimization and Validation Program proposed for the Kiggavik Project.

6.3.2 Geochemical Evaluation – Uranium

Figure 6.3-1 shows the total uranium concentrations corresponding to Tests 1 and 3 as a function of time since final neutralization was attained. Most significant is the observation that all concentrations of uranium were less than 0.03 mg/L. A consistent pattern of behavior as a function of time is not immediately apparent. For example, the Test 1 low pH data set appears to decrease and "level off". The Test 3 high pH results show an increase over time. The other two data sets are intermediate in the amount of increase. Further review of the data indicates that the strong relationship between pH and uranium remains apparent as is shown on Figure 6.3-2. The pH values for Test 1 (low pH data set) appear to decrease as a function of time. Similarly, for the Test 3 high pH data set the pH shows an increase over time.

A geochemical model of the tailings neutralization process was prepared using PHREEQC (Parkhurst and Appelo, 1999) to evaluate uranium behaviour in the neutralized tailings. The model started with the final solution from the Resin In Pulp testing program. Details of the model are included in Attachment C.

Table 6.3-1 summarizes the Test 5, 6 and 7 uranium concentrations and also lists the model derived values. Measured uranium concentrations are low and range from 0.11 mg/L to 0.14 mg/L. Table 6.3-1 shows that the geochemical models for the Test 5, 6 and 7 conditions all tend to predict lower concentrations. It is believed that for this configuration the geochemical models likely over predict the amount of surface complexation of uranium onto HFO and hence a lower concentration is predicted in pore water.

Table 6.3-1 Measured and PHREEQC Derived Uranium Concentrations for Tests 5, 6 & 7

Description	pH	U (mg/L)
Test 5		
• Initial condition	1.55	9.51 (measured concentration)
• Neutralized tailings	6.95	0.14 (measured concentration)
• Model	6.95	0.009 (modeled concentration)
Test 6		
• Initial condition	1.68	6.58 (measured concentration)
• Neutralized tailings	6.95	0.11 (measured concentration)
• Model	6.95	0.0042 (modeled concentration)
Test 7		
• Initial condition	1.59	9.51 (measured concentration)
• Neutralized tailings	7.33	0.11 (measured concentration)
• Model	7.33	0.0036 (modeled concentration)

Based upon a review of the uranium concentration data from the SGS laboratory and coupled with a series of geochemical models, the following conclusions can be been made:

- Uranium concentrations measured on neutralized tailings are lower than 1 mg/L confirming the conclusions of the initial geochemical evaluation (see Section 6.2).

- For the Test 1 and 3 samples, uranium concentrations of less than 0.007 mg/L at a pH of 6.92 were attained based upon the two stage neutralization process, with increasing pH the value increased to 0.028 at a pH of 7.84.

- Measured concentrations for the Test 5, 6 and 7 Tests produced slightly higher uranium concentrations. Measured concentrations ranged from 0.11 to 0.14 mg/L. The initial uranium concentrations in these samples were greater than the initial uranium concentration used in the Test 1 and 3 experiments. This higher initial concentration of uranium in these tests may be partially responsible for these differences.

- The concentrations of uranium observed in these experiments are too low to be explained by mineral precipitation reactions only. It appears that surface complexation primarily upon the precipitated ferrihydrite is a key process that removes uranium from these solutions.

- A concentration of 0.14 mg/L (Test 5 measured concentration) is proposed for the long term uranium pore water concentration in tailings. This value is considered to be a conservative estimate as lower values were measured in the Test 1 and 3 experiments.

6.3.3 Geochemical Evaluation – Choride and Sulfate

Chloride

Chloride (Cl^-) concentrations in the Test 6 and 7 experiments were generally in the 300 to 600 mg/L range, with most concentrations at less than 500 mg/L. Chloride is considered to be a conservative species and so attenuation reactions are expected to be slight. This is confirmed by the laboratory measurements; neutralization with slaked lime did not show any significant change in Cl^- concentrations. An estimate for chloride in the tailings pore waters of 500 mg/L is selected.

Sulfate

The behavior of sulfate (SO_4^{-2}) in the barren stream and in the subsequently neutralized solutions is more complicated than chloride. Several different geochemical processes can occur with sulfate. The dominant process is the formation of gypsum ($CaSO_4 \cdot 2H_2O$). Surface complexation onto HFO also occurs but sulfate tends to desorb with increasing pH. At a pH of 7 surface complexation of sulfate is not considered to be a significant process. Much of the gypsum precipitation occurs in the low pH region as bisulfate (HSO_4^-) and is converted to sulfate (SO_4^{-2}). This conversion takes place at a pH of approximately 2.0. With increasing calcium additions as the pH is raised to 7.0, additional gypsum will form.

Concentrations of sulfate in the Kiggavik neutralized tailings range from 8,000 mg/L to 12,000 mg/L. These concentrations are much higher than the values in the JEB pit pore waters (AREVA 2011), which are currently mesured at 1800 mg/L. A comparison of gypsum saturation indices between the laboratory generated solutions (Tests 1, 3, 5, 6 and 7) and the long term concentrations in the pore waters of the JEB pit (AREVA, 2011) indicates that both sets of waters are near or at saturation with respect to gypsum.

Calcium concentrations are slightly greater (15%) for the pore waters collected from the JEB pit with an average of around 532 mg/L, compared to 463 mg/L for the Kiggavik test solutions. Therefore other factors must be operating to keep sulfate concentrations so high.

The primary reason for the difference in sulfate for the two locations is the much greater concentration of dissolved magnesium (Mg) in the Kiggavik samples. Magnesium concentrations in the Kiggavik samples range from 1390 mg/L to 4440 mg/L (Test 7 low pH solution), with an average Mg concentration of 2508 mg/L. In the 2008 JEB pit pore water samples, Mg concentrations ranged from 9.1 to 190 mg/L with an average concentration of 90 mg/L. The $MgSO_4°$ ion pair can sequester a significant percentage of sulfate, which explains

the high sulfate concentrations and the simultaneous equilibration with gypsum. In the Kiggavik samples, the $MgSO_4°$ ion pair holds on average 35.5 percent of the sulfate in solution with a maximum exceeding 50% of the total sulfate in one sample, elimination of the samples with initial pH values of less than 2 raises the average to 39.6%. For the JEB TMF pore waters the average percentage of total sulfate bound in the $MgSO_4°$ ion pair is about 6 percent.

Another factor responsible for the differences is related to the different ionic strengths, and the resulting differences in activity coefficient values. The ionic strength of pore waters from the JEB TMF is about 0.05 m, while the Kiggavik samples have an ionic strength of 0.35 m. This changes the activity coefficient of Ca^{+2} from 0.47 in the JEB pore waters to 0.30 in the Kiggavik samples, as the SO_4^{-2} ion is also divalent similar differences in the activity coefficient of SO_4^{-2} are also expected.

It appears that the primary driver for all of these factors is related to the higher total magnesium concentration, which increases the proportion of the $MgSO_4°$ ion pair in these solutions, which lowers the activity of the SO_4^{-2} ion in these solutions. This also increases the ionic strength and lowers the activity coefficients in these solutions. The ion exchange process appears to be responsible for the elevated magnesium concentrations and the slightly decreased calcium concentrations noted in these waters.

Using the mean weighted average for sulfate of 1802 mg/L (AREVA, 2011) and after adjusting for the 15 % difference in calcium, the impact of the $MgSO_4°$ ion pair and for the activity coefficient effects provides a range of concentrations from 7800 to 10,000 mg/L sulfate. This range has been selected as representative of the sulfate concentrations in the pore waters. These concentrations are comparable to many of the sulfate concentrations noted in the experiments performed at SGS Canada (Lakefield).

6.3.4 Geochemical Evaluation – Trace Metals

The previous sections show that the proposed treatment system for the Kiggavik tailings successfully removes uranium from the tailings pore water. This treatment is also expected to remove most of the metals that would be released during the leaching of the ores.

All of the tailings neutralization tests conducted at SGS Lakefield followed a similar procedure, consistent with the proposed mill flow sheet. After some initial preparation including addition of $BaCl_2$ (see Section 3.2), the samples were neutralized with slaked lime to a pH of 4 and after approximately 2 hours the samples were the neutralized to their final specified pH values.

The geochemical model developed to evaluate the behavior of trace metals in the tailings relied primarily on the PHREEQC program (Parkhurst and Appelo, 1999). The model combined several distinct geochemical processes including neutralization of the initial low pH solution with slaked lime [$Ca(OH)_2$], mineral precipitation reactions, surface complexation and coprecipitation reactions (solid solution). Precipitation of “possible” phases including gypsum, ferrihydrite

[$Fe(OH)_3$], amorphous aluminum hydroxide [$Al(OH)_3(a)$], calcite ($CaCO_3$), strengite ($FePO_4 \cdot 2H_2O$), hydroxyapatite [$Ca_5(PO_4)_3OH$], barite ($BaSO_4$) as an end member in solid solution reactions with radium, tenorite (CuO), rhodochrosite ($MnCO_3$), magnesite ($MgCO_3$), hausmannite (Mn_3O_4), or in earlier versions manganite (MnOOH) was also allowed. Some of the later models were constructed to assess specific issues, and in those cases additional minerals were included. Possible phases are permitted to form if the solution is oversaturated with respect to the specific phase. The partial pressure of carbon dioxide gas [$CO_2(g)$] was fixed at $10^{-3.4}$ atmospheres and in most simulations the partial pressure of oxygen was fixed at $10^{-0.7}$ atmospheres. Some additional modeling was conducted using the Geochemist's Workbench program (GWB) (Bethke, 2008, Bethke and Yeakel, 2010). This program provides detailed reaction path models that supplement the PHREEQC derived results.

Summaries of the geochemical behavior for the elements examined as part of the tailings neutralization evaluation are included in Attachment C. The behaviour of the following elements was examined: major cations, iron, aluminum, silicon, antimony, arsenic, barium, beryllium, boron, bismuth, cadmium, cobalt, chromium, copper, lead, lithium, manganese, molybdenum, nickel, phophate, selnium, silver, strontium, thallium, tin, titanium, vanadium, zinc and radium. For each element tailings pore water concentrations were modelled and compared to measured concentrations during the aging tests. The models attempted to reproduce observations based on a number of geochemical features including pH and redox condition, mineral precipitation and adsorption processes.

6.4 SUMMARY

Based upon a review of the uranium and metals concentration data from the SGS laboratory testing program and coupled with a series of geochemical models, pore water concentrations for metals in the neutralized tailings were selected to estimate post-decommissioning long term concentrations in the Kiggavik TMFs. Pore water concentrations in the neutralized tailings were selected based primarily upon the laboratory results. The selected values are summarized in Table 6.4-1.

Geochemical modeling was also performed to support and better understand the reactions occurring during neutralization. These models, described in detail in Attachment E, ranging from simple Eh-pH diagrams to full reaction path models, have been used to understand the behavior of these different constituents, and ultimately to support conclusions obtained from the selection process.

As summarized in Table 6.4-1 the estimated pore water concentrations for uranium and most metals are lower than 1 mg/L. The one exception is zinc where the selected concentration is 18 mg/L based on modeled concentrations. As opposed to most elements the modeled and measured concentrations for zinc show some inconsistencies and further evaluation of the test results is recommended.

In addition to uranium and trace metals such as arsenic, nickel and selenium one of the elements of concern at a uranium tailings management facility is radium. As part of the tailings treatment operation, barium chloride will be added to the barren stream to produce additional barium sulfate. Upon precipitation barite will sequester radium in a coprecipitate along with the dominant barium ion. The SGS laboratory tests coupled with the geochemical models developed for radium confirm the performance of this process for the Kiggavik tailings. The laboratory results and the model suggest that at least 99.9% of the radium is removed. The resulting radium concentration in tailings pore water is estimated at 0.08 Bq/L.

Table 6.4-1 Estimated Kiggavik TMF Long Term Solute Concentrations

Constituent		Units	Concentration in tailings pore water	Comments on selected value
Aluminium	Al	mg/L	0.50	Based upon consistency between measured and modelled concentrations
Arsenic	As	mg/L	0.02	Greatest value from measured concentrations
Cadmium	Cd	mg/L	0.003	Selected greater of two neutralized values from Test 6 and 7
Chromium	Cr	mg/L	0.35	Selected greatest value from model result, although low measured concentration indicates possible attenuation
Cobalt	Co	mg/L	0.10	Selected greatest value from model result, although low measured concentration indicates possible attenuation
Copper	Cu	mg/L	0.40	Based upon consistency between measured and modelled concentration
Iron	Fe	mg/L	5.0 to 0.1	Measured concentration significantly greater than modelled concentration
Lead	Pb	mg/L	0.04	Selected measured concentration because greater than modeled value
Manganese	Mn	mg/L	10 to less than 1.0	Selected range based on measured concentrations and model results
Molybdenum	Mo	mg/L	0.20	Greatest initial measured concentration
Nickel	Ni	mg/L	0.40	Selected measured value
Radium-226	^{226}Ra	Bq/L	10	Weighted average of Results from Tests 3, 5 and 6
Selenium	Se	mg/L	0.05	Based upon measured values
Uranium	U	mg/L	0.14	Greatest value from measured concentrations
Vanadium	V	mg/L	0.70	Selected average of the two greater values Tests 6 and 7
Zinc	Zn	mg/L	3.0	Based upon Test 5 measured concentrations

7 POST-DECOMMISSIONING EFFECTS

7.1 INTRODUCTION

Field data acquisition, laboratory testing and modelling programs were developed to assess the potential long-term effects of tailings management activities. Groundwater is identified as the principal pathway for potential interactions between constituents of the tailings and the receiving environment. As a result, the assessment of long-term effects of tailings disposal focuses on the post-decommissioning groundwater flow regime in the Kiggavik area, the source terms (tailings geochemical behaviour as a function of time) and the constituent release and transport mechanisms.

Two scenarios were considered for the assessment of potential long-term post-decommissioning effects. The first scenario considers persistence of current permafrost conditions. The second scenario assumes complete melting of the permafrost as a result of climate change.

The effects of climate change on the project in the long term will depend on the degree and rate of warming. A compilation of the factors affecting global climate and a discussion of the cumulative effects of these factors are provided in Technical Appendix 4D (Baker Lake Long Term Climate Scenario). The warming trend used for modeling purposes of the Project area considers a 5^{o}C rise in the mean annual surface temperature (MAST) over the next 100 years followed by a long-term plateau at 5^{o}C above the current MAST (see Section 4.6). This trend is considered to be conservative as it anticipates a greater temperature increase for the Baker Lake area than what is suggested based on the analysis and scenario presented in Appendix 4D. Model results (Section 4.6) show that if the mean annual surface temperature rises the change is manifested as a reduction in depth of permafrost at the base, and not at the surface. The warming trends are expected to result in long term permafrost depths decreasing from about 220m in the Kiggavik area to either 90m from surface for the first trend (e.g., -7 °C to -2 °C) or 40m from surface for the warmer trend (e.g., -6 to -1 °C).

To assess the worst case potential from a groundwater flow and contaminant transport perspective a conservative approach was used and complete melting of permafrost was considered. The absence of permafrost would be a significant change to the groundwater flow system. With removal of the confining permafrost layer, piezometric levels would equilibrate to near ground surface levels, except in low topographical locations, which would act as discharge zones for the groundwater system. Surface components of the hydrological system would become connected to the underlying hydrogeological flow system across the region. This would have an effect on the pressure distribution and hydraulic heads. A no-permafrost ground water flow model was developed to predict groundwater flow conditions in a very long term scenario,

with the assumption that a warming trend greater than the 5°C rise has melted the permafrost completely and that the hydrogeological system has stabilized to a new pseudo-equilibrium state. The development of this model is presented in Technical Appendix 5D (Groundwater Flow Model).

The following sections present application of the current permafrost and no-permafrost models to predict the potential change in solute transport from the Main Zone, Centre Zone and East Zone TMFs to potential receptors.

7.2 METHODOLOGY

Methods employed to characterize the physical and chemical properties of the tailings and the groundwater flow regime of the Kiggavik site are discussed in this section. The groundwater flow regime of the Kiggavik site dictates flows that will occur in and around the decommissioned Kiggavik TMFs. Several groundwater flow parameters are required to assess the long-term effects of the decommissioned facility, including the infiltration through the tailings cover, the flow through the placed tailings within the decommissioned TMFs and the groundwater flow in the formations surrounding the tailings mass.

7.2.1 Infiltration through Tailings Cover

Thermal modelling results presented in Section 4 show that under current climate conditions there will be establishment of a frozen zone in the tailings cover. The mine rock cover is expected to cool and freeze across at surface over a short period of time (i.e., one winter) creating a barrier to either downward or upward flow. This result is consistent with the thermal and water transport modelling for the waste rock piles and TMF presented in Technical Appendix 5G. Based on these results the tailings pits were modelled with a frozen layer at the top, and a no-flow boundary condition was used to simulate the tailing cover surface under current climate conditions.

Under climate change conditions the results presented in Section 4 also suggest that as long as the mean annual air temperature remains below zero, a frozen barrier is expected to establish at the surface of the cover. Therefore a climate trend warmer than +6 °C, approximately, would be required to significantly slow the progress of freeze back post cover placement. This conclusion is partially confirmed by the thermal and water transport modelling for the waste rock piles and TMF presented in Technical Appendix 5G. Model results included in Technical Appendix 5G suggest that under certain surface and climate change conditions some infiltration could occur through uncovered waste rock piles and TMF cover. Based on these results a recharge condition was used to simulate the tailing cover surface under climate change conditions. The recharge value was taken at 15 mm/year in a manner consistent with the maximum reasonable recharge rate used in the no-permafrost groundwater flow model (Technical Appendix 5D).

7.2.2 Groundwater Flow Regime

Initial Condition

Groundwater flow simulations were performed under steady-state conditions that would exist following decommissioning, in order to calculate the groundwater flow rates through the tailings and surrounding formation. The three dimensional MODFLOW model presented in Technical Appendix 5D "Groundwater Flow Model" was used to conduct the ground water flow simulations for both the current permafrost and no-permafrost scenarios. The flow rates through the decommissioned TMFs were calculated using the ZONE BUDGET option of MODFLOW.

Figure 7.2-1 illustrates the baseline (pre-mining) groundwater flow conditions in the Kiggavik area, as simulated by the regional groundwater flow model. Under pre-mining conditions, and under the current permafrost conditions, groundwaters flowing through the Kiggavik area eventually discharge to Pointer Lake, which is considered to be wide and deep enough to support the development of an open talik (see Technical Appendix 5D). Figure 7.2-2 illustrates the conceptual model of groundwater flow in the Kiggavik area under current conditions.

Boundary Conditions

The boundary conditions for the post-decommissioning model are similar to the baseline (pre-mining) model and include constant head and no flow boundaries (see Technical Appendix 5D).

As discussed in Technical Appendix 5D, to account for the expected change in hydrology groundwater recharge from precipitation was included as a boundary condition in the no-permafrost groundwater flow model. A recharge value of 15 mm/year was used. In addition drain boundary conditions were used along stream channels at the top surface of the no-permafrost model in order to prevent excessive mounding of the water table as a result of the applied recharge flux, particularly in areas away from lakes. The stream channels were simulated as drains allowing groundwater to exit the model but not recharge the model. This assumption is considered to be reasonable because the water table is close to ground surface and the drainage channels are the lowest points along topography.

The recharge condition was also applied on surface of the tailings cover for the no-permafrost model while the tailings pits were modelled with a frozen layer at the top in the current permafrost model, resulting in a no-flow boundary condition used to simulate the tailing cover surface under current climate conditions.

Hydraulic Conductivity Distribution

The hydraulic conductivity distribution for bedrock materials in the post-decommissioning model is identical to the distribution used in pre-mining model (see Tables 7.2-1 and Technical Appendices 5D and 5E). Under no-permafrost conditions the hydraulic conductivity distribution

changes for units that were previously located in the permafrost layer is changed. The hydraulic conductivity distribution presented in Table 7.2-1 is used to characterize basement units previously located in permafrost.

Material properties of fully consolidated tailings and rock covers in the TMFs are shown in Table 7.2-1. For both the current permafrost and no-permafrost scenarios the tailings are assumed to be fully consolidated, with all excess pore pressure dissipated prior to model scenario running.

Based on results of thermal and consolidation modelling presented in Sections 4 and 5, the consolidated tailings in the Main Zone, Centre Zone and East Zone TMFs were simulated as unfrozen material with a hydraulic conductivity of $5x10^{-8}$ m/s. Both mine rock and till in the overlying cover were modelled with a hydraulic conductivity of $1x10^{-6}$ m/s for the no-permafrost scenario.

Table 7.2-1 Hydraulic Conductivity Distribution

Depth (m)	HYDRAULIC CONDUCTIVITY (m/s)						
	Permafrost	Granite	Meta-sediment	Gneiss	Ortho-quartzite	Syenite	Barrensland Group
0-5	$1x10^{-12}$	$5x10^{-05}$	$5x10^{-05}$	$5x10^{-05}$	$5x10^{-05}$	$5x10^{-05}$	$5x10^{-05}$
5-100	$1x10^{-12}$	$5x10^{-07}$	$5x10^{-09}$	$5x10^{-08}$	$1x10^{-07}$	$8x10^{-08}$	$3x10^{-07}$
100-215	$1x10^{-12}$	$5x10^{-08}$	$5x10^{-10}$	$5x10^{-09}$	$1x10^{-08}$	$8x10^{-09}$	$3x10^{-08}$
215-450	-	$1x10^{-08}$	$1x10^{-10}$	$1x10^{-09}$	$5x10^{-09}$	$3x10^{-09}$	$8x10^{-09}$
450-900	-	$1x10^{-09}$	$1x10^{-11}$	$1x10^{-10}$	$5x10^{-10}$	$3x10^{-10}$	$8x10^{-10}$

Table 7.2-2 Hydraulic Conductivity Properties of TMF Materials

Material	Thickness (m)	Hydraulic Conductivity K (m/s)
Overburden cover – All TMFs	1	$1x10^{-06}$
Mine rock Type 2 cover – All TMFs	5-10	$1x10^{-06}$
Mine rock Type 3 – Main Zone TMF only	12	$1x10^{-06}$
Tailing	>80	$5x10^{-08}$

7.2.3 Source Term Characterization

Concentrations of solutes within the tailings pore water are of concern since they represent the portion of chemical constituents available for transport out of the tailings mass. The following constituents were considered in the assessment of long-term effects: aluminium (Al), arsenic (As), cadmium (Cd), cobalt (Co), chromium (Cr), copper (Cu), iron (Fe), lead (Pb), manganese (Mn), molybdenum (Mo), nickel (Ni), selenium (Se), vanadium (V), zinc (Zn), uranium (U) and radium-226 (^{226}Ra).

The source term characterization of tailings for long-term predictions was based on laboratory studies related to the control of constituents of concern in tailings pore water. The geochemical characteristics of tailings to be placed within the Kiggavik TMFs are presented in Section 6 (see also Attachment C). Table 6.4-1 presents a summary of the selected solute source concentrations in the decommissioned Kiggavik TMFs. These source term concentrations were simulated in the transport model with a constant concentration boundary, until release of the maximum leachable mass (*i.e.*, pulse-type function). The two parameters required for this approach are, for each constituent, the value of the constant source concentration and the duration of the pulse. The duration of the pulse was determined according to the flow through the tailings mass. Given the small flow through the TMFs (see Section 7.3-1) and the large inventory of soluble constituents in the tailings the duration of the pulse is very long (> 10,000 years).

7.2.4 Solute Transport

Solute transport analyses describe the movement of solute between a source and receptor, considering the groundwater flow velocity, mixing or dispersion, and attenuation along the pathway due to sorption behaviour and decay of the contaminant.

The solute transport calculation performed for the decommissioned Kiggavik TMFs couples a semi-analytical solution to the one-dimensional advection-dispersion equation with a particle tracking analysis output from the flow model. This method was used to calculate the mass of contaminant arriving at the surface water bodies from the Kiggavik TMFs over time. The particle analysis was performed using the MODPATH module of the Visual MODFLOW environment. MODPATH (Pollock 1998) allows forward and backward tracking particles to be released at specific locations within the flow model domain.

The hydraulic head distribution calculated using MODFLOW is used to calculate the flow path followed by each particle assigned by the user. The output file generated by the code records travel time as a function of travel distance for each particle path. Travel times are calculated according to effective porosity values specified by the user. The output file may be used to calculate the total travel distance from release point to receptor and the average linear velocity for each path line.

The source term model described in the preceding section was applied to calculate a contaminant concentration at the location of the released particles. Particles were released from the cells within the flow model adjacent to the source cells and tracked to surface water receptors. The one-dimensional advection-dispersion equation was solved analytically for each path line using the concentration calculated by the source term model as a boundary condition and the travel distance and average linear velocity along each path line. Analytical models provide a simple and effective means for gaining insight into the relative importance of various transport parameters. Their utility is not constrained by computational difficulties, such as convergence and stability problems.

The analytical solution provided by van Genuchten (1985) was selected to solve the advection-dispersion equation, giving the concentration at the end of each path line as a function of time. This solution is very general in nature and has the capability of solving transport of four solutes involved in sequential first-order decay reactions. Various boundary conditions can be considered, including concentration-type or flux-type conditions declining or pulse-type input functions. Finally, all the particle paths were integrated to calculate the mass flux arriving at the receptor, given the flow associated with the path lines as calculated from the flow model.

The governing equation for one-dimensional transport of a single solute can be written as:

$$R \cdot \frac{\partial c}{\partial t} = D \cdot \frac{\partial^2 c}{\partial x^2} - u \cdot \frac{\partial c}{\partial x} - \lambda \cdot R \cdot c$$

with $u = V_D / n_e$ and $R = 1 + \rho_D K_D / n_e$

where

- V_D =Darcy velocity (L/T)
- u =pore water velocity (L/T)
- R =retardation factor
- ρ_D =bulk dry density (M/L^3)
- K_D =distribution coefficient (L^3/M)
- n_e =effective porosity (-)
- D =dispersion coefficient in the direction of flow (L^2/T)
- t = time (T)
- x =position in the direction of flow (L)
- c =solute concentration (M/L^3)
- λ =first-order decay rate (T^{-1})

The reader is referred to van Genuchten (1985) for the expression of the analytical solution.

Input parameters used for solute transport calculations are summarized in Table 7.2-3. The following is a discussion of the selection the various input parameters.

Table 7.2-3 Mass Flux Calculation Input Parameters

Parameter	Selected Value
Travel Distance (x)	Model Output, from 2700 m to 4000 m
Groundwater Velocity (v)	Model Output
Longitudinal Dispersivity (α)	0.1*x
Distribution Coefficient (K_D)	Base case Kd=0 (no sorption) Sensitivity case Kd=1 L/kg
Decay rate (λ)	^{226}Ra: 4.28×10^{-4} 1/y (T ½ = 1620 y)

[a] L/kg = litres per kilogram.

Travel Distance

The travel distance (*x*) was calculated directly from the particle paths analysis. Each particle path has its own flow path length. The calculated distances range from 2,700 m to 4,000 m. Under current permafrost conditions the calculated travel distances to Pointer lake average 3,600 m. Under the no-permafrost scenario the calculated travel distances average 3,100 m for particles discharging to Pointer Lake.

Arrival Time and Groundwater Velocity

Particle arrival time and groundwater velocity (*v*) were calculated directly from the particle paths. An effective porosity of 45% (0.45) was considered for the consolidated tailings to reflect the porous nature of the material. An effective porosity of 0.1 % (0.001) was used for the unfrozen basement rock. This value is approximately an order of magnitude lower than the average total porosity value determined from 18 metasediments and granite samples in the Main Zone area (see Technical Appendix 5B "Geology and Hydrogeology Baseline"). As mentioned in the Groundwater Flow Model Technical Appendix 5D a low effective porosity value is supported by the following observations:

- Data from 90 tracer experiments performed in low-permeability fractured media have been studied to explore correlations among parameters controlling flow and transport, including hydraulic conductivity and effective porosity (Guimera and Carrera, 2000). The results presented by these authors suggest that effective porosity values between 0.0001 and 0.01 cover the main data set, with a central value of about 0.001.
- These values are supported by the work conducted at the Yucca Mountain test site, Nevada (Bechtel SAIC, 2005). The value used in the assessment at Yucca Mountain was reported to be 0.0001 for granites that form the basement rocks beneath the alluvial basins at depths greater than 300 m (Smith, 2010, personal communication).

- A value of 0.003 was suggested for fractured bedrock in the Whiteshell Research Area (Ophori et al., 1996).

Figure 7.2-3 presents the histograms of particle arrival times to Pointer Lake for both current permafrost conditions and the no-permafrost scenario. Under current permafrost conditions particle arrival times to Pointer Lake are extremely long, ranging from approximately 88,000 years to more than 10 million years. The arrival times histograms shows two peaks, corresponding to particles lower and higher in the tailings. Particles arrival times in the no permafrost scenario range from approximately 420 years to more than 10,000 years. Although significantly reduced relative to the current permafrost conditions the arrival times in the no permafrost case are also long, illustrating the small hydraulic gradient and the low hydraulic conductivity of the unfrozen rock in the Kiggavik area.

Each particle path is associated with a distinct average groundwater velocity. Under current permafrost conditions the calculated groundwater velocity is extremely slow, ranging from 3.8 10^{-4} m/year to 4.1 10^{-2} m/year. In the no-permafrost case the calculated groundwater velocity increases, ranging from 0.2 m/year to 8.2 m/year.

Longitudinal Dispersivity

Longitudinal dispersivity (α) is a scale-dependent parameter that accounts for mechanical mixing during transport of solute through an aquifer. Dispersivity is generally recognized to increase with flow path distance. Based on a literature review, it may be noted that typically longitudinal dispersivity is observed to be approximately 10% of the flow path distance (Gelhar *et al*. 1992). As such, for transport calculations the longitudinal dispersivity was systematically taken to be 10% of the travel distance of each particle. Dispersivity values ranged from 270 m to 400 m.

Distribution Coefficient

Partitioning of solute between liquid and solid phases along the pathway may be described in terms of a distribution coefficient (K_d). The distribution coefficient is the slope of a linear sorption isotherm and represents the ratio of the amount of solute sorbed to solid phase to the concentration of dissolved solute for an instantaneous and fully reversible sorption process. Sorption behaviour acts to reduce the rate of solute migration with respect to the rate of groundwater movement during transient transport conditions, in which concentrations at a point along the pathway change with time. Therefore, sorption behaviour simply delays the breakthrough time of solute at a receptor, but does not affect the steady-state concentration or mass flux where decay does not occur along the pathway. In the case of decay of the solute along the pathway, greater sorption will result in reduced mass flux to the receptor since more mass is lost due to decay over longer transport times.

Solute transport analyses were conducted for two assumptions. In the first assumption attenuation along the pathway due to sorption behaviour was neglected. Therefore all the constituents were assigned distribution coefficients of zero (*i.e.,* no sorption assumption). In the second assumption, which is less conservative, reversible sorption behaviour along the groundwater flow path was accounted for through the application of distribution coefficients.

Sixteen sorption tests were conducted on 8 basement rock samples collected from the Kiggavik Main Zone site (SRC, 2011). The tests focussed on Kd determinations for sorption of uranium and radium-226. Results indicated a distribution coefficient ranging from 0.1 L/kg to 6.2 L/kg, with a mean value of 2.2 L/kg for sorption of uranium on Kiggavik Main Zone granite. These values are consistent with the value of 5 reported by AECL for Canadian Shield material (listed in McKinley and Scholtis, 1993 and US EPA, 1999). Distribution coefficients determined for sorption of radium-226 on Kiggavik Main Zone granite were found to be higher, ranging from 44 to 644 L/kg, approximately, with a mean value of 177 L/kg. These values are consistent, although higher, than values reported for sandstone units within the Athabasca basin (i.e., 3.8 L/kg to 128 L/kg, COGEMA 1997).

Based on these results a conservative Kd value of 1 L/kg was used to simulate sorption of uranium and radium-226 during solute transport. A distribution coefficient of 1 L/kg was also selected to simulate sorption of other trace metals based on values previously used in Saskatchewan EISs. Given a porosity of 1% and a bulk dry density of 2.5 Mg/m^3, a K_d of 1 L/kg translates to a retardation factor of approximately 250. That is to say that the constituent would move at a rate 250 times slower than groundwater.

Radioactive Decay

Radioactive decay (λ) was incorporated into the transport simulations for radium-226.

7.2.5 Significance of Long-Term Predictions

Long term incremental concentrations in surface water receptors were predicted based on calculated mass flux values from the solute transport analysis and average surface water flow rates. Resulting concentrations in surface water were determined by summing the incremental and baseline concentration for each receptor. The predicted long-term concentrations in surface water receptors were compared to currently applicable water quality objectives and aquatic toxicity benchmarks to determine if further assessment of risk was warranted.

7.3 RESULTS

7.3.1 Groundwater Flow

The post-decommissioning flow regime of the Kiggavik area was modelled based on the groundwater flow model discussed in Section 7.2.2 and Technical Appendix 5D. Groundwater flow simulations were performed under steady-state conditions that would exist following decommissioning, in order to calculate the groundwater flow rates through the tailings and surrounding basement rock.

Figures 7.3-1 and 7.3-2 show the simulated hydraulic head distribution and results of the particle path analysis for the current permafrost and no-permafrost post-decommissioning scenarios where the three TMFs are fully backfilled with an expected tailings hydraulic conductivity of 5×10^{-8} m/s.

The hydraulic head distributions in the Kiggavik area for the baseline and post-decommissioning cases are similar. The effect of the tailings mass on the head distribution is localized due to the relatively small area occupied by the tailings. Compared to the current permafrost conditions the simulated steady-state heads with the no-permafrost model show a stronger surface water impact on groundwater flow. Particles were released in the model throughout the Kiggavik TMFs to track the advective groundwater flow paths to discharge locations. The particles discharged to Pointer Lake according to the local topography.

The groundwater flow rates through the tailings were calculated using the ZONE BUDGET option of Visual MODFLOW. The calculated flow rates are presented in Table 7.3-1.

Table 7.3-1 Predicted Groundwater Flow through Kiggavik Tailings Management Facilities

Description	Current permafrost conditions	No-Permafrost Scenario
Groundwater Flow (m^3/day) through Tailings Management Facility		
• Main Zone	0.01	0.88
• Centre Zone	no flow	0.32
• East Zone	no flow	0.23

Under the current permafrost conditions, the flow through the tailings mass in Main Zone TMF was simulated to be 0.01 m^3/day. Flow through the tailings in Main Zone increases to 0.88 m^3/day for the no-permafrost scenario. The increase is due in part to the increased hydraulic

conductivity of the surrounding unfrozen rock mass. The increase is also attributable to the increased amount of surface recharge that reaches the tailings through the unfrozen cover. Under the current permafrost conditions Centre Zone and East Zone TMFs are located entirely within permafrost and there is virtually no groundwater flow through the tailings mass. In the no-permafrost case the calculated flow through the tailings in Centre Zone and East Zone increases to 0.32 m^3/day and 0.23 m^3/day, respectively.

7.3.2 Solute Migration and Fate

As described in Section 7.2-4, solute transport calculations were performed for the path lines associated with the particles released from the Kiggavik TMFs within the post-decommissioning groundwater flow model. The solute transport analysis was performed based on expected source concentrations of constituents of concern in the tailings material (Table 6.4-1). The results of solute transport modeling are presented in terms of mass flux to and solute concentrations at the outlet of Pointer Lake. The average annual flow out of Pointer Lake (0.48 m^3/s), see Technical Appendix 5A "Hydrology Baseline", was used to calculate the incremental surface water concentration from the predicted mass fluxes.

Table 7.3-2 presents predicted steady state mass fluxes to Pointer Lake and resulting peak incremental surface water concentrations for all constituents of concern and for both the current permafrost conditions and the no-permafrost scenario. Table 7.3-2 also presents baseline concentrations for each constituent (site specific baseline water chemistry data were taken from Technical Appendix 5C "Aquatic Environment").

Current permafrost conditions

In the current permafrost case the predicted flow through the tailings is very limited, approximately 0.01 m^3/day. Subsequently there is a very small flux to Pointer Lake for all constituents resulting in negligible incremental concentration in relation to baseline concentrations.

As an example the mass flux of uranium from groundwater to Pointer Lake is plotted with respect to time in Figure 7.3-4 for the current permafrost conditions assuming no sorption along the flow path (K_d =0). The corresponding predicted surface water concentrations are also shown in Figure 7.3-4. The concentration increases to about $2x10^{-4}$ µg/L after approximately 3 million years, illustrating the very slow solute transport conditions in this geological environment.

No-permafrost scenario

In the no-permafrost scenario the predicted flow through the tailings is increased, relative to the current permafrost conditions, as a result of both the recharge rate applied on surface of the tailings cover and the slightly higher hydraulic conductivity of the rock mass surrounding the TMFs. However, the fluxes are still small as illustrated in Figure 7.3-5.

As an example the mass flux of uranium from groundwater to Pointer Lake is plotted with respect to time in Figure 7.3-5 for the no sorption assumption (K_d =0). Figure 7.3-5 illustrates the flux contributions from the various TMFs. The Main Zone TMF is the largest contributor due to the larger groundwater flow through the Main Zone pit (see Table 7.3-1). The corresponding predicted surface water concentrations are also shown in Figure 7.3-5. In the no-permafrost case and assuming no sorption along the flow path the long term uranium flux to Pointer Lake is 0.07 kg/year. The corresponding incremental concentration peaks at about 0.005 µg/L at approximately 2000 years.

The effect of sorption along the flow path is illustrated in Figure 7.3-6, where loadings to Pointer Lake and incremental concentrations are plotted with respect to time for K_d=0 and K_d=1 L/kg. Including sorption in the solute transport simulation translates to significantly lower fluxes and incremental surface water concentrations.

Significance of Long Term Effects

Predicted long-term water concentrations of solutes in Pointer Lake are compared to baseline and to the applicable surface water quality objectives in Table 7.3-2, for the no sorption case. All predicted concentrations are well below applicable water quality objectives and for most constituents incremental concentrations calculated for both the current permafrost and no-permafrost conditions are negligible in relation to baseline concentrations. For these reasons, a human and ecological risk assessment (as the one developed for the assessment of the operational effects, see Technical Appendix 8A) was not deemed necessary for the long-term scenario.

Table 7.3-2 Predicted Peak Incremental Loadings to Pointer Lake and Resulting Incremental Surface Water Concentrations

Constituent	Reference Values		Predicted Flux and Resulting Incremental Surface Water Concentration (no sorption)			
			Current Permafrost		No Permafrost	
	Baseline (µg/L)[a]	Guideline (µg/L)[b]	Mass Flux (kg/year)	Concentration (µg/L)	Mass Flux (kg/year)	Concentration (µg/L)
Al	21	5 to 100	1.53E-03	1.01E-04	2.61E-01	1.72E-02
As	0.2	5	6.10E-05	4.04E-06	1.04E-02	6.90E-04
Cd	<0.1	0.017	9.15E-06	6.06E-07	1.57E-03	1.03E-04
Cr	<0.5	1 to 8.9	1.07E-03	7.07E-05	1.83E-01	1.21E-02
Co	<0.1		3.05E-04	2.02E-05	5.22E-02	3.45E-03
Cu	0.8	2	1.22E-03	8.08E-05	2.09E-01	1.38E-02
Fe	45	300	1.53E-02	1.01E-03	2.61E+00	1.72E-01
Pb	0.1	1 to 7	1.22E-04	8.08E-06	2.09E-02	1.38E-03
Mn	2.4		3.05E-03	2.02E-04	5.22E-01	3.45E-02
Mo	<0.1	73	6.10E-04	4.04E-05	1.04E-01	6.90E-03
Ni	0.4	25 to 150	1.22E-03	8.08E-05	2.09E-01	1.38E-02
Se	<0.1	1	1.53E-04	1.01E-05	2.61E-02	1.72E-03
U	<0.1	15	4.27E-04	2.83E-05	7.31E-02	4.83E-03
V	0.1		2.14E-03	1.41E-04	3.65E-01	2.41E-02
Zn	5.8	30	9.15E-03	6.06E-04	1.57E+00	1.03E-01
Constituent	**Baseline (Bq/L)**	**Guideline (Bq/L)**	**Mass Flux (Bq/year)**	**Concentration (Bq/L)**	**Mass Flux (Bq/year)**	**Concentration (Bq/L)**
^{226}Ra	<0.005	0.5	2.06E+04	1.36E-06	3.53E+06	2.33E-04

a = Baseline, September 2008 (See Technical Appendix 5C)

b = Guideline, Canadian Council of Mininters of the Environmen's (CCME) Canadian Water Quality Guidelines (CWQG) for the protection of aquatic life (2011)

c = Guideline, Health Canada Guidelines for Canadian Drinking Water Quality(2010)

8 MONITORING AND FOLLOW-UP PROGRAM

8.1 GENERAL

Monitoring of the Kiggavik TMF will be integrated with the operational and long-term compliance monitoring system. To provide information on TMF long-term performance and containment, the monitoring program will focus on the following areas:

- Tailings chemical and physical properties
- Tailings delivery and deposition
- Thermal conditions
- Groundwater flow and chemistry conditions

8.2 TAILINGS PROPERTIES

Contingency plans are intended to address unforeseen circumstances which could result in a significant increase in the mass flux of solutes to the receptors. Extensive investigations into the chemical and physical properties of tailings has been undertaken at Kiggavik and will continue to be undertaken as part of a Tailings Optimization and Validation Program (TOVP), similar to the program that was initiated at McClean Lake Operation and has been a successful audit program for the behaviour of the tailing produced at that site in Northern Saskatchewan.

8.3 TAILINGS DELIVERY AND DEPOSITION

The tailings delivery pipe will be equipped with a leak detection system and will be inspected regularly. To prevent freezing, the pipe will also be equipped with an electric heat tracing system.

The depth of water under the barge and the buildup of tailings will be monitored with an ultrasonic level monitor. A manual sludge gun may also be used to monitor the accuracy and reliability of the ultrasonic level monitor.

8.4 THERMAL CONDITIONS

Thermal data will continue to be collected from the rock mass surrounding the TMF and the groundwater system below the permafrost as a means of calibrating the modelled thermal behaviour of the system as a whole in order to support long-term performance predictions. The temperature of the tailings, at the point of discharge and in the TMF, will be measured regularly.

8.5 GROUNDWATER

Groundwater monitoring will consist of an array of monitoring points to track changes in pressure gradients (flow direction) and water quality. The proposed monitoring system will be phased in as the project moves from planning and design, through operations, and finally into closure. Groundwater pressures and chemistry will be established in the rock mass surrounding the proposed TMF prior to excavation of the pits, and then monitored as the excavation base penetrates the permafrost base and as the pit is filled with tailings material. This will require an increasing array of monitoring points in order to detect changes brought about by the mining activities.

As the monitoring system will be operating in a deep permafrost environment, it will need to operate at temperatures well below 0°C. Pressure monitoring below permafrost will be carried out regularly using electronic transducers that are connected to the surface via an electrical wire. Regarding water sampling it is considered that a viable method will be to use a closed pipe system that can be used with an antifreeze fluid in the permafrost interval.

8.6 CLIMATIC

Climatic data (air temperature, precipitation, evaporation, etc.) will be collected as part of the overall site monitoring and will be used in the TMF operating evaluation process.

9 CONCLUSION

An assessment was completed to characterize the physical and geochemical properties of the tailings expected from the development of the Kiggavik Project as they relate to long term environmental management of the site and surrounding area. The proposed tailings management plan for the Project was developed and evaluated in relation to potentially adverse effects of tailings on the receiving environment. The assessment included field, laboratory and modelling studies to determine the management strategy.

The proposed tailings management plan for the Kiggavik Project has been designed to avoid interaction between tailings and natural water bodies, to maximize the use of mine workings for long-term management of tailings and to ensure the long-term protection of terrestrial, aquatic and human environments. The proposed option consists of producing thickened tailings that will be neutralized and treated to control uranium, radium-226 and trace metal concentrations. Tailings will be deposited in three open pits (or Tailings Management Facility, TMF) at the Kiggavik site. Based on the current mine schedule, tailings will be deposited into the East Zone TMF, followed by the Centre Zone and Main Zone TMFs. Tailings will be deposited subaqueously to prevent freezing of the tailings and enhance radiation protection. The natural surround concept will be used. At closure, the tailings will be covered using mine rock to enhance consolidation and prevent wind and water erosion. A final cover of overburden will be added to facilitate revegetation.

Several numerical models were developed to assess the potential long term effects of tailings management activities at the Kiggavik Project, including thermal, geotechnical, groundwater flow and geochemical models. The models were first calibrated against field and laboratory results then used to predict potential operational and long-term behaviours. Potential long-term effects were assessed under current permafrost conditions and for a conservative scenario assuming no permafrost.

Laboratory and geochemical models confirmed the performance of the proposed tailings treatment system for the Kiggavik mill, with estimated long term pore water concentrations for uranium and most metals lower than 1 mg/L.

Groundwater flow and solute transport models confirmed the performance of the tailings containment system and the limited interaction between tailings and natural surface water bodies. Pointer Lake was identified as the main receptor with the potential to be affected over the long term (i.e., after several hundred years) by tailings management activities. Predicted long-term water concentrations of solutes in Pointer Lake were compared to baseline and to the applicable surface water quality objectives. All predicted concentrations were found to be well below applicable water quality objectives and for most constituents incremental concentrations

calculated for both the current permafrost and no-permafrost conditions were found to be negligible in relation to baseline concentrations.

A monitoring and follow-up program is proposed to validate the predicted operational and long-term effects of tailings management activities. To provide information on TMF long-term performance and containment, the monitoring program will focus on tailings chemical and physical properties, tailings delivery and deposition, thermal, groundwater flow and chemistry conditions.

10 REFERENCES

AREVA Resources Canada, Inc. (2011). McLean Lake Operation - Tailings Optimization and Validation Program, Validation of Long Term Tailings Performance Report (2009). April 26th, 2011

AREVA Resources Canada (2011). Kiggavik EIS – Tier 3 Technical Appendix – Appendix 4D Baker Lake Long Term Climate Scenario, December 2011

AREVA Resources Canada (2011). Kiggavik EIS – Tier 3 Technical Appendix – Appendix 5A Hydrology Baseline, December 2011

AREVA Resources Canada (2011). Kiggavik EIS – Tier 3 Technical Appendix – Appendix 5B Geology and Hydrogeology Baseline, December 2011

AREVA Resources Canada (2011). Kiggavik EIS – Tier 3 Technical Appendix – Appendix 5C Aquatics Baseline, December 2011

AREVA Resources Canada (2011). Kiggavik EIS – Tier 3 Technical Appendix – Appendix 5D Groundwater Flow Model, December 2011

AREVA Resources Canada (2011). Kiggavik EIS – Tier 3 Technical Appendix – Appendix 5G Thermal and Water Transport Modelling of the Waste Rock Piles and TMF, December 2011

BGC Engineering (2003). Indian and Northern Affairs Canada - Implications of Global Warming and the Precautionary Principle in Northern Mine Design and Closure. Project 0131-009-02, March 27, 2003

Bechtel SAIC (2005). Saturated Zone Flow and Transport Model Abstraction, Bechtel SAIC, August 2005. Doc. No. 20050808.0004

Bethke, C.M., 2008. Geochemical and Biogeochemical Reaction Modeling, 2nd ed. Cambridge University Press. Cambridge. 543 p.

Bethke, C.M., and Yeakel, S., 2010. The Geochemist's Workbench, Release 8.0 GWB Essentials, Available From Rockware, Golden, CO.

Canadian Nuclear Safety Commission (CNSC) (2011). Management of Uranium Mine Waste Rock and Mill Tailings. Draft Regulatory Document RD/GD-370, July 2011

COGEMA Resources Inc. (1997). McClean Lake Project JEB Tailings Management Facility, December 1997.

Danilek G.T. and Laine D.L (2001). Costs and Benefits of Geomembrane Liner Installation CQA. In the Proceedings of 2001 Geosynthetic Conference.

Erickson, P.M (1995). Reclamation of the North Rankin Nickel Mine Tailings. NWT, Dept of Publci Works and Services. Yellowknife.

Gelhar, L.W., C. Welty, K. R. Rehfeldt. 1992. A Critical Review of Data on Field-Scale Dispersion in Aquifers. Water Resources Research, 28 (7):1955-1974.

GINGER CEBTP (2009). Compressibility Tests Results – Pulp Sample, SLG3-9-402, March 2009

GINGER CEBTP (2011). Compressibility Tests Results – Pulp Sample, SLG6-B-0007, April 2011

Golder Associates (2005). Final Report on Consolidation Sensitivity Analysis, JEB Tailings Management Facility, Report 03-1362-096, May 2005

Golder Associates (2010). JEB TMF Expansion Project. Analysis and Design of Soil Liner, Report 08-1362-0590/1600/1620, October 2010

Guimera J., and J. Carerra (2000). A comparison of hydraulic and transport parameters measured in low-permeability fractured media. Journal of Contaminant Hydrology 41: 261–281

Jang, J., Dempsey, B. and Burgos, W.D., (2006). Solubility of schoepite: comparison and selection of complexation constants for U(VI). Water Research, Vol. 40. P 2738 – 2746.

Kays, W.B. (1977). Construction of Linings for Reservoirs, Tanks and Pollution Control Facilities. A Wiley-Interscience Publication. John Wiley & Sons Inc. New York

Langmuir, D., (1997). Aqueous Environmental Geochemistry: Prentice Hall, Upper Saddle River, NJ, 600 p.

Liao W.A (1989). Polymer/Bentonite/Soil Admixtures as Hydraulic Barriers. SPE Drilling Engineering, 4(2):153-161.

Mahoney, J.J., Cadle, S.A, and Jakubowski, R.T., (2009a). Uranyl adsorption onto hydrous ferric oxide – a re-evaluation for the diffuse layer model database. Environ. Sci. and Technol., vol. 43, no. 24, p. 9260-9266. DOI 10.1021/es901586w.

Mahoney, J.J., Jakubowski, R.T. and Cadle, S.A., (2009b). Corrections to the diffuse layer model database for uranyl adsorption onto hydrous ferric oxide - Ramifications for solute transport modeling. (Poster presented at U2009 Global Uranium Symposium, May 2009 Keystone, CO.)

Mahoney Geochemical Modelling (2011). Geochemical Evaluation of Uranium in Raffinate and Neutralized Tailings – Kiggavik Project, April 2011

Mahoney Geochemical Modelling (2011). Geochemical Evaluation of Uranium in Barren Stream and Neutralized Tailings – Kiggavik Project, October 2011

Mahoney Geochemical Modelling (2011). Geochemical Evaluation of Metals in Barren Stream and Neutralized Tailings – Kiggavik Project, October 2011

McKinley, G., and A. Scholtis (1993). A Comparison of Radionuclide Sorption Databases Used I Recent Performance Assessments. Journal of Contaminant Hydrology, 13:347-363.

Meldrum, J.L. (1988). The determination of sulphide oxidation potential of mine tailings from Rankin Inlet, Nunavutm at sub-zero temperature. M.Sc. Thesis, Geological Engineering, Queen's University.

Meldrum, J.L., Jamieson, H.E. and Dyke, L.D (2001). Oxidation of mine tailings from Rankin Inlet, Nunavut at subzero temperatures. Cdn. Geotechnical Journal, Vol. 38. pp 957-966.

MEND (2004). Covers for Reactive Tailings Located in Permafrost Regions Review. MEND Report 1.61.4, October 2004

MEND (2009). Mine Waste Covers in Cold Regions. MEND Report 1.61.5a, March 2009

Merkel, B. J., and Planer-Friedrich, B. (2008). Groundwater Geochemistry, a practical guide to modeling of natural and contaminated aquatic systems. 2nd Edition. Edited by Nordstrom, D.K., Springer, Berlin, 230 p.

Ophori, D.U., Brown, A., Chan, T., Davison, C.C., Gascoyne, M., Schier, N.W., Stanchell, F.W., and Stevenson, D.R., 1996. Revised Model of Regional Groundwater Flow in the Whiteshell Research Area. AECL Whiteshell Laboratories, Pinawa, Manitoba.

Parkhurst, D.L., and Appelo, C.A.J., 1999, User's guide to *PHREEQE* (version 2) - a computer program for speciation, batch-reaction, one-dimensional transport, and inverse geochemical calculations. U.S. Geological Survey Water Resources Investigation Report 99-4259, 312 p.

United States Environmental Protection Agency (1999). Understanding Variation in Partition Coefficient, Kd, Values. Volume II. EPA Report 402-R-99-004B, August 1999.

Van Genuchten M.Th. (1985). Convective – Dispersive Transport of Solutes Involved in Sequential First-Order Decay Reactions. Computer & Geoscience, Vol A, No. 2, pp 129 - 147

Figures

Projection: NAD 1983 UTM Zone 14N
Creator: CDC
Date: 05/24/2011 Scale: 1:16,000,000
File:
Data Sources: *Natural Resources Canada, Geobase®, Nation Topographic Database, Geological Survey of Canada, AREVA Resources Canada Inc.*

FIGURE 1.1-1
GENERAL LOCATION OF PROPOSED KIGGAVIK PROJECT IN CANADA

Kiggavik Project

AREVA

AREVA Resources Canada Inc - P.O. Box 9204 - 817 - 45th Street West - Saskatoon, SK - S7K 3X5

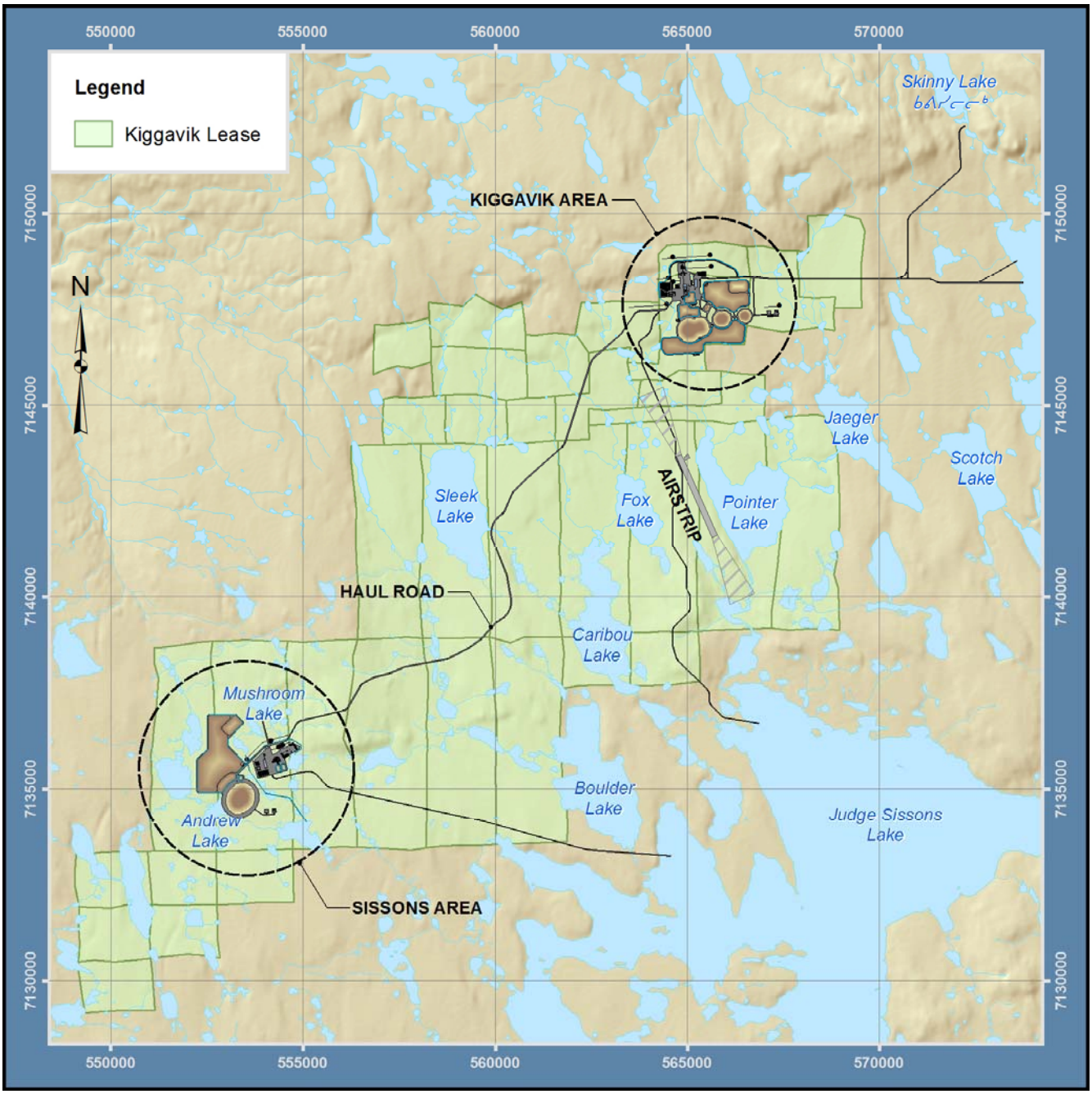

Technical Appendix 5J
Tailings Characterization and Management
Dec., 2011

Figure 1.1-2
Site base map

Kiggavik Project

AREVA

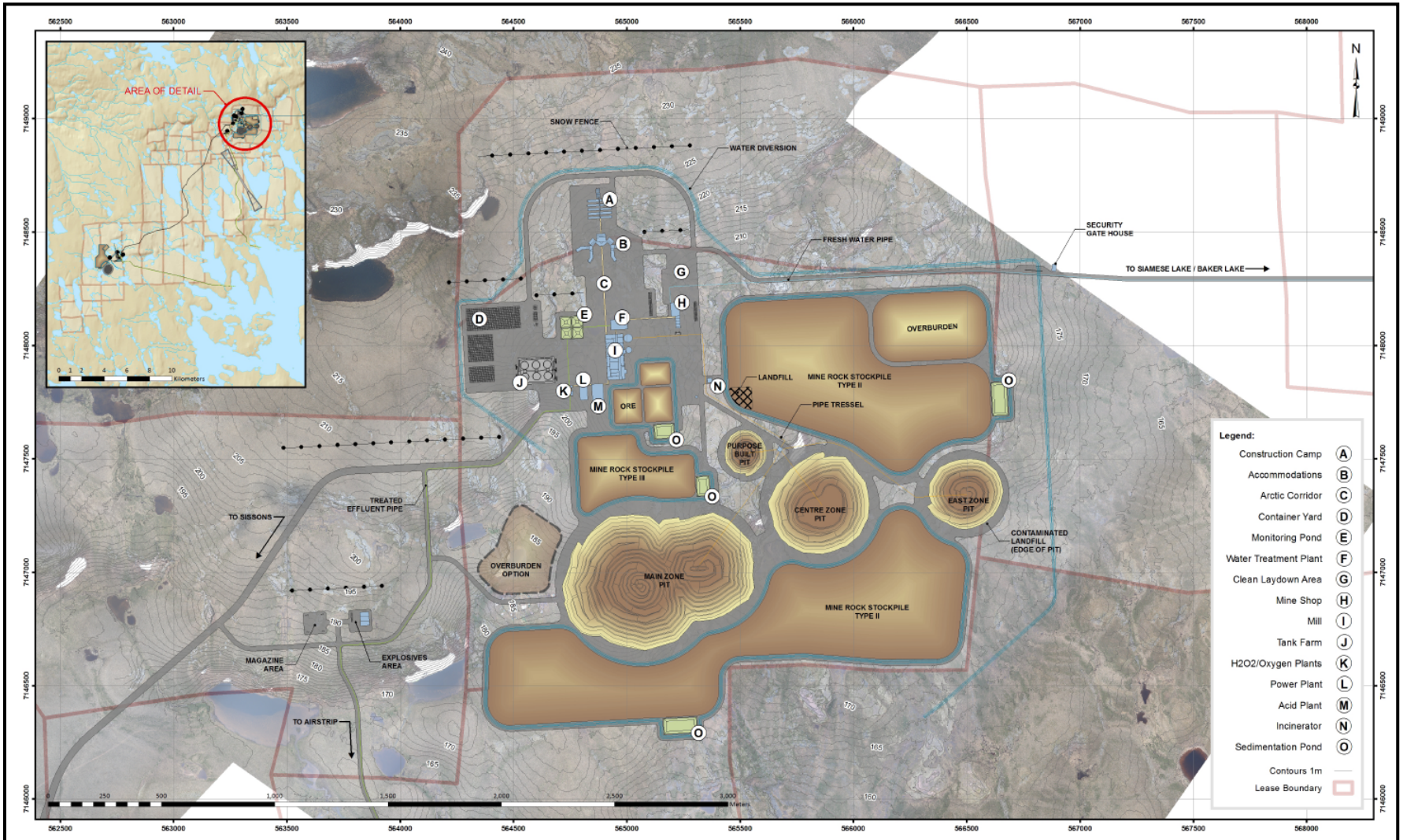

Technical Appendix 5J
Tailings Characterization and Management
Dec., 2011

Figure 1.1-3
Kiggavik site layout

Kiggavik Project

AREVA

Areva Resources Canada Inc.- P.O Box 9204 – 817 – 45th Street W – Saskatoon – S7K 3X5

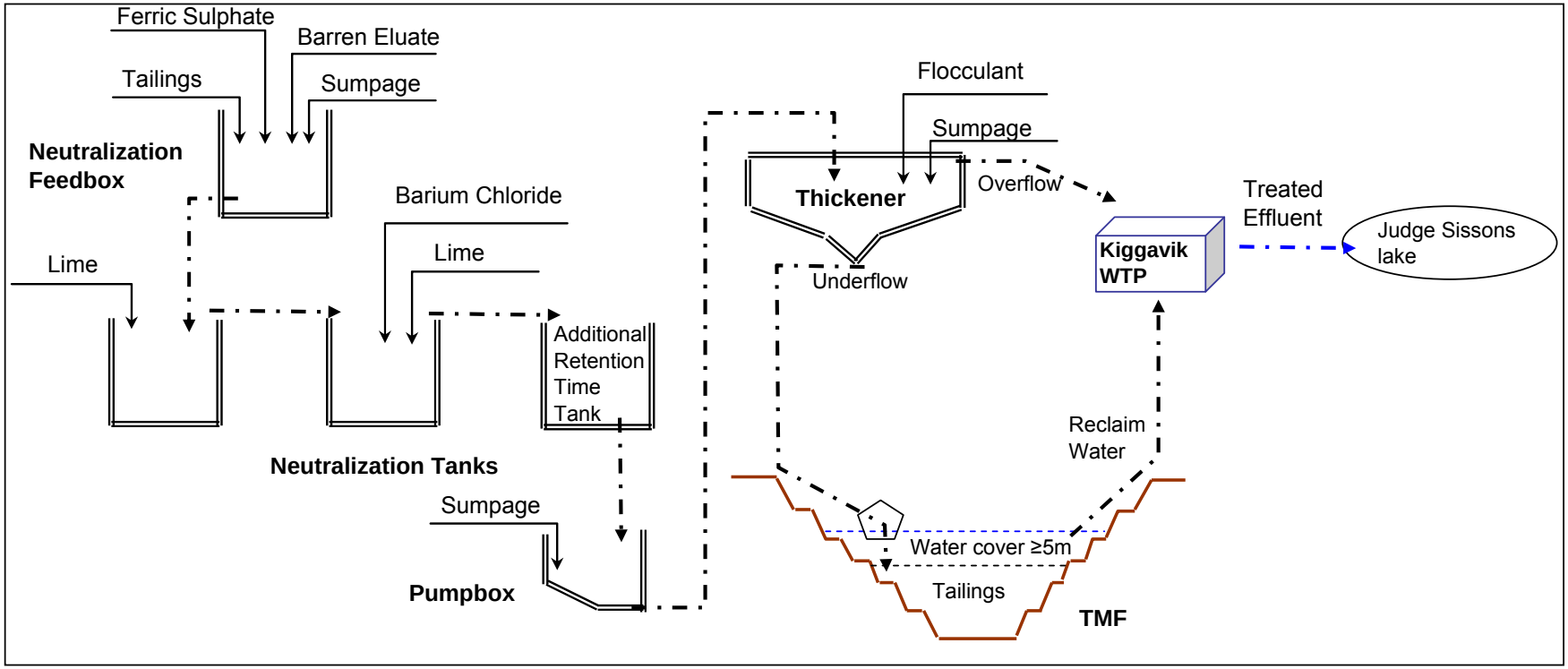

Technical Appendix 5J
Tailings Characterization and Management
Dec., 2011

Figure 3.1-1
Kiggavik tailings management system schematic diagram

Kiggavik Project

AREVA

Areva Resources Canada Inc.- P.O Box 9204 – 817 – 45th Street W – Saskatoon – S7K 3X5

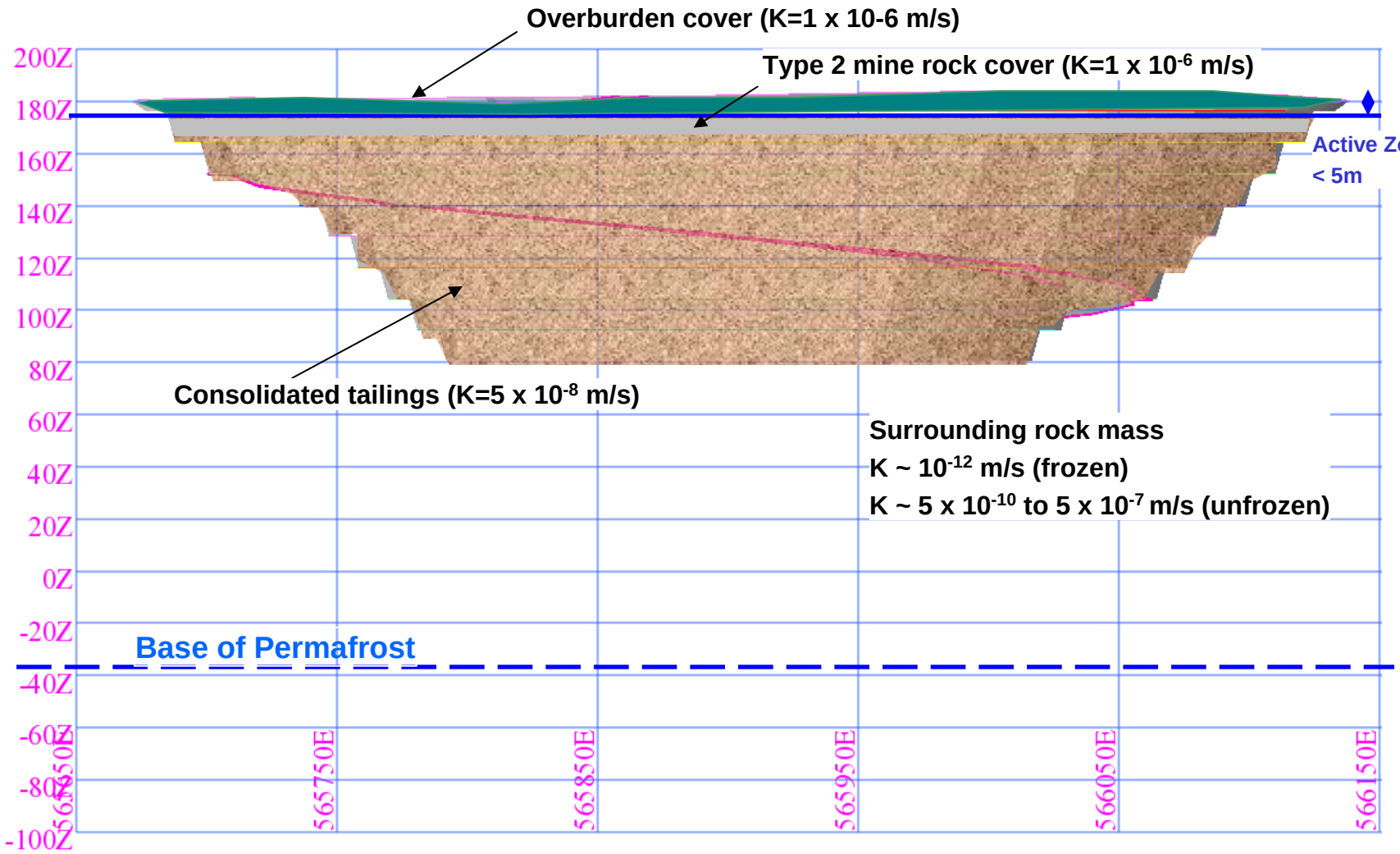

Technical Appendix 5J
Tailings Characterization and Management
Dec., 2011

Figure 3.9-1
Centre Zone and East Zone decommissioning concept

Kiggavik Project

AREVA

Areva Resources Canada Inc.- P.O Box 9204 – 817 – 45th Street W – Saskatoon – S7K 3X5

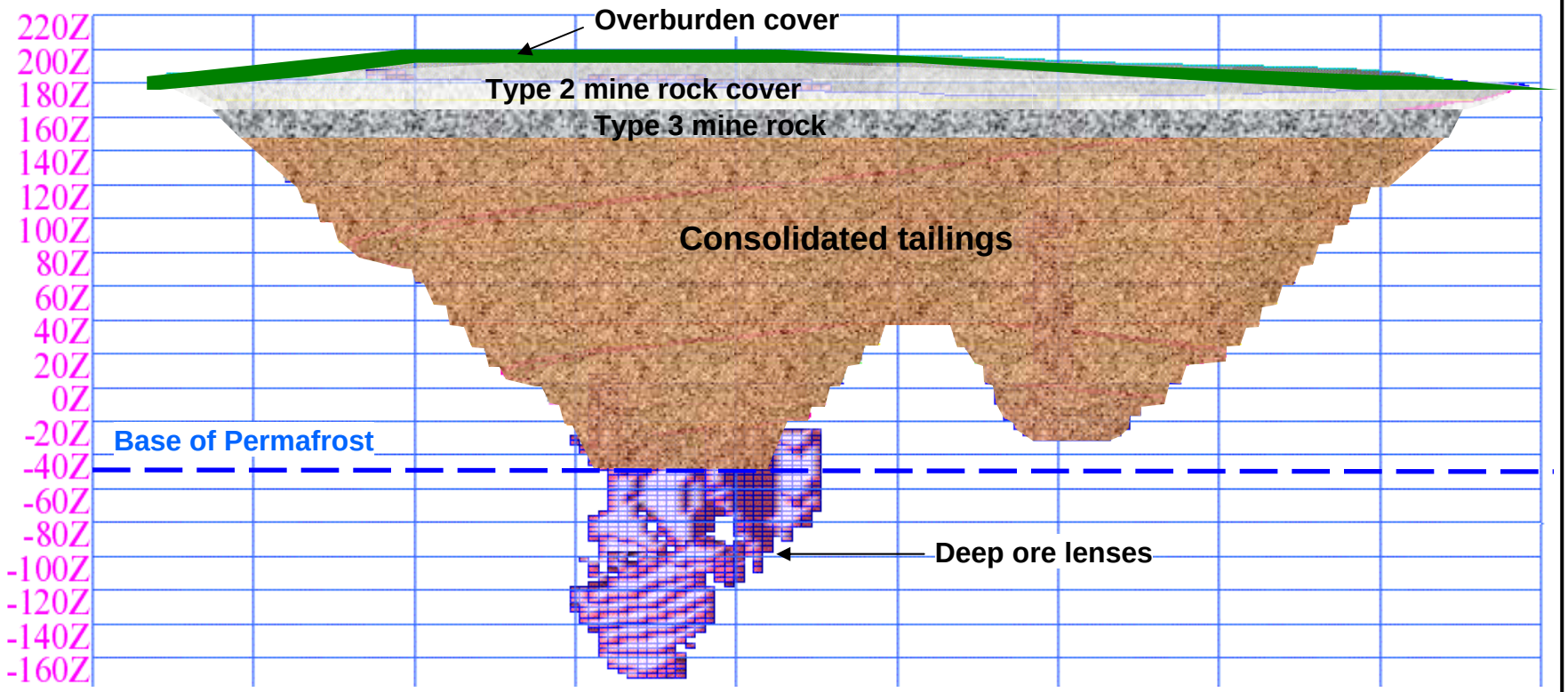

Technical Appendix 5J
Tailings Characterization and Management
Dec., 2011

Figure 3.9-2
Main Zone decommissioning concept

Kiggavik Project

AREVA

Areva Resources Canada Inc.- P.O Box 9204 – 817 – 45th Street W – Saskatoon – S7K 3X5

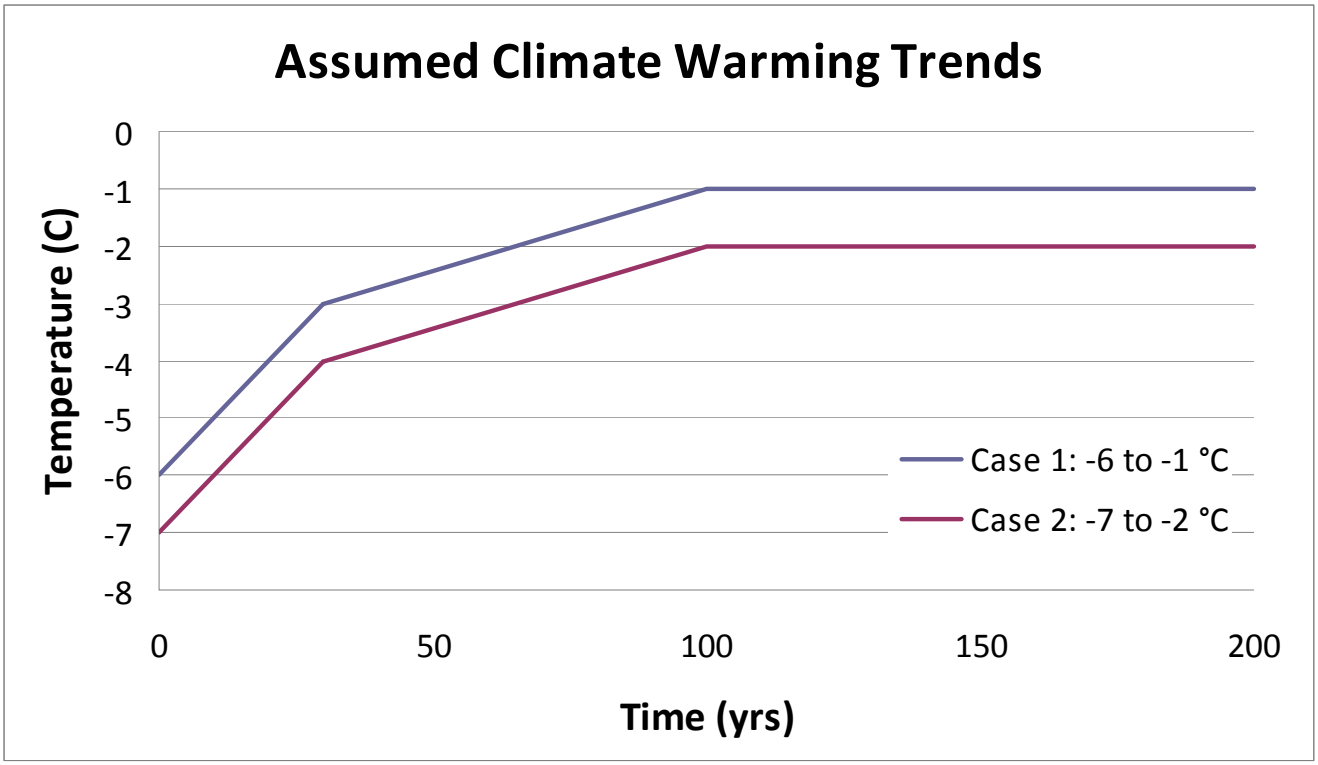

Figure 4.1-1
Climate change trends applied to ground surface mean temperature

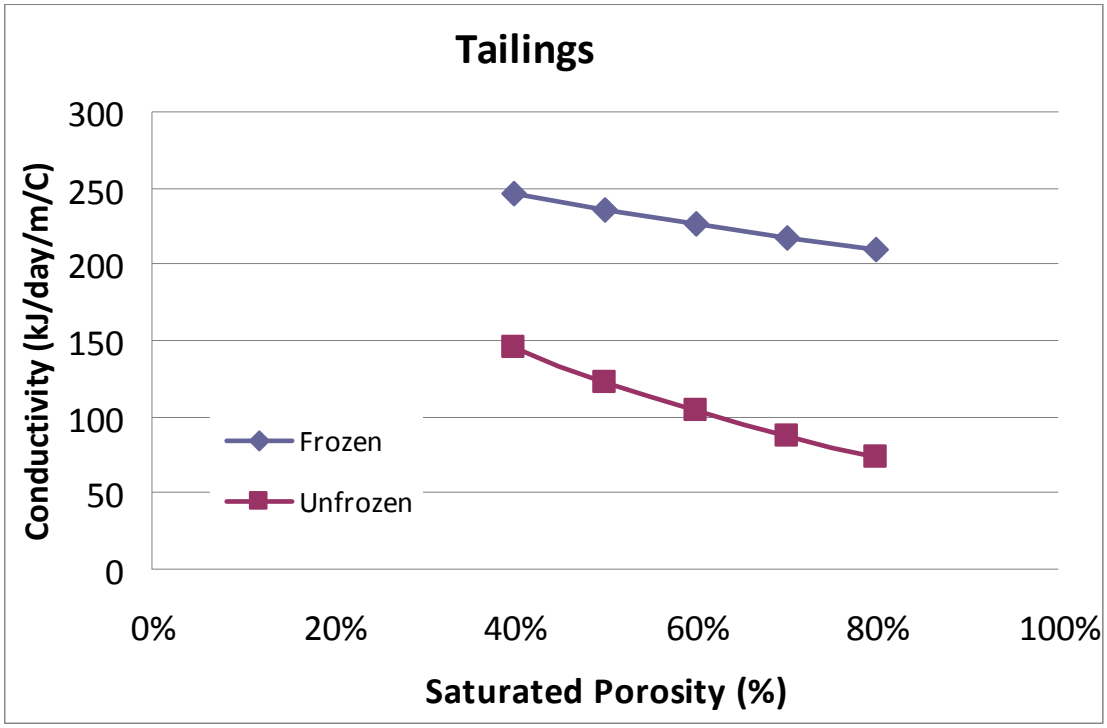

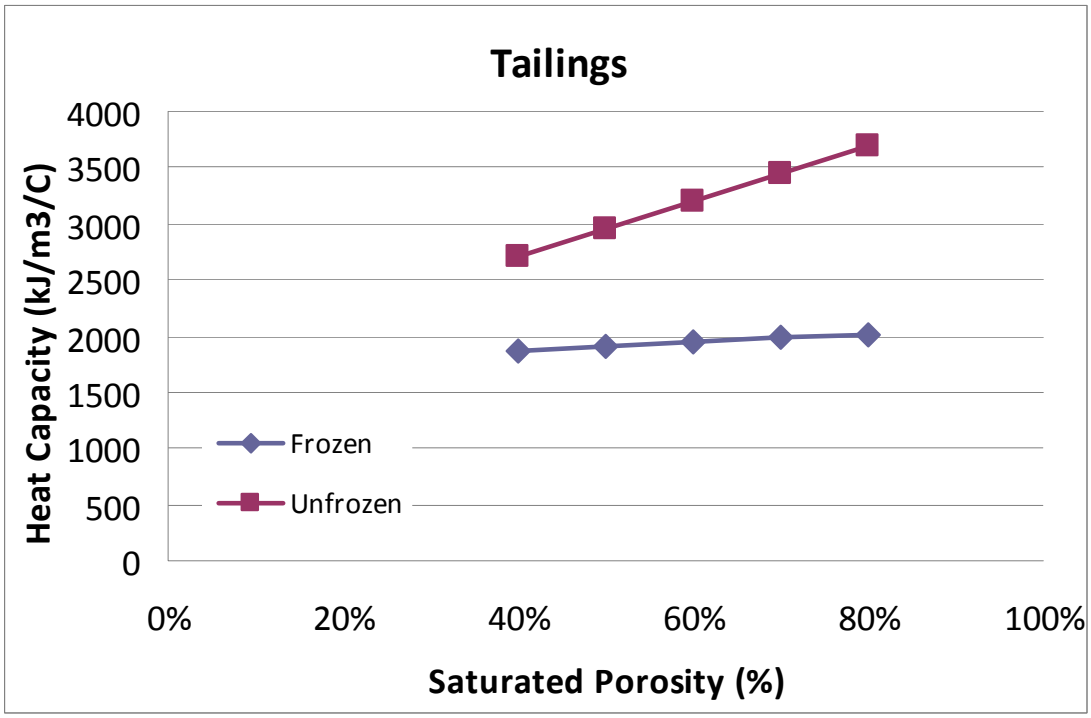

Figure 4.2-1
Thermal properties of tailings

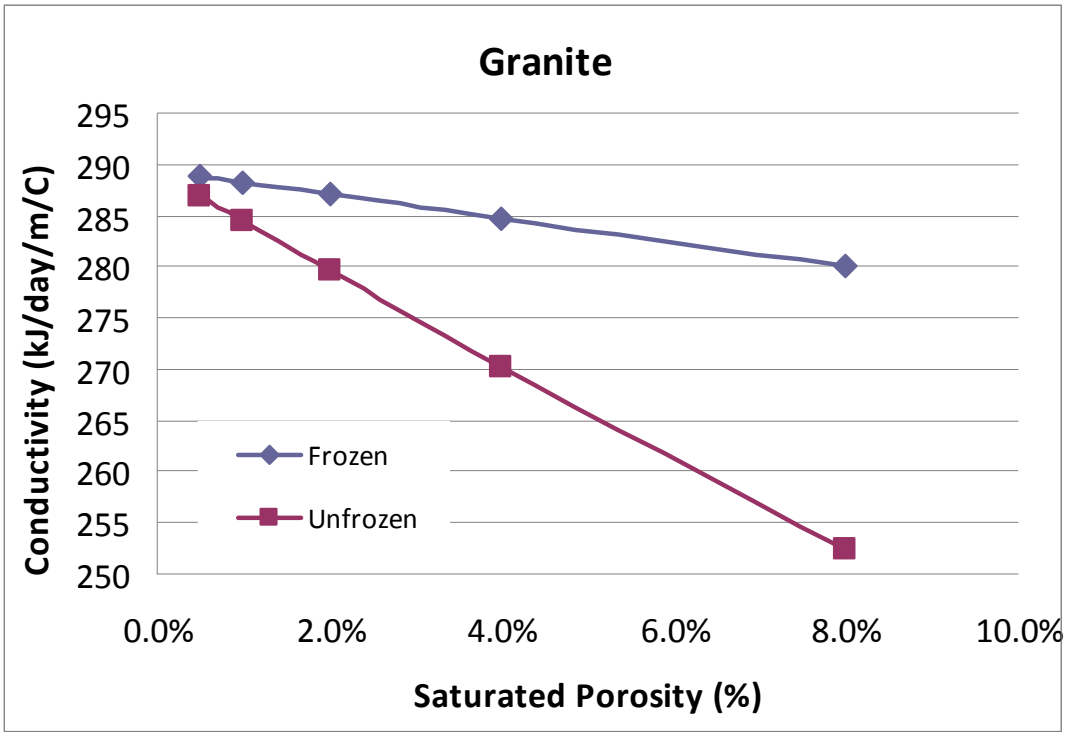

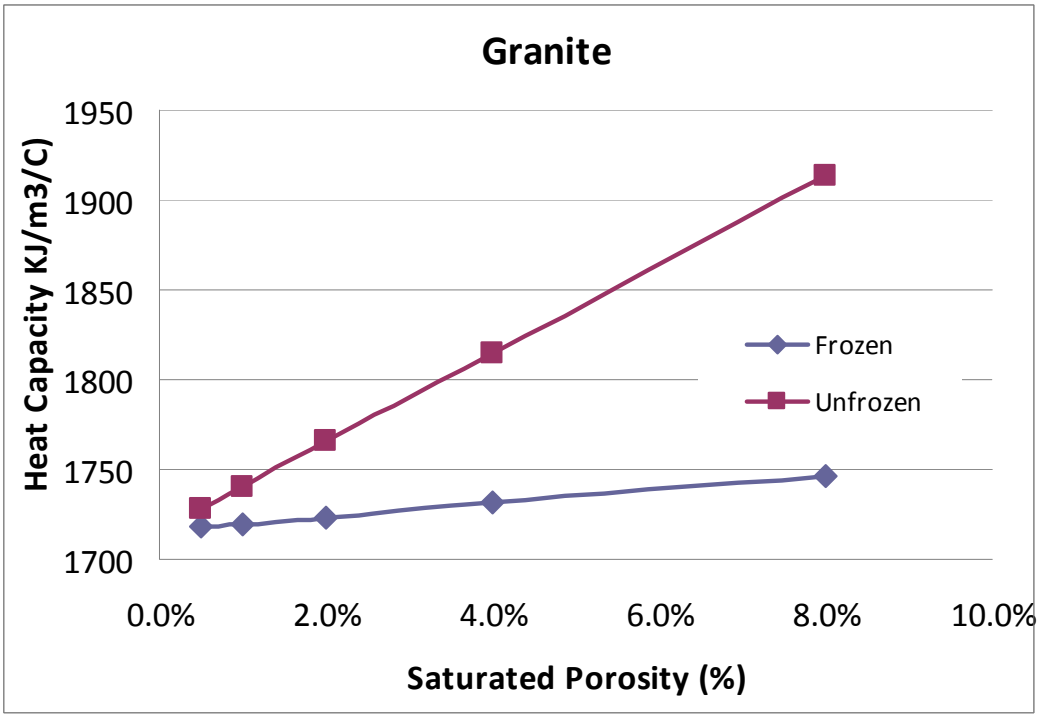

Figure 4.2-2
Thermal properties of host rock

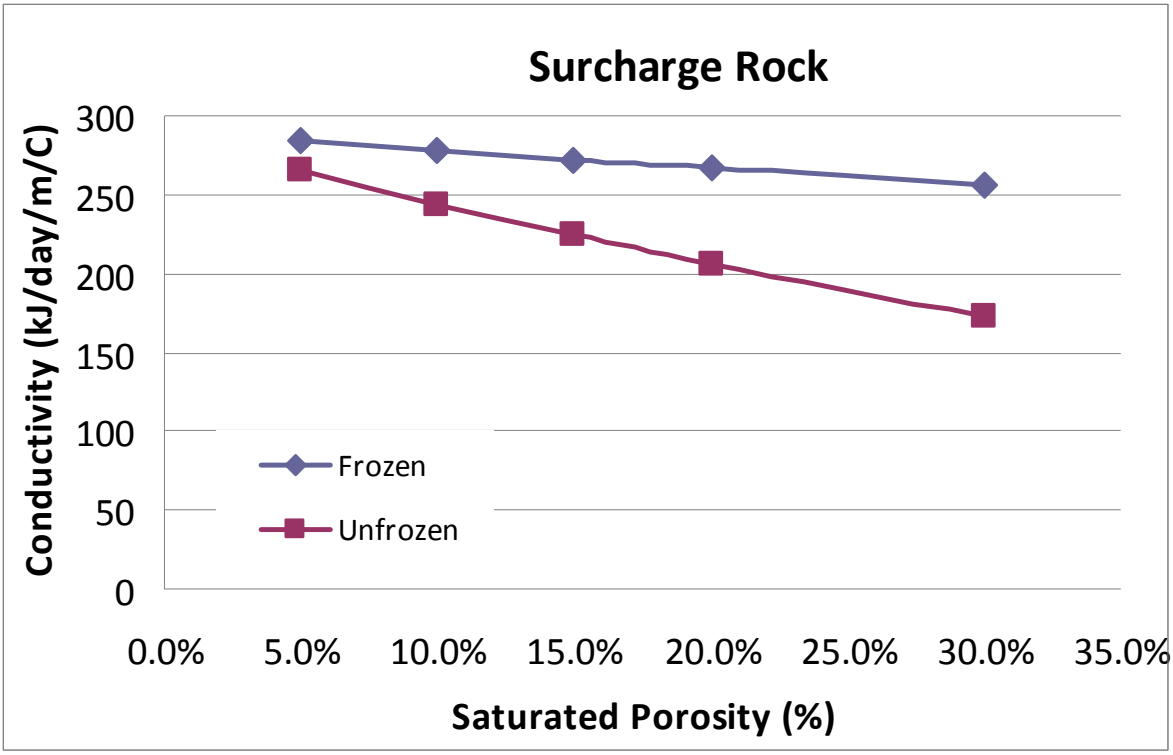

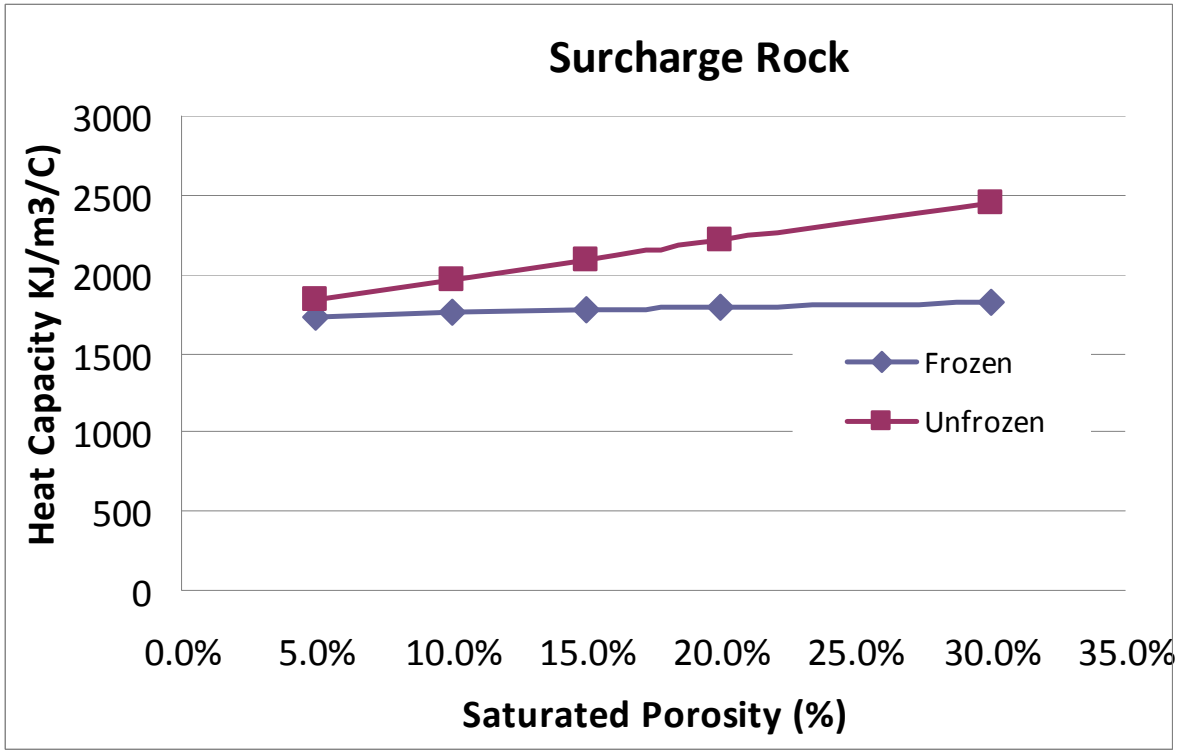

NEWMANS GEOTECHNIQUE

Figure 4.2-3
Thermal properties of surcharge mine rock

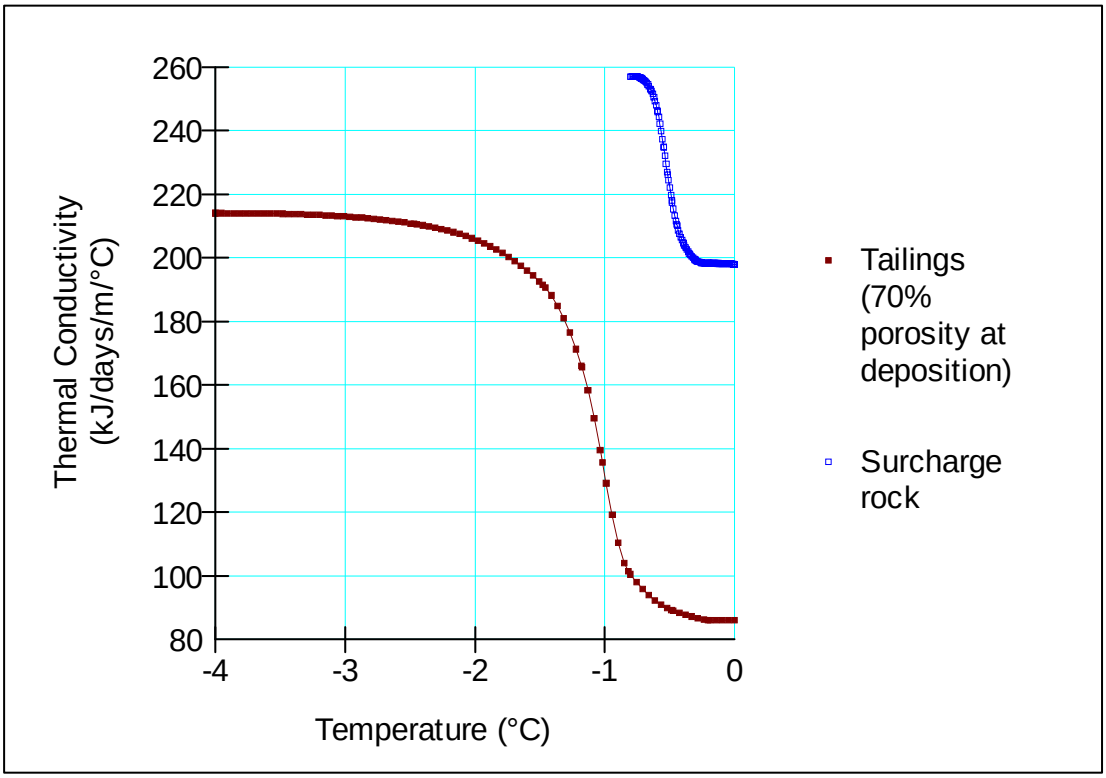

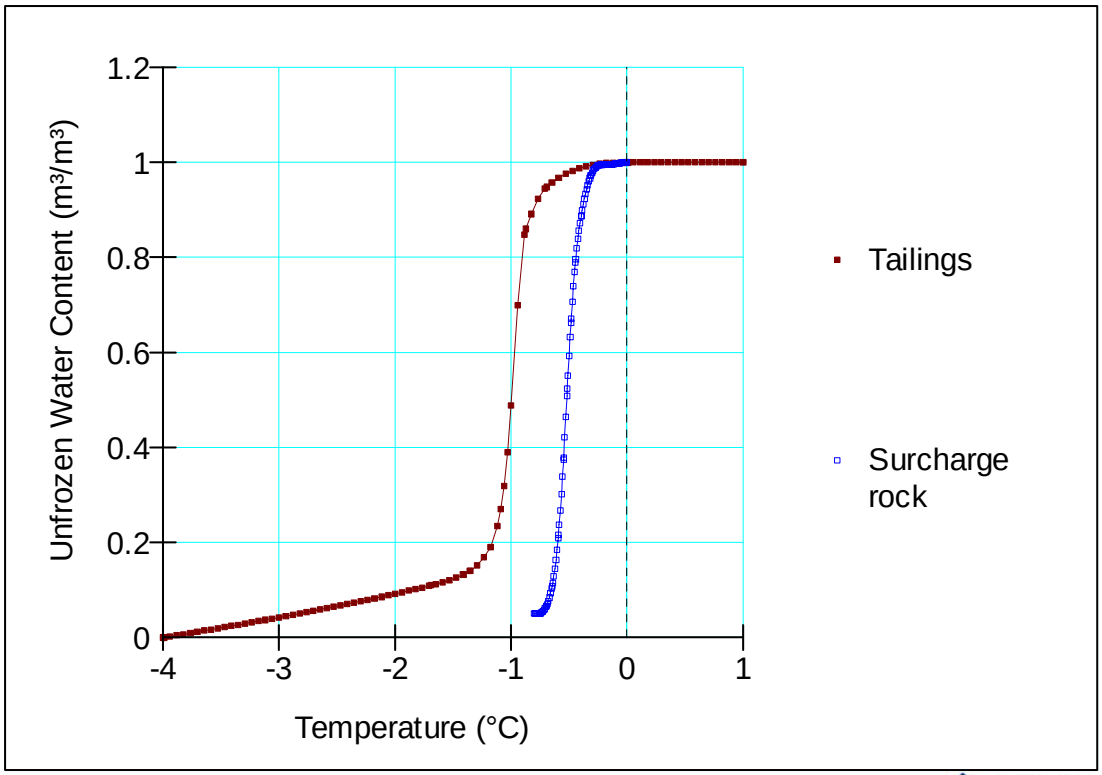

NEWMANS GEOTECHNIQUE

Technical Appendix 5J
Tailings Characterization and Management
Dec., 2011

Figure 4.2-4
Thermal functions showing transition between thawed and frozen states

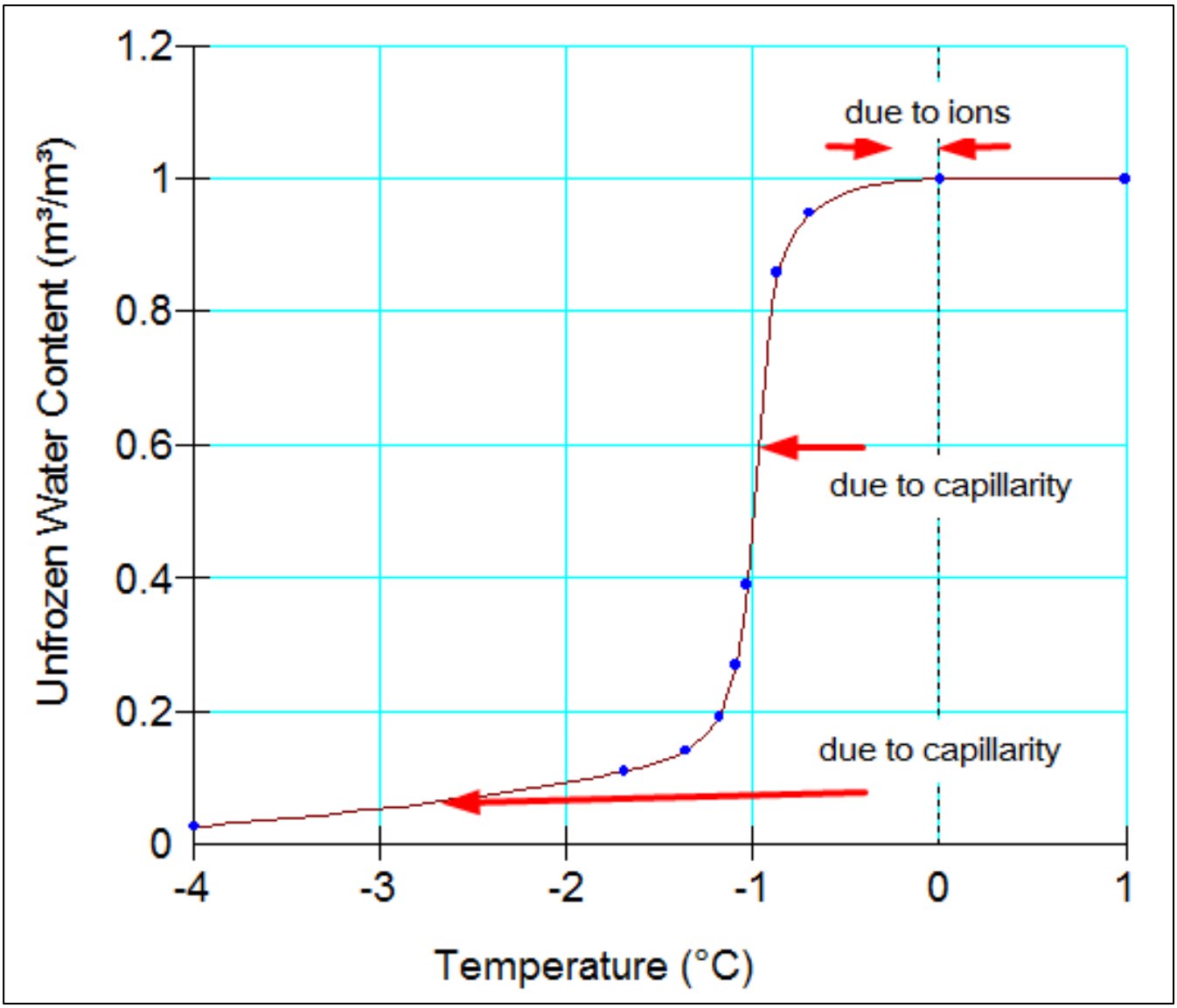

Figure 4.2-5
Combining ion and capillarity freezing point depression

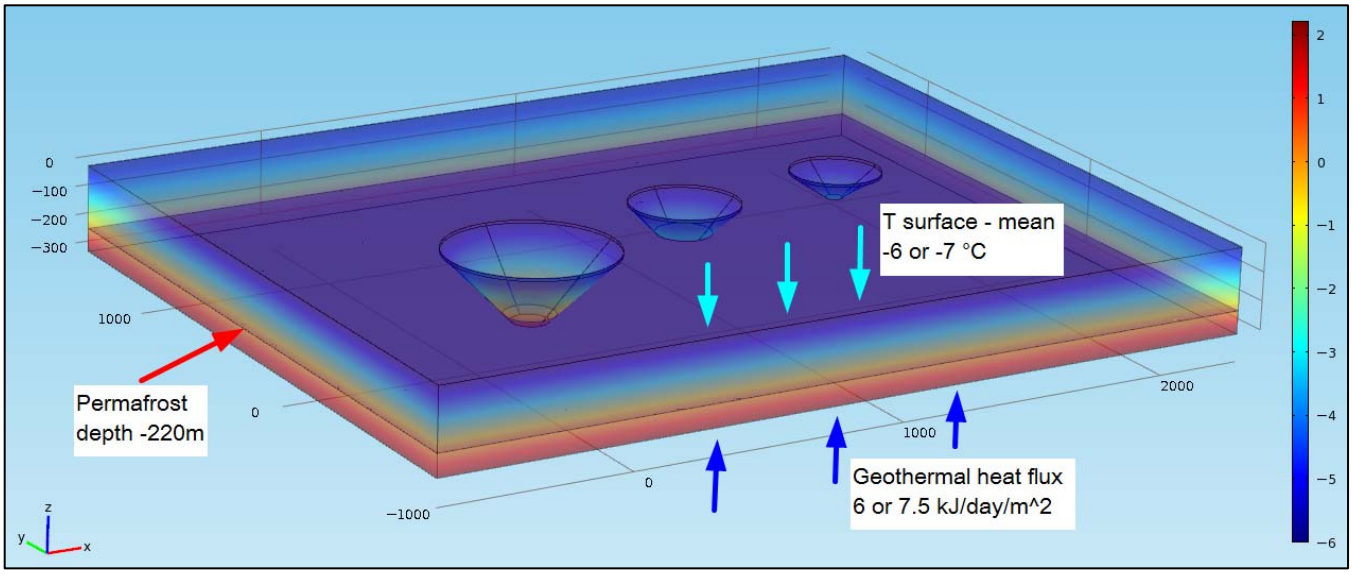

Figure 4.3-1
3D thermal model – Initial and boundary conditions

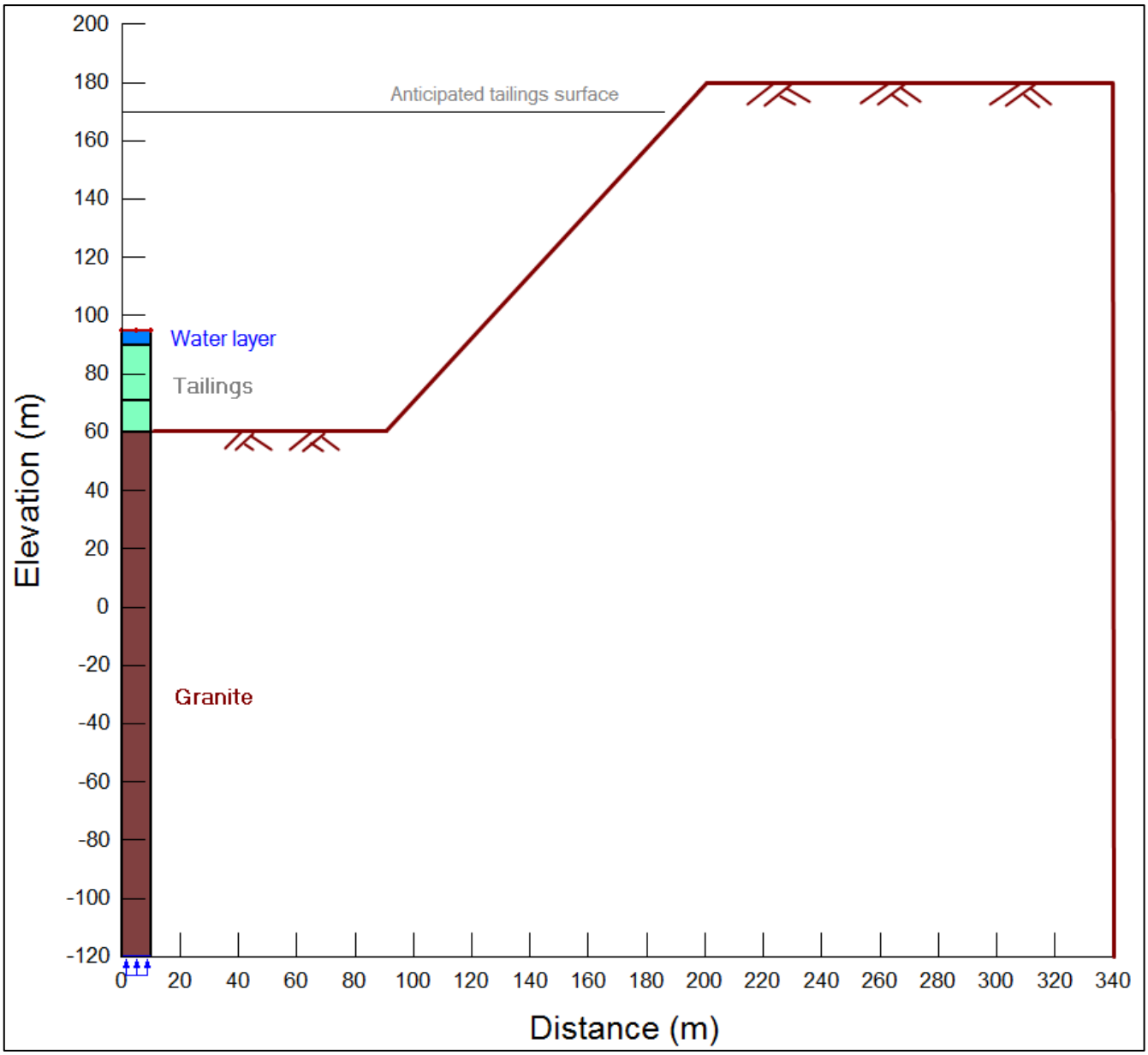

Figure 4.4-1
Example of 1-D model domain (relative to pit geometry) used for water layer analysis

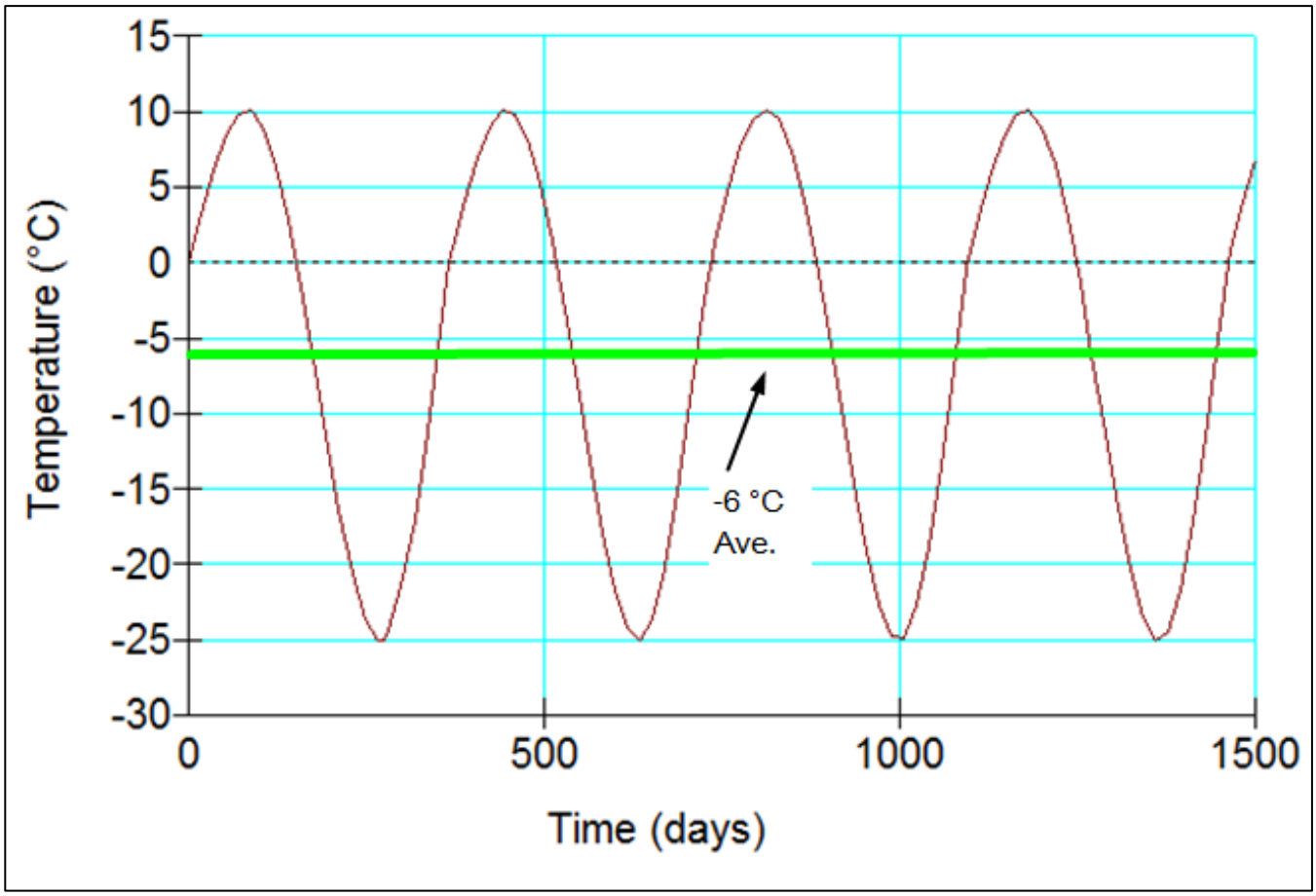

Figure 4.4-2
Transient water surface temperature function

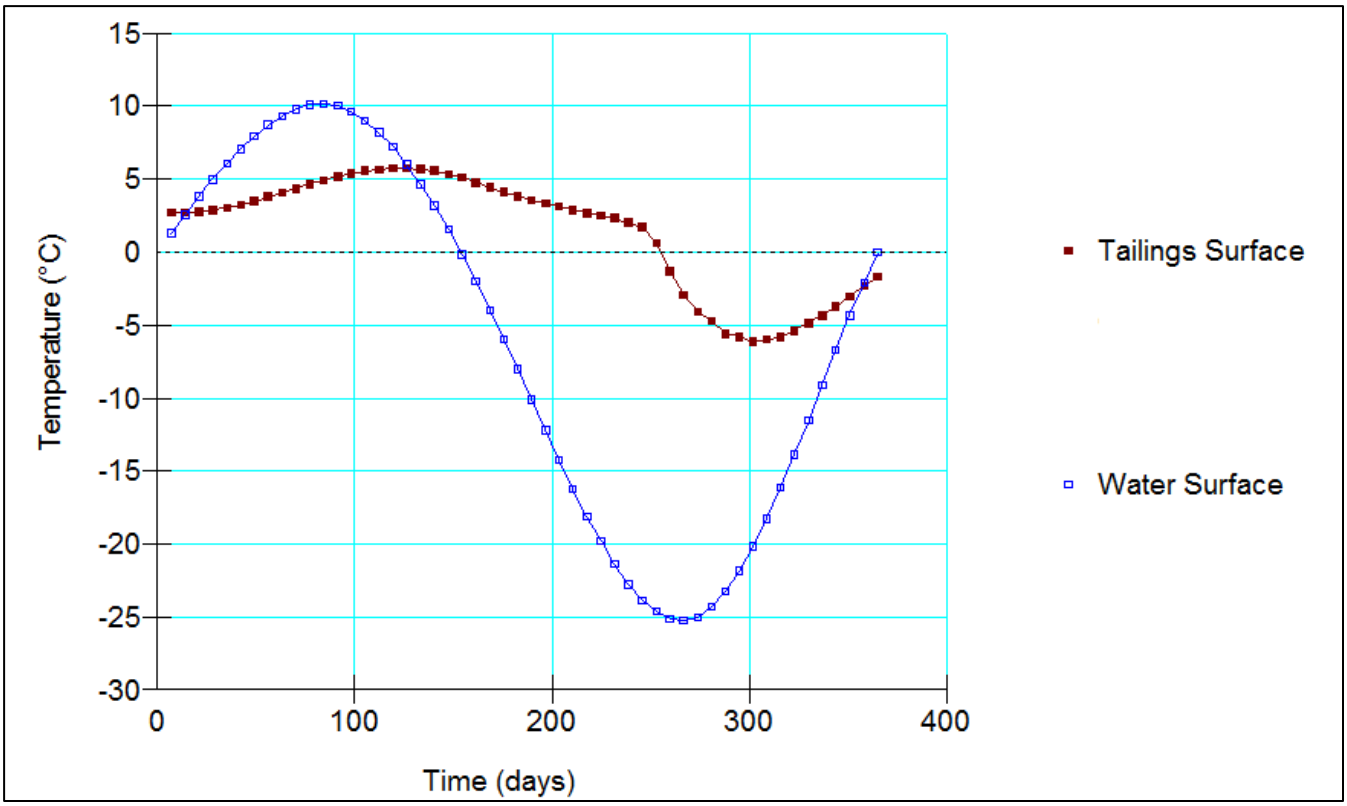

Figure 4.4-3
Tailings and water surface temperatures for 1m water layer

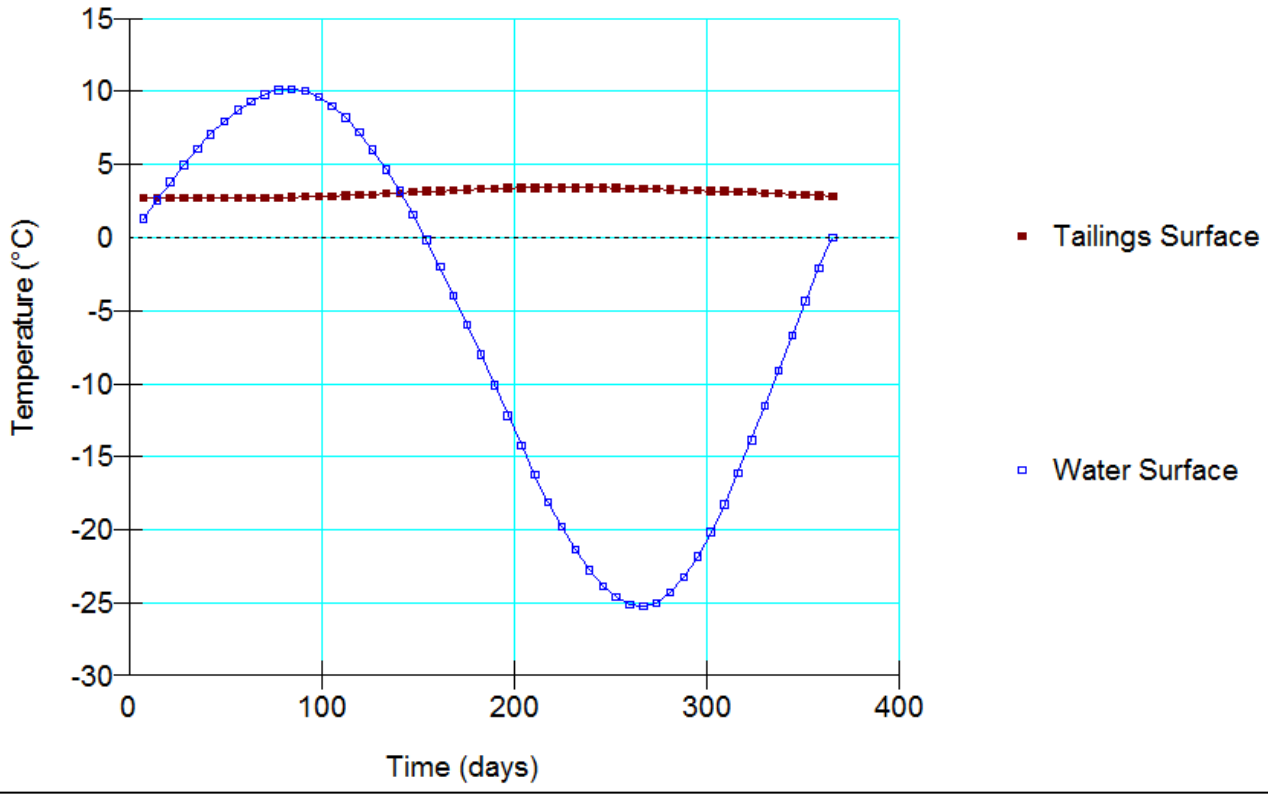

Figure 4.4-4
Tailings and water surface temperature for 3m water layer

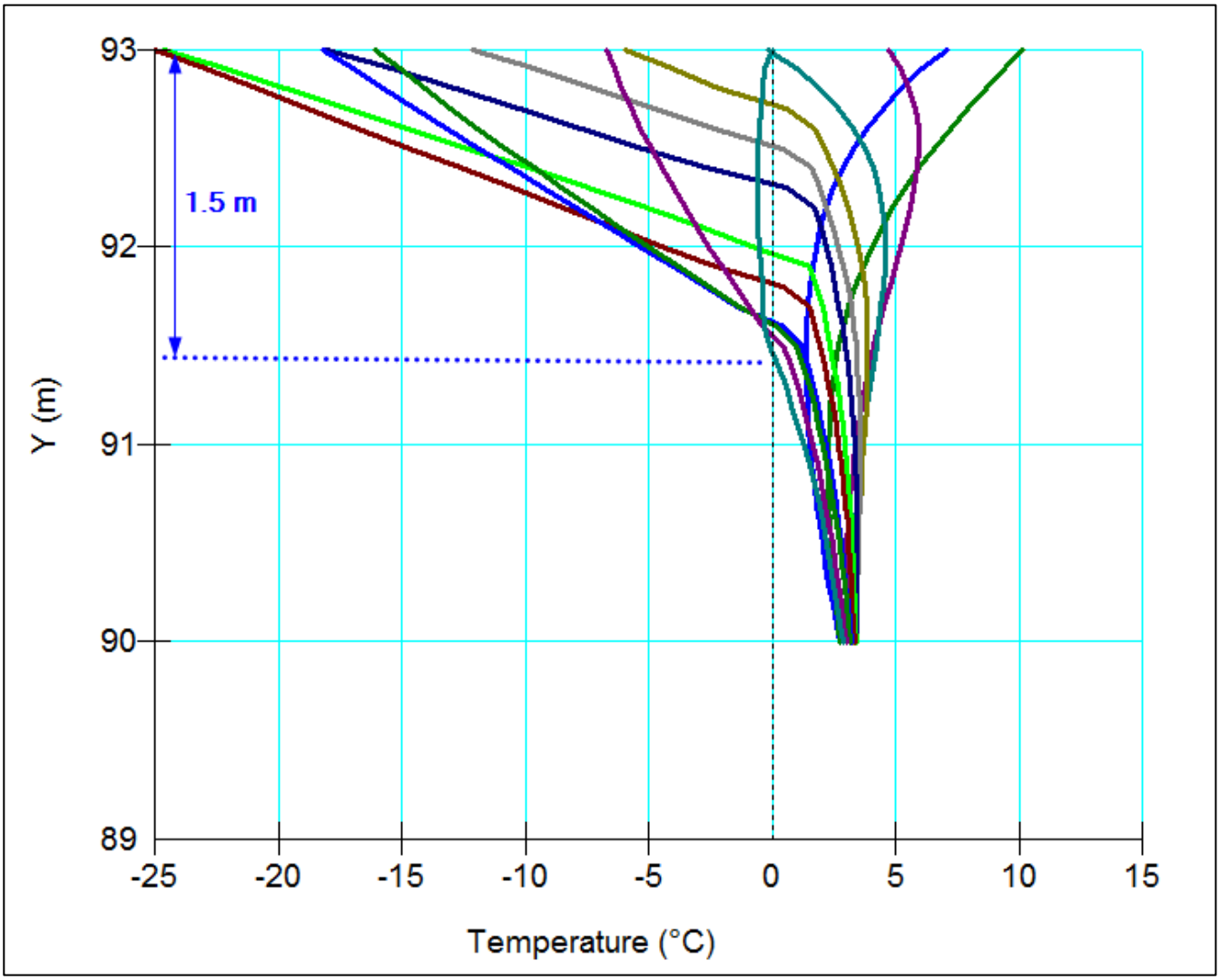

NEWMANS GEOTECHNIQUE

Technical Appendix 5J
Tailings Characterization and Management
Dec., 2011

Figure 4.4-5
Temperature profiles over time showing positive values below 1.5 m depth

Kiggavik Project

AREVA

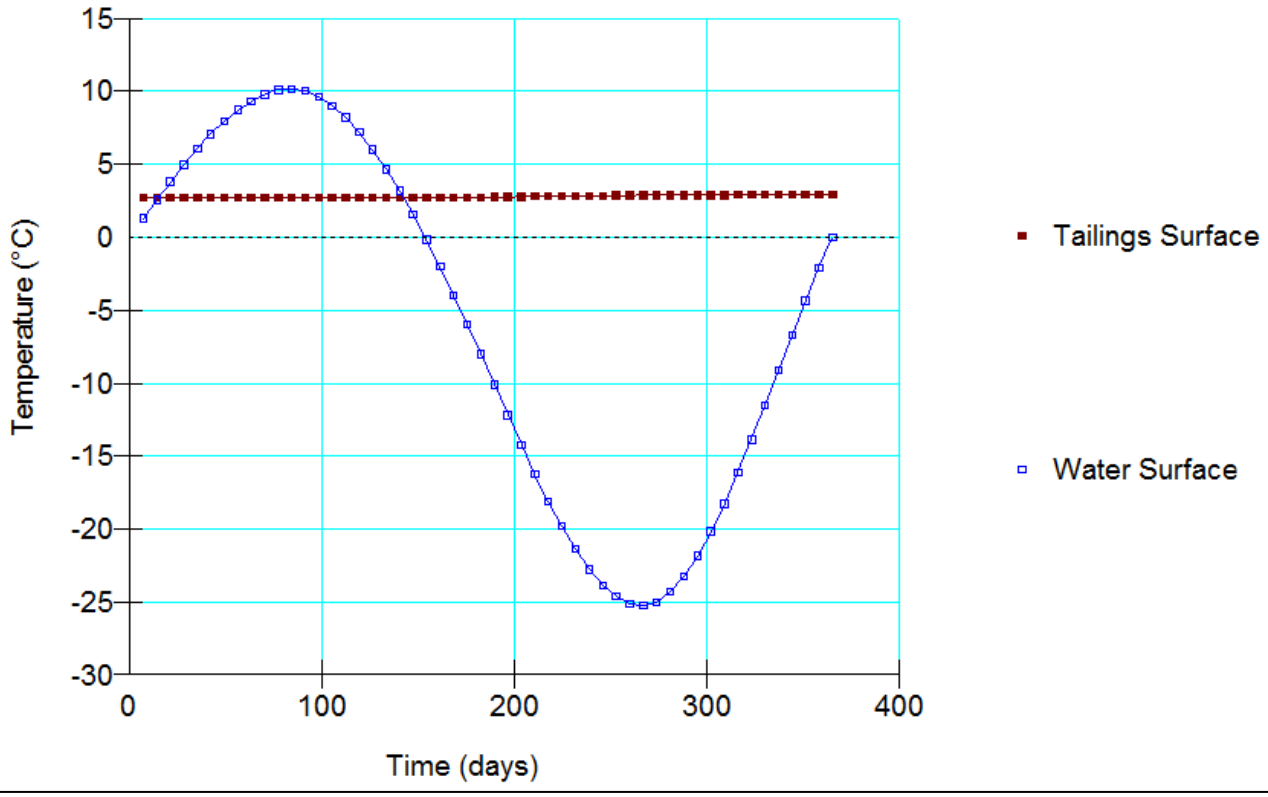

Figure 4.4-6
Tailings and water surface temperature for 5m water layer

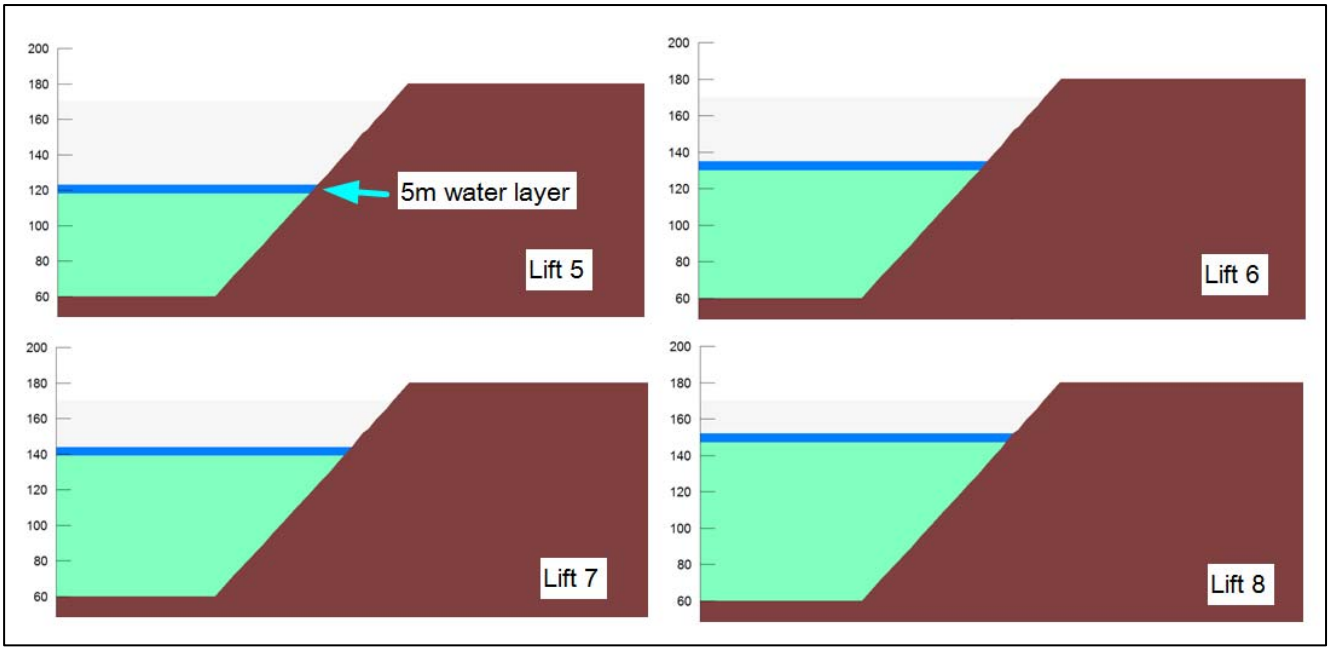

Figure 4.5-1
Example of transient depositional sequence with 5m water layers

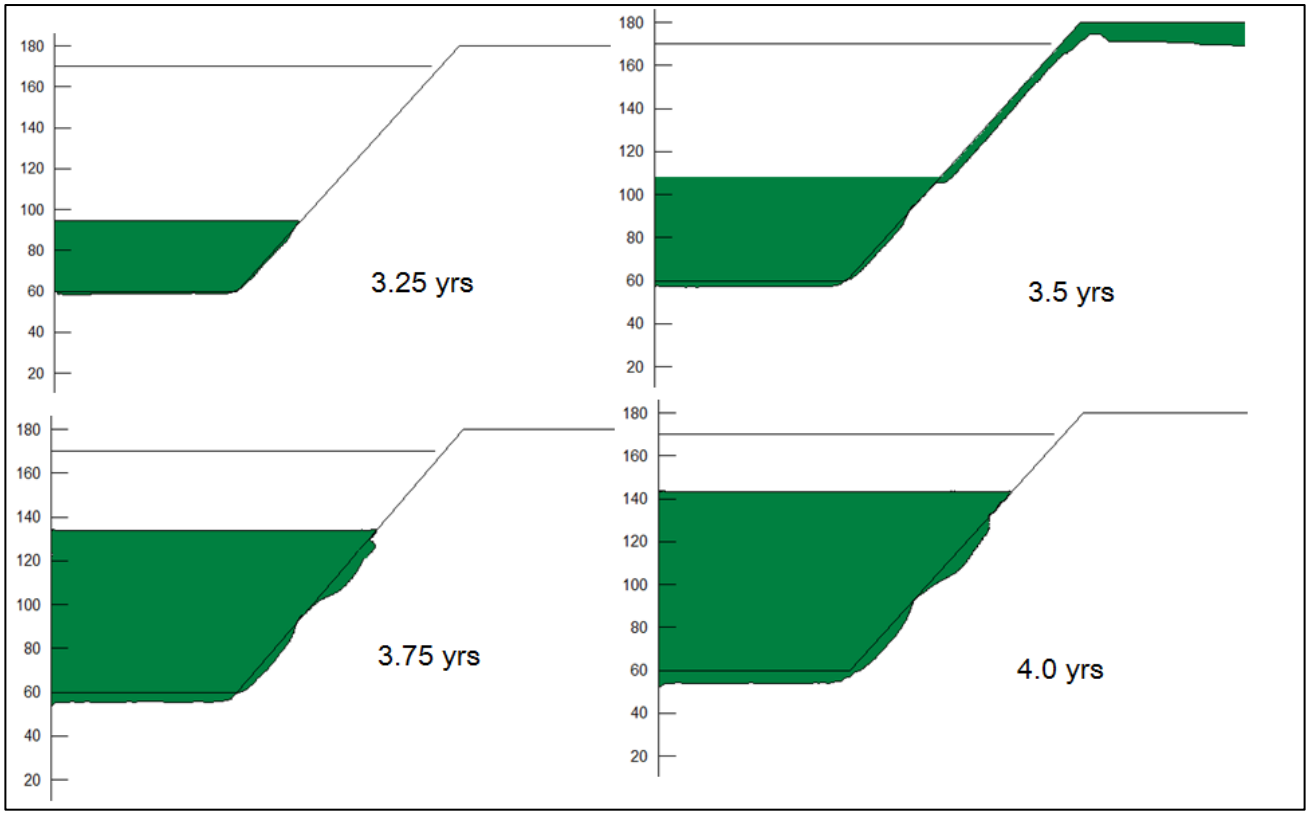

NEWMANS GEOTECHNIQUE

Figure 4.5-2
Unfrozen zones at selected time intervals with 5m water layers during deposition

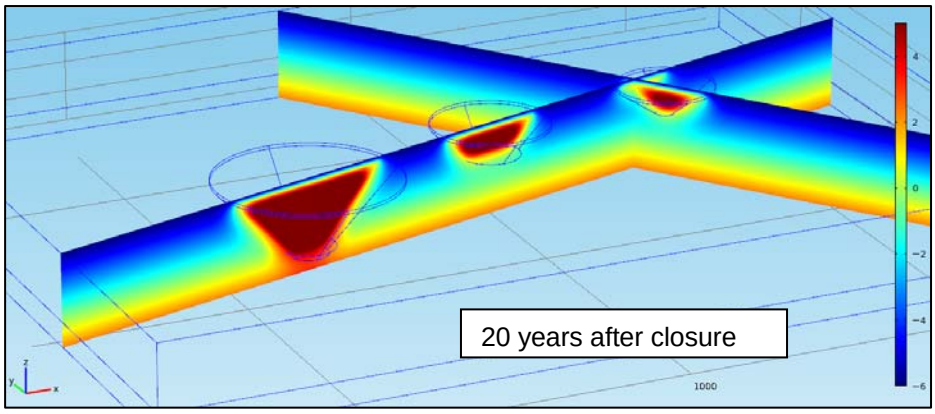

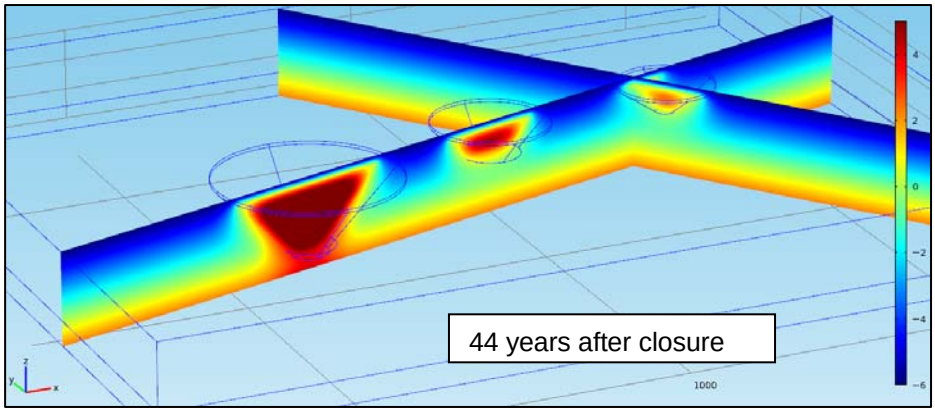

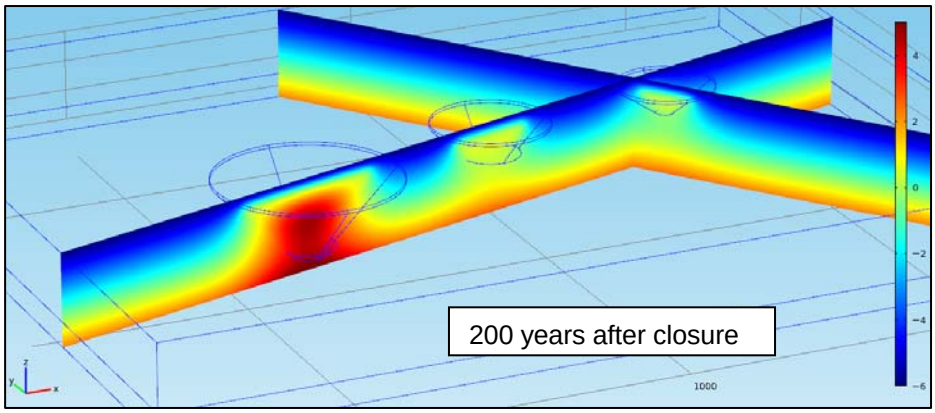

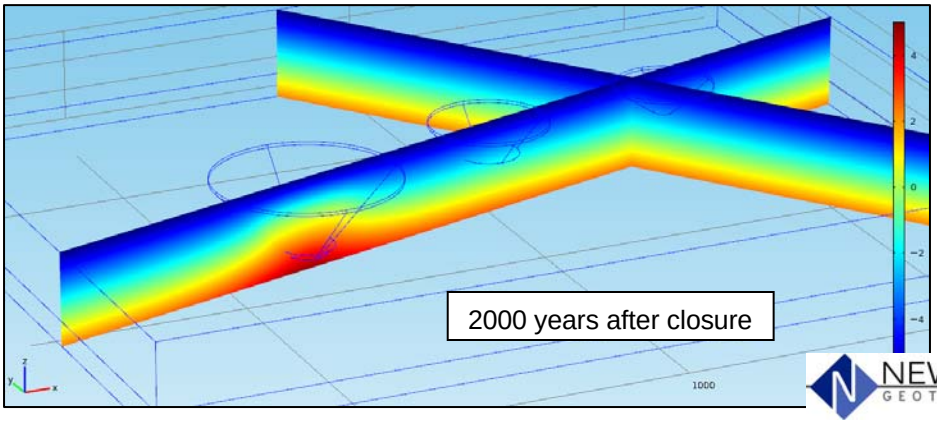

NEWMANS GEOTECHNIQUE

Figure 4.5-3
Thermal profile in pits

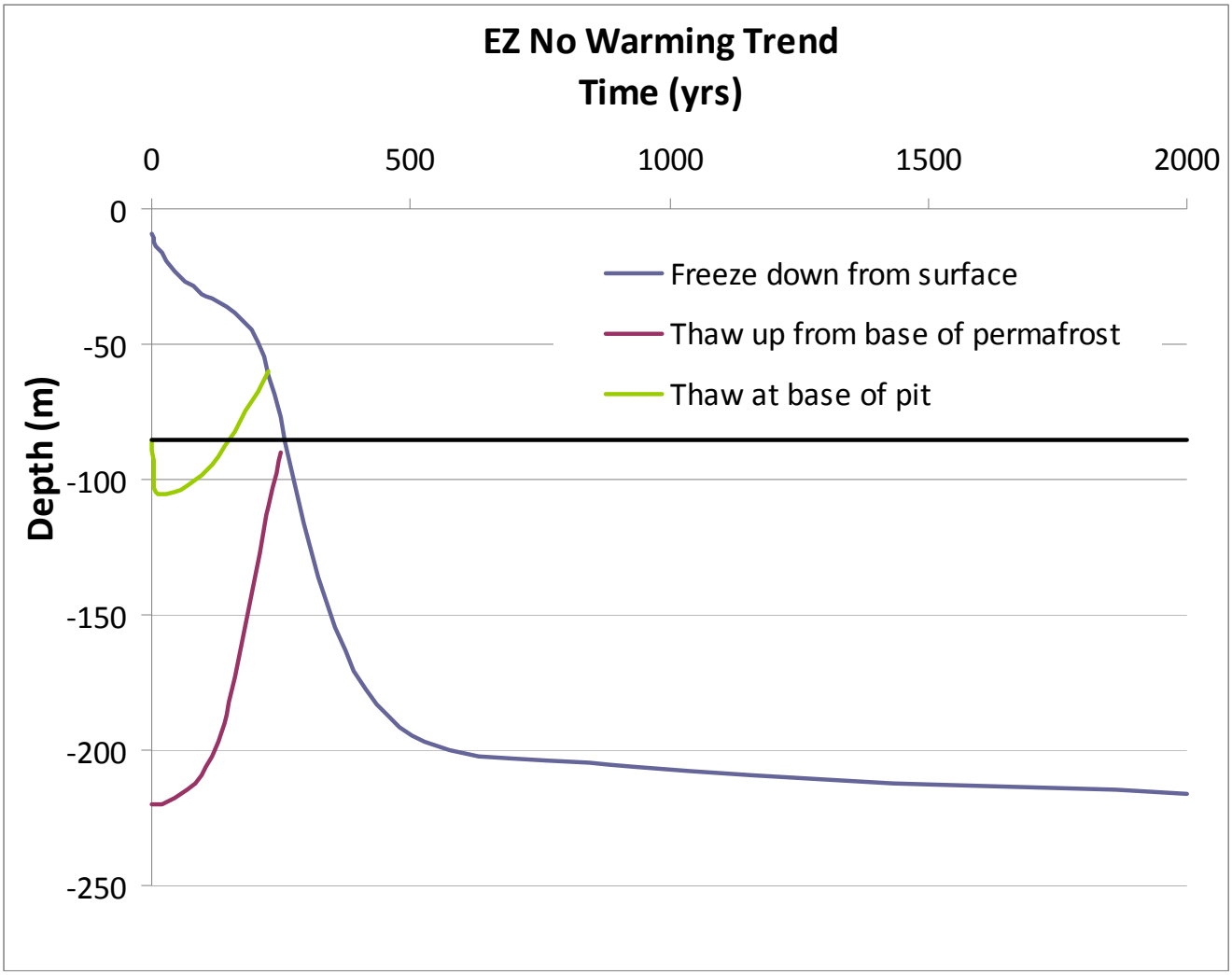

Figure 4.5-4
East Zone permafrost status with depth and time – No warming trend

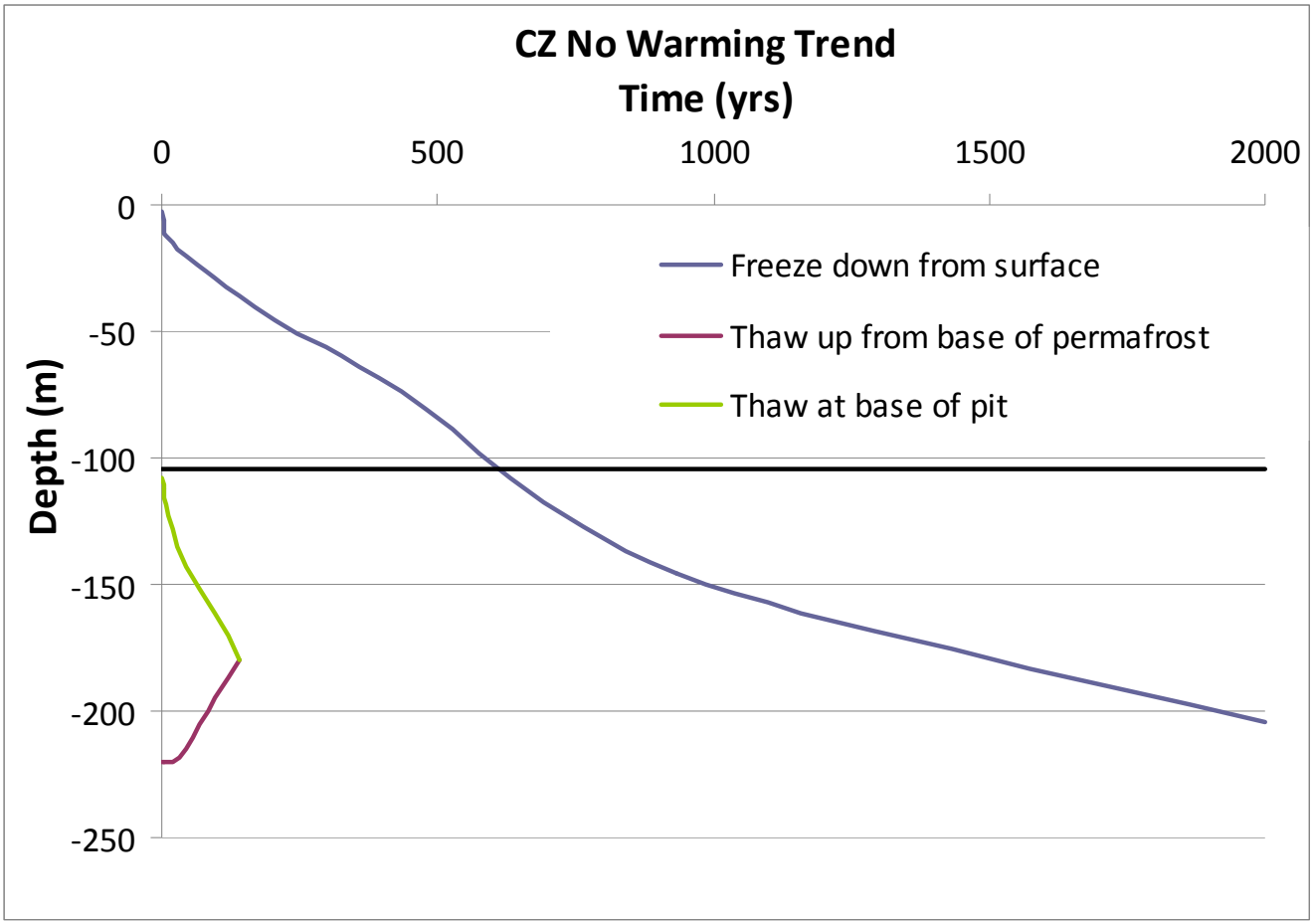

Figure 4.5-5
Centre Zone permafrost status with depth and time – No warming trend

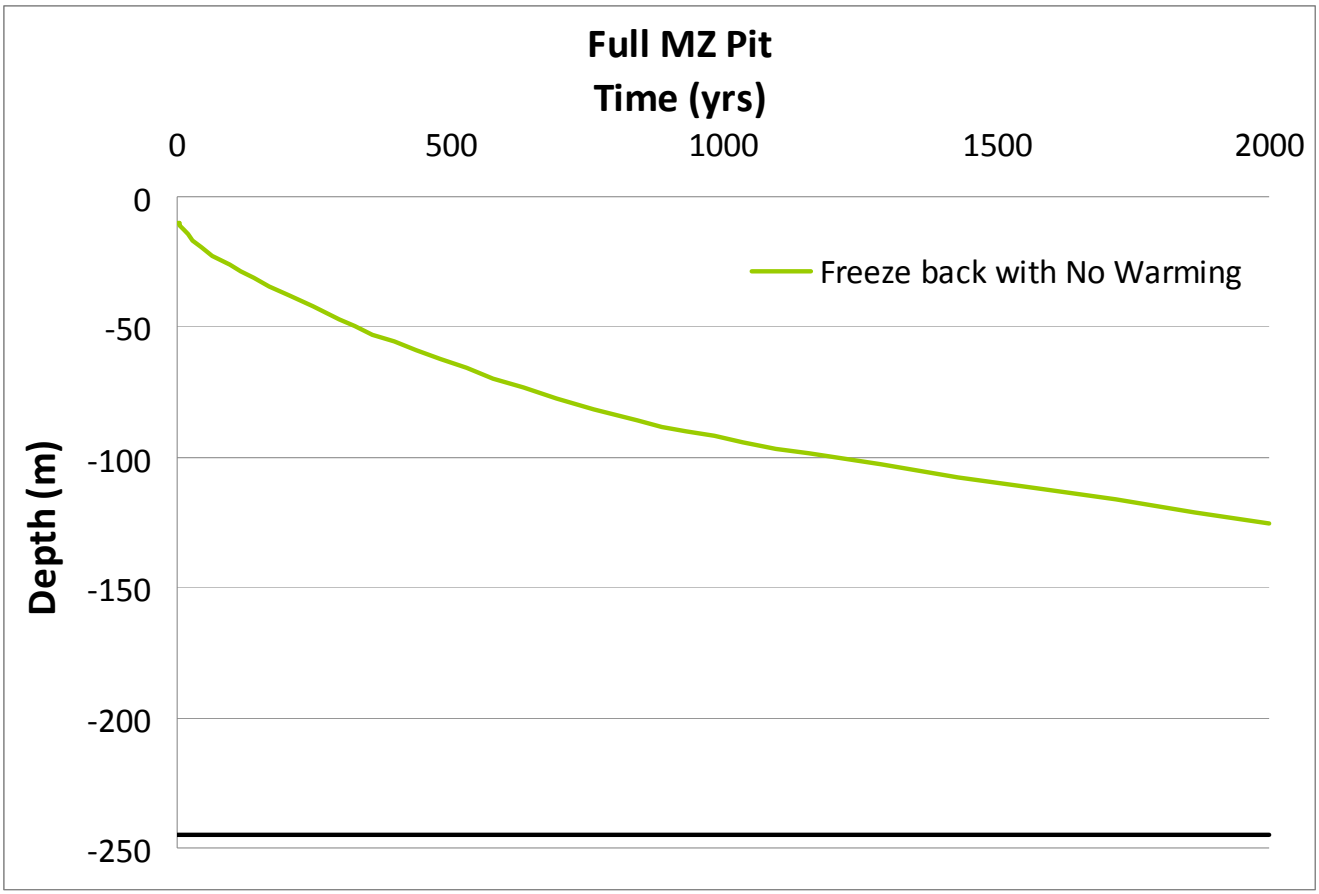

Figure 4.5-6
Main Zone permafrost status with depth and time – No warming trend

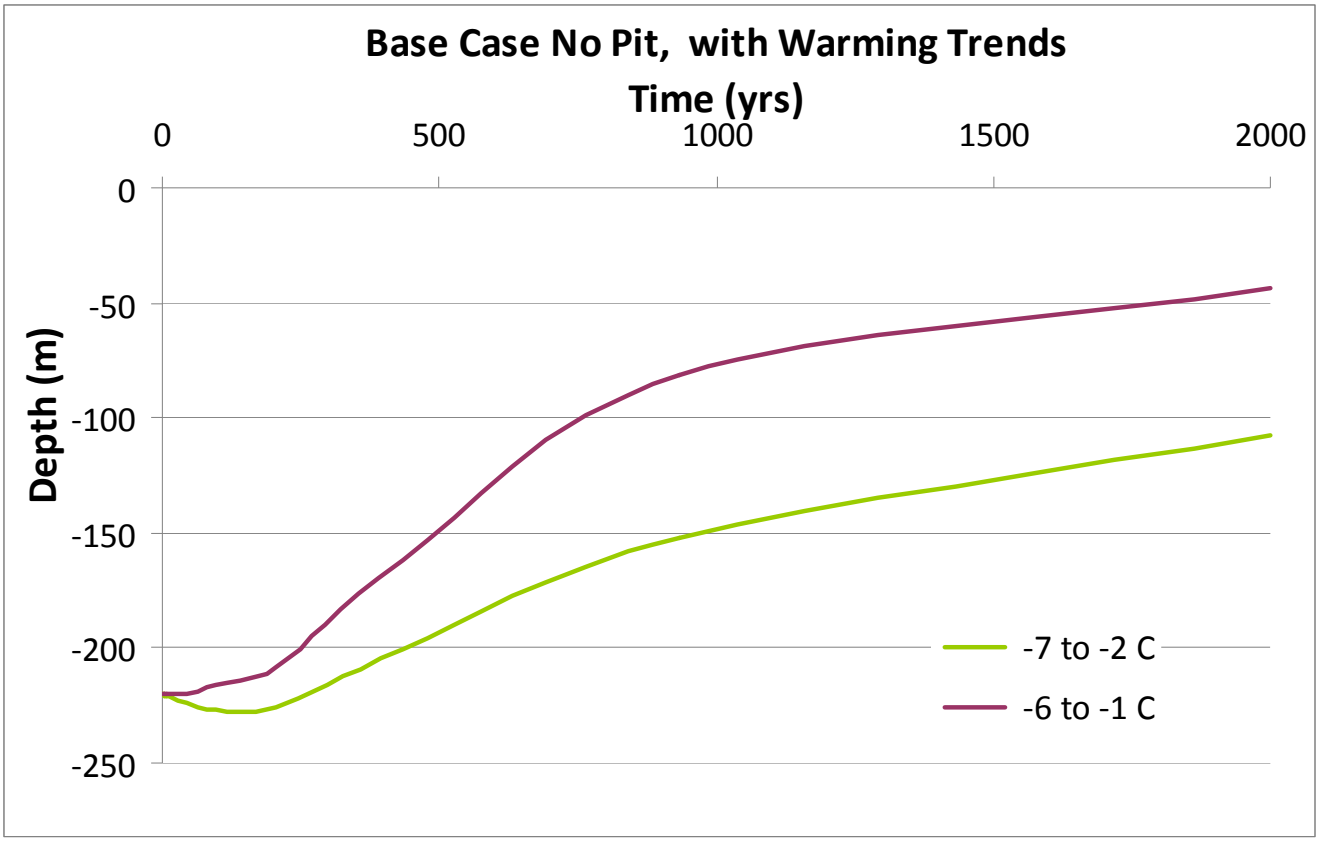

Figure 4.6-1
Natural ground permafrost degradation with climate warming

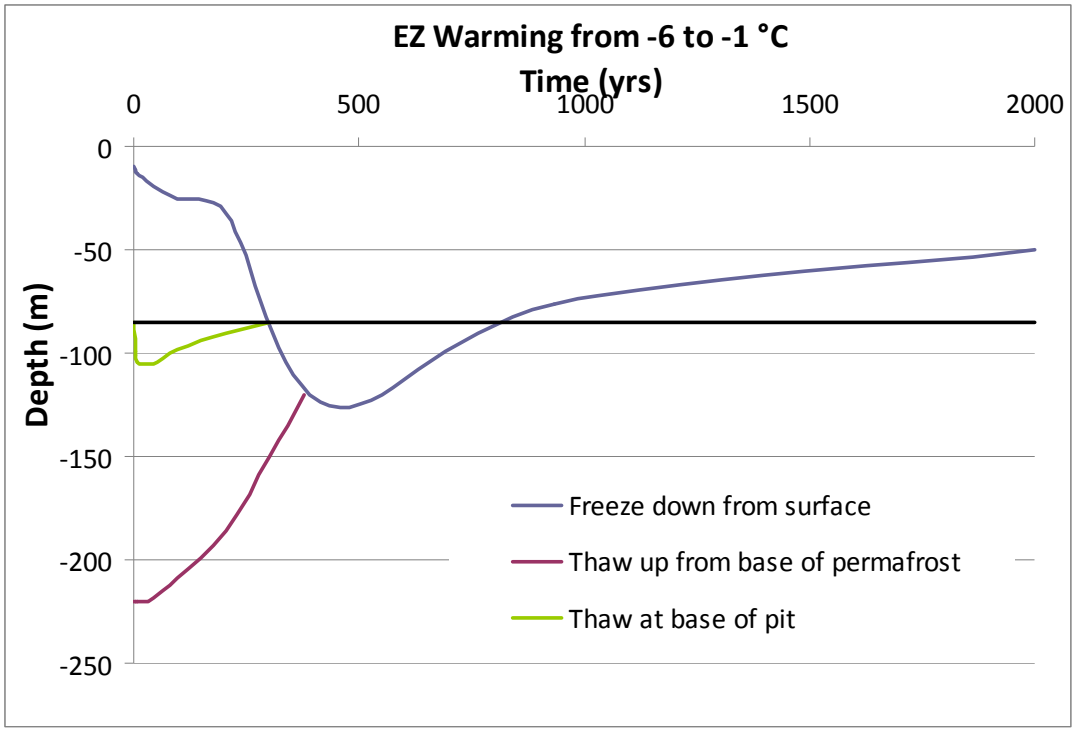

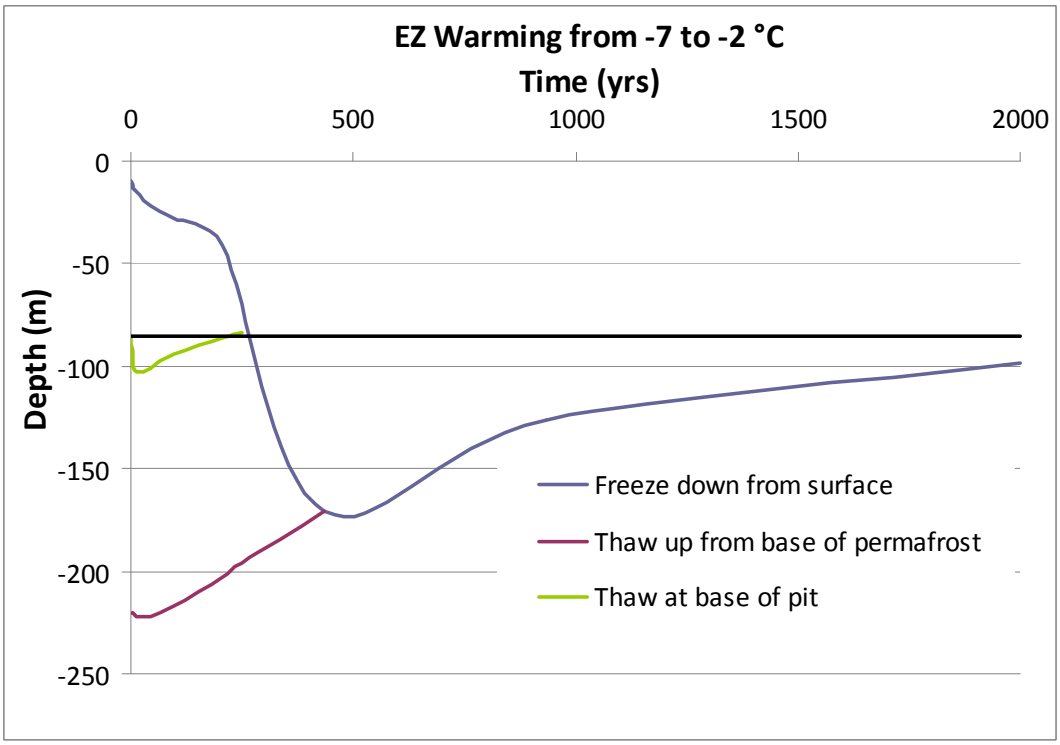

NEWMANS GEOTECHNIQUE

Technical Appendix 5J
Tailings Characterization and Management
Dec., 2011

Figure 4.6-2
East Zone permafrost status with warming trends

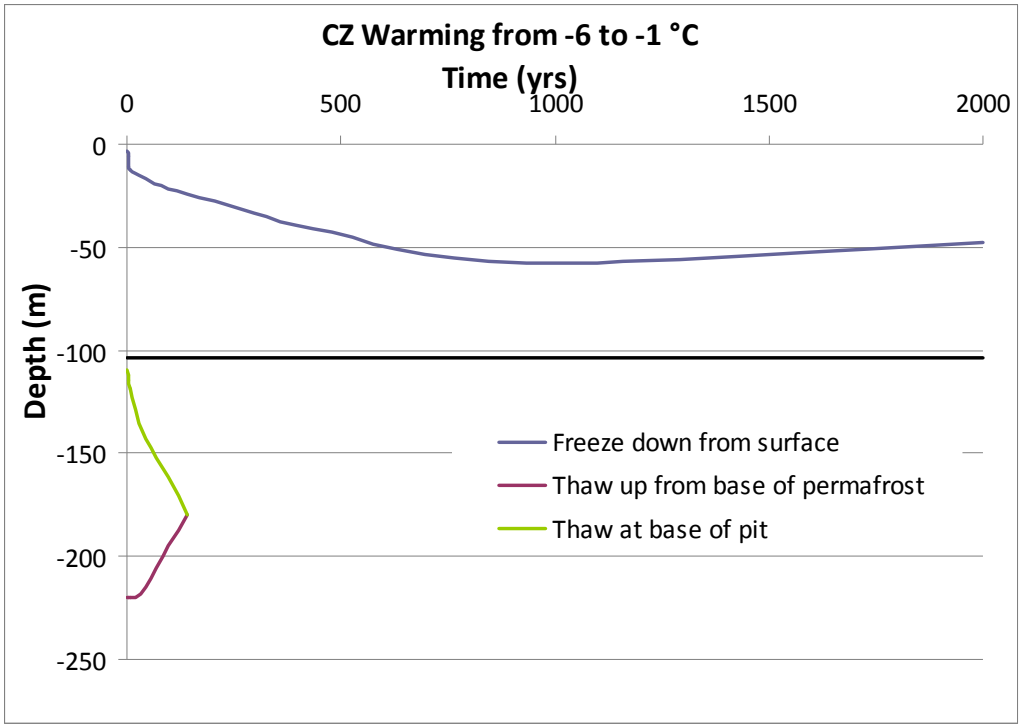

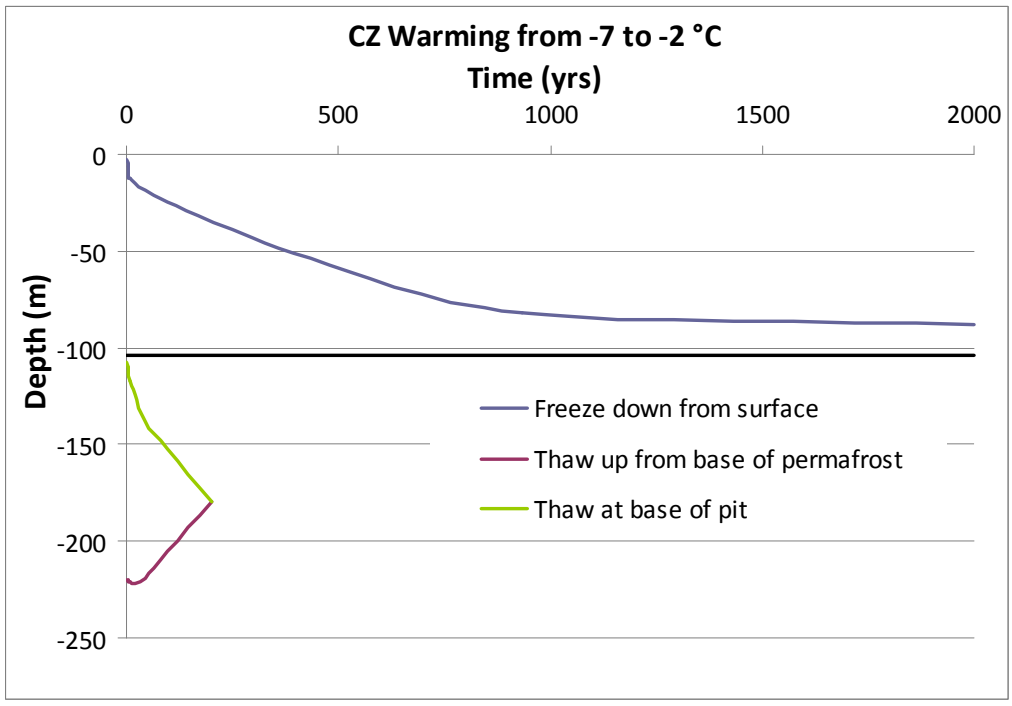

Figure 4.6-3
Centre Zone permafrost status with warming trends

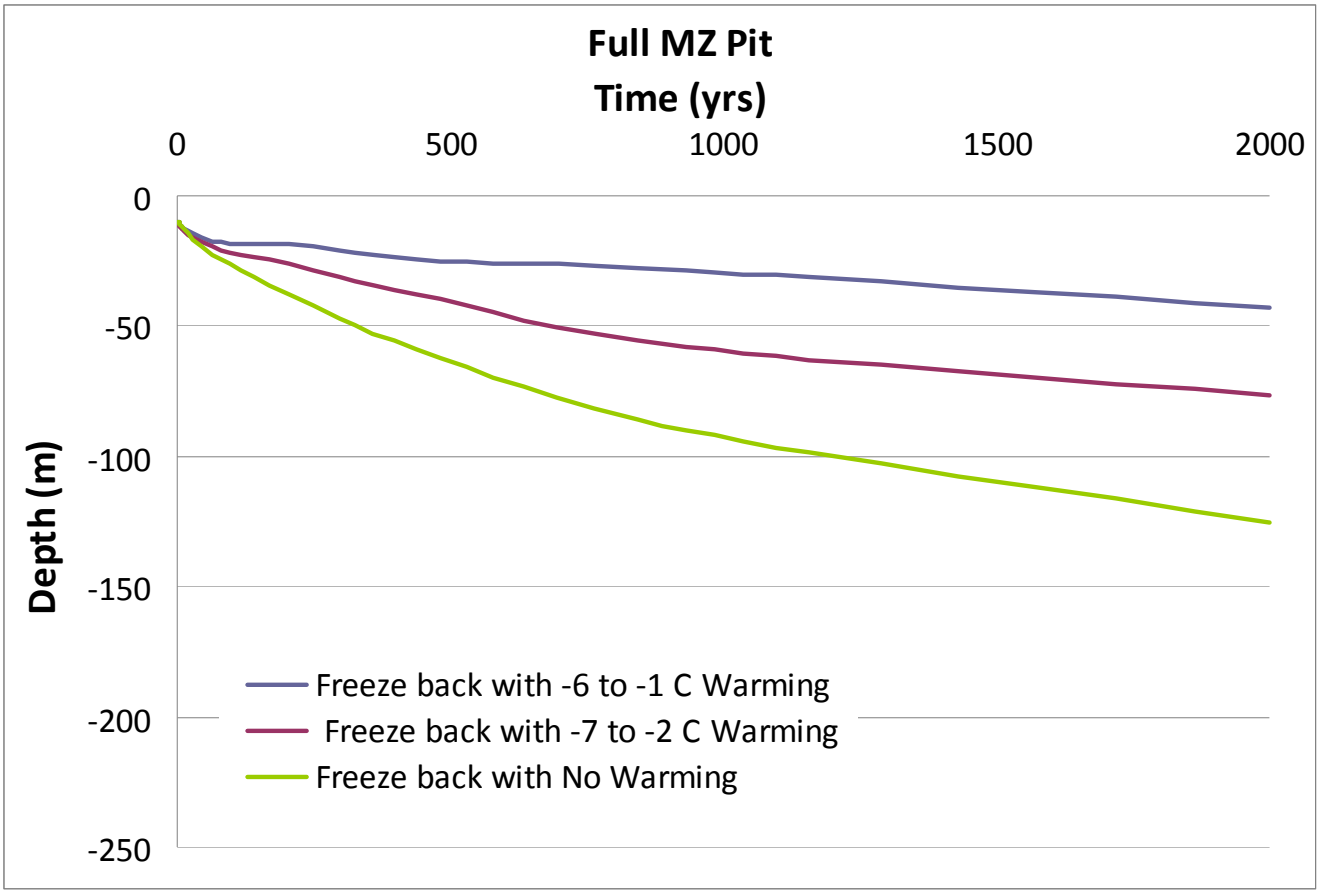

Figure 4.6-4
Main Zone permafrost status for a full pit case

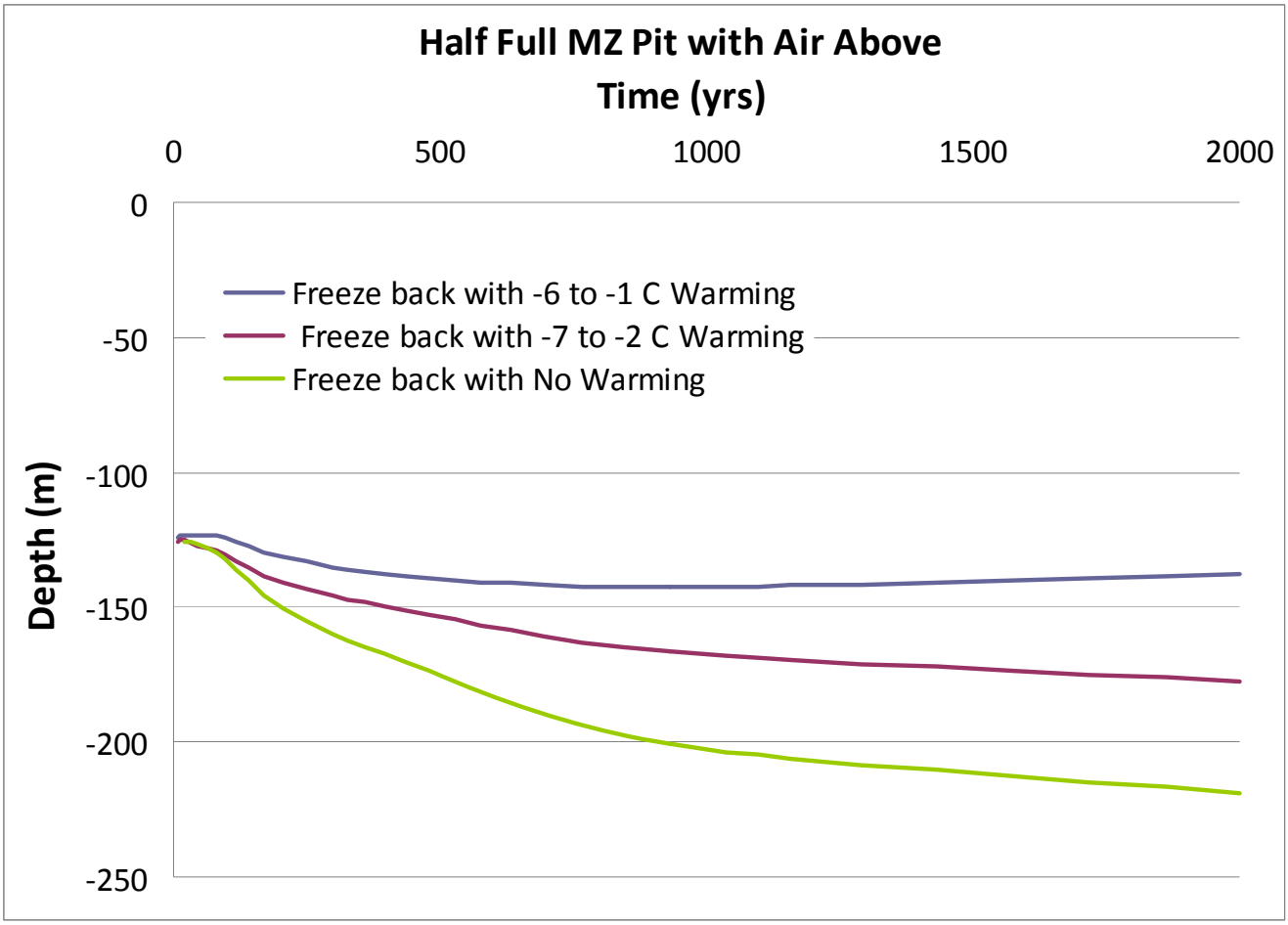

Figure 4.6-5
Main Zone permafrost status for a half full pit case

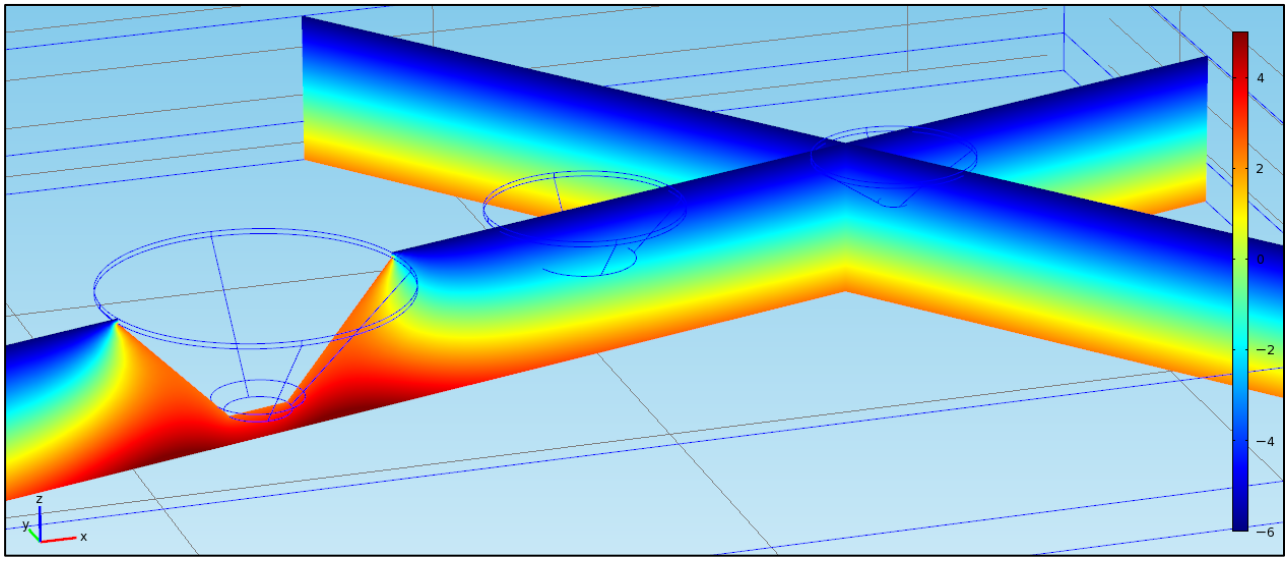

Figure 4.6-6
Simulated long term thermal regime with Main Zone water filled

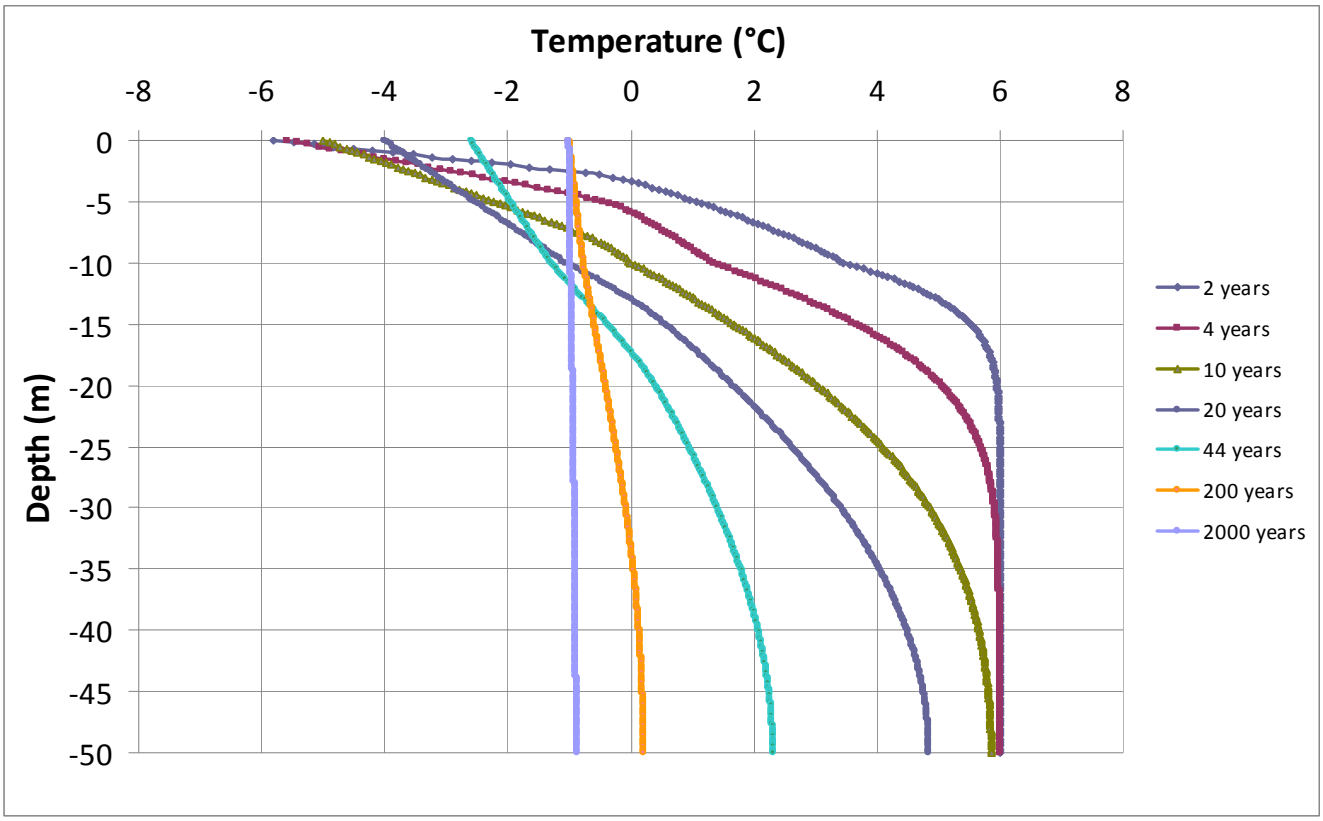

Figure 4.6-7
Temperature profile and freeze back through TMF cover (10 m deep)

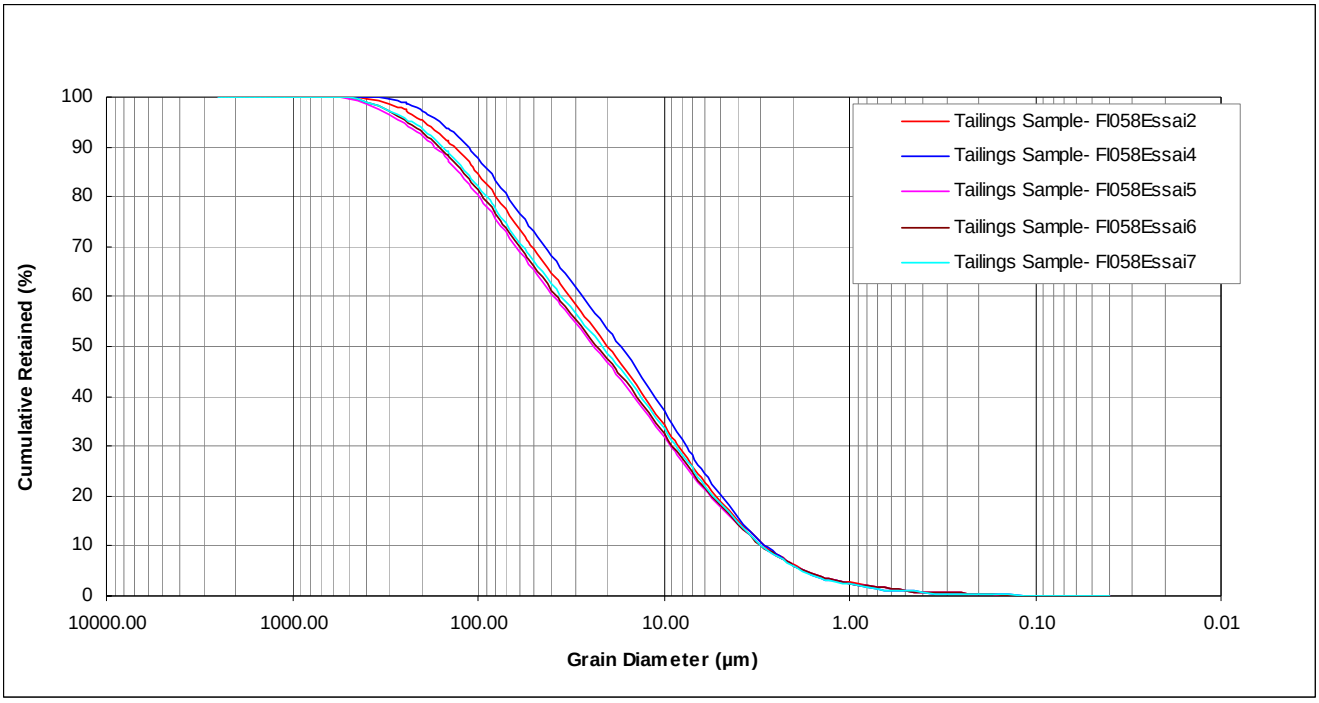

Figure 5.2-1
Grain size distribution curves of laboratory produced tailings

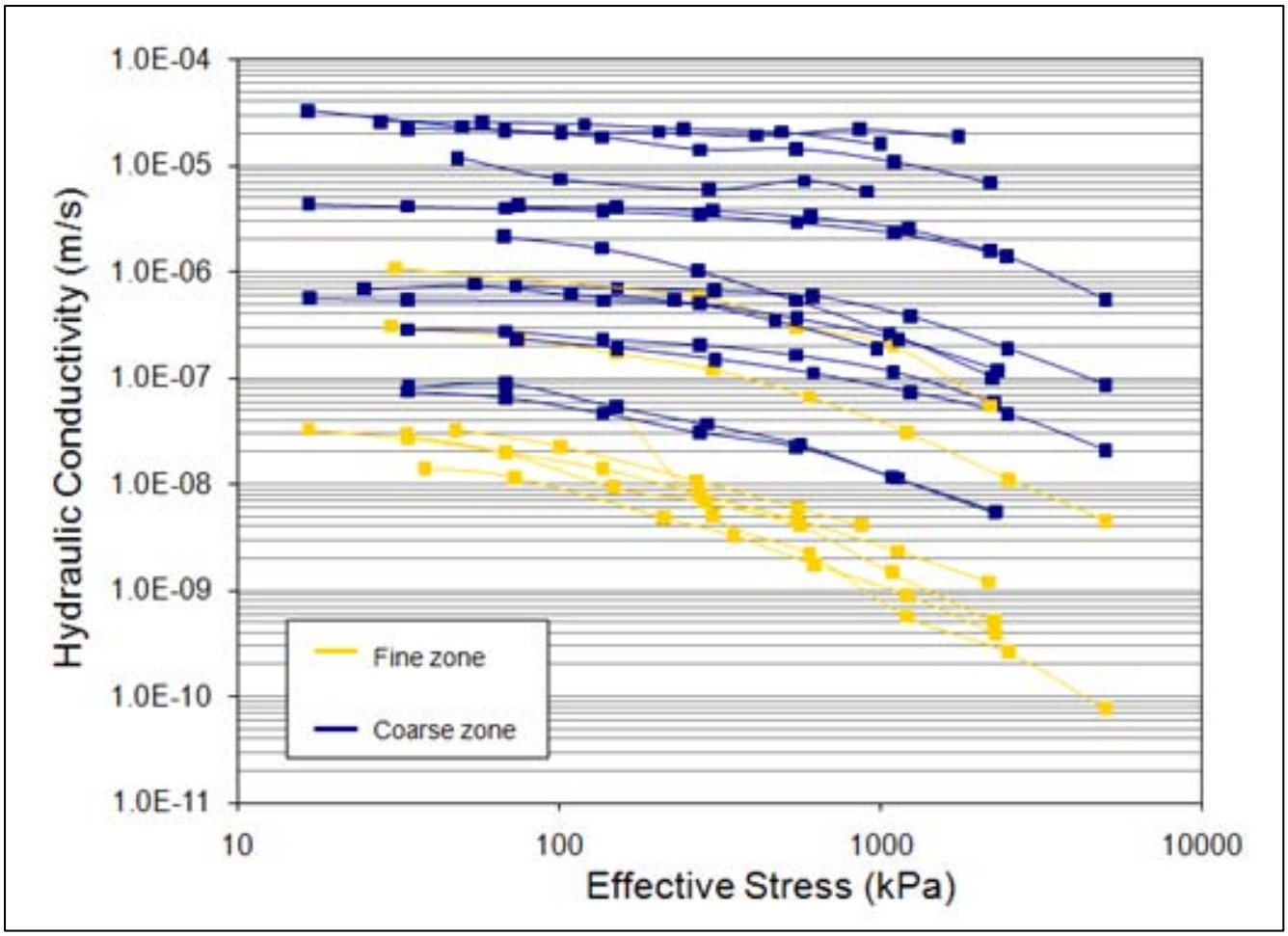

Figure 5.2-2
Range of hydraulic conductivity values observed in the McClean Lake JEB TMF

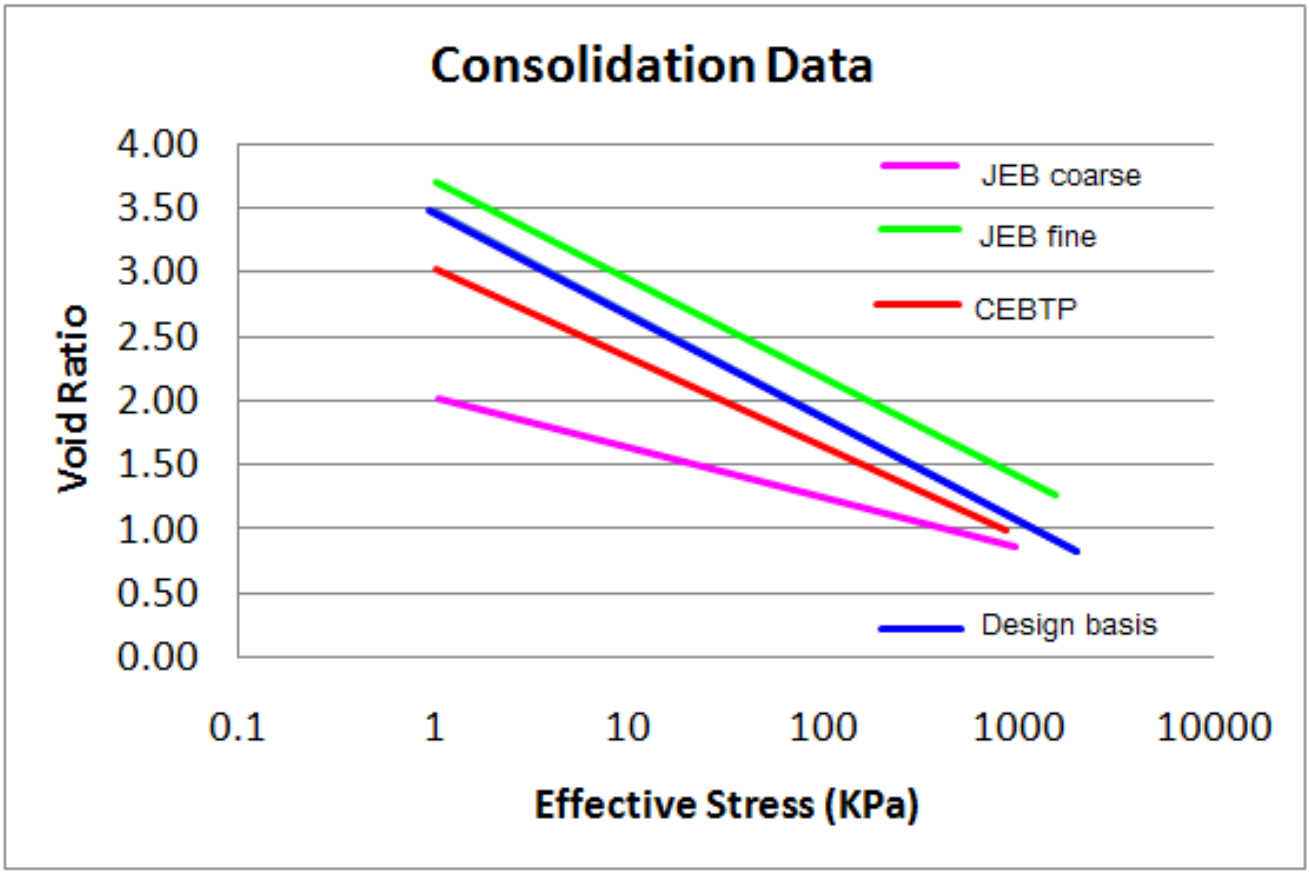

Figure 5.2-3
Applied void ratio versus effective stress relationship

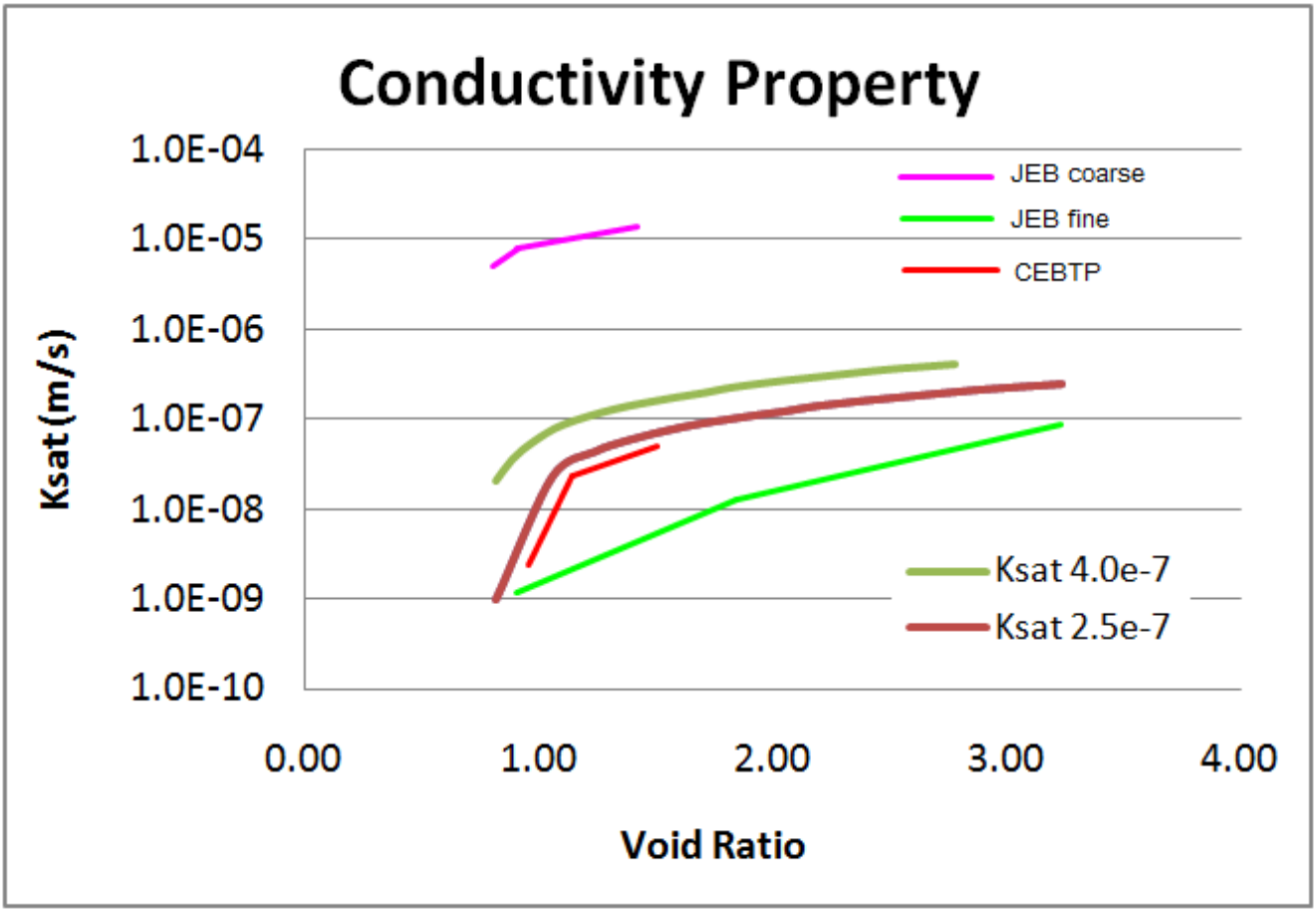

Figure 5.2-4
Applied hydraulic conductivity versus void ratio relationship

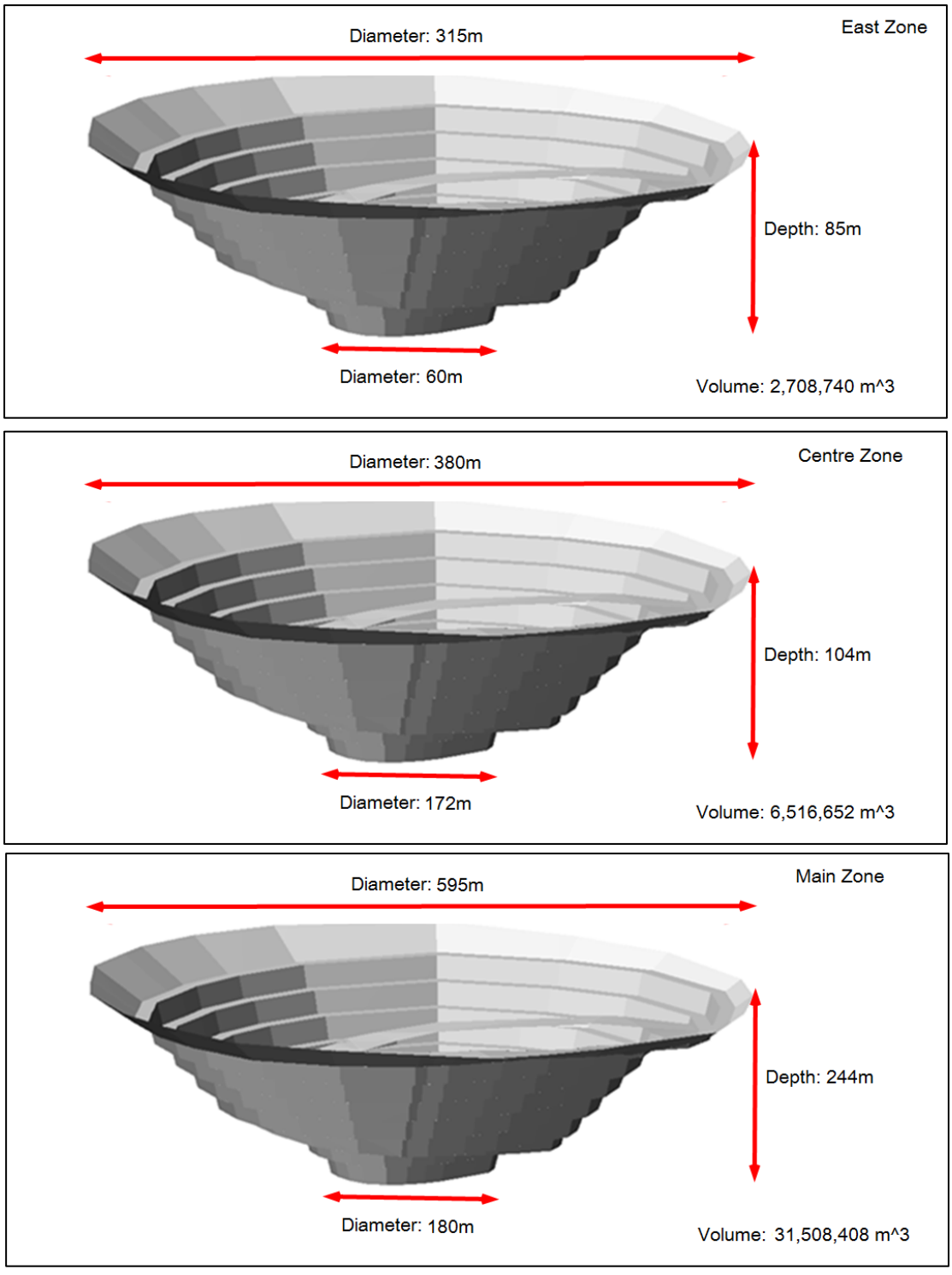

NEWMANS GEOTECHNIQUE

Technical Appendix 5J
Tailings Characterization and Management
Dec., 2011

Figure 5.3-1
Simulated pit geometry and TMF volumes

Kiggavik Project

AREVA

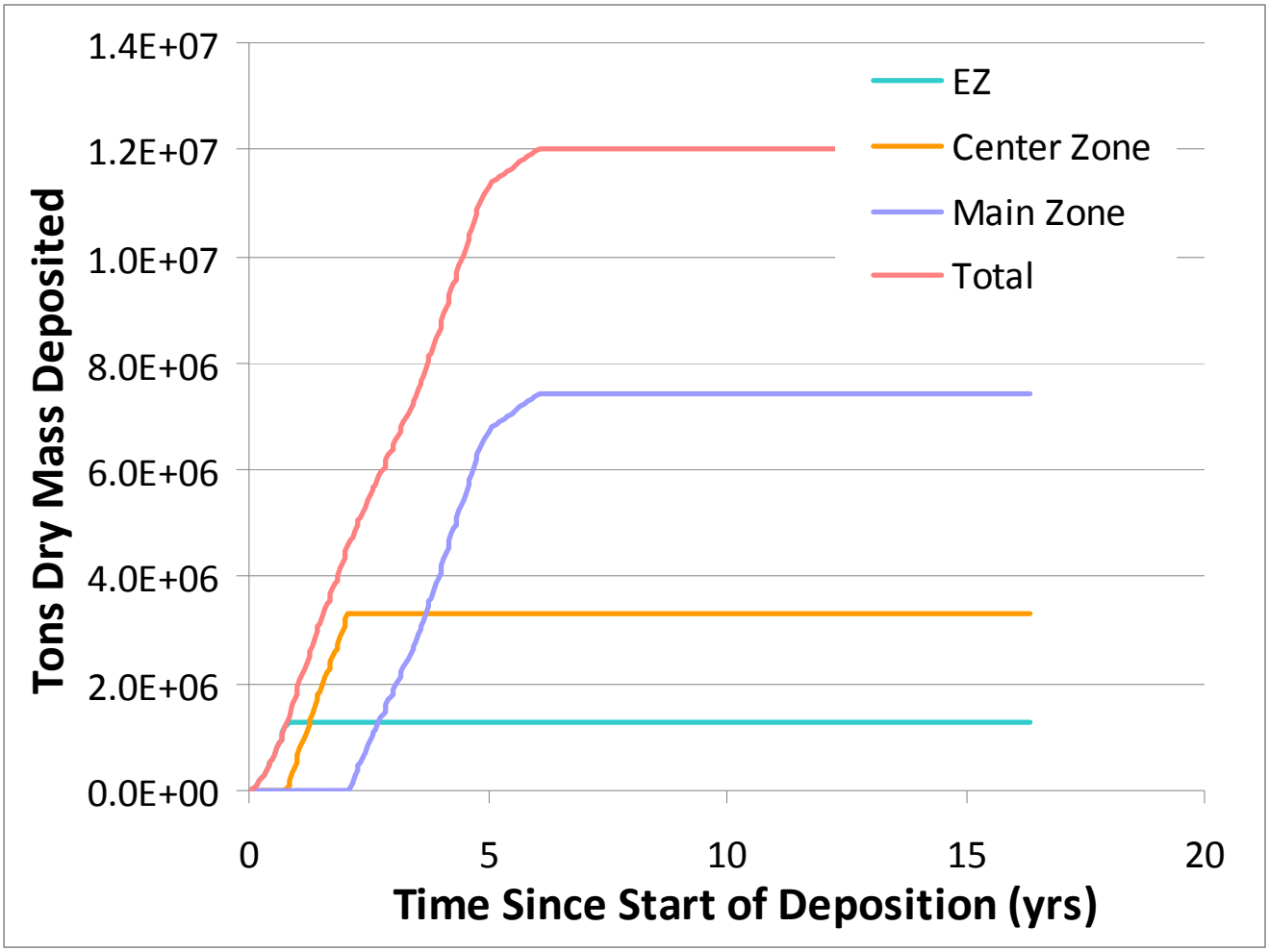

Figure 5.3-2
Dry mass deposition rates applied in FSCONSOL model

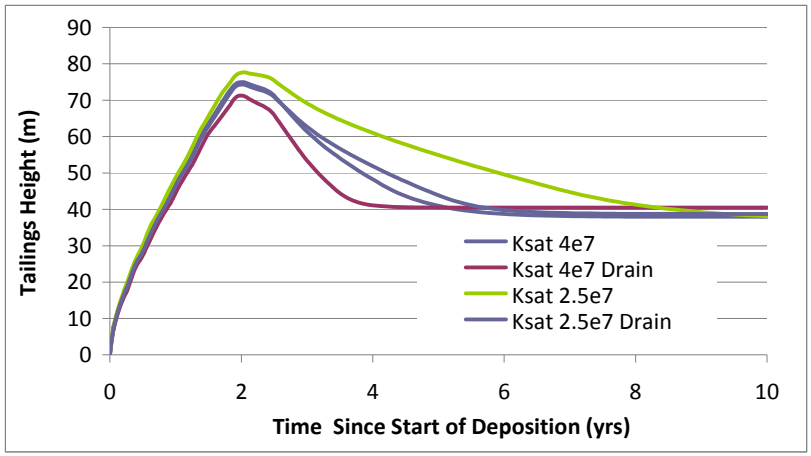

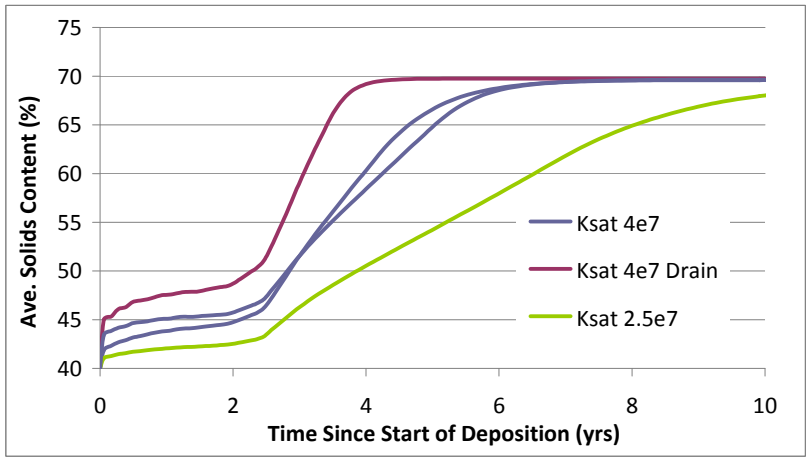

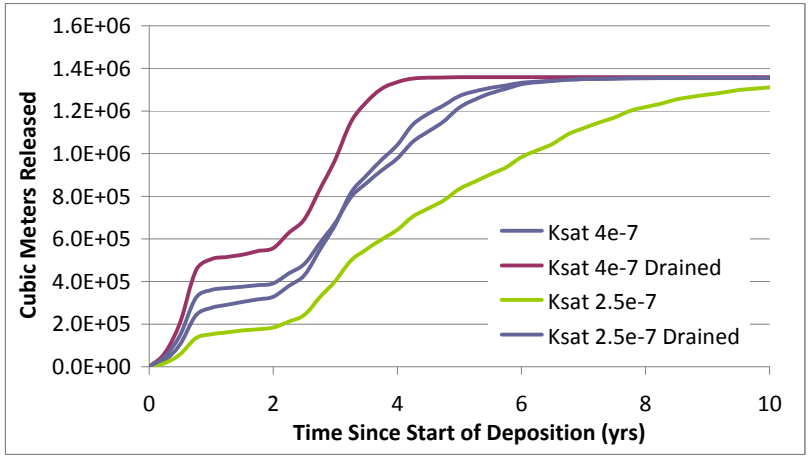

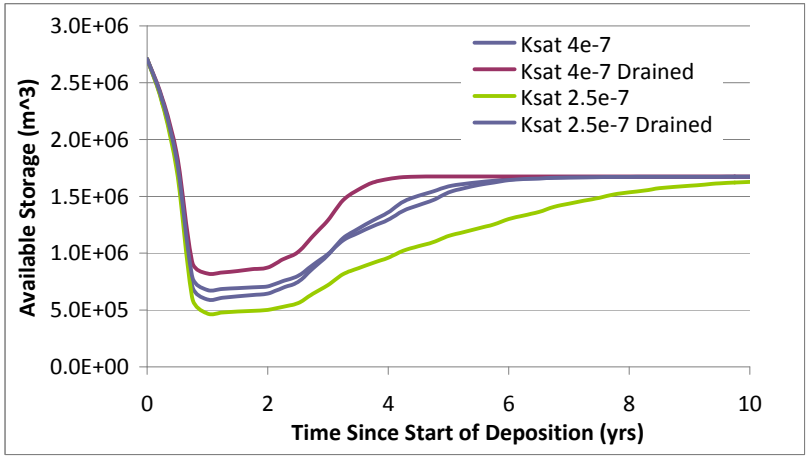

NEWMANS GEOTECHNIQUE

Technical Appendix 5J
Tailings Characterization and Management
Dec., 2011

Figure 5.4-1
East Zone Consolidation and water expulsion results

Kiggavik Project

AREVA

Areva Resources Canada Inc.- P.O Box 9204 – 817 – 45th Street W – Saskatoon – S7K 3X5

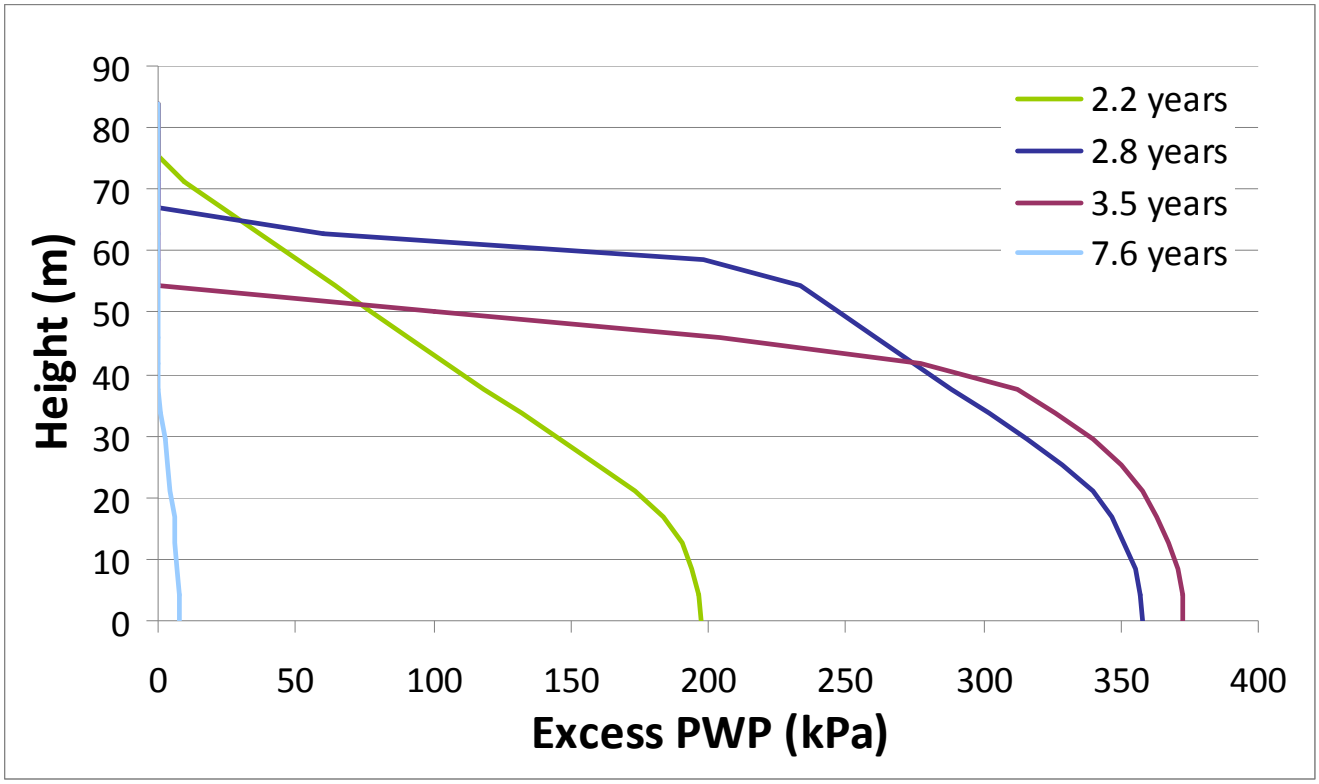

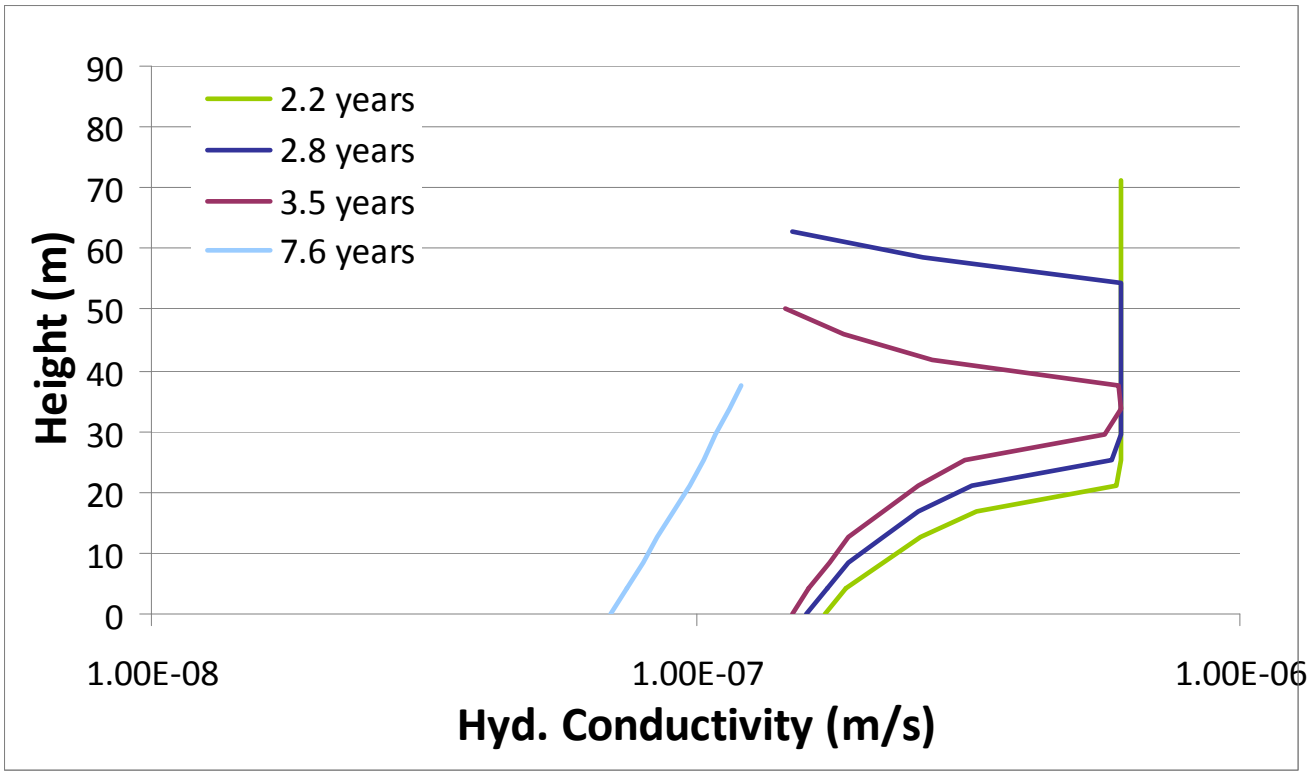

NEWMANS GEOTECHNIQUE

Technical Appendix 5J
Tailings Characterization and Management
Dec., 2011

Figure 5.4-2
Excess pore water pressure and hydraulic conductivity profile in East Zone

Kiggavik Project

AREVA

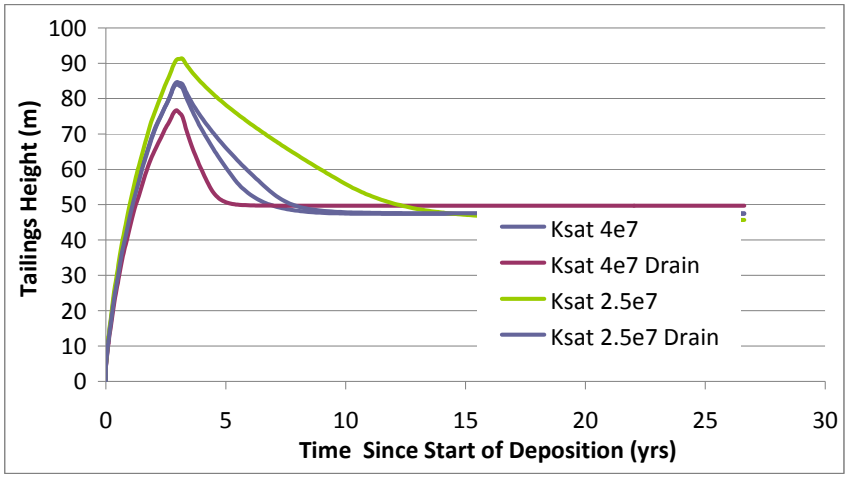

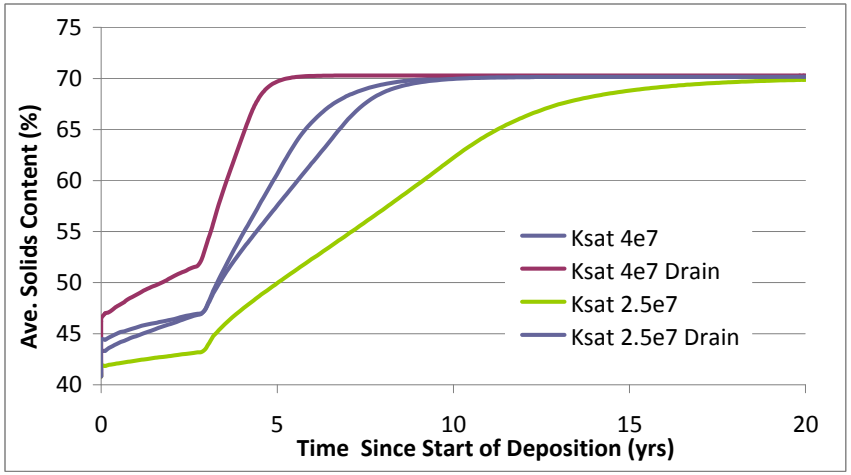

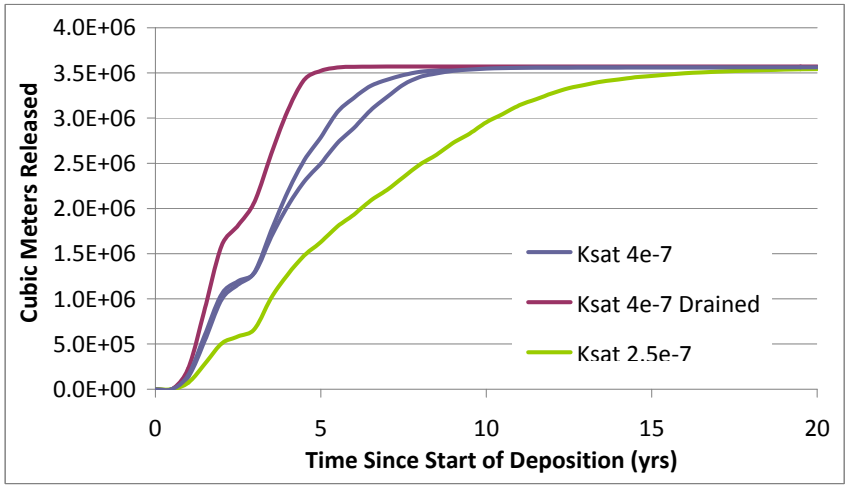

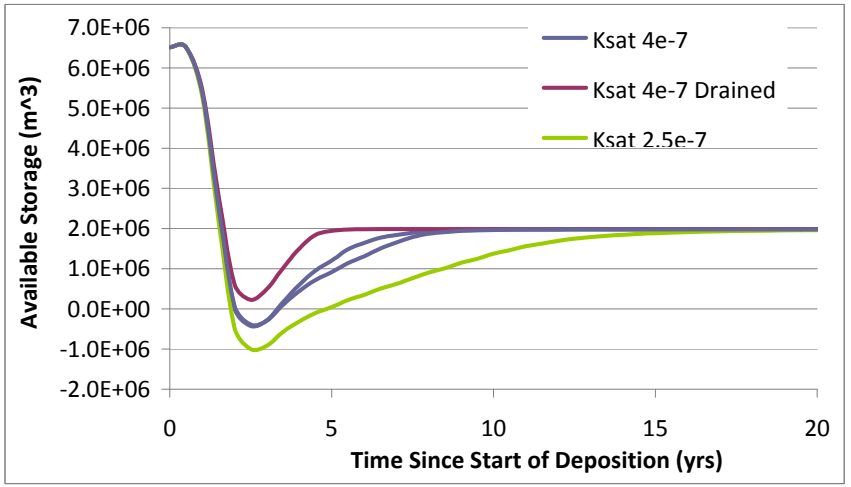

NEWMANS GEOTECHNIQUE

Technical Appendix 5J
Tailings Characterization and Management
Dec., 2011

Figure 5.4-3
Centre Zone Consolidation and water expulsion results

Kiggavik Project

AREVA

Areva Resources Canada Inc.- P.O Box 9204 – 817 – 45th Street W – Saskatoon – S7K 3X5

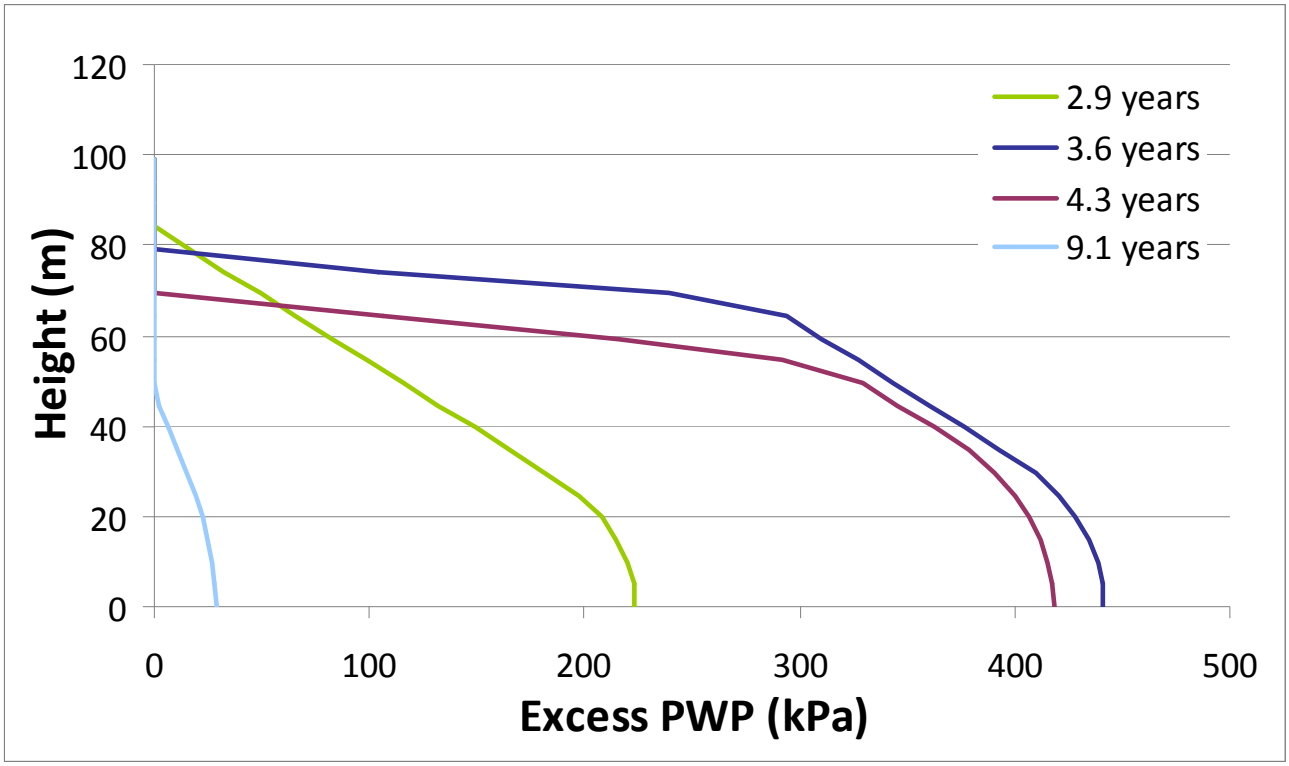

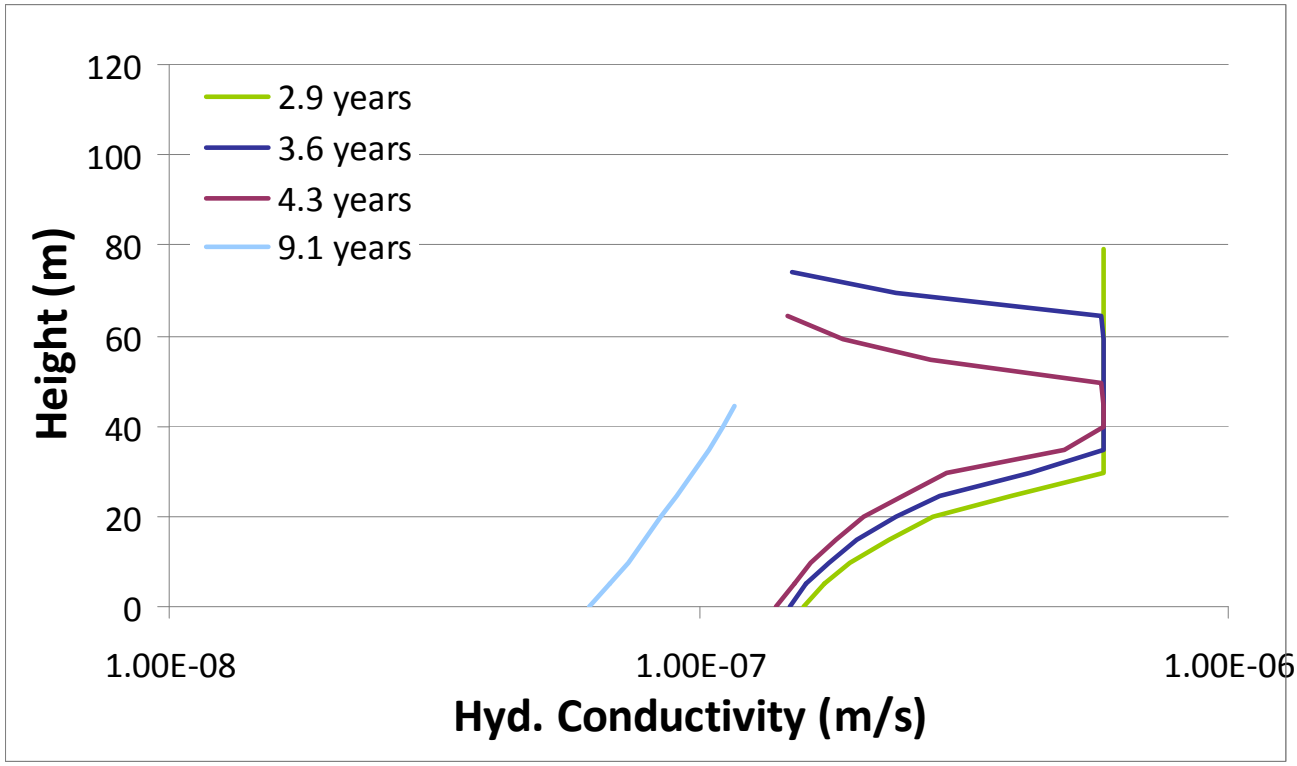

NEWMANS GEOTECHNIQUE

Figure 5.4-4
Excess pore water pressure and hydraulic conductivity profile in Centre Zone

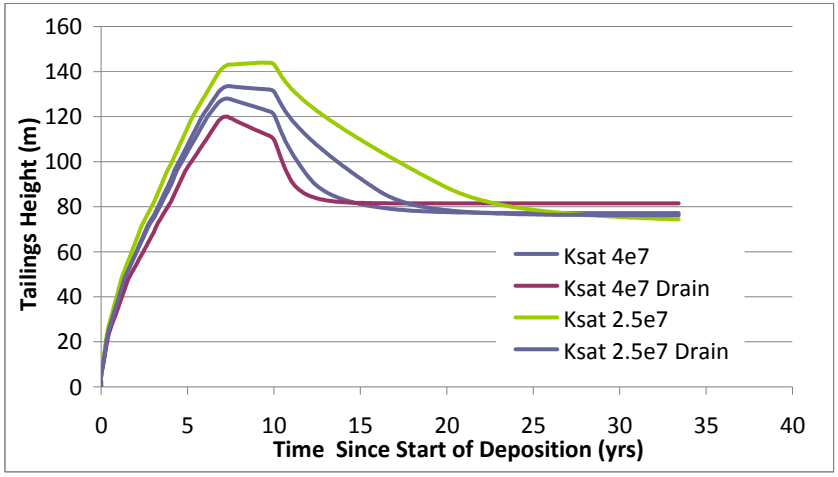

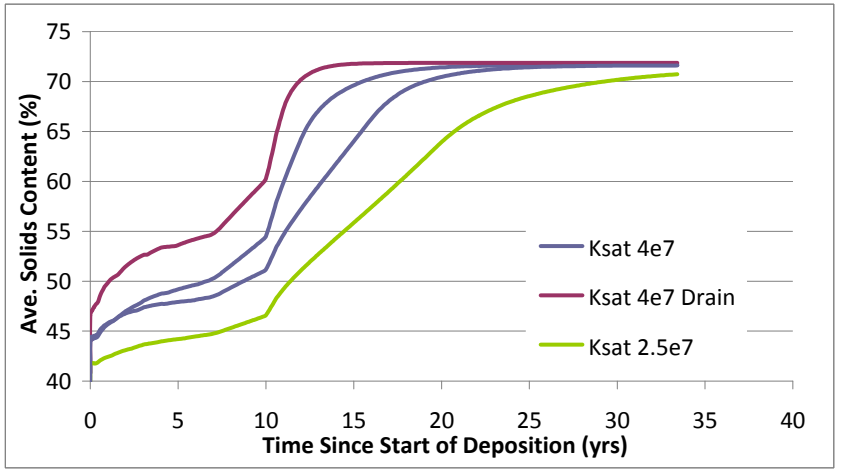

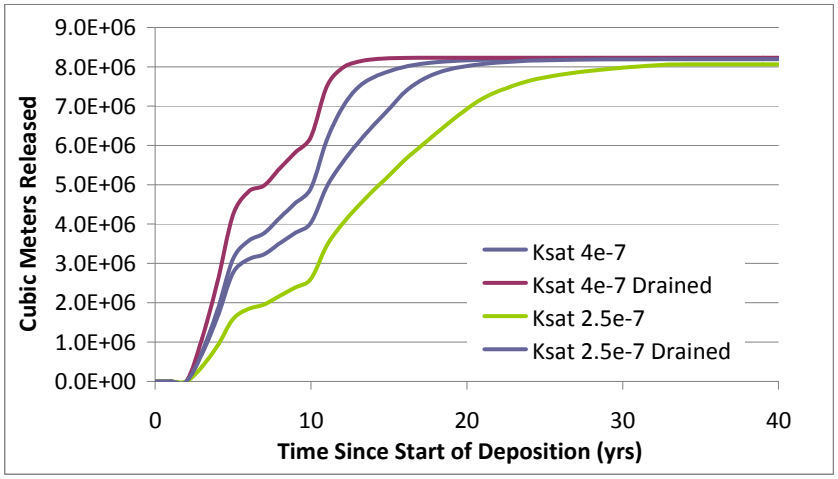

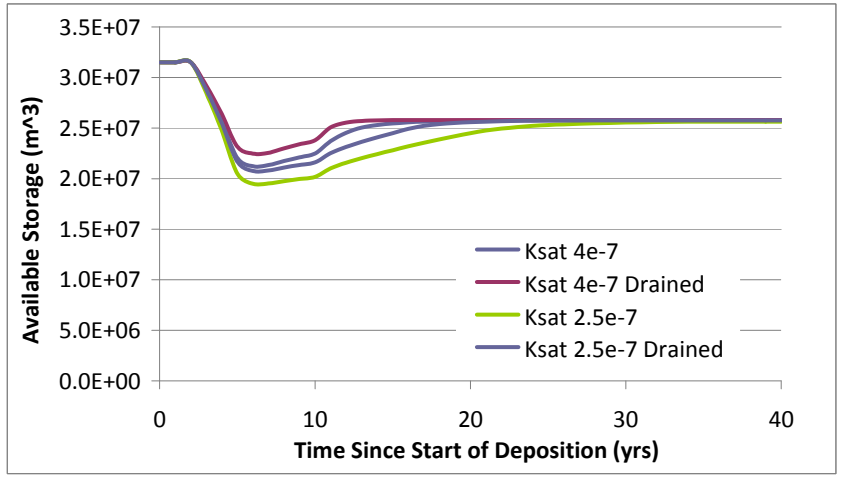

NEWMANS GEOTECHNIQUE

Technical Appendix 5J
Tailings Characterization and Management
Dec., 2011

Figure 5.4-5
Main Zone Consolidation and water expulsion results

Kiggavik Project

AREVA

Areva Resources Canada Inc.- P.O Box 9204 – 817 – 45th Street W – Saskatoon – S7K 3X5

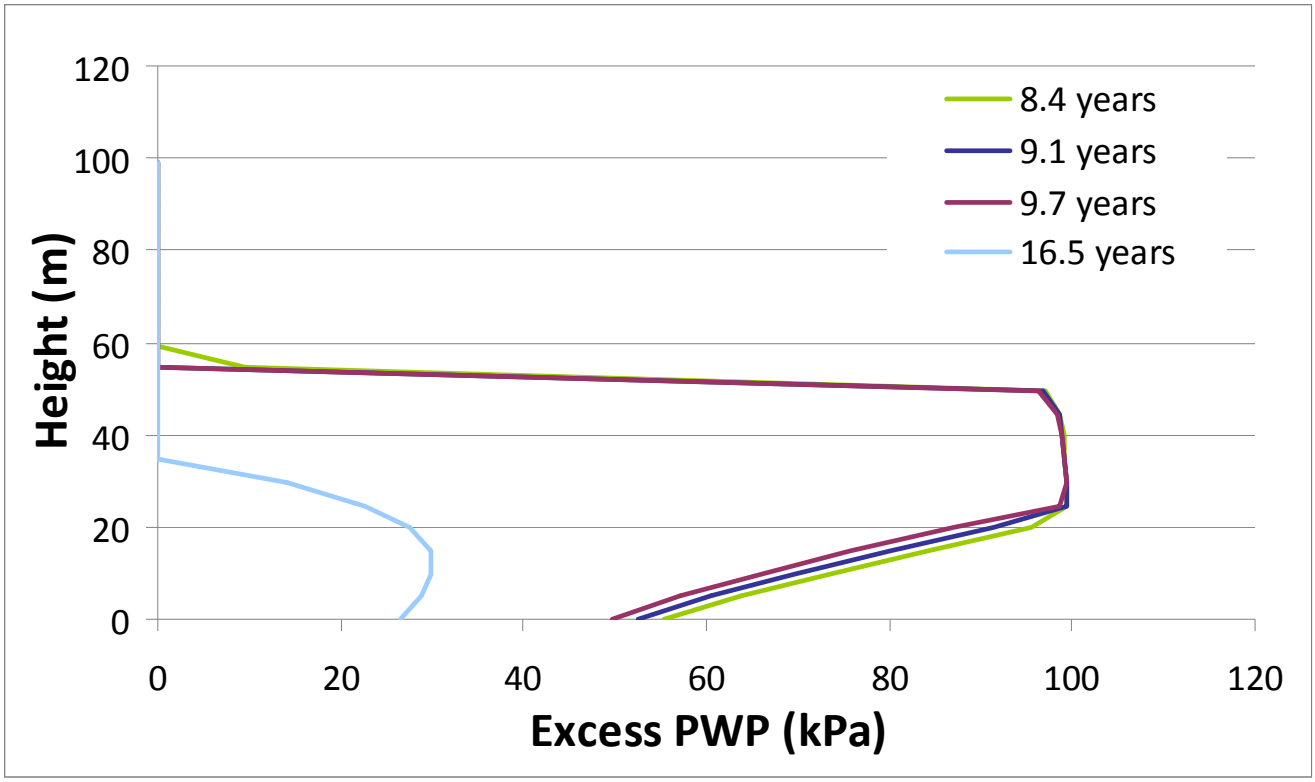

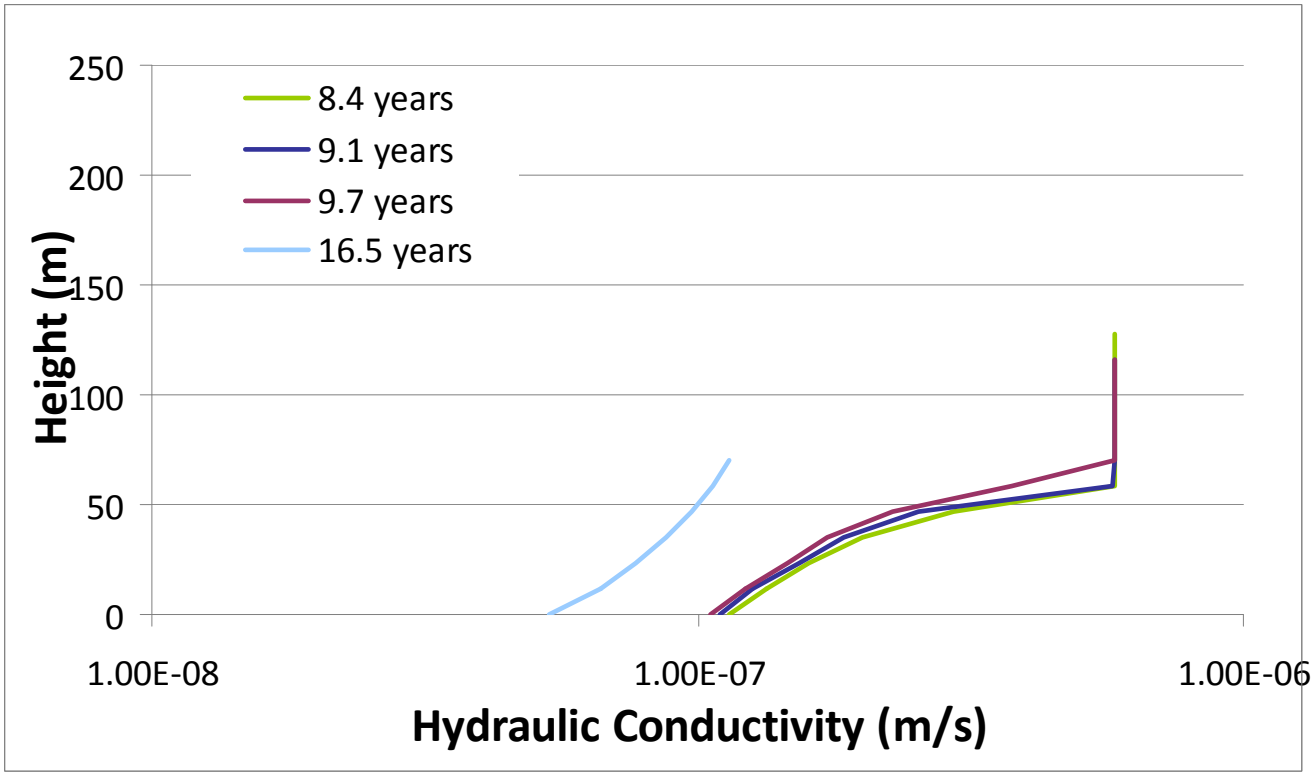

NEWMANS GEOTECHNIQUE

Figure 5.4-6
Excess pore water pressure and hydraulic conductivity profile in Main Zone

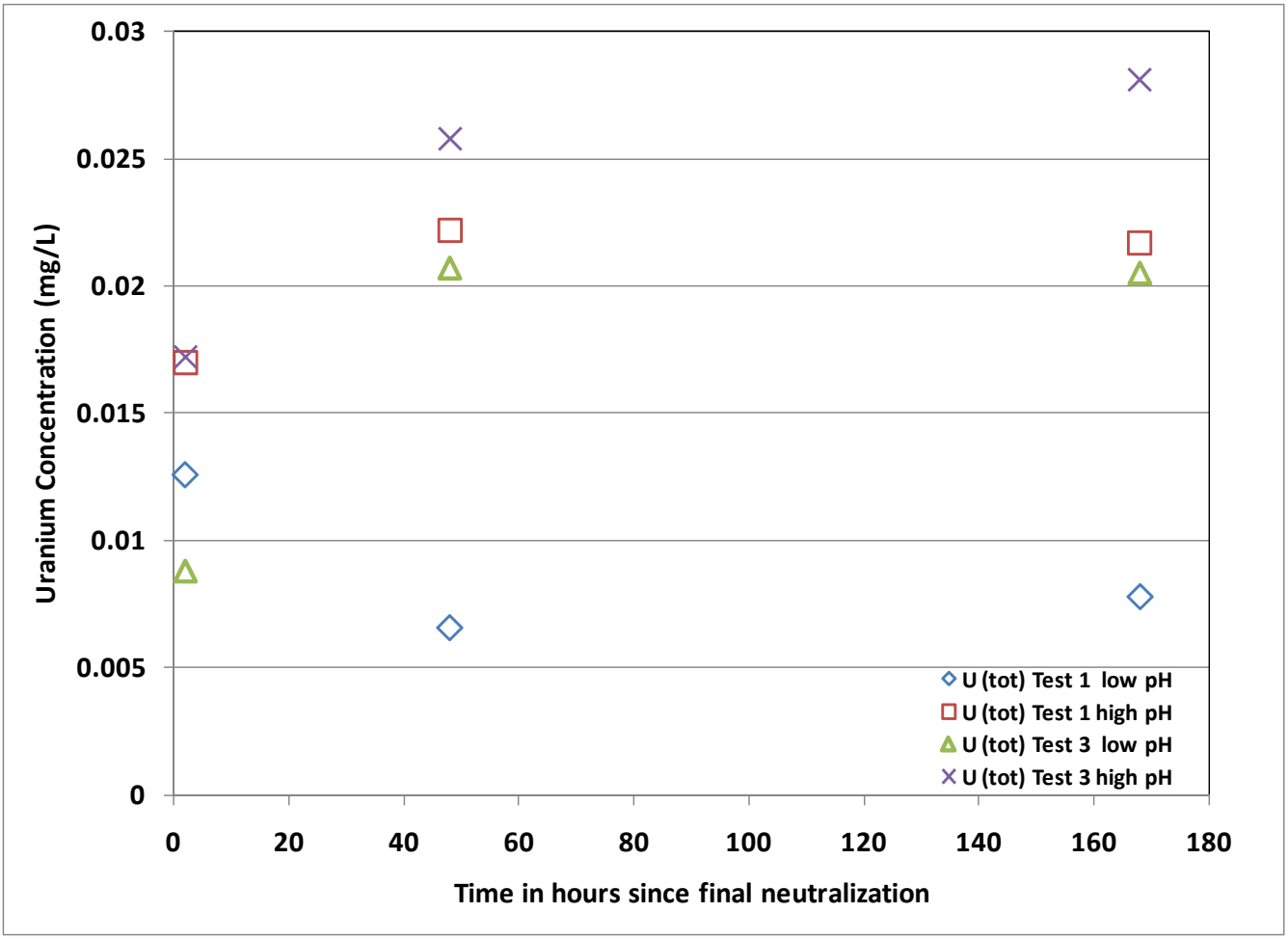

MGC
MAHONEY GEOCHEMICAL CONSULTING

Figure 6.3-1
SGS Lakefield testing - Aging test results for Uranium (Tests 1 and 3)

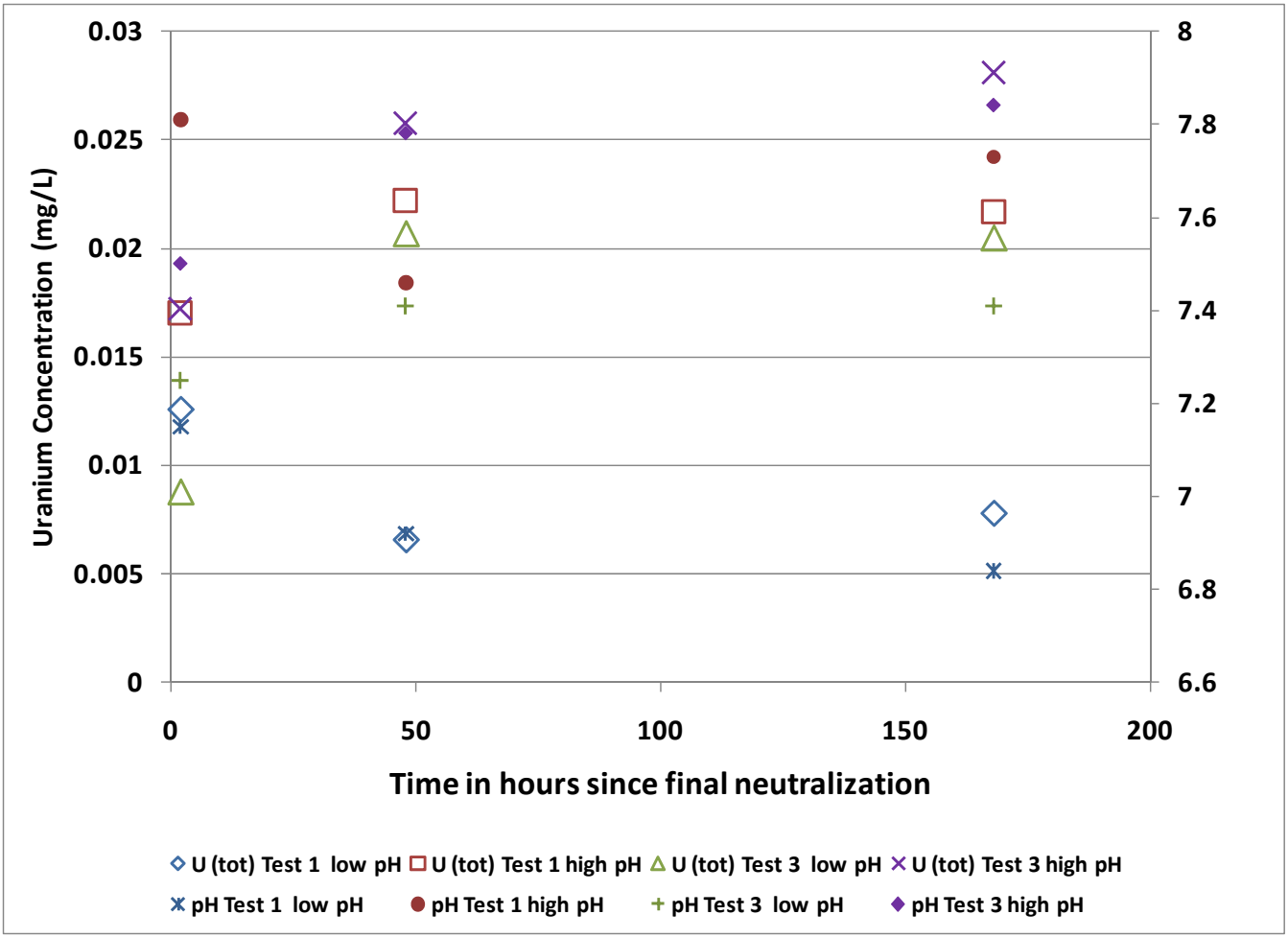

MGC MAHONEY GEOCHEMICAL CONSULTING

Technical Appendix 5J
Tailings Characterization and Management
Dec., 2011

Figure 6.3-2
SGS Lakefield testing - Aging test results; Uranium and pH value versus time

Kiggavik Project

AREVA

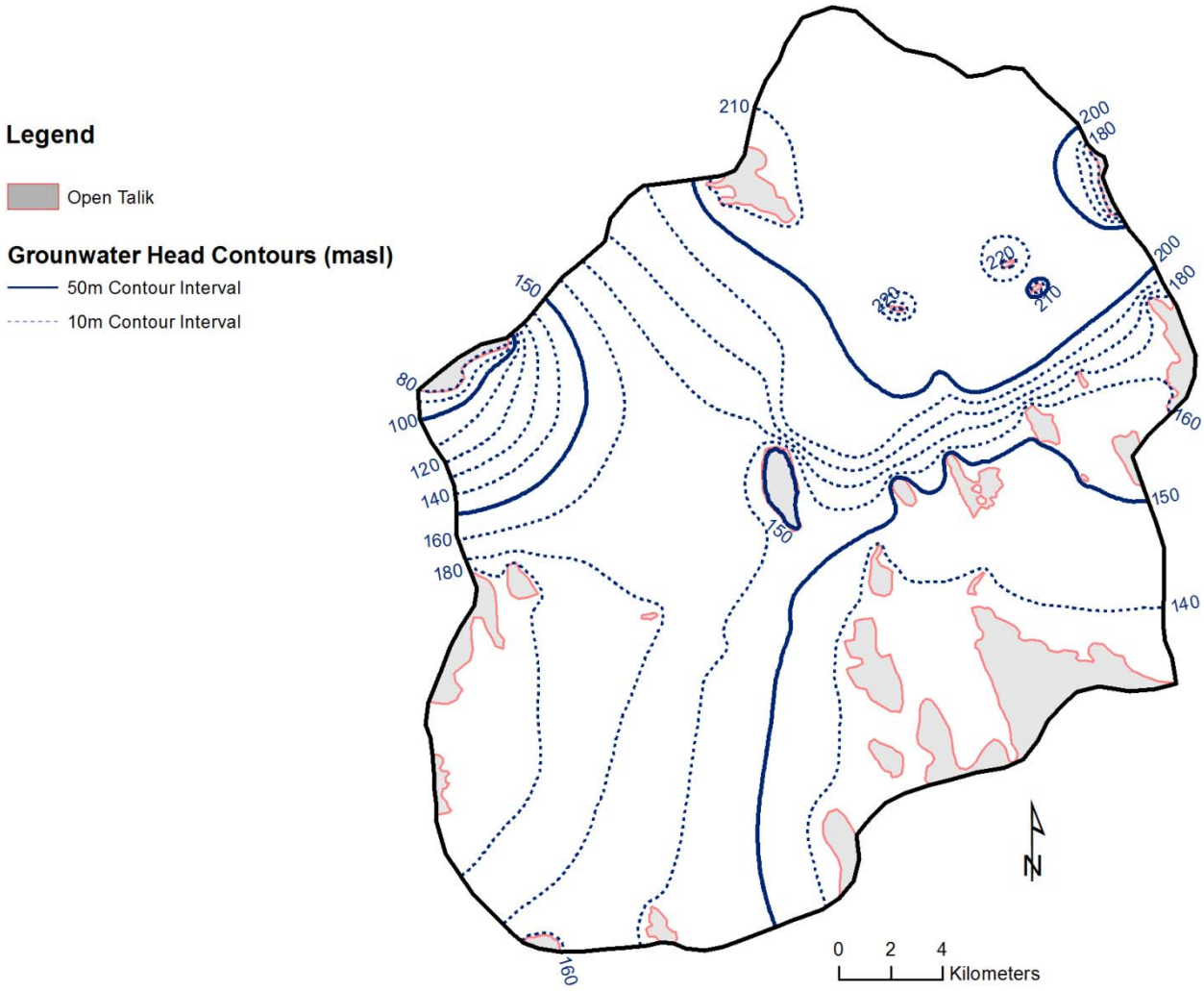

Technical Appendix 5J
Tailings Characterization and Management
Dec., 2011

Figure 7.2-1
Baseline (pre-mining) groundwater flow conditions in the Project area

Kiggavik Project

AREVA

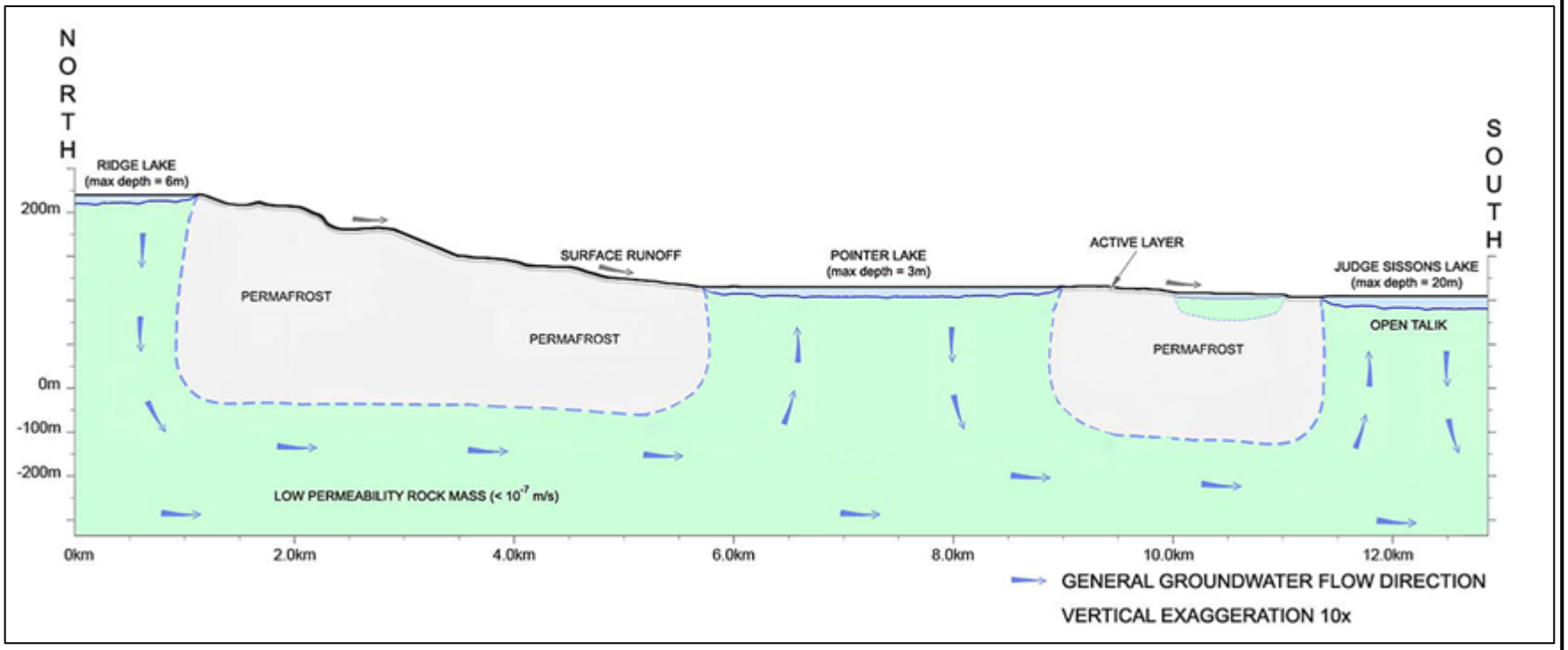

Technical Appendix 5J
Tailings Characterization and Management
Dec., 2011

Figure 7.2-2
Conceptual model of groundwater flow in the Kiggavik area

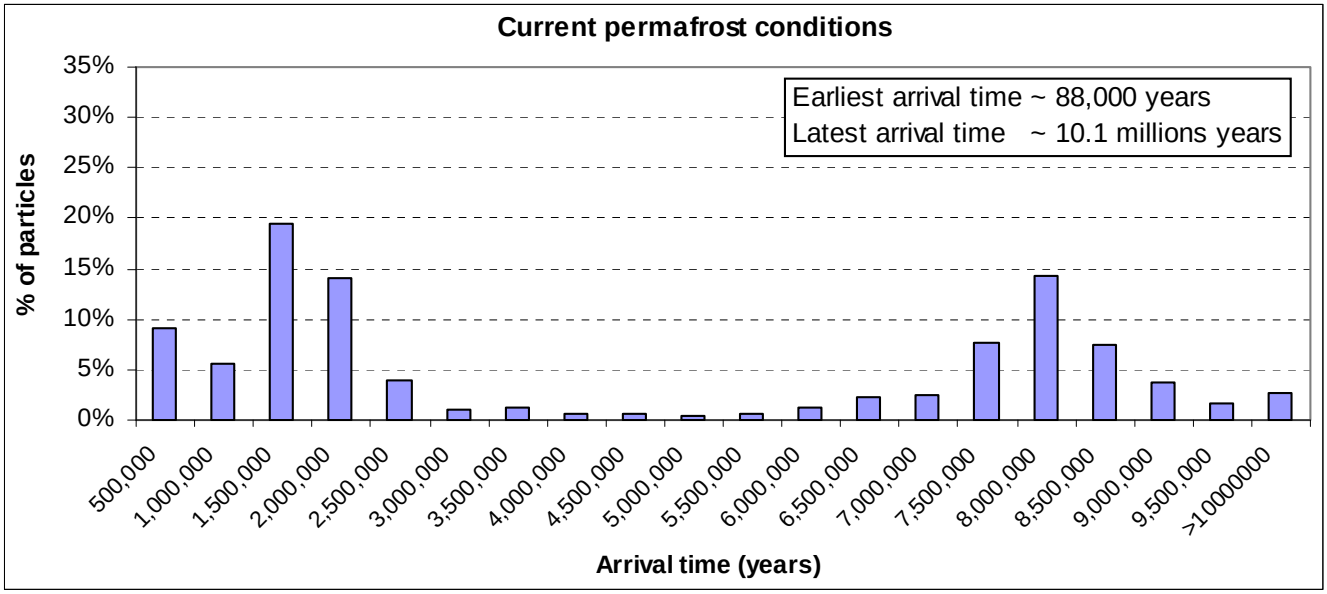

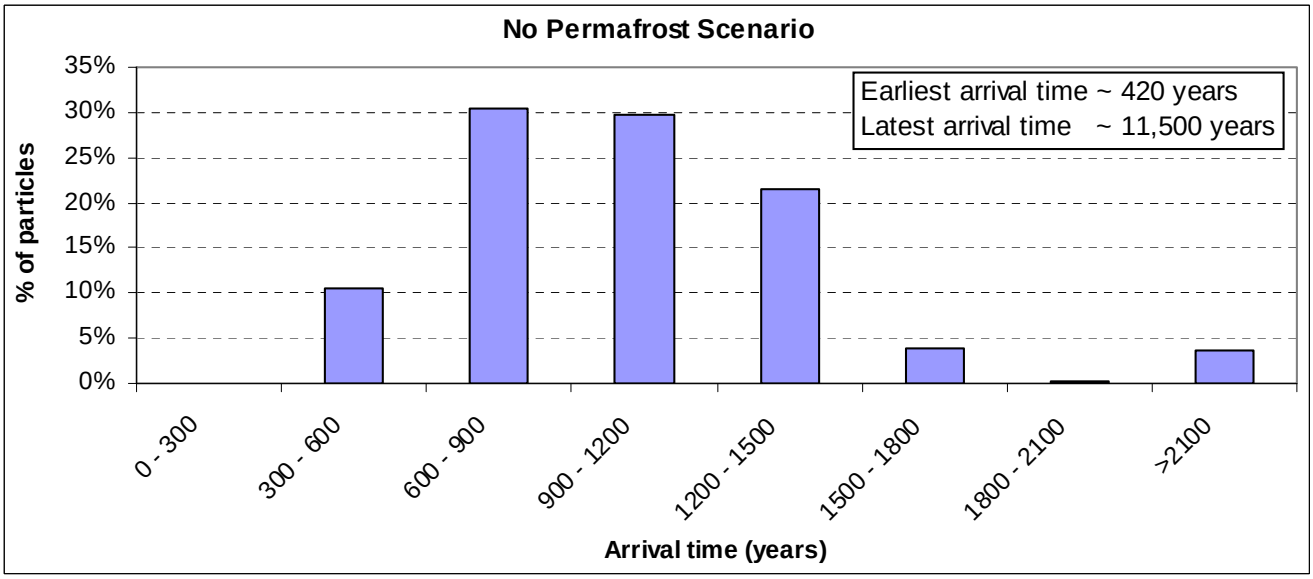

Figure 7.2-3
Histogram of particle arrival times to Pointer Lake

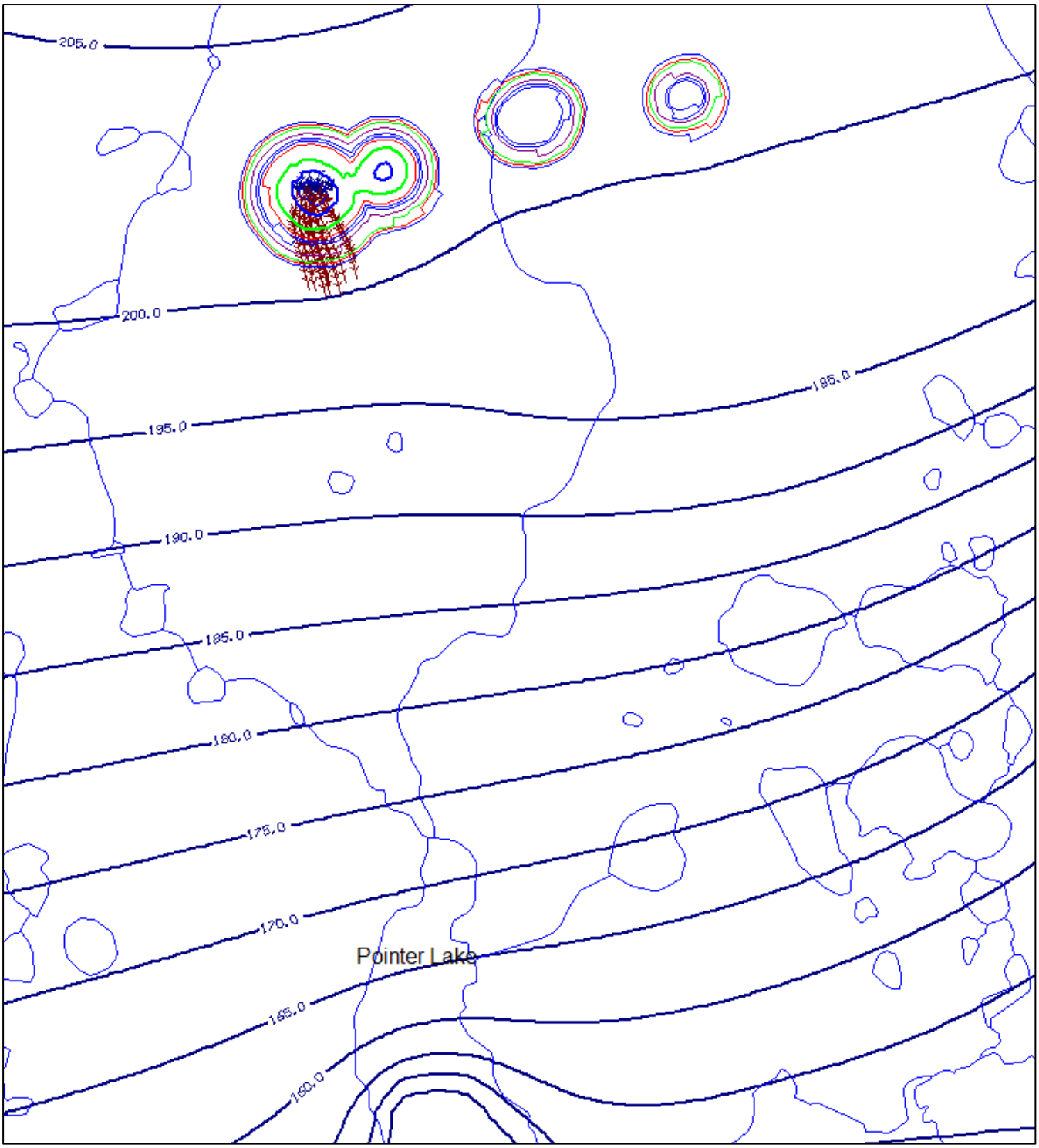

Technical Appendix 5J
Tailings Characterization and Management
Dec., 2011

Figure 7.3-1
Pathlines from tailings for current permafrost conditions (pathlines for 10000 years, ticks every 1000 years)

Kiggavik Project

AREVA

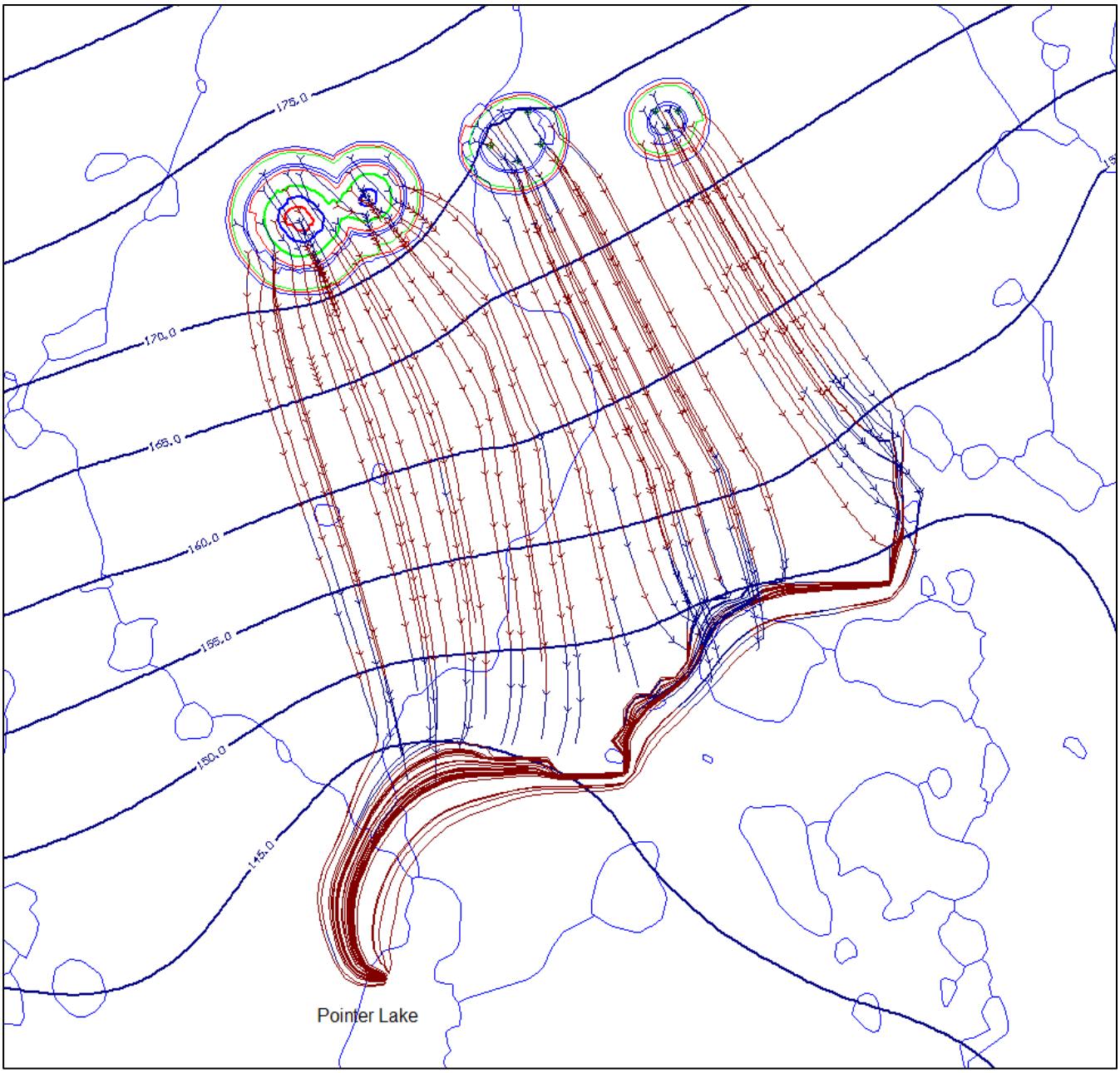

Technical Appendix 5J
Tailings Characterization and Management
Dec., 2011

Figure 7.3-2
Pathlines from tailings for the no permafrost scenario (pathlines for 1000 years, ticks every 100 years)

Kiggavik Project

AREVA

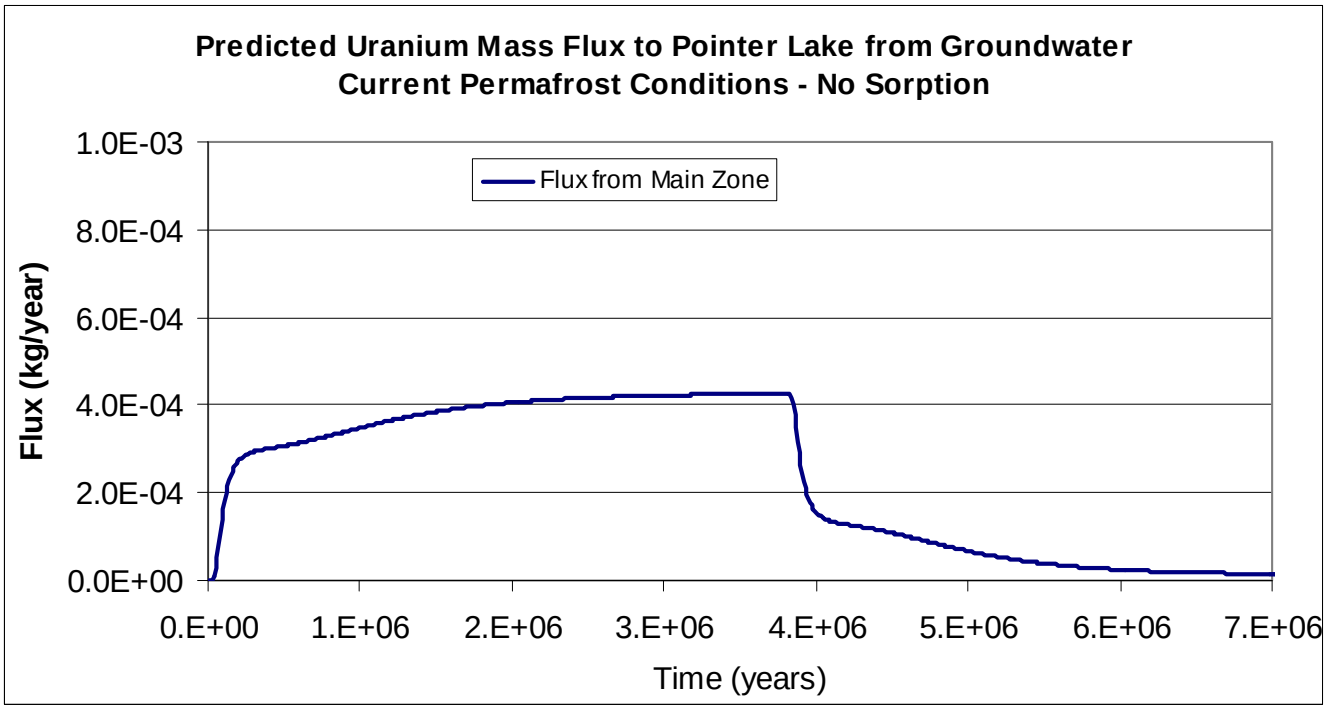

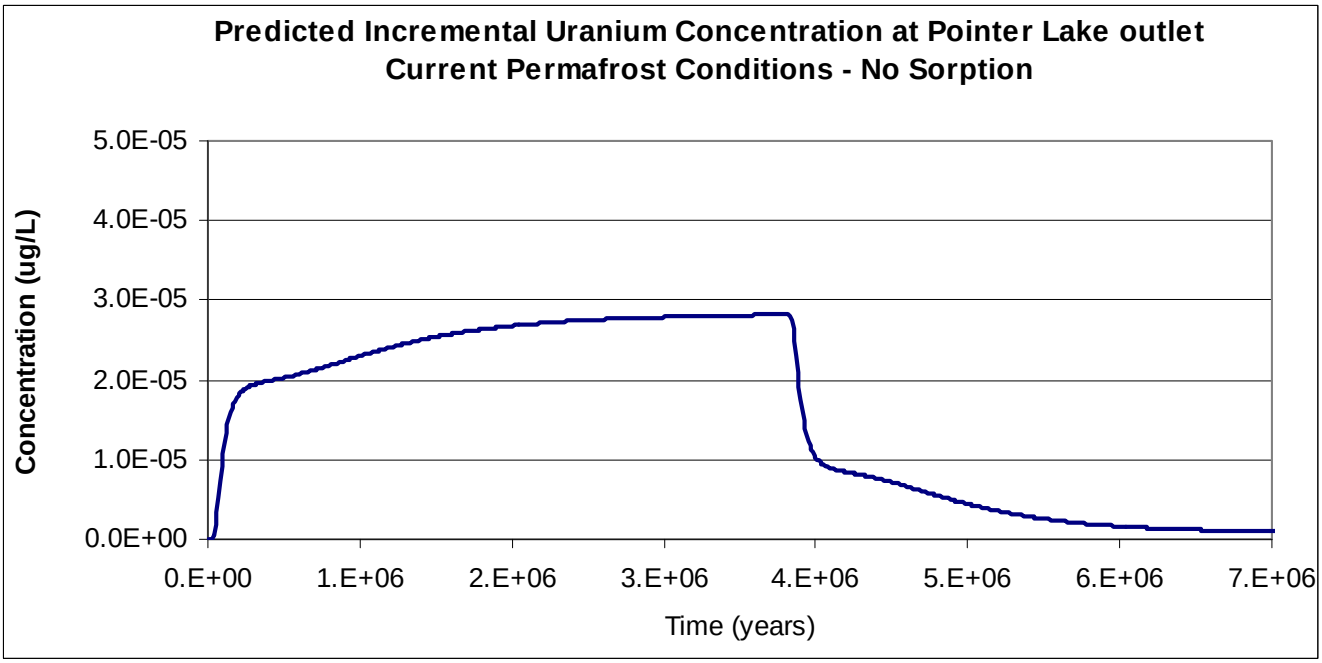

Figure 7.3-4
Predicted uranium mass flux to Pointer Lake and resulting incremental concentrations in Pointer Lake Current Permafrost, no sorption

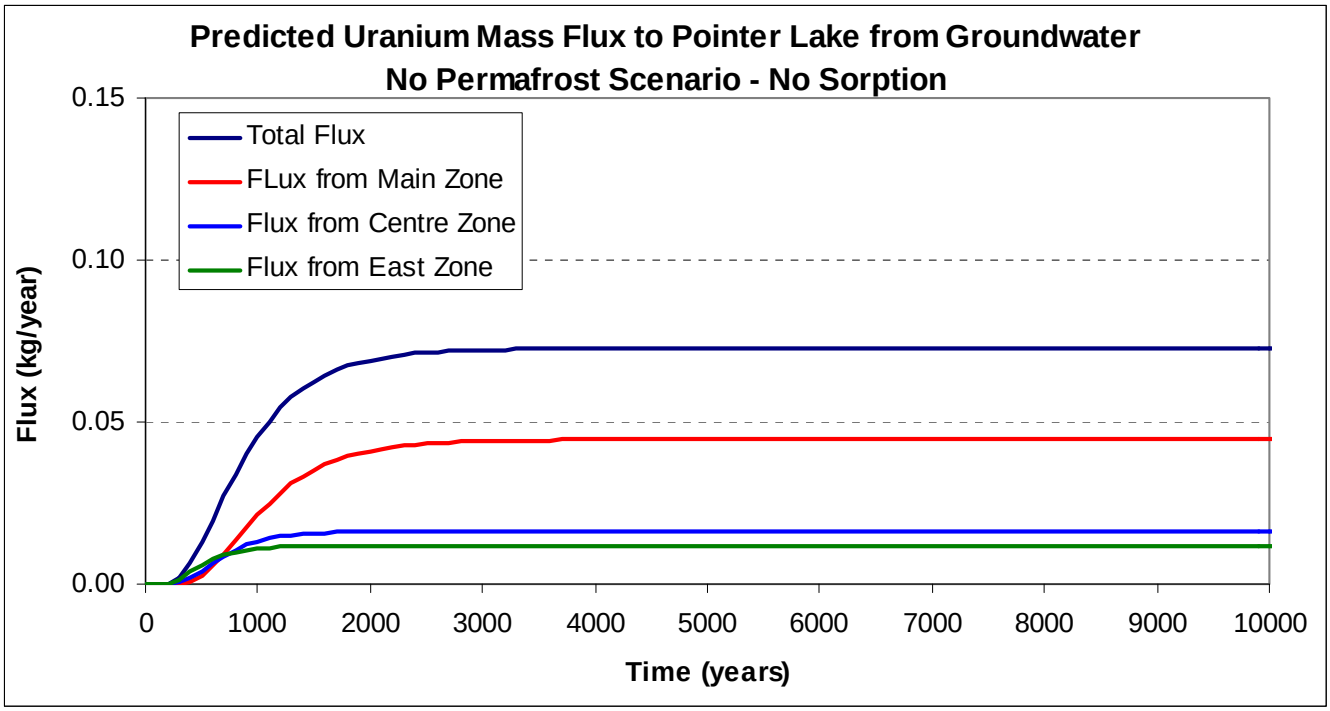

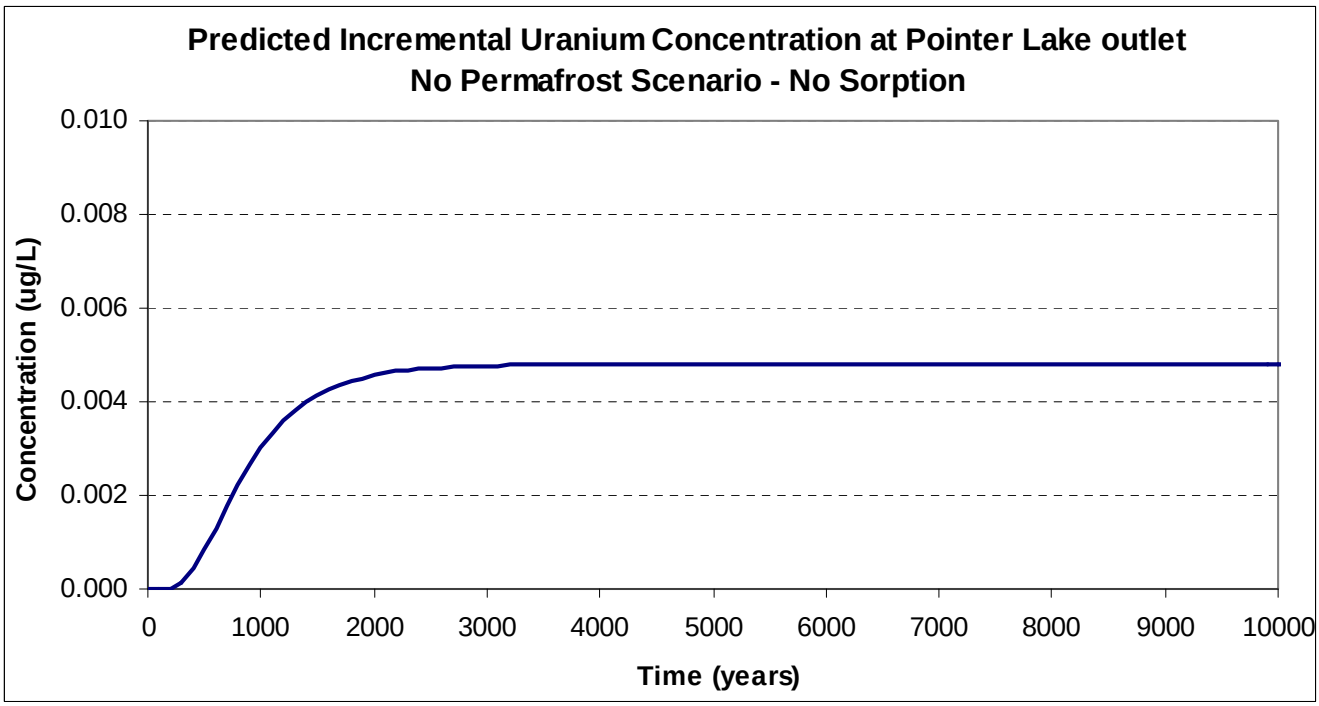

Figure 7.3-5
Predicted uranium mass flux to Pointer Lake and resulting incremental concentrations in Pointer Lake
No Permafrost, no sorption

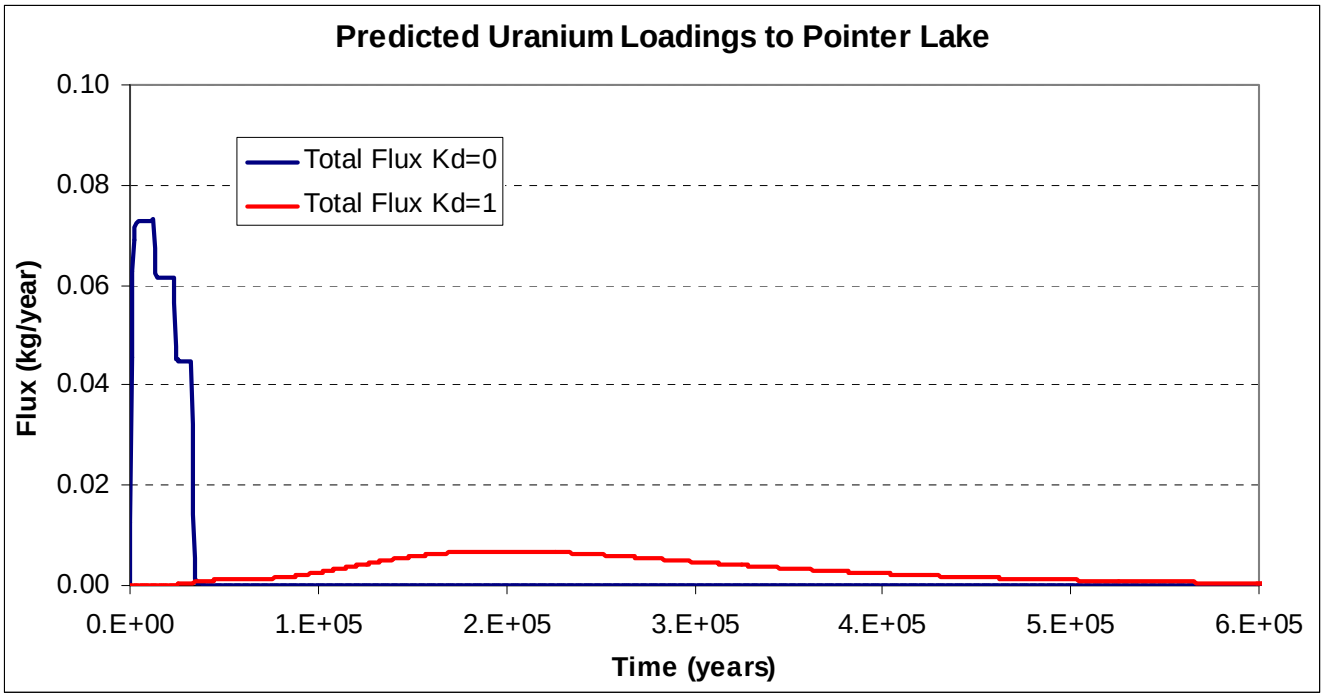

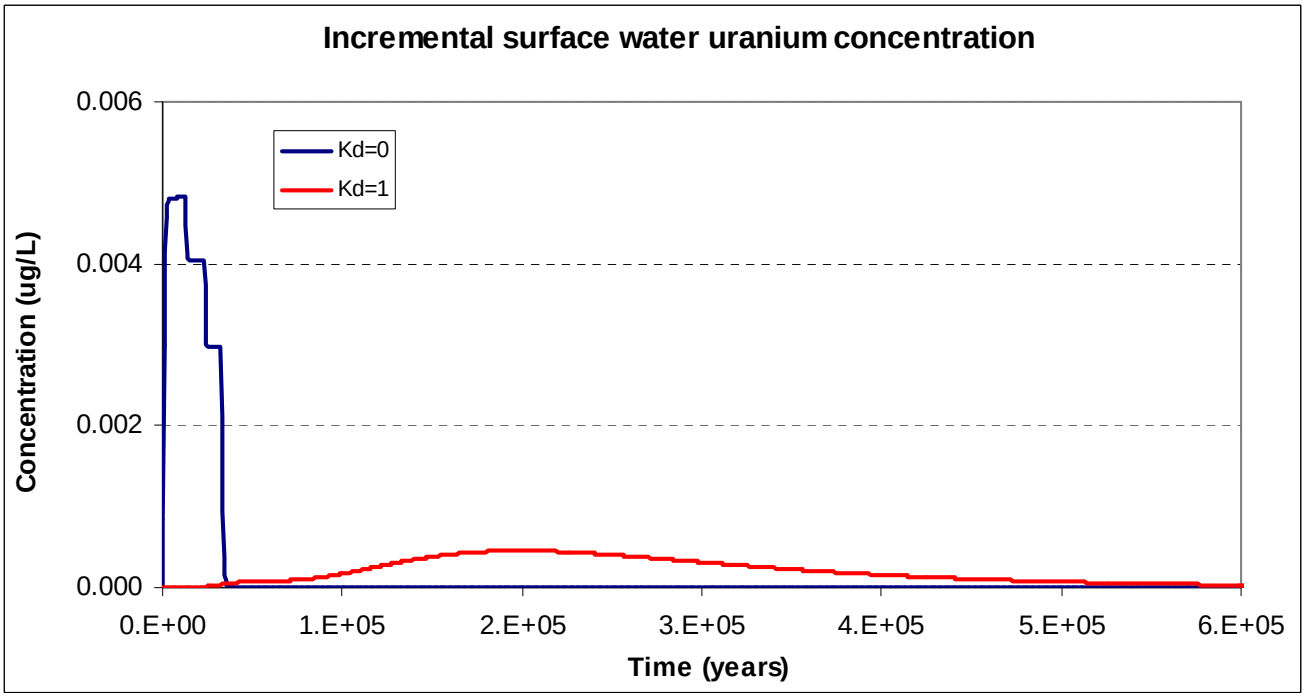

Technical Appendix 5J
Tailings Characterization and Management
Dec., 2011

Figure 7.3-6
Impact of sorption assumptions on predicted uranium transport to Pointer Lake - No permafrost scenario

Attachment A

Tailings Hydraulic Conductivity – Sensitivity Analysis

As part of the process in understanding how to best represent the wide scatter in material properties as they vary spatially throughout the pit, a comparison of water expulsion from a simple one-dimensional column with initial excess pore water pressure was carried out. Three different conductivity distribution conditions were applied:

- a homogeneous value equal to the median conductivity of all measured points,
- a randomly assigned log-normal distribution with the median conductivity and an allowable range of +/- 2 orders of magnitude,
- and a randomaly assigned log-uniform distribution with a median conductivity and 2 order magnitude allowable range.

The conductivities was assigned randomly throughout the domain, for each distribution pattern, as shown in the figure A1 below.

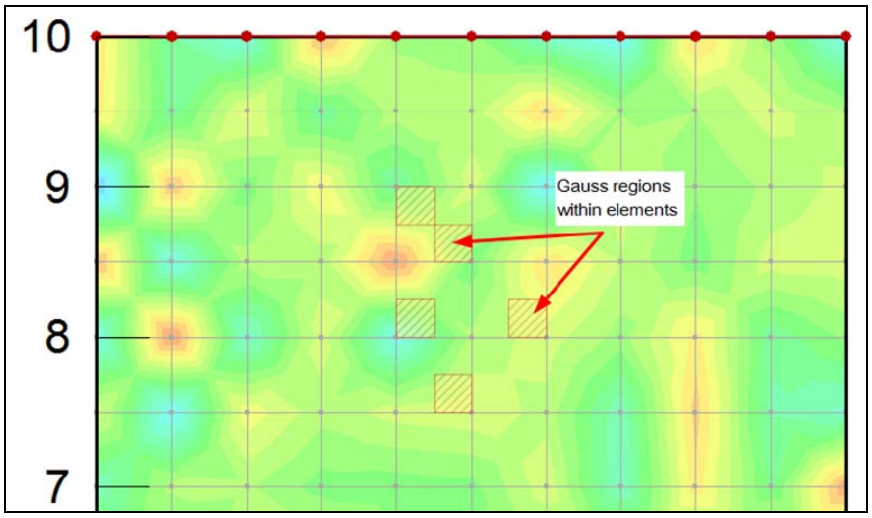

Figure A1: Example of random assignment of conductivity to model elements

Figure A2 shows the computed water dissipation volumes as a function of time for the three cases considered in the test model. Both the log-normal and log-uniform distribution cases show faster consolidation than the homogeneous case with the median conductivity applied.

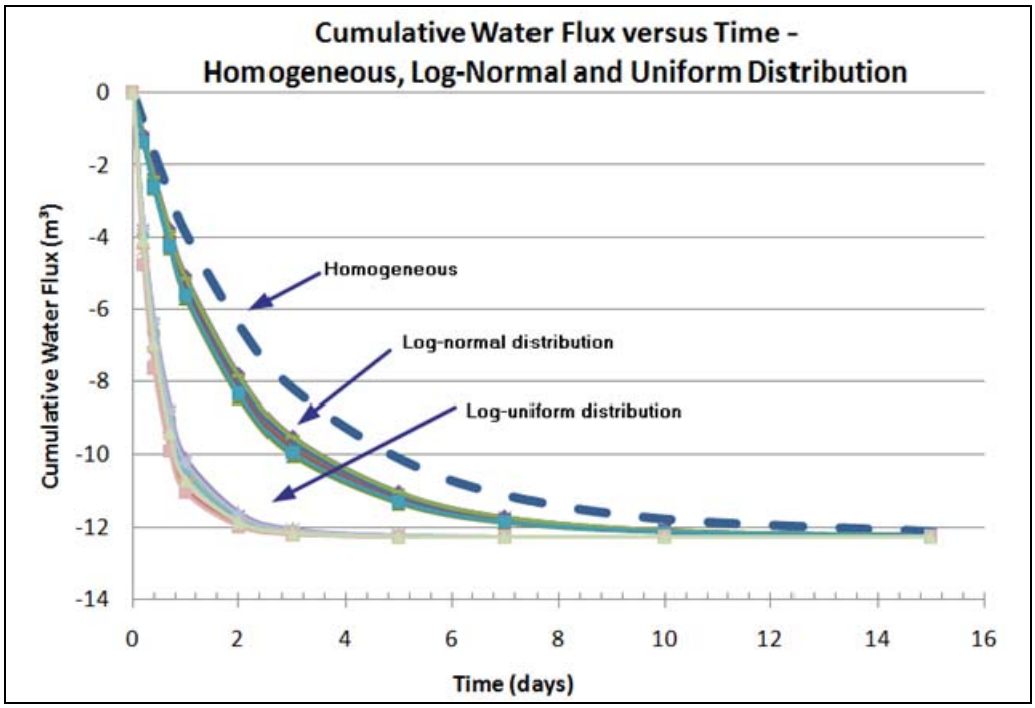

Figure A2 Sensitivity of consolidation to distribution of conductivity

Closer inspection of the results helps explain why this is. Figures A3 and A4 show all model data points and how the conductivity was randomly assigned to the model element regions. Figure A3 is for an assumed log-normal distribution and Figure A4 is for a log-uniform distribution.

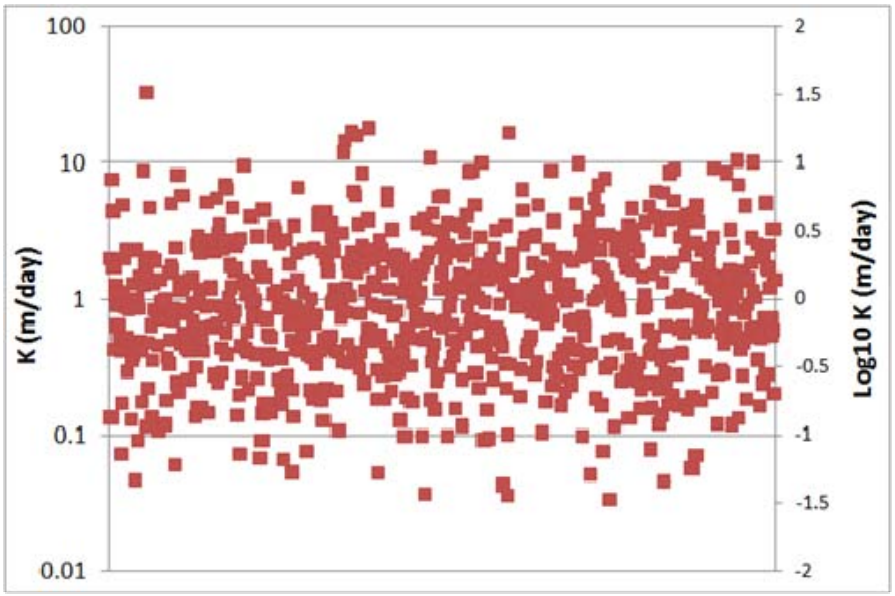

Figure A3 All model data point conductivities with a log-normal distribution.
K_{median} = 1m/day, K_{avg}=1.6 m/day

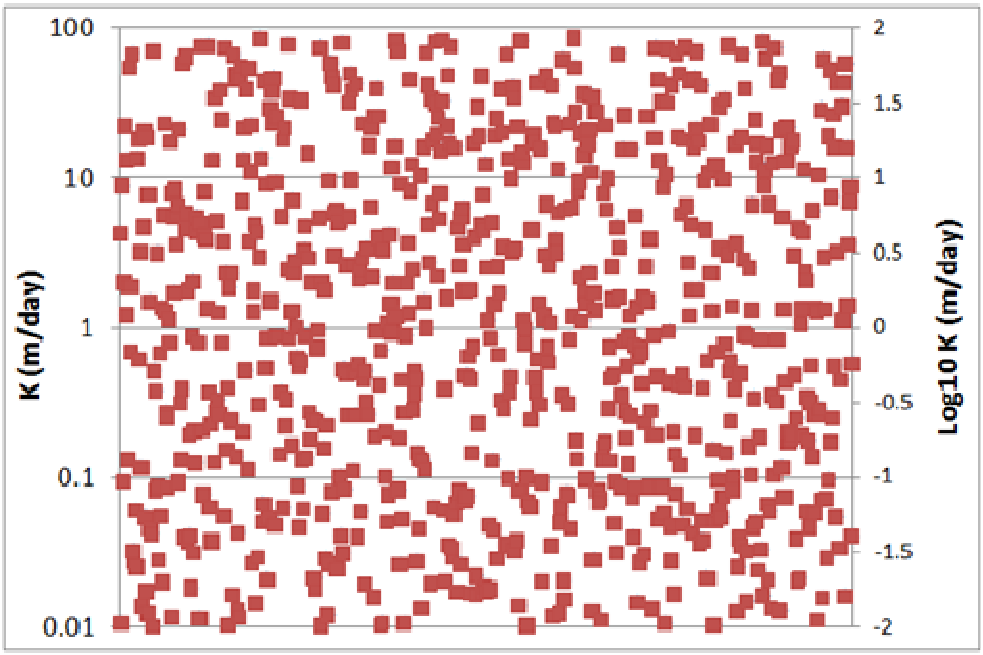

Figure A4 All model data point conductivities with a log-uniform distribution. K_{median} = 1m/day, K_{avg}=9.4 m/day

For the log-normal case, while the median input conductivity is 1 m/day, the average of all points is computed to be 1.6 m/day. For the log-uniform case, the median is the same 1 m/day, but the average of the points is now 9.4 m/day. The implication of this is that the knowledge of a random distribution of conductivity within the pit allows the assumption to be made that the average equivalent conductivity of the over-all pit is a higher value than the measured median conductivity. We know that the JEB pit conductivity values range between 2×10^{-9} m/s and 2×10^{-5} m/s and has a median of about 2×10^{-7} m/s. Using the findings of the random distribution study, it can be concluded that the likely in-pit hydraulic performance can be expected to behave as if the average equivalent homogeneous conductivity is somewhat higher than the mean.

Attachment B

Consolidation Theory

CONSOLIDATION MODEL

The computer program FSCONSOL was selected to simulate the consolidation behaviour of the deposited tailings in the JEB TMF. FSCONSOL implements a volume fraction theory of one-dimensional, finite strain, nonlinear consolidation of loaded and accumulating layers of a saturated soil. FSCONSOL is a commercial computer program available from "GWP Software Inc. of Edmonton, Alberta".

Nonlinear Finite Strain Theory

A brief overview of the nonlinear finite strain theory for one-dimensional consolidation of saturated soil by Dr. R. L Schiffman, Vlasta Szavits-Nossan and John M. McArthur is presented in the following section.

The nonlinear finite strain theory was developed within the Lagrangian (material) coordinate system. The theory considered:

- conservation of linear momentum and the equilibrium of the solid and pore water;
- conservation of pore water mass; and,
- conservation of solid mass.

Constitutive Equations

The constitutive equations in the nonlinear finite strain theory include the material functions, the coupling equations and the equations of state.

There are two material functions: the void ratio - effective stress relationship and the void ratio - hydraulic conductivity relationship. In both instances the assumption of homogeneity and monotonic loading requires that void ratio, e, is a single valued function of the effective stress, s' and the hydraulic conductivity, k.

Equations for void ratio - effective stress relationship include:

$$e = f(s') \quad (1.1)$$

$$a_v = -\frac{de}{ds'} \quad (1.2)$$

Where,

e : void ratio

s' : effective stress

f(s') : function of effective stress

a_v : coefficient of compressibility

Equation for void ratio - hydraulic conductivity is:

$$k = f(e) \quad (1.3)$$

Where,

k : hydraulic conductivity

f(e) : function of void ratio

Coupling equations are the pore water pressure equation, the effective stress principle and the flow equation. The pore water pressure equation is:

$$u(\xi, t) = u_w(\xi, t) + \gamma_w \xi + C \quad (1.4)$$

Where,

u : excess pore water pressure

u_w : pore water pressure

ξ : Lagrangian coordinates a function of (a,t) satisfying x(a,0)=a

t : time

γ_w : unit weight of water

C : constant, determined from the boundary condition

The pore water pressure equation as defined by Lamb Whitman 1969 and Gibson et al. 1989 is:

$$u_e = u_w - u_{ss} \qquad (1.5)$$

Where,

u_e : excess pore water pressure

u_w : pore water pressure

u_{ss} : steady state pore water pressure

In a linear theory when the hydraulic conductivity is a constant, the static pore water pressure given by (3,4) is a special case of u_{ss}. However, when the hydraulic conductivity is a function of the void ratio, the steady state pore water pressure is also a function of the void ratio (Schiffman et al. 1994).

The effective stress principle equation based on the effective stress equation by Terzaghi 1943 is:

$$s' = s^{(s)} + (n-1)u_w \qquad (1.6)$$

Where,

s' : effective stress

$s^{(s)}$: volume averaged stress

n : porosity

The flow equation is the Darcy-Gersevanov relationship which is Darcy's law modified by Gersevanov (1934):

$$v_w - v_s = -\frac{k(e)}{n\gamma_w}\frac{\partial u}{\partial \xi} \quad (1.7)$$

Where,

v_w : seepage velocity of the pore water

v_s : velocity of the solid

k(e) : hydraulic conductivity as a function of void ratio

The Equations of State are:

γ_w : constant

γ_s : constant

These underly the physical assumption that both solid and pore water are incompressible.

Governing Equations

Derivation of the governing equations was based on the conservation of mass, continuity of the volume of solids and the continuity of the mixture. The governing equation takes the form of:

$$\frac{\partial}{\partial a}\left[\frac{k(e)}{\gamma_w a_v(e)}\left(\frac{1+e_0}{1+e}\right)\frac{\partial e}{\partial a}\right] - f(e)\frac{\partial e}{\partial a} = \frac{1}{1+e_0}\frac{\partial e}{\partial t} \quad (1.8)$$

where the self weight term is:

$$f(e) = \left(\frac{\gamma_s}{\gamma_w} - 1\right)\frac{\partial}{\partial e}\left[\frac{k(e)}{1+e}\right] \quad (1.9)$$

which is the volume fraction formulation of the nonlinear, finite strain theory of one-dimensional consolidation.

Attachment C

Geochemical Evaluation of Uranium and Other Constituents in Barren Stream and Neutralized Tailings

(Mahoney Geochemical Consulting, November 2011)

Geochemical Evaluation of Uranium and Other Constituents in Barren Stream and Neutralized Tailings: Kiggavik Project

Prepared by
Mahoney Geochemical Consulting, LLC
Lakewood, CO 80226

Prepared for

AREVA Resources Canada, Inc.

November 2011

TABLE OF CONTENTS

LIST OF TABLES

LIST OF FIGURES

15 GWB reaction path model showing changes in concentration for Silicon (as Silica) and aluminum

16 GWB reaction path model showing mineral precipitation and dissolution reactions

17 Eh-pH diagram for the system Sb-O-H at 25°C

18a Eh-pH diagram for the system Bi-S-O-H at 25 °C. (note: higher concentration of Bi).

18b Eh-pH diagram for system Bi-S-O-H at 25 °C (note: lower concentration of Bi)

19a Eh-pH diagram for the system Cr-O-H at 25°C. Figure shows most stable solids

19b Eh-pH diagram for the system Cr-O-H at 25°C. Figure replaces Cr_2O_3(cr) with chromium hydroxide [$Cr(OH)_3$(cr)]

20 Results from alternative geochemical model for chromium lowered Eh. Partial pressure of O_2(g) equals 10^{-30} atmospheres. $Cr(OH)_3$ allowed to precipitate

21 Eh-pH diagram for the system Co-O-H at 25°C. Cobalt at ~ 4 mg/L.

22 Eh-pH diagram for the system Cu-O-H at 25°C

23 Distribution of copper (adsorbed and mineral phases) in geochemical model simulations. Comparison of tenorite and malachite precipitated phases

24 Eh-pH diagram for the system Mn-C-O-H at 25°C

25 GWB based reaction path model showing the formation and subsequent dissolution of Strengite

26 Concentrations of selected parameters for GWB reaction path model shown on Figure 19.

27 Results from geochemical model (sweep) showing dissolution of strengite and formation of hydroxyapatite and intermediate adsorption of phosphate

28 Eh-pH diagram for the system Se-S-Fe-O-H at 25°C

29 Eh-pH diagram for the system Tl-O-H at 25°C, Tl concentration of 0.04 mg/L

30 Barite ($BaSO_4$) crystal structure showing replace of barium ions (red spheres) with radium (blue spheres) sulfur – yellow spheres, oxygen - white spheres

1.

2. INTRODUCTION

This report provides an assessment of the geochemical behavior of uranium and other constituents in the tailings neutralization tests conducted for AREVA Resources Canada, Inc. for the Kiggavik Project. Besides uranium, the remaining constituents include the major ions and elements which are generally considered the trace metals. A primary reason for this evaluation is to estimate source term concentrations for these constituents in the tailings pore waters.

The proposed tailings neutralization system will use a two stage process that will initially neutralize the slurry to a pH of 4, and then in the second stage the pH of the slurry is increased to approximately 7. The neutralized slurry will then be sent to an in pit tailings management facility (TMF). This is similar to the treatment process used at AREVA's McClean Lake operation in northern Saskatchewan.

At this time, five different tailings neutralization tests have been conducted at the SGS Laboratory (formerly Lakefield Research). For reasons explained later in this report, these tests are called Tests 1, 3, 5, 6 and 7. The test results generally show significant decreases in concentrations as the barren stream is neutralized. In addition to describing the actual test results, this report will also describe results from a series of geochemical models that were constructed to better understand the reactions that control the concentration of metals during the neutralization process. The laboratory results and the geochemical modeling described in this report will be used to provide the expected pore water concentrations for these various constituents.

As part of the geochemical modeling efforts various processes were initially evaluated using PHREEQC (Parkhurst and Appelo, 1999), which also served as the primary modeling program. The model was originally developed to study the uranium adsorption reactions. A secondary role of the geochemical modeling was to provide initial assessments related to the long term behavior of the other trace metals present in the barren stream. Besides using the primary PHREEQC based model additional approaches were often employed to gain additional insight

into the geochemical behavior of the different constituents. In some cases, methods as simple as examination of Eh-pH diagrams were used. While in other cases, alternative models were prepared using PHREEQC. These alternative models often assumed different redox conditions. Finally for some constituents, even more sophisticated reaction path modeling programs, such as Geochemist's Workbench (Bethke, 2008, Bethke and Yeakel, 2010), were employed to confirm conclusions originally indentified in the earlier modeling efforts.

The data from the various tests and modeling efforts were then taken as an aggregate and used to estimate the likely pore water concentrations for the various constituents in the emplaced tailings.

3. LABORATORY NEUTRALIZATION PROCEDURE

The laboratory testing program conducted by SGS Lakefield was primarily designed to evaluate the addition of ferric sulphate to the barren stream to lower uranium concentrations to below 1.0 mg/L. The proposed treatment system was based upon the successful two stage process developed at AREVA's McClean Lake operation (Mahoney et al., 2007). This treatment system will also remove most of the metals that would also be released to solution during the leaching of the ores.

The first test matrix that was prepared consisted of four primary tests. The testing plan was specifically designed to adjust some of the conditions prior to the first neutralization, which was set at a pH of ~4.0. The variables under consideration included presence or absence of leach residue solids and increasing the Fe/U ratio, through ferric sulphate addition. Another goal of the program was to assess the influence of the final pH particularly on the concentration of uranium.

The preliminary modeling efforts [Mahoney Geochemical Consulting (MGC), 2011] demonstrated that increases in pH (beyond approximately 7) tended to cause desorption of uranium due to several factors including: 1) changes to the surface charge on the HFO, 2) increased significance of uranyl tricarbonate complexes, and 3) the increase of several ternary uranyl complexes; $CaUO_2(CO_3)_3^{-2}$, $Ca_2UO_2(CO_3)_3°$, and $MgUO_2(CO_3)_3^{-2}$ (Dong and Brooks, 2006, 2008). Therefore, two different pH conditions, one initially less than pH 7 and the other closer to pH 8, were selected for the "final" pH values in the first tests. This was accomplished by splitting the sample into two aliquots two hours after the pH in the initially neutralized solution reached 4 and then raising the pH to the target levels. For the Test 1 and 3 experiments, the testing matrix required that after neutralization at pH 4, the solutions be split and neutralized at pH values of 6.3 to 6.7 or 7.8 to 8.1. Based upon the results of these initial tests, in subsequent tests (Tests 5, 6, and 7) a target pH of 7 was specified.

The original test matrix specified that Test 1 used only the solution (no solids), Test 2 used the solution with added ferric sulphate, Test 3 used solution and solids, and Test 4 included solution, solids and added ferric sulphate. However, when the testing program was initially developed, Tests 2 and 4 assumed higher uranium concentrations and significantly lower total iron concentrations in the barren stream (solution expected to require treatment prior to being discharged). The laboratory testing program at SGS Canada (Lakefield) demonstrated that the uranium recovery process using a resin-in-pulp (RIP) process would produce a solution with a final concentration of around 3 mg/L total uranium, and an iron concentration greater than 3,000 mg/L (a measured value of 3,970 mg/L). Based upon these values, and the initial geochemical modeling, which indicated that these solutions could, upon neutralization, produce satisfactorily low uranium concentrations without added ferric sulphate, it was decided to postpone Tests 2 and 4 until the results of Tests 1 and 3 became available. Because of the extremely low uranium concentrations obtained in the first two tests, the originally proposed Tests 2 and 4 were cancelled. Tests 1 and 3 were also designed to provide some initial information about the aging of these neutralized samples.

All of the tailings neutralization tests conducted at SGS Lakefield followed a similar procedure. After some initial preparation including addition of $BaCl_2$, the samples were neutralized with slaked lime to a pH of 4 and after approximately 2 hours the samples were then neutralized to their final specified pH values. Specifics related to the preparation of the Test 5 samples are listed in Table 1. For the Test 1 and 3 setups, aliquots were also taken from the pH 4 neutralized solutions (Tables 2 and 3). Results for the Test 5 measurements are summarized in Table 4.

Tests 6 and 7 were set up primarily to provide longer duration aging test results. The tests were run at ambient (Test 6 - fluctuating between 18°C to 25°C) and low temperatures (Test 7 - approximately 4°C). Initial results are available and are included in Tables 5 (Test 6) and 6 (Test 7). The aging tests were still being run when this report was prepared, so only the initial results (all collected at ambient temperatures) will be discussed at this time.

For the aqueous samples the parameter list included; pH, Electrical Conductance, Oxidation Reduction Potential, Total Dissolved Solids, and ICP scan for Total Metals and Dissolved

Metals, as well as the following additional parameters - Fe^{+2}, Fe^{+3}, PO_4, SO_4, NO_3, NH_4, Si, Alkalinity (HCO_3^- and CO_3^{-2}).

4. DESCRIPTION OF GEOCHEMICAL MODELING

The geochemical model relied primarily on the PHREEQC program (Parkhurst and Appelo, 1999) to evaluate saturation indices, model the neutralization process, and calculate the extent of mineral precipitation and surface complexation. The model can combine several distinct geochemical processes in user defined steps. These processes include neutralization of the initial low pH solution with slaked lime [$Ca(OH)_2$], equilibration with atmospheric gases such as carbon dioxide, mineral precipitation reactions, surface complexation and coprecipitation reactions (solid solution). Precipitation of "possible" phases including gypsum ($CaSO_4 \cdot 2H_2O$), ferrihydrite [$Fe(OH)_3$], amorphous aluminum hydroxide [$Al(OH)_3(a)$], schoepite [$UO_2(OH)_2 \cdot H_2O$], calcite ($CaCO_3$), strengite ($FePO_4 \cdot 2H_2O$), hydroxyapatite [$Ca_5(PO_4)_3OH$], barite ($BaSO_4$) as an end member in a solid solution reactions with radium, tenorite (CuO), rhodochrosite ($MnCO_3$), magnesite ($MgCO_3$), hausmannite (Mn_3O_4), or in earlier versions manganite (MnOOH), was also allowed. Some of the later models were constructed to assess specific issues, and in those cases additional minerals were included. Possible phases are permitted to form if the solution is oversaturated with respect to the specific phase. The partial pressure of carbon dioxide gas [$CO_2(g)$] was usually fixed at $10^{-3.4}$ atmospheres and in most simulations the partial pressure of oxygen was fixed at $10^{-0.7}$ atmospheres.

In some of the latter models, the partial pressure of oxygen was reduced in order to define a more reducing condition. These changes in partial pressure were primarily used to evaluate the behavior of redox sensitive species such as selenium and chromium.

In many situations the data evaluation/modeling process used different approaches to explain the behavior of a specific constituent. The different approaches related to modeling the neutralization process involve equilibrium with atmospheric gases (specifically carbon dioxide and oxygen), mineral precipitation, surface complexation, and formation of possible coprecipitated solids. In many cases the geochemical behavior of a specific element can be often

better understood after examination of an Eh-pH diagram. All the Eh-pH diagrams prepared in this report were prepared with the HYDRA/MEDUSA Software package (Puigdomenech, 2009), and relied upon the database included with that program. Some additional modeling was conducted using the Geochemist's Workbench program (GWB) (Bethke, 2008, Bethke and Yeakel, 2010). This program provides detailed reaction path models that supplement the PHREEQC derived results. This report includes several figures prepared with GWB.

As a general rule in this report the term concentration will apply to a laboratory measured result. The term value will generally apply to a model derived number. The expression "pH value(s)" may apply to either measured or modeled results.

For the first model calculations, the geochemical model was a simple step model in which the initial solution was raised to a specific pH; additional reactions were allowed to occur simultaneously with the neutralization step. Thus for the Test 1 and Test 3 results two separate models were developed. The composition of the solution used for the Test 1 and 3 models is listed in Table 7. The first model started with the low pH barren stream and the pH was raised to 4. In the second model the low pH barren stream was raised to user specified pH values from about 6.75 to 7.65, each of these models started with the low pH barren stream. As a check on this assumption, a few simulations were run in a two step path and results were similar to the simpler one step models.

Surface complexation (adsorption) onto the precipitated ferrihydrite surface was also included in the model. This process has been discussed in numerous books and papers (Mahoney et al. 2009a, 2009b, Langmuir, 1997, Merkel and Planer-Friedrich, 2008), and the method is commonly employed by water treatment facilities to remove various metals from water. The PHREEQC program tracks the amount of ferrihydrite that precipitates and calculates the concentration of surface sites based upon user specified parameters. For all constituents except uranium, the surface complexation model relies upon the diffuse layer database (Dzombak and Morel, 1990) provided with the PHREEQC program. This database has also been included in other geochemical modeling packages, and it is considered an industry standard for these type of

applications. As discussed below in more detail, the adsorption reactions for uranium as uranyl were updated with the reactions defined in Mahoney et al. (2009a).

One other minor correction was added to the diffuse layer database. The surface complexation constants for radium were corrected based upon the linear free energy relationships developed in Dzombak and Morel (1990). These are regression equations are based upon the relationship between the first hydrolysis constant (for divalent metals it is the formation of the $MeOH^+$ complex) and surface complexation constants that used reliable laboratory data to develop their respective values. In some cases these regressions, such for as uranium (See Mahoney et al. 2009), have been shown to produce poor results. But because of the similarity of the barium and radium ions, particularly in terms of ionic potential, these regressions appear to produce reasonable values. Indeed prior to these adjustments, it was common industry practice to use the values derived for the barium surface complexation constants for the radium surface complexes. In this revised database, the radium surface complexation constants were recalculated using data for the formation of the $RaOH^+$ ion presented in Langmuir and Riese (1985). Compared to the values in the original database, the adjustments to the radium surface complexation constants are slight. Furthermore, under conditions present in the neutralized tailings, and because of the presence of barite, the sorption of barium and radium is also slight. These corrections were originally prepared for another project. In this situation the adjustments provide mainly an improvement in database traceability and defensibility.

For the Test 1 and 3 evaluations, the model only included metals that had reported concentrations in the starting solution (Table 7). Concentrations for several parameters in the initial solution were reported at less than 3 or even 5 mg/L. As starting concentrations are critical to any reaction type geochemical model, it was decided that such uncertainties could not be tolerated in these calculations. Consequently, several elements such as antimony (<1mg/L), arsenic (<3mg/L), molybdenum (<0.6 mg/L) selenium (<3 mg/L), silver, (<0.08 mg/L), thallium (<3 mg/L) and lead (<5 mg/L) were not included in the initial PHREEQC simulations. This does not mean that subsequent results at pH 4 and 7 are not available, merely that certain parameters could not be modeled using the Test 1 and 3 results.

Three constituents were not included in the geochemical database selected for the modeling of the later results. These parameters include tin, bismuth and titanium. Therefore they were not included in the PHREEQC based geochemical models. Measured concentrations are included in the summarized laboratory data sheets (Tables 2 through 6). Selection of pore water concentrations are primarily based upon a review of those measured values. Given their low initial concentrations and their subsequent decreases in concentration upon neutralization it is believed that none of these three elements is expected to be of environmental significance.

To properly model the radium attenuation process the model also include a coprecipitation (solid solution) model that involved barite ($BaSO_4$), celestite ($SrSO_4$) and $RaSO_4$. The details related to this model will be included in a later section of this report (Section 6).

One point should be noted and that is that PHREEQC, because of the method it uses to calculate concentrations, tends to apparently increase concentrations. In most models, concentrations are generally entered in units of mg/L, however PHREEQC calculates using the primary unit of mg/Kgw (kilogram of water), and it doing these calculations the program tracks the amount of water available in each step. In dilute solutions these differences are commonly minimal and can be ignored. However, in these concentrated solutions, some of the water undergoes hydrolysis with ions like Fe^{+3} which reduces the amount of water available in solution and concentrates the dissolved parameters. Furthermore, as gypsum precipitates it removes two moles of water (as waters of hydration) for every mole of gypsum that forms. For these models the combination of these processes can increase final concentrations by approximately 10%. Rather than perform additional corrections, the values as reported by PHREEQC are retained. These increases in concentration also provide an additional and more conservative[1] margin in the estimation of the pore water concentrations.

4.1 Specifics of the Geochemical Model as it Pertains to Uranium

[1] For the purposes of this report, the term "conservative" will mean any process or assumption that will tend to increase predicted concentrations.

As described previously, surface complexation (adsorption) onto the precipitated ferrihydrite surface was the primary attenuation process included in the PHREEQC geochemical model. In some of the simulations used to further evaluate the behavior of uranium, mineral precipitation reactions involving schoepite [$UO_2(OH)_2 \cdot 2H_2O$], carnotite (KUO_2VO_4) and tyuyamunite [$Ca(UO_2)_2(VO_4)_2$] were also evaluated.

For uranium reactions the database was updated to the recently specified NEA values (Guillaumont et al., 2003). Also the Ca or Mg ternary uranyl carbonate complexes as defined by Dong and Brooks (2006, 2008) were included in the database.

For all constituents except uranium, the surface complexation model relies upon the diffuse layer database for the ferrihydrite surface (Dzombak and Morel, 1990) provided with the PHREEQC program. However, the adsorption reactions for uranyl were updated with the reactions defined in Mahoney et al. (2009a, b). Site concentrations were based upon 0.2 moles of weak sites (Hfo_wOH), and 0.005 moles of strong sites (Hfo_sOH) per mole of precipitated ferrihydrite.

Inclusion of the uranyl surface complexation reactions defined in Mahoney et al. (2009) solved several long term issues with the reactions and values present in the original Dzombak and Morel compilation. Unlike the estimated values provided in Dzombak and Morel (1990) the surface complexation reactions in Mahoney et al. (2009) were fit to numerous peer reviewed experimental datasets. The original values for uranium sorption reported by Dzombak and Morel (1990) were estimated using a regression equation, and these estimated values tended to overestimate uranyl adsorption by almost an order or magnitude under low pH conditions (non carbonate). Also as shown below, the Mahoney et al. data set also included uranyl carbonate surface complexation reactions, while the earlier database did not include such reactions. Therefore, the replacement surface complexation reactions tend to provide a more realistic assessment of uranium adsorption when carbonate is present.

The following surface complexation reactions were used to describe uranium (as uranyl) adsorption onto hydrous ferric oxide:

$$Hfo\_sOH + UO_2^{+2} = Hfo\_sOUO_2^{+} + H^{+} \qquad Log\ K = 3.736$$

$$Hfo\_wOH + UO_2^{+2} = Hfo\_wOUO_2^{+} + H^{+} \qquad Log\ K = 2.534$$

$$Hfo\_wOH + UO_2^{+2} + CO_3^{-2} = Hfo\_wOUO_2CO_3^{-} + H^{+} \qquad Log\ K = 9.034$$

$$Hfo\_wOH + UO_2^{+2} + 2CO_3^{-2} = Hfo\_wOUO_2(CO_3)_2^{-3} + H^{+} \qquad Log\ K = 15.28$$

In addition to the uranyl adsorption reactions, two additional reactions (Appelo et al., 2002) were added to the database. These reactions are defined below:

$$Hfo\_wOH + CO_3^{-2} + H^{+} = Hfo\_wOCO_2^{-} + H2O \qquad Log\ K = 12.78$$

$$Hfo\_wOH + CO_3^{-2} + 2H^{+} = Hfo\_wOCO_2H + H2O \qquad Log\ K = 20.37$$

Preliminary models also evaluated quartz as a potential sorbent phase (along with the ferrihydrite surface). However, the extent of uranyl sorption was smaller than observed in the data and so another surface was selected. This second alternative model included a montmorillonite surface instead of quartz. Although this mineral is not strictly present in the tailings, at this time we can use it as a surrogate for other clay minerals, like illite which is present in the alteration zones (Wollenberg, 2010) and will report to tailings. The chief advantage of using the montmorillonite surface is that it has a much greater surface area than quartz, and this can result in a much smaller solid to liquid ratio for a similar amount of sorption.

The model included adsorption onto a montmorillonite surface at a concentration of 25 g/L. This surface only adsorbed uranium and it was added to better fit some of the data evaluated in the preliminary assessment (MGC, 2011). Because of the better agreement between the measured concentrations and the model derived values, particularly at a pH of 4, the montmorillonite surface has been retained in these latter models. In the Test 5, 6 and 7 models (pH 6.95) the percentage of uranium retained on the montmorillonite surface at pH of 7 is around 20 percent. This is probably related to the large amounts of competition for surface sites on the ferrihydrite. Because of the improvements in fitting data, particularly at a pH of 4, the surface has been retained in these later models. In the Test 5, 6 and 7 models, the percentage of uranium retained on the montmorillonite surface at pH of 7 is around 20 percent. This is probably related to the large amounts of competition for surface sites on the ferrihydrite. Additional rationale for the

inclusion of this surface is provided in Mahoney Geochemical Consulting (MGC) (2011). Surface complexation parameters for the montmorillonite surface were obtained from Pabalan et al. (1998).

Pabalan et al. (1998) selected a surface area of 9.7m^2/g for montmorillonite; the same authors reported a surface for quartz of 0.03m^2/g. They also assumed the same site density of 2.3sites/nm^2. The montmorillonite surface contained both >AlOH° sites and >SiOH° type sites, at a ratio of 0.83 (45% >AlOH° sites and 55% >SiOH° sites).

The following reactions were used to define the montmorillonite surface.

Mont_aOH = Mont_aOH
log_k 0.0

Mont_aOH + H+ = Mont_aOH2+
log_k 8.33

Mont_aOH = Mont_aO- +H+
log_k -9.73

Mont_aOH +UO2+2 = Mont_aOUO2+ +H+
log_k 2.70

Mont_aOH +3UO2+2 + 5H2O = Mont_aO(UO2)3(OH)5 + 6H+
log_k -14.95

Mont_sOH = Mont_sOH
log_k 0.0

Mont_sOH = Mont_sO- + H+
log_k -7.2

Mont_sOH +UO2+2 = Mont_sOUO2+ +H+
log_k 2.6

Mont_sOH +3UO2+2 + 5H2O = Mont_sO(UO2)3(OH)5 + 6H+
log_k -15.29

Where the *Mont_sOH* site represents the >SiOH°, and the *Mont_aOH* site represents the >AlOH° site.

4.2 Overview of Geochemical Modeling Results

The Test 1 and 3 data sets were used in the initial geochemical modeling efforts. Tables 2 and 3 summarize the laboratory derived results from the Test 1 and 3 Setups. Figures 1 and 2 plot the data for selected trace elements as function of pH for these testing conditions.

Because of the lower detection limits obtained in the subsequent tests, the bulk of the modeling efforts used the Test 5, 6 and 7 results. Therefore, discussion of the modeling results from the Test 1 and 3 experiments will be limited. However, some of the Test 1 and 3 results will be discussed when pertinent to a specific constituent.

The barren streams used in Tests 5, 6, and 7 became the primary source to define the starting compositions in the PHREEQC based geochemical model. Because of the lower reporting limits those results also provided a more complete set of data for the geochemical model. Table 10 provides a summary of the laboratory results for these tests and it also includes model derived values. The table is color coded. The barren stream concentrations for these three tests are in uncolored columns, laboratory concentrations of the neutralized streams are in yellow and model results are in green. There are two model result columns for Test 7. This is because the final pH of the Test 7 experiment was 7.33, while the target pH was 7.0. The Test 5 and 6 samples, both with final pH values of 6.95, are considered close enough to 7.0 to not warrant any adjustment in the pH of these models. However, with the 7.33 pH for the Test 7 sample it was decided to provide two pH values; one comparable to the Test 5 and 6 values at 6.95 and other at the 7.33 value.

Table 11 provides comments that are related to the laboratory testing and modeling efforts. The table also defines the expected pore water concentrations, and summarizes the rationale for the selection of the pore water value.

For most elements, the neutralized concentrations show significant decreases with increasing pH. However, the geochemical model results are not always consistent with the measured values.

The reasons for these differences will be discussed as the various parameters are evaluated. As mentioned previously, in some cases additional models were prepared to better understand these differences.

Because of the abundance of dissolved iron in the barren stream, the geochemical model relies heavily upon surface complexation of the dissolved constituents onto Ferrihydrite [Hydrous Ferric Oxide (HFO)]. Figures 3 through 8 show the percentage of constituent adsorbed as a function of pH for selected constituents (trace metals and oxyanions) from Tests 5, 6 and 7. These figures were generated by defining (fixing) a series of pH values. This is sometimes referred to as a pH sweep. These sweep based calculations provide additional insights into the behavior of the different components during the neutralization process.

Parameters selected for inclusion on Figures 3 through 8 were those that showed measurable adsorption on a percentage scale from zero to 100 percent (Because PHREEQC tends to recalculate concentrations based upon moles/Kgw some percentages were slightly greater than 100% and so the scale goes to 120%). Parameters such as calcium, magnesium, sulfate, cobalt, antimony, thallium and radium generally show less than 1 percent sorption and so plotting those results on a percentage scale would not provide any useful information. Other parameters are influenced by redox conditions such as chromium and selenium. They will be covered in subsequent figures when these elements are discussed in detail. Because barium is added as part of the neutralization process the percent adsorbed become significantly greater than 100 percent, so they have been eliminated. The model calculations start at a pH of 4 and generally stop at pH of 7.5 or 7.65. The resulting curves show adsorption edges, which indicate how pH affects the surface complexation of the different constituents. Usually the adsorption edge is identified as the pH at which 50 percent is sorbed. There are various factors that determine the location of an adsorption edge. These factors include amount of sorbent, initial concentration of sorbate and the presence of competing sorbates. As these solutions start with high dissolved metal concentrations, competition for adsorption sites on the HFO is a significant factor.

Figures 3, 4 and 5 show the behavior of selected cations (trace metals) for the three tests, and Figures 6, 7 and 8, show the behavior of the oxyanions. Some of these curves show percent

adsorbed values slightly greater than 100 %. This is because during the model calculations approximately 2.5 percent of the water initially present is lost to mineral precipitation reactions, primarily gypsum precipitation, so the solutions have become more concentrated and this is reflected in values slightly greater than 100 percent.

Cation adsorption onto HFO (Figures 3, 4 and 5) is characterized by increases in percent adsorbed values with increasing pH. Different cations display different percentages. Uranium is strongly adsorbed so it shows an adsorption edge at low pH. Lead shows an adsorption edge around 4.25 to 4.5 depending upon the composition of the solution. Cadmium is not strongly adsorbed and it shows an adsorption edge that is greater than 7.

With increasing pH, the oxyanions (Figures 6, 7 and 8) tend to decrease the amount of sorption but these simulations also demonstrate that a target pH of around 7 is low enough to retain most of these constituents on the HFO surface. Phosphate behavior is unusual in that is shows a rise and then a rapid decrease between pH 5 to 7. The behavior of phosphate under these conditions is related to the initial formation of strengite and the subsequent formation of hydroxyapatite. More details will be provided in the discussion related to phosphate in Section 5 of this report.

5. EVALUATION OF URANIUM

5.1 Tests 1 and 3 - Laboratory Results and Model Calculations

Uranium (U) in aqueous systems is dominated by two valence states (Figures 9a and 9b). Uranous is the U(IV) or reduced valence, and uranyl [U(VI)] is dominant under oxidizing conditions. The mineral uraninite (UO_2) is the (IV) stable form under reducing conditions. The Eh pH diagrams (Figures 9a and 9b) show dissolved U(IV) species only under extremely low or high pH conditions. Figure 9a is color coded, with grey representing the metallic uraninite solid; most uranyl minerals are yellow and so the schoepite field has been colored yellow. The dissolved species are in blue.

Upon oxidation uranyl (UO_2^{+2}) becomes dominant (Figure 9b). The simple uranyl minerals tend to be more soluble than the U(IV) phases, and therefore dissolved species and surface complexation reactions control the concentration of uranium under oxidizing conditions. Baring the presence of vanadium or phosphate in solution, schoepite [$UO_2(OH)_2 \cdot H_2O(cr)$] is the most likely U(VI) bearing phases that will form. Uranyl complexes strongly with hydroxyl groups and even more strongly with carbonate (Figure 9b). Under the conditions selected for Figure 9b, the uranyl carbonate complexes becomes important at pH values greater than approximately 4.8, with formation of the uranyl monocarbonate complex. The dicarbonate starts to dominate at a pH of 6.8, and the uranyl tricarbonate becomes dominant at a pH of approximately 8.1. The importance of this complex is also apparent in the slight dip observed along the boundary with uraninite. Although schoepite can control uranium concentrations in many waters, other phases are more stable and can produce even lower concentrations. In particular these phases are the uranyl vanadates; carnotite (KUO_2VO_4) and tyuyamunite [$Ca(UO_2)_2(VO_4)_2$]. The barren streams contain abundant vanadium, but geochemical modeling predicts uranium concentrations much lower than observed in the experimental results. This suggests that these minerals are not forming.

Laboratory derived concentrations for Tests 1 and 3 are summarized in Tables 2 and 3. The tables list total concentrations; except for uranium, where both total and dissolved concentrations have been included. A comparison of the total and dissolved concentrations for most parameters indicated that only slight differences in concentrations were noted; with total concentrations in most, but not all situations, slightly greater than dissolved concentrations.

Total and dissolved concentrations for uranium are shown for Tests 1 and 3 on Figure 10. The results demonstrate the general consistency between total and dissolved concentrations. One of the most significant differences is noted among the pH 4 samples; the Test 3 results are significantly lower than the Test 1 results. This suggests that sorption of uranium onto mineral phases (leached residue) may play a role under these lower pH conditions. This had been identified as a possible to influence uranium concentration in an earlier report (MGC, 2011). As the differences in uranium concentrations decrease in the higher pH samples, it appears that this mechanism plays a lesser role as the pH approaches or exceeds ~ 7.0.

The increase in uranium concentrations with increasing pH can be readily seen on Figure 10. This trend demonstrates the role of pH in increasing uranium concentrations due to the formation of various carbonate complexes.

5.2 Aging of Tests 1 and 3

Figure 11 shows the total uranium concentrations as a function of time since final neutralization was attained. A consistent pattern of behavior as a function of time is not immediately apparent. For example, the Test 1 low pH data set appears to decrease and "level off". The Test 3 high pH results show an increase over time. The other two data sets are intermediate in the amount of increase. Further review of the data indicates that the strong relationship between pH and uranium remains apparent as is shown on Figure 12. The pH values for Test 1 (low pH data set) appear to decrease as a function of time. Similarly, for the Test 3 high pH data set the pH shows an increase over time. It appears that the variation in pH is driving the variation in U concentrations and this process may be related to the presence of some excess base (added lime that took time to react), or possibly a desorption process on the mineral surfaces. The extent of

this pH shift will be examined as part of the evaluation of the currently ongoing Test 6 and 7 aging tests. In those tests there is a requirement to monitor pH on a daily basis.

5.3 Geochemical Modeling of the Test 1 and 3 Results

A geochemical model of the tailings neutralization process was prepared using PHREEQC (Parkhurst and Appelo, 1999). The model started with the final solution from the RIP testing program. The concentrations for the starting solution are listed in Table 7.

The model calculations used the solution composition listed in Table 7 as a starting solution and then in subsequent modeling steps the pH was fixed to 4 or to 6.75, 7.0, 7.35, 7.5 or 7.65 with the addition of $Ca(OH)_2$ (essentially slaked lime). These models always started with the composition listed in Table 7 and then the pH was brought up to the selected value. Convergence issues prevented model calculations above a pH of approximately 7.65. Possible mineral phases and other equilibrium conditions were described in Section 3.0.

The first two surface complexation based models only considered the role of uranyl sorption onto precipitating ferrihydrite; surface complexation reactions onto mineral surfaces other than the precipitated HFO were included in the third model. Figure 13 compares the results from two models with the total and dissolved uranium concentrations from Tests 1 and 3. The model derived values show good agreement with the corresponding measured concentrations. The pH effect, discussed previously, is similarly observed in the model derived concentrations. The initial model did not include vanadium in the solution and the lower concentrations indicate that the model tends to overestimate adsorption of uranyl. The inclusion of vanadium in the second model improved the fits, particularly for the high pH data. This is probably a result of competition for surface complexation sites.

Another model evaluated carnotite precipitation (results not plotted). In those calculations, uranium concentrations dropped to levels that were significantly lower than those measured in these tests, although other vanadium phases were suppressed. Therefore, it appears that carnotite

is not forming, and that surface complexation (sorption) reactions appear to be the most reasonable mechanism available to explain the decrease in uranium concentrations.

The first two models were constructed to evaluate the Test 1 results and as this test did not include solids, no consideration was given to sorption of uranyl onto other mineral phases such as clays and other silica bearing minerals. The Test 3 results showed lower concentrations at a pH of 4, suggesting that the presence of the leached solids did play a role in reducing uranium concentrations at least in the low pH solutions. Therefore, a third model was prepared that included 25 grams of montmorillonite sorbent per liter. The rest of the model assumptions, including the surface complexation onto HFO, remained the same. The concentration of 25 grams was selected in the earlier modeling efforts as providing a reasonable first approximation to some preliminary data (MGC, 2011), the value was retained in the latter models. Details related to the definition of the surface complexation reactions for this surface are provided in Section 3 (above).

The montmorillonite surface was selected not because montmorillonite is present in the mineral assemblage, but rather because there is a paucity of uranium surface complexation reaction data for other clay minerals, such as illite and chlorite. Sorption onto montmorillonite is well documented, and typically it would be expected to be a stronger sorbing surface than many of the other clay minerals. Consequently, the amount of montmorillonite needed to remove a specified amount of uranium, would be expected to be less than if other sorbent surfaces were present. The model clearly demonstrates that adsorption onto another surface present in the solids matrix is a likely process, and that with increasing pH the effectiveness of the adsorption on that alternate surface appears to decrease as the amount of ferrihydrite increases. With increased formation of uranyl carbonate complexes, the importance of this "clay" surface to sequester uranium becomes less important. Because montmorillonite is not actually present in the leached solids, it was decided that no additional benefit would be derived from preparing additional iterations to estimate the amount of montmorillonite needed to get better agreement with the Test 3 uranium concentrations at pH of 4.0.

The surface complexation models generally showed that the various schoepite solids were consistently undersaturated. Removal of the surface complexation reactions from the model indicated that only the most stable schoepite would potentially precipitate at pH values of 6.75 and 7.0. This particular version is identified in the database as Schoepite_NEA, because the stability constant used for this particular phase is based upon the value reported in Guillaumont et al. (2003). The NEA selected value was 4.81 (written in the proton form), it should also be noted that the NEA compilation selects only the most stable solids and it is unlikely that such a stable phase would form under the short time frame and ambient temperatures present in the labortory tests. The next most stable schoepite stability product constant was 5.40, and using that version in the same model did not cause the precipitation of schoepite. As concentrations from the tests are much lower than the values predicted in the schoepite models, it is reasonable to assume that schoepite is not controlling the concentrations of uranium in these tests. Because of the large amount of ferrihydrite available to adsorb uranium under these conditions, any initially precipitated schoepite would dissolve and transfer that uranium to the ferrihydrite surface.

Reaction path models using Geochemist's Workbench (Bethke 2008, Bethke and Yeakel 2010) suggest that the high iron concentrations would favor the formation of strengite under low pH conditions, which would limit the concentration of phosphate and preclude the formation of autunite [$Ca(UO_2)_2(PO_4)_2$] phases. Section 5.21 of this report also demonstrates that strengite decomposes with increasing pH to hydroxyapatite, with some additional formation of ferrihydrite. During this transition some phosphate is "temporarily" adsorbed onto the HFO as the pH increases. In all of the PHREEQC based surface complexation models, the various autunite phases (including the true Ca bearing, as well as H-, Na- and Sr- versions) were consistently undersaturated. Only the K-autunite phase appears to be slightly oversaturated at pH's of 6.75 and 7.0. As all three of the surface complexation models discussed above tend to underestimate uranium concentrations under these conditions only a further decrease in U concentration would result. No benefit would be obtained if K-autunite was included as a possible phase.

5.4 Tests 5, 6 and 7- Laboratory Results and Model Calculations

Based upon an initial review of the Test 1 and 3 results, and because of the apparent increase in U concentrations with increasing pH it was decided that a pH of 7 would provide a reasonable final pH value. Tests 5, 6 and 7 were prepared to provide that information at a pH of approximately 7. Test 5 was primarily prepared for tailings for additional geotechnical evaluations and Tests 6 and 7 were designed to provide additional confirmation of the Test 1 and 3 results, and to provide longer aging tests (60 days). The three additional test required the preparation of a new barren leach composition (identified as pulp filtrate in Tables 4, 5 and 6), and for the analysis of this sample lower detection limits were used for many of the trace metals. This allowed for a more complete geochemical model for these elements. For these tests only results from the final pH range (around 7) were obtained.

Table 4 lists the concentrations both total and dissolved values for the Test 5 samples. The subsequent geochemical modeling used total concentrations. For uranium, the initial concentrations were approximately 8.5 mg/L (rounded average of total and dissolved U), upon neutralization the concentrations dropped to approximately 0.14 mg/L. The starting concentration of uranium was greater than the concentration used in Tests 1 and 3. However, the iron concentration was also greater in these latter tests.

Tests 6 and 7 were set up primarily to provide longer duration aging test results. These ongoing tests are being stored at ambient (Test 6 - fluctuating between 18°C to 25°C) and low temperatures (Test 7 - approximately 4°C). At this time only the initial results are available and are included in Table 5 (Test 6) and Table 6 (Test 7). The aging tests were still being run when this report was prepared so only the initial results (all collected at ambient temperatures) will be discussed at this time.

Table 8 summarizes the Test 5, 6 and 7 uranium concentrations and also lists the model derived values. For Test 5 (Table 8), geochemical modeling results produced a modeled uranium value of 0.009 mg/L. The initial U concentration was 8.65 based upon total U and the separate ferric and ferrous iron concentrations of 4470 mg/L Fe(3) and 13.8 mg/L Fe(2) were used. A final pH of 6.95 was used. For the Test 5 data, the modeled value is more than an order of magnitude

smaller than the measured concentration. There are several possible factors that are responsible for this lower value.

The additional results for Tests 6 and 7 are also included on Table 8. Two different models were run for Test 7, one near the target pH of 7 (6.95) and one consistent with the laboratory measured pH of 7.33. The pH value of 6.95 was considered close enough to the target pH of 7 that it was retained. Keeping the measured pH in the model removed one more variable and allowed for a more direct comparison between the laboratory concentrations and the modeled values. Alkalinities are also included and the model estimated alkalinities tend to be significantly lower than the measured values. The low alkalinities are probably at least partially responsible for the lower model estimated U values.

The geochemical models for the Test 5, 6 and 7 conditions (Table 8) all tended to over predict the amount of surface complexation of uranium onto HFO and hence a lower concentration was predicted in pore water based upon the models. This was also observed in the Test 1 and 3 results, but to a lesser extent. Uranium surface complexation is a complicated process that is influenced by pH and carbonate concentration. In these models the carbonate concentration is essentially controlled by the partial pressure of carbon dioxide gas. In these models a partial pressure of $10^{-3.4}$ atms (or a log value equal to -3.4) was used. This value corresponds to the current partial pressure in the atmosphere and so it should represent the long term equilibrated condition. The PHREEQC calculated partial pressures for $CO_2(g)$ for the neutralized samples were all significantly greater than the partial pressure fixed in the model.

Because of the difference between the measured and model defined partial $CO_2(g)$ pressures additional, simulations were run to evaluate the influence of this factor on dissolved uranium concentrations. The influence of carbon dioxide partial pressure on the modeled uranium concentrations are shown in Table 9.

The models are also sensitive to the initial pH. A difference between an assumed pH of 1.0 and the reported pH of 1.55 changed the uranium concentration from 0.038 mg/L to 0.009 mg/L. This difference is related to the greater amount of $Ca(OH)_2$ required to increase the pH to 6.95

when the pH is assumed to be 1.0. This causes an increase in the total Ca^{+2} concentration in solution which increases the abundance of $Ca_2UO_2(CO_3)_3$ and $CaUO_2(CO_3)_3^{-2}$. Under these conditions these two complexes are responsible for carrying a large percentage of uranium in solution (> 90 %).

Figure 14 shows the Eh-pH diagram for vanadium, potassium and uranium. The diagram indicates a large stability field for carnotite (KUO_2VO_4). One version of the geochemical model, using these three starting solutions, was developed that included carnotite and tyuyamunite as a possible mineral phases. Because of the stability of carnotite, uranium concentrations dropped from the previously modeled values by two to three orders of magnitude; in some situations the difference was even greater. Tyuyamunite was undersaturated. Vanadium concentrations did not change significantly. It appears that uranium acts a limiting reagent in these simulations. Because of the extremely low concentrations for uranium in these models and the disagreement between these modeled and the measured uranium concentrations models that use carnotite as a possible phase have been eliminated from further consideration. Although there is good evidence that carnotite is a relatively insoluble phase (Tokunaga, 2009) as reflected in its generally low solubility, it is possible that its thermodynamic stability, as defined by its low solubility product constant, has been misestimated.

The section on vanadium (Section 5.28) discusses additional models prepared with carnotite (KUO_2VO_4) and tyuyamunite [$Ca(UO_2)_2(VO_4)_2$]. In those models uranium concentrations dropped to even lower limits. Because the model estimated values were significantly lower than the measured concentrations it was decided that the uranyl vanadates were not present in the neutralized solutions.

5.5 Summary and Selection of Uranium Pore Water Concentration

Based upon a review of the uranium concentration data from the SGS laboratory and coupled with a series of geochemical models, the following conclusions have been made:

- For the Test 1 and 3 samples, uranium concentrations of less than 0.007 mg/L at a pH of 6.92 were attained based upon the two stage neutralization process, with increasing pH value increased to 0.028 at a pH of 7.84.

- Measured concentrations for the Test 5, 6 and 7 Tests produced slightly higher uranium concentrations. Measured concentrations ranged from 0.14 to 0.11 mg/L. The initial uranium concentrations in these samples were greater than the initial uranium concentration used in the Test 1 and 3 experiments. This higher initial concentration may be partially responsible for these differences.

- The concentrations of uranium observed in these experiments are too low to be explained by mineral precipitation reactions that involve schoepite without additional surface complexation of uranium onto HFO. If schoepite had initially formed, and there is no evidence that this happened because of the large concentration of iron initially in solution, the uranium in any early formed schoepite would have completely transferred to the HFO phase.

- Models suggest that the high initial concentrations of vanadium would produce final uranium concentration lower than observed in these tests if carnotite were present.

- The only other alternative process that might explain the behavior of uranium would be some type of coprecipitation process, but that process would likely sequester the uranium deeper in the primary precipitating phase and so the concentrations would be expected to be lower than those indicated by the surface complexation models and the response to pH increases would also probably behave in a different manner that would more likely reflect the breakdown of the primary solid.

- Surface complexation models appear to provide the best explanation of the processes that are controlling uranium in these tests. The initial decreases in uranium concentrations observed in the pH 4 samples cannot be explained by a simple mineral precipitation process. Previous modeling efforts (MGC, 2011) demonstrated that schoepite would not

- At pH values around 7 the models tend to overestimate uranyl surface complexation but with increasing pH, as shown in the Test 1 and 3 results, these differences test to become smaller. There are several reasons for these differences. Chief among the reasons is that the model tends to underestimate alkalinity.

Therefore, it appears that surface complexation, primarily upon the precipitated ferrihydrite, is the dominant process that removes uranium from these solutions.

A concentration of 0.14 mg/L (Test 5 measured concentration after neutralization) has been selected as the pore water concentration for uranium. This value is considered to be a conservative estimate as significantly lower values were measured in the Test 1 and 3 experiments.

6. EVALUATION OF DATA AND ESTIMATION OF PORE WATER CONCENTRATIONS - NON URANIUM CONSTITUENTS

What follows are summaries of the geochemical behavior for the other constituents (major ions and trace elements) examined as part of the tailings neutralization evaluation.

6.1 Major Cations

The effort to match the major ion [calcium (Ca), magnesium (Mg), sodium (Na) and potassium (K)] concentrations to modeled values were limited. Calcium is added in the form of slaked lime and it is allowed to precipitate either as gypsum or calcite. In the Test 5 results at neutralization the modeled calcium exceeded the measured concentration by nearly a factor of 3. In the Test 6 and 7 measurements there was a slight decrease in Ca upon neutralization, and the reported calcium concentrations were slightly greater than the modeled value. These differences are probably related to the amount of lime needed to attain the specified pH, as well as the activity of sulfate as it controls gypsum solubility.

Sodium concentrations are generally in the 100 to 250 mg/L range. Some decreases in Na are noted upon neutralization, but the model did not include any process to adjust Na concentrations. Potassium values in the tests showed initial values around 2,200 mg/L and concentrations upon neutralization are about half the initial values. Magnesium concentrations also decreased with neutralization. The most likely explanation is that a cation exchange process is influencing the major ion concentrations in these samples. As these four elements are not considered to be of environmental concern a detailed evaluation of the ion exchange process was not performed as part of this study.

6.2 Chloride

Chloride (Cl^-) concentrations in the Test 6 and 7 experiments were generally in the 300 to 600 mg/L range, with most concentrations at less than 500 mg/L. In some preliminary tests, chloride concentration data were not available as the reporting limit was 800 mg/L and all samples had concentrations less than the 800 mg/L reporting limit. Chloride is considered to be a conservative species and so attenuation reactions are expected to be slight. This is confirmed by the laboratory measurements; neutralization with slaked lime did not show any significant change in Cl^- concentrations. An estimate for chloride in the tailings pore waters of 500 mg/L is selected.

6.3 Sulfate

The behavior of sulfate (SO_4^{-2}) in the barren stream and in the subsequently neutralized solutions is more complicated than chloride. Several different geochemical processes can occur with sulfate. The dominant process is the formation of gypsum. Surface complexation onto HFO also occurs but sulfate tends to desorb with increasing pH. At a pH of 7, surface complexation of sulfate is not considered to be a significant process. Much of the gypsum precipitation occurs in the low pH region as bisulfate (HSO_4^-) is converted to sulfate (SO_4^{-2}). This conversion takes place at a pH of approximately 2.0. With increasing calcium additions as the pH is raised to 7.0, additional gypsum will form.

Initial concentrations of sulfate in the Kiggavik Test solutions are at times greater than 50,000 mg/L. Upon neutralization, concentrations decrease to around 12,000 to 8,000 mg/L. These concentrations are much higher than the values in the JEB pit pore waters (AREVA, 2011), which in 2008 averaged around 1800 mg/L. The current estimate of a sulfate source term in the JEB pit pore water is ~1800 mg/L. A comparison of gypsum saturation indices (SI) between the laboratory generated solutions (Tests 1, 3, 5, 6 and 7) and the long term concentrations in the pore waters of the JEB pit (AREVA, 2011) indicates that both sets of waters are near or at saturation with respect to gypsum.

PHREEQC calculates saturation indices (SI) to determine whether a solution (water) is at equilibrium, or undersaturated or oversaturated with respect to certain phases (minerals). The

precipitation and dissolution reactions of gypsum ($CaSO_4 \cdot 2H_2O$) can be represented by the following equation:

$$CaSO_4 \cdot 2H_2O \leftrightarrow Ca^{+2} + SO_4^{-2} + 2H_2O$$

and quantified by the following relationship:

$$K_{sp} = \frac{\left(Ca^{+2}\right)\left(SO_4^{-2}\right)}{\left(CaSO_4 \cdot 2H_2O\right)}$$

where K_{sp} is the solubility product constant, and the items in parentheses represent chemical activities[2] of the calcium and sulfate ions. The K_{sp} for gypsum is $10^{-4.59}$. At equilibrium the pure solid phase $CaSO_4 \cdot 2H_2O$ is present, and it is assigned an activity of 1.0. Water also has an activity of one, as long as the solution remains dilute, and it can be eliminated from the K_{sp} equation. In this example, the product $(Ca^{+2})*(SO_4^{-2})$ is commonly called the ion activity product (IAP). In this case, because it is a simple 1:1 product, if the solution is already at equilibrium, and if that equilibrium is disturbed by increasing the activity of sulfate, then more gypsum should precipitate and the activity of the calcium ion should decrease by a corresponding amount. The most common way for increasing the activity of an ion in solution is to increase its concentration. For this example, a soluble form of sulfate could be added by adding sulfuric acid. More gypsum would form and some calcium would be removed from solution, and as a result of the precipitation Ca^{+2} activity would decrease, the activity of the sulfate would re-equilibrate and would show a corresponding increase, but the ion activity product would remain the same.

The saturation index (SI) compares the ion activity product with the solubility product constant, and the following relation is used to calculate the saturation index:

$$SI = \log \frac{IAP}{K_{sp}}$$

[2] The activity of an ion ($\mathbf{a_i}$) is defined by the molality ($\mathbf{m_i}$) of the ion times an activity coefficient ($\boldsymbol{\gamma_i}$).

$$\mathbf{a_i} = \boldsymbol{\gamma_i}\, \mathbf{m_i}$$

Because a log function is used in the definition, a saturation index of 0.0 means the saturation ratio equals 1.0. The IAP equals the K_{sp} and the solution is in equilibrium with the mineral; the solution is at saturation and no change in composition should take place. Positive SI values mean that the solution is supersaturated with respect to the mineral. Baring kinetic constraints, the mineral should then precipitate and concentrations in solution should decrease. Negative SI values mean that the solution is undersaturated and the mineral, if present, should dissolve. Because of the log scale, an SI of 1.0 means the solution is oversaturated by a factor of 10, when compared to an SI of 0.0. Usually some leeway is given to the interpretation of SI values. For gypsum, values of ± 0.1 units suggest that the solution is at equilibrium with that solid. The best way to evaluate the saturation state is to examine a number of water samples from a site.

For the 17 Kiggavik specific samples (neutralized with pH 4 to 7.33) that were evaluated, the average SI was 0.04, and the lowest values was -0.03. For the 61 JEB pit pore waters collected in 2008 that were examined, the average SI for gypsum was -0.02, with a maximum of 0.06, and a minimum of -0.054. However, sulfate concentrations in the Kiggavik solutions are much greater than the levels in the JEB pit. Calcium concentrations are slightly greater (15%) for the pore waters collected from the JEB pit with an average of around 532 mg/L, compared to 463 mg/L for the Kiggavik test solutions. Therefore, other factors must be operating to keep sulfate concentrations so high.

The primary reason for the difference in sulfate for the two locations is the much greater concentration of dissolved magnesium (Mg) in the Kiggavik samples. Magnesium concentrations in the Kiggavik samples range from 1,390 mg/L to 4,440 mg/L (Test 7 low pH solution), with an average Mg concentration of 2,508 mg/L. In the 2008 JEB pit pore water samples, Mg concentrations ranged from 9.1 to 190 mg/L with an average concentration of 90 mg/L. The $MgSO_4°$ ion pair can sequester a significant percentage of sulfate, which explains the high sulfate concentrations and the simultaneous equilibration with gypsum. In the Kiggavik samples, the $MgSO_4°$ ion pair holds on average 35.5 percent of the sulfate in solution with a maximum exceeding 50% of the total sulfate in one sample, elimination of the samples with

initial pH values of less than 2 raises the average to 39.6%. For the JEB TMF pore waters the average percentage of total sulfate bound in the $MgSO_4°$ ion pair is about 6 percent.

Another factor responsible for the differences is related to the different ionic strengths, and the resulting differences in activity coefficient values. The ionic strength of pore waters from the JEB TMF is about 0.05 m, while the Kiggavik samples have an ionic strength of 0.35 m. This changes the activity coefficient of Ca^{+2} from 0.47 in the JEB pore waters to 0.30 in the Kiggavik samples, as the SO_4^{-2} ion is also divalent similar differences in the activity coefficient of SO_4^{-2} are also expected. These effects are multiplied in calculation of the ion activity product. The product of the activity coefficients for the JEB pore water is 0.2209, and the product for the Kiggavik solution is 0.09, so the effective activity coefficient product is 2.45 (0.2209/0.09) greater in the JEB pit, and so a corresponding decrease in the total sulfate concentration can be accommodated in the JEB pit (or an increase in the Kiggavik solutions). Fortunately, if dilution does take place in the Kiggavik TMF the activity coefficients will increase and more gypsum will precipitate and lower sulfate concentrations in the pore waters.

It appears that the primary driver for all of these factors is related to the higher total magnesium concentration, which increases the proportion of the $MgSO_4°$ ion pair in these solutions, and lowers the activity of the SO_4^{-2} ion in these solutions. This also increases the ionic strength and lowers the activity coefficients in these solutions. So even lower overall activities of SO_4^{-2} and Ca^{+2} result. When used to calculate an ion activity product for equilibrium with gypsum the resulting condition requires that more sulfate remain in solution to maintain the equilibrium between the added calcium (which is limited by the condition that the pH not exceed 7.0), and gypsum.

Using the mean weighted average for sulfate of 1802 mg/L (AREVA, 2011) and after adjusting for the 15 % difference in calcium, the impact of the $MgSO_4°$ ion pair and for the activity coefficient effects provides a range of concentrations from 7,800 to 10,000 mg/L sulfate. This range has been selected as representative of the sulfate concentrations in the pore waters. These concentrations are comparable to many of the sulfate concentrations noted in the experiments performed at SGS Canada (Lakefield). Comparison of the measured concentrations to the model

estimated values also demonstrates that equilibrium with gypsum, is the dominant control process on sulfate even though the sulfate concentrations much greater than those measured in the JEB pit.

As discussed elsewhere, the ion exchange process appears to be responsible for the elevated magnesium concentrations and the slightly decreased calcium concentrations noted in these waters. A better understanding of the ion exchange process might help to reduce the magnesium concentrations and also reduce sulfate concentrations. The elevated ionic strength noted in these waters starts with the extremely high initial sulfate concentrations used in the pilot plant leaching tests. If sulfuric acid consumption can be reduced in the mill then there should be several benefits. Chief among them will be a decrease sulfate pore water concentrations. Certainly the first effect of lessened sulfate consumption will be a decrease in ionic strength and an increase in the activity coefficients for the Ca^{+2} and SO_4^{-2} components. At this time, it is difficult to assess the impact of reducing sulfuric acid consumption on the release of magnesium. If this is dominantly an ion exchange process it may not have much impact. But if much of the initial leaching releases magnesium from clay minerals, such as chlorite, then it may be worthwhile to investigate this further. Better control of leaching conditions to reduce sulfate consumption and if possible magnesium concentrations could have a significant effect on the final concentration of sulfate in the pore waters.

6.4 Iron

The geochemical model relies primarily upon the precipitation of an iron hydroxide phase typically called ferrihydrite. This phase provides the surface upon which all of the trace metals will adsorb in accordance with the general principles of the surface complexation model. Measured iron concentrations in the laboratory obtained solutions range from 0.01 mg/L to 4.6 mg/L (total iron). The dissolved concentrations are usually less. The activity of Fe^{+3} is controlled by the following reaction;

$$Fe(OH)_3 = Fe^{+3} + 3OH^-$$

and, the resultant K_{sp} is defined as:

$$Ksp = \frac{\left(Fe^{+3}\right)\left(OH^{-}\right)^{3}}{\left(Fe(OH_{3})\right)} = 10^{-37.1}$$

Ferrihydrite type minerals have a range of stabilities, and the $10^{-37.1}$ is a commonly accepted value for this solid. A larger value of the log K_{sp} will produce a less stable mineral, that will be more soluble and the resultant iron concentration may be larger. For these solutions the model calculated iron concentration is 0.025 mg/L at a pH of 6.95. The differences between the observed and modeled concentrations are related to two factors. The first is redox conditions. The largest total iron concentration (after neutralization) was noted in the Test 5 sample at 4.59 mg/L (Table 4). The corresponding dissolved concentration was 0.155. It is possible that the sample still contained some Fe^{+2} in solution. During the time required to filter the sample it might have undergone additional oxidation and precipitated as more ferrihydrite. This lower redox condition would explain the behavior of the selenium and chromium results in this sample. An alternative explanation is that the ferrihydrite was less stable because of the short time available for precipitation.

6.5 Aluminum and Silicon

Because the geochemistry of aluminum and silicon (as silica or SiO_2) are interrelated in the tailings neutralization reactions the two components will be discussed together.

Aluminum (Al) concentrations in the initial solution used in the Test 1 and 3 experiments were around 7,100 mg/L. In the later tests (Tests 5, 6, and 7) the concentrations were around 9000 mg/L. For all experiments concentrations drop significantly when the solutions were neutralized. In the Test 1 system the concentration of Al at a pH of 4 was 1,800 mg/L. For the Test 3 setup, which included leach residue solids the concentration dropped to 900 mg/L. Upon further neutralization, Al concentrations (for all tests) decreased to less than 1 mg/L; with the lowest value of 0.35 mg/L in the Test 5 neutralized solution.

Silicon (Si) concentrations in the untreated barren stream used in Test 5, 6 and 7, ranged from 242 mg/L in the Test 5 initial solution to values of about 100 mg/L (96 and 106) in the Test 6 and 7 samples. Upon neutralization to a pH of 6.95 or greater, silica concentrations dropped to values of 3.51 to 1.91 mg/L. As silicon is not generally considered to be an element of environmental concern silicon phases were not included in the PHREEQC based geochemical model. However, a separate model was developed using Geochemists' Workbench (GWB) (Bethke, 2008, Bethke and Yeakel, 2010) to rapidly assess possible reaction paths (Figures 15 and 16). For that model the Test 1, and 3 the initial solution was augmented with silica at 520 mg/L (as SiO_2). This corresponds to the 242 mg/L Si noted in the Test 5 initial solution. With such a high initial silica concentration all SiO_2 polymorphs in the database (amorphous SiO_2, quartz, tridymite, chalcedony, cristobalite (alpha and beta), and coesite) needed to be suppressed. The models tended to precipitate a silica phase at low pH and drop the Si concentration to levels that were usually less than 50 mg/L. The first model also selected two nontronite (a type of clay mineral) phases and produced unrealistically low concentrations for Si and Al. In subsequent models of this system, the nontronites were also suppressed. Bethke (2008) states that the thermodynamic parameters for the nontronites are probably suspect in most of the current databases and that in the models that include these nontronites in their databases they appear to be more stable than they actually are in nature. Geochemical modeling programs tend to select the most stable phases in the database for most modeling calculations. The modeler must guide the mineral selection process through either selection of appropriate phases as in PHREEQC or for programs like GWB through the suppression of certain phases. The garnet andradite appeared in some of the early path calculations and as it is unlikely to form at low temperatures it was also eliminated. Even with the high initial concentration of silica, the final concentrations were estimated to be around 2 to 5 mg/L (Figure 15). Aluminum concentrations appear to be significantly underestimated in the model. An additional model was run using a lower initial silicon concentration (based upon the 90 mg/L concentrations noted in Test 6 and 7), a silica concentration of 200 mg/L was used. It had little impact on the final concentrations. This failure to change the silicon and aluminum concentrations is a result of the phase rule that states that it is not necessarily the amounts of material present in a mineral assemblage that will control final concentrations but it is the presence or absence of certain phases in an assemblage that will dictate the concentrations in solution. The amounts of phases may have changed in the second

model, but this did not change the basic assemblage, i.e., the same minerals were present. Therefore, the thermodynamic activities of the components remained the same and so the concentrations in solution remained the same.

Saturation indices calculated using PHREEQC indicated that basaluminite ($Al_4(OH)_{10}SO_4$) was oversaturated in the neutralized solutions. Therefore, a series of simulations were run that allowed for the precipitation of basaluminite. However, the modeled Al concentrations were significantly lower than the observed values and so the model based upon the formation of $Al(OH)_3$(am) was retained as the preferred model for aluminum.

The PHREEQC model used an amorphous aluminum hydroxide phase [$Al(OH)_3$(am)] and the predicted Al concentrations using that simpler model were in excellent agreement with the measured concentrations (Table 10). Therefore a concentration of 0.5 mg/L has been selected to represent the pore water concentration for aluminum (Table 11).

Using the highest value reported from the Test 5 measurements 3.51 mg/L Si, and examining the output from the GWB reaction path model silicon concentrations are expected to fluctuate between 2 to 5 mg/L and so a value of 5 mg/L has been defined. Basically, the 3.51 mg/L value has been rounded up to 5 mg/L (Table 11).

6.6 Antimony

Antimony (Sb) concentrations were below the 1.0 mg/L reporting limit for the initial solution used in the Test 1 and 3 results. Consequently, antimony was not included in the neutralization model for the Test 1 and 3 datasets. The testing program (Tests 1 and 3) demonstrated that upon neutralization, the pH 4 samples had concentrations of 0.022 and 0.009 mg/L (Sb). For the samples with pH value greater than 6.75 all concentrations were below the 0.02 mg/L reporting limit. Surface complexation onto the precipitated hydrous ferric oxide is the most likely process that is controlling final concentrations of antimony. In the Test 5, 6 and 7 results (Table 10), the initial antimony concentrations were approximately between 0.0015 to 0.018 mg/L. These low concentrations in the barren stream suggest that antimony will not be of environmental concern.

The sample with the lowest initial concentration of 0.0017 mg/L upon neutralization produced a concentration of 0.00014 mg/L. However, for the Test 6 and 7 samples which had greater starting concentrations such a significant reduction in concentration was not noted and the neutralized concentrations were similar to the initial concentrations. The geochemical model also did not demonstrate any decrease in concentrations. This was caused primarily by an apparent limitation in the surface complexation database. In the geochemical model database the surface complexation reactions for antimony are based upon the $Sb(OH)_4^-$ component, which represents the Sb(3) valence, while the dominant component in the primary model is Sb(5), which is represented by $Sb(OH)_6^-$ (Figure 17). An alternative model was run at a lower partial pressure of oxygen primarily to evaluate Cr(III) behavior. The Eh for this alternative model was still not low enough to favor the $Sb(OH)_4^-$ component. Based upon experience gained at McClean Lake, the redox requirement to allow for the dominance of the $Sb(OH)_4^-$ component is not a reasonable representation of the tailings neutralization process; it is simply too low an Eh. Therefore a third model with an even lower Eh is not justified. Significant attenuation of antimony as represented by the laboratory results and confirmed by the geochemical model as currently constructed is not expected to occur. A pore water concentration similar to the unneutralized samples noted in Tests 6 and 7 of approximately 0.016 mg/L has been selected (Table 11).

6.7 Arsenic

In the Test 1 and 3 results, arsenic concentrations showed concentrations of 0.09 mg/L and 0.074 mg/L at a pH of approximately 4. Arsenic was reported at < 3 mg/L in the initial low pH solution and so a model was not developed for the Test 1 and 3 conditions. Concentrations decrease to generally less than 0.01 mg/L when the pH is raised to 6.75 to 8. Crystalline scorodite ($FeAsO_4 \cdot 2H_2O$) may be at saturation in the lower pH samples as saturation index values of 0.53 and 0.59 were observed for these samples and the more soluble amorphous scorodite (sometimes called ferric arsenate) phase was undersaturated in all cases (Langmuir et al., 2006). For the pH ~ 4 samples the SI values averaged around -2.4. For the higher pH samples, SI's were all well below zero, with values between -4.5 to –7.4 for the amorphous scorodite. These values suggest that another process is probably responsible for the lowered

arsenic concentrations in these higher pH samples. Sorption onto hydrous ferric oxide surfaces or coprecipitation onto the precipitated ferrihydrite is the most probable process controlling arsenic. Given the low initial metal concentrations and high initial concentration of iron in the tailings discharge solution this is expected. Furthermore, these processes are closely related so they may be difficult to distinguish and they are probably responsible for attenuation of many of the trace metals examined in this report.

These observations are confirmed when the Test 5, 6 and 7 results are examined. Initial concentrations in the barren stream are between 1.1 and 1.8 mg/L. Concentrations decrease to approximately 0.02 mg/L upon neutralization to a pH around 7. The geochemical model estimates even lower concentrations with values of 0.001 to 0.004 mg/L (Table 10).

The dip in the percent adsorbed curves between pH 4 and 4.75 (Figures 6, 7 and 8) is believed to be caused by competition with other oxyanions for adsorption sites on the HFO surface. The most significant is competitive sorption caused by the high concentrations of sulfate. However, the percentage adsorbed is small and so sulfate was not included in the figures. Sulfate also tends to display a low pH for a desorption edge. Review of the sulfate adsorption data confirms that the extent of sulfate adsorption is decreasing at pH values greater than 4.

AREVA Resources has considerable experience in controlling arsenic concentration in uranium mill tailings (Mahoney et al., 2007). The low initial concentrations of arsenic expected in the Kiggavik ores and the high iron concentrations in the barren stream will result in low concentrations of arsenic in the pore waters. We have selected a value of 0.02 mg/L based upon the Test 6 laboratory results and the similarity in the Test 6 geochemical model (Table 11).

6.8 Barium

Barium (Ba) concentrations for the surface complexation model (no barium mineral precipitation) did not show any significant decrease upon neutralization. The surface complexation constants for barium are not large, and so at these near neutral pH values barium is only slightly adsorbed onto the HFO surface. The addition of barium to the solution to treat for

radium changes the nature of the percent adsorbed calculations, and in the case of barium the calculations are no longer representative of the sorption process. Therefore barium has not been included on Figures 3, 4 or 5.

One model included barite precipitation (results shown on Figure 1) and that model predicted lower concentrations than observed. This was consistent with the earlier measured saturation indices that generally indicated an oversaturated condition with most SI values around 1.0±0.2. In many different waters from sites around the world, oversaturated conditions for barite with SI values often around 0.5 or greater have been noted. It may be possible that a less stable barite phase actually precipitates under ambient near surface conditions. That phase may have a log K_{sp} of closer to -9.0 rather than the generally accepted value of -9.97. This is believed to be the case in these waters as in the Test 5 results barium concentrations in the initial solution and in the neutralized sample both had Ba concentrations of approximately 0.13 to 0.14 mg/L. (The Test 6 and 7 barium concentrations were not available at the time this report was prepared). These waters are oversaturated with respect to Barite (log K_{sp} = -9.97) by about one log unit. It should also be appreciated that the neutralized solution had been treated with an addition of $BaCl_2$, which effectively increased the Ba concentration to nearly 100 mg/L prior to precipitation of additional barite. However, in Test 6 the initial concentration changed from 0.138 to 0.134 mg/L after the addition of the $BaCl_2$. The Test 1 and 3 samples (Tables 2 and 3) showed lower concentrations, around 0.05 mg/L after some aging.

The geochemistry of radium is intimately connected to barium and these two parameters will be discussed in more detail in Section 6 of this report. However, based upon the slightly oversaturated conditions noted in the laboratory samples, which is supported by observations in various water samples from locations around the world, we have selected a concentration of 0.15 mg/L for barium (Table 11).

6.9 Beryllium

Beryllium (Be) concentrations in the initial solutions (Tests 5, 6 and 7) average around 1.0 mg/L. Upon neutralization these concentrations drop to less than 0.01 mg/L, and in the case of the Test

5 results the laboratory reported concentration was 0.0006 mg/L. Model results (Table 10) show even greater decreases in concentrations with final values in the 0.00001 mg/L or lower predicted values.

Figures 3, 4 and 5 indicate the beryllium is strongly adsorbed. Furthermore, its ionic potential (charge/ionic radius) suggests that it should readily form insoluble oxide or hydroxide phases (Railsback, 2003). The parameters used to model beryllium surface complexation reactions onto HFO were derived from a linear regression described by Dzombak and Morel (1990). The surface complexation constants for Be as reported by Dzombak and Morel were not obtained with experimentally determined sorption data, but rather were estimated using a relationship between the first hydrolysis constant for hard cations and their model fitted surface complexation constants. This method has previously been shown to overestimate uranyl adsorption (Mahoney et al., 2009a, 2009b). Furthermore, Gustafsson (2003) demonstrated that surface complexation constants for tungstate and molybdate that were estimated using a similar linear regression method did not produce reliable fits under a range of conditions. It is reasonable to assume that that these surface complexation constants may be too "strong" and they may have a tendency to overestimate surface complexation of beryllium. The experimental data suggest approximately a 99% or greater removal for beryllium upon neutralization. Figures 3, 4 and 5 demonstrate that the adsorption edge for Be is well below a pH of 4. Therefore, a value of 0.01 mg/L has been selected as a conservative estimate of the pore water concentration for beryllium (Table 11), actual values may be lower than the selected value.

6.10 Boron

For the low and near neutral pH values expected for the tailing neutralization process, boron (B) is present as $B(OH)_3$ (boric acid). This species has a neutral charge and the corresponding surface complexation constant is one of the smaller constants in the database. In the calculations used to generate Figures 3 through 8, boron adsorption was always less than 1.0 percent. Review of the data used by Dzombak and Morel (1990) demonstrates that surface complexation of boron is slight. Therefore, it would be expected that surface complexation would not be a significant process that could remove boron from these solutions and this is confirmed by the model results

(Table 10). Concentrations appear to increase for these neutralized solutions. As discussed previously, these apparent increases are related to the removal of water as gypsum forms and as ferrihydrite and aluminum hydroxides precipitate. Nonetheless, it demonstrates that boron is geochemically mobile. The neutralization tests show a slight decrease in concentration (at best about 80% removal). For example, in Test 7 an initial concentration of 17.8 mg/L B is reduced to 3.2 mg/L. This is probably related to some small amount of coprecipitation, but it should not be relied upon. As some attenuation is noted in these experiments, the concentration from the Test 6 neutralized solution of 4.4 mg/L (rounded to 4.5 mg/L) has been selected to represent the boron pore water concentration in the neutralized tailings (Table 11). This number also represented the highest of the three concentrations for the second set of neutralized tailings experiments.

6.11 Bismuth

As mentioned previously, bismuth (Bi) was not included in the database selected for the PHREEQC geochemical model. Dzombak and Morel (1990) do not include estimated constants for surface complexation in their compilation, so any model that even considered surface complexation of bismuth could not be readily developed. Only one starting concentration was available from the SGS testing program. The Test 5 sample had a concentration of 0.299 mg/L (total Bi). Neutralized samples do show a significant decrease in concentration; values for total Bi are reported at 0.00015 mg/L. Comparable and sometimes even lower Bi concentrations were reported for the Test 1 and 3 results. For those tests the lowest quantified concentration was 0.00002 mg/L and several samples had concentrations less than 0.00001 mg/L. The lowest concentrations generally applied to the higher pH samples. A review of several Eh-pH diagrams (Figures 18a, b) indicate that at higher concentrations (around 3 mg/L) $Bi_2O_3(s)$ is stable, but at the lower initial concentrations as represented by the results from Test 5 a separate solid will not form and the dominant species in solution is $Bi(OH)_3°$. However, bismuth could be incorporated into a coprecipitate, consisting of the precipitating Al and Fe hydroxides.

Because of the limited data, a value equal to the total Bi concentration in the neutralized sample from Test 5 has been selected. The selected value is 0.00015 mg/L (Table 11).

6.12 Cadmium

Cadmium (Cd) concentrations show significant decreases with increasing pH. However, the surface complexation based model does not predict such low concentrations (Table 10) (Figures 3, 4, and 5). For these conditions the adsorption edge for cadmium is commonly greater than a pH of 7. Cadmium tends to require pH value greater than those used in the model before significant surface complexation will occur. In many cases, it is possible that a coprecipitation reaction, possibly with calcite may control cadmium (Mahoney 1998, 2001). Examination of saturation indices in the measured samples suggests than calcite may be oversaturated in many of the samples from the Test 1 and 3 Series. Otavite ($CdCO_3$) is undersaturated with most SI values ranging from -1.57 to -3.3. However, the model simulations are, for most of the steps, slightly undersaturated with respect to calcite, so it may require some changes in the model to get a calcite coprecipitate to form in the model. These undersaturated conditions are the result of the low alkalinities generated in the model. Alkalinities are significantly higher in the test samples and so it is possible that a calcite dominant coprecipitate could form in the actual neutralization process.

Among the Test 5, 6 and 7 results, no significant changes in Cd concentrations were noted in the Test 5 samples, the concentration apparently increased and therefore an analytical error is suspected. However significant decreases in Cd were noted in the Test 6 results. This may possibly be caused by a coprecipitation reaction. Saturation indices for calcite for the two laboratory generated neutralized solutions from Tests 6 and 7 suggest that calcite could form. The Test 6 sample had an SI of -0.16 and the Test 7 neutralized sample was slightly oversaturated with an SI of 0.07. Based upon the difference in Cd concentrations between the two tests it is most likely that calcite did form in the Test 6 solution and it is also possible that calcite did form in the Test 7 experiment, but to a lesser extent. Because of the inconsistent behavior in the laboratory results between the Test 6 and 7 samples we have eliminated the less conservative value (0.0007 mg/L) from the Test 6 experiment (see discussion related to zinc in section 5.29). A coprecipitation model with calcite and otavite was not prepared because of the low alkalinities predicted in the primary model. Also the current sorption based model has

shown that cadmium displays a limited amount of attenuation due to the demonstrated sensitivity to the initial concentrations, particularly if the final pH is near or slightly less than 7.0. The concentration of 0.003 mg/L from the Test 7 laboratory results is probably caused by a coprecipitation process. Consequently, that value has been selected as representative of cadmium concentration in the tailings pore water.

6.13 Chromium

Because of the high oxidation potential defined in the primary geochemical model the dominant chromium (Cr) species was Cr(6), [as chromate (CrO_4^{-2}) and bichromate ($HCrO_4^-$)]; no chromium bearing minerals were included as possible phases so only surface complexation was available as an attenuation process. The primary geochemical model used to evaluate the behavior of most of the elements described in this report assumed a fixed partial pressure of oxygen of $10^{-0.7}$ atms. The primary model assumes the solution is in equilibrium with atmospheric oxygen at a partial pressure of 0.2 atmospheres (log value -0.7 atms). For the Test 1 and 3 model simulation, chromium does not show a reduction in value (Figure 1) that is similar to the reduction in the measured concentrations. Similarly, the results from the Test 5, 6 and 7 models (Table 10) show some attenuation, but the measured concentrations are typically two or more orders of magnitude greater. The discrepancy between measured and modeled results is believed to be related to the assumptions about Eh conditions in the primary geochemical model.

The high Eh condition used in the initial models meant that chromium was assumed to be predominantly Cr(6) (Figures 19a,b), and surface complexation reactions were the only process that could attenuate chromium. In the primary model, sorption of Cr(6) was slight to moderate (Figures 6, 7 and 8) and so modeled Cr concentrations remained high, and the resulting modeled values were significantly greater than the laboratory measured concentrations. Based upon this difference additional modeling was performed.

Cr(3) tends to form insoluble precipitates such as Cr_2O_3(cr) and $Cr(OH)_3$ (Figures 19a,b) so it is most likely that some type of mineral phase was precipitating in the neutralized solutions. This could be a distinct mineral or possibly in a coprecipitate with the dominant ferrihydrite. It is also

reasonable that the actual oxidation reduction potential of the neutralized tailing slurry is much lower than the value used in the early models which were based upon equilibrium with atmospheric oxygen. It had been demonstrated that for conditions present in the McClean Lake tailings that redox condition are commonly influenced by reactions between ferric hydroxide and ferrous iron (Mahoney et al., 2007). These intermediate redox conditions were approximated in a subsequent model that lowered the partial pressure of oxygen to 10^{-30} atmospheres. This is a means to adjust redox conditions through the following reaction that is present in the PHREEQC database and defines the upper stability limit of water:

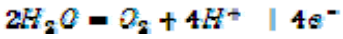

Rearranging terms to define an Eh, one obtains

$$Eh = E° + 0.059/4 log PO_2[H^+]^4$$

or

$$Eh = 1.23 + 0.0148 log PO_2 - 0.059 pH$$

At a pH of 7.0 and a partial pressure of oxygen of 10^{-30} atmospheres, this produces an Eh of 0.373 volts. Using the partial pressure of $10^{-0.7}$ atmospheres would produce an Eh of 1.044 volts. A true partial pressure of 10^{-30} atmospheres is unrealistically low, it represents a condition equivalent to one molecule of O_2(g) in all the oceans (Anderson, 2005), but in PHREEQC it provides a method that can be used to fix an Eh that will change as the pH changes. This partial pressure has been set mainly to define an approximate area in Eh-pH space. The alternative is to define an Eh as one would define a fixed pH or other phase. Deliberately fixing the Eh has a shortcoming if the pH changes but the Eh remains constant. Using a method that fixes a partial pressure allows for some variation in Eh as pH's are changed in pH sweep calculations.

The Eh-pH diagram (Figure 19a) shows a large stability field for Cr_2O_3(cr), which indicates that oxide, and even the less stable hydroxides such as $Cr(OH)_3$(cr) (Figure 19b) solids are able to

form under a wide range of Eh-pH conditions. Figure 19b also includes the Eh-pH conditions for the additional geochemical models that were run (Lined X's). The geochemical models constructed to better evaluate the chromium reactions included either $Cr(OH)_3$ or Cr_2O_3 as possible precipitating phases. These initial simulations were run at the previously selected pH of 6.95. Models that allowed for formation of $Cr(OH)_3$ produced a chromium concentration of 0.72 and 0.67 mg/L for the Test 6 and Test 7 initial compositions (Figure 20). Increasing the pH to the measured value of 7.33 decreased chromium concentrations from 0.67 to 0.36 mg/L. These values are close to the reported concentrations of 0.32 and 0.34 mg/L. Selection of the more stable Cr_2O_3 phase resulted in vastly lower concentrations with values at a pH of 6.95 of 0.00028 (Test 6) and 0.00026 mg/L (Test 7). Because the Cr_2O_3 phase results were so low, additional simulations based upon the Cr_2O_3 phase were not prepared. Give the short time for precipitation to occur in the laboratory tests the less stable $Cr(OH)_3$ phase is expected to precipitate rather than a more crystalline Cr_2O_3. This is in accordance with Ostwald's Step Rule.

Because of the close agreement between the laboratory derived concentrations and the model calculated values it appears that the precipitation of a $Cr(OH)_3$ phase is most likely responsible for controlling chromium concentrations in these samples.

Based upon the results from Test 6, a value of 0.35 mg/L has been selected as representing the chromium concentrations in the tailings pore waters. Geochemical modeling supports this value.

6.14 Cobalt

Initial concentrations of cobalt (Co) were 4.6 mg/L in the discharge solution used in the Test 1 and 3 systems (Tables 2 and 3). Concentrations dropped slightly to between 3.9 and 3.8 mg/L at pH 4. The cobalt in the samples dropped further with increasing pH with a final concentration of approximately 0.2 mg/L at pH 6.75. The geochemical model only employed surface complexation of cobalt onto the precipitated ferrihydrite surface, but the amount of complexation was limited and concentrations did not decrease in the modeled results to the degree seen in the actual results. In the model sweep calculations adsorption of cobalt was less than 1.0 percent. Two cobalt bearing phases were identified in some solutions as being potentially oversaturated.

These include Spinel-Co (Co_3O_4) and $CoFe_2O_4$, both of these phases are related to spinels, which are generally high temperature phases, and they probably do not form under low temperature conditions. However, Krupka and Serne (2002) suggest that Co_3O_4 may be stable at ambient temperatures. Figure 21 is an Eh-pH diagram for cobalt that was prepared using the HYDRA/MEDUSA program and database (Puigdomenech, 2009). Instead of the Co_3O_4 phase suggested by Krupka and Serne, it identifies a $Co(OH)_3$ phase, the stability field for that solid encompasses the conditions expected in the neutralization tests. Additional model simulations did not confirm the precipitation of a cobalt phase and so a coprecipitation mechanism is likely.
In the second series of tests (Table 10) initial concentrations were similar to the Test 1 and 3 values and concentrations decreased to similar or lower values. The models did not show any significant attenuation. The modeled values listed in Table 10 appear to show an increase in concentration (these values for the Test 6 and 7 model results have been included to demonstrate how PHREEQC can apparently increase concentrations). A value 0.1 mg/L, based upon the Test 6 neutralized sample, has been selected to represent the pore water concentration for cobalt (Table 11).

6.15 Copper

For the Test 1 and 3 results, measured copper (Cu) concentrations for the samples with pH values greater than 6 are in generally good agreement with the model predicted concentrations. Initial copper concentrations in the Test 1 and 3 simulations were 434 mg/L (Table 7). Measurements in the pH 4 solutions show decrease in copper concentrations to approximately 250 mg/L. However, the modeled concentration did not demonstrate this reduction in concentration but rather remained at a concentration just slightly less than the initial value; the model at pH 4 showed only a 24 mg/L decrease in copper concentration. At a fixed pH of 4.0, the only available method for copper removal was through surface complexation onto precipitating ferrihydrite; tenorite [CuO(cr)] was strongly undersaturated at this pH (Figure 22). As the extent of copper adsorption at a pH of 4 is limited (Figures 3, 4, 5 and 23) there is a slight possibility that a copper iron coprecipitate may have formed under these conditions and this material removed about half of the initial copper. For the higher pH samples, copper concentrations decreased to less than 0.5 mg/L with some values as low as 0.022 mg/L (these

low concentrations were noted in the higher pH samples). Under the higher pH conditions, the model allowed for tenorite precipitation, and for samples with a pH of 6.75 or greater tenorite precipitated. Other copper sulfate hydroxide minerals such as antlerite [$Cu_3(OH)_4SO_4$] or brochantite [$Cu_4(OH)_6SO_4$] were not oversaturated in these simulations. Agreement between the Test 1 and 3 models and the measured results (Figure 1) is good.

Tests 5, 6 and 7 had similar starting concentrations with a low of 327 mg/L in the Test 5 sample to nearly 500 mg/L in the Test 7 barren stream. Upon neutralization concentrations decreased significantly. A measured copper concentration of 0.19 mg/L was noted in the pH 6.95 solution obtained from the Test 5 setup. The geochemical model for the Test 5 solution had a comparable concentration of 0.13 mg/L. The Test 5 pH 6.95 solution was undersaturated with respect to tenorite. The geochemical model was similarly undersaturated with respect to tenorite and the model indicated that the copper was removed from the solution through surface complexation (Figure 3). The surface complexes Hfo_wOCu$^+$ and Hfo_sOCu$^+$ were the most abundant surface complexes on the HFO surface. As the initial copper concentrations were greater than 300 mg/L this is not unexpected.

The Test 6 and 7 neutralized solutions displayed concentrations of 2.8 and 2.6 mg/L, respectively. The modeled values were about an order of magnitude lower. For the laboratory neutralized solutions, both samples were oversaturated with respect to tenorite; and in the models prepared for these conditions tenorite precipitated. Both the measured concentrations and the model derived values indicate that copper concentrations can be greatly reduced using the proposed treatment method.

Further evaluation of the copper system was undertaken and additional simulations were prepared. Figure 23 shows the distribution of copper as moles of adsorbed surface complexes or in minerals for two of those additional models; both models are based upon the Test 6 initial solution. The first one assumes tenorite is the precipitating phase and the second model assumes that malachite [$CU_2(OH)_2CO_3$] precipitates rather than tenorite. In both cases copper modeled values remained in or around the 0.3 mg/L range an order of magnitude lower than the measured concentrations. One other model was prepared that adjusted the stability of tenorite and made it

more soluble by an order of magnitude. This model showed only a slight change in the dissolved copper concentration. In that model as in the tenorite/malachite comparisons, the "excess" copper was adsorbed through surface complexation onto HFO.

Reasons for the discrepancies between the Test 1, 3 and 5 results, which produced concentrations less than 0.5 mg/L and the Test 6 and 7 results, which had concentrations around 2 to 3 mg/L, have not been identified. However, based upon the predominance of evidence (from Tests 1, 3 and 5) and the support for concentrations less than 0.5 mg/L from the model calculations a source term of 0.4 mg/L has been selected for copper (see Test 1 result of 0.357 mg/L, Table 2). Copper concentrations are sensitive to increases in pH so it may be possible to lower concentrations through increasing the pH. Additional efforts to better understand the reasons for the differences in the experiments should be undertaken.

6.16 Lead

Lead (Pb) concentrations in the expected tailings discharge solution (untreated) were below the reporting limit of 5 mg/L. Consequently an initial model was not developed for the Test 1 and 3 setups. As expected, lead concentrations drop with increasing pH. Using the Test 5, 6 and 7 data we can assume that the initial lead concentration in these samples was likely around 3 mg/L. For the Test 1 and 3 datasets the pH sample 4 lead values drop to approximately 0.2 mg/L (with a range of 0.12 to 0.28 mg/L). Concentrations continued to decrease to values below 0.01 mg/L for the higher pH ranges. The two samples with the longest aging times have the lowest lead concentrations.

In Tests 5, 6 and 7 (Table 10) the average initial lead concentrations were around 3 mg/L. The neutralized solution (pH 6.95 to 7.33) had lead concentrations of 0.04 to 0.016 mg/L. The model only allowed for surface complexation of Pb^{+2} onto hydrous ferric oxide (HFO). Lead ions are strongly attached to the HFO surface. It was this strong affinity of lead for the HFO surface that was a primary reason that strong sites were added to the diffuse layer model developed by Dzombak and Morel (1990). Model estimated values for lead are approximately an order of magnitude less than the measures concentrations. This has been observed in several

parameters and there may be several reasons for these discrepancies. For example, a difference in surface charge of the actually precipitated ferrihydrite when compared to the simpler model derived ferrihydrite may explain some of these discrepancies. For lead, the pore water concentration of 0.04 mg/L (Table 11) has been selected based upon the measured concentration in the Test 6 experimental work.

6.17 Lithium

Initial lithium (Li) concentrations ranged from approximately 30 to 43 mg/L. Neutralization tests indicated some attenuation, but most of the decrease was noted in the Test 1 and 3 samples that had target pH values in the 7.8 to 8.1 range and that had at least 48 hours of aging. The geochemical model did not include surface complexation constants for Li. Most likely Li concentrations are influenced by the major ions, most specifically sodium. Ion exchange may play some role in controlling lithium concentrations. A value of 20 mg/L has been selected as the pore water concentration. This is based upon the greatest value noted after neutralization of Tests 5, 6 and 7 (Table 10).

6.18 Manganese

In most cases, estimating equilibrium based manganese (Mn) concentrations is difficult. There are numerous reasons that hinder such a prediction. Fortunately, for drinking water at least, Mn is considered a secondary standard and mainly deals with esthetics and possible staining of plumbing fixtures and perhaps staining of clothing. From a theoretical basis, manganese is generally considered to be insoluble so over the long term particularly for oxygenated waters concentrations are expected to be low.

One of the most significant issues in estimating Mn concentrations is slow precipitation kinetics that prevents the attainment of a final equilibrium concentration. Related to this is the fact that manganese has several important valences states including Mn(II), Mn(III) and Mn(IV). This is seen in the Eh-pH diagram (Figure 24) where three different oxide solids are present. The Mn(IV) valence is represented by MnO_2(cr), the Mn(III) valence is represented by Mn_2O_3(cr),

and a mixed valence solid consisting of Mn(3) and Mn(2) is seen in Mn_3O_4(c). In some cases auto-oxidation occurs among the three valences, which adds additional complications to the reaction kinetics and subsequent stability of the solids. Furthermore, there is also an abundance of possible Mn bearing minerals and most of these appear to be extremely stable. The presence of these low solubility minerals complicates any assessment related to Mn solubility as selection of these phases tends to result in extremely low model derived values. These low values are commonly unrealistic when compared to the observed concentrations. One way to alleviate this issue is to select the more soluble manganese carbonate rhodochrosite. For these models, rhodochrosite ($MnCO_3$) was included in the list of possible phases, and saturation indices were reviewed for the neutralized waters. In the database used for this evaluation rhodochrosite has been assigned two different solubility product constants. The more stable (more crystalline form) has a log K_{sp} of -11.13. The more soluble form [identified with a (d) for disordered] has a log K_{sp} of -10.39. Many of the neutralized solutions from the SGS testing program (near neutral pH samples) have ion activity products between the solubility product constants for these two phases. This is evidence that a rhodochrosite of intermediate stability could be formed during neutralization.

Because of the high initial acidity in the untreated barren stream, the geochemical model has tendency to produce a low alkalinity as the solution is neutralized. This low alkalinity is responsible for undersaturated conditions for carbonate minerals including calcite, magnesite and rhodochrosite. These solids were included as possible phases, but even for the low solubility rhodochrosite these solids can precipitate as long as rhodochrosite is the only Mn bearing phase available. An additional model was constructed and using the final pH noted in the Test 7 sample (7.33, rather than the 6.95 noted in the other datasets, which is similar to the design specified pH) and using the stable rhodochrosite phase a value of 14.9 mg/L was obtained. For the assumptions related to these model calculations the value is comparable to the 5.9 mg/L Mn concentration noted in the Test 7 neutralized sample. For manganese a range between 10 to less than 1.0 mg/L has been selected as representing the pore water composition (Table 11).

6.19 Molybdenum

The concentration of molybdenum (Mo) in the Test 1 and 3 and initial solution (barren stream) was less than 0.6 mg/L. Consequently, a model for molybdenum attenuation was not included in the Test 1 and 3 models. In the Test 5, 6 and 7 datasets, molybdenum concentrations in the initial solutions ranged from 0.16 to 0.20 mg/L. Concentrations decreased only slightly upon neutralization; concentrations ranged from 0.18 to 0.14 mg/L. Model concentrations showed some reduction in value, ranging from 0.05 to 0.02 mg/L. Review of saturation indices for Mo bearing minerals [$FeMoO_4$, Ferrimolybdate ($Fe_2(MoO_4)_3 \cdot 8H_2O$), Powellite ($CaMoO_4$) and $NiMoO_4$) indicated that the initial and neutralized solutions (Tests 5, 6, and 7) were all undersaturated with respect to these minerals.

The model assumed only surface complexation for molybdenum, using the reactions and constants published by Gustafsson (2003) (Figures 6, 7, and 8). It should also be understood that the dominant molybdenum ion under the conditions present in the laboratory studies and in the model is molybdate (MoO_4^{-2}). The molybdate ion is an oxyanion and it has a negative charge and so the greatest amount of adsorption will take place under low pH conditions when the ferrihydrite surface has the greatest positive surface charge. However sulfate tends to occupy HFO surface sites that could complex with Mo under these low pH conditions. With increasing pH, molybdate adsorption will decrease. In many cases the pH has to be greater than 7 to see significant decreases in surface complexed Mo. The models tend to overestimate Mo attenuation in these experiments. Based upon this assessment the laboratory derived concentrations have been deemed to be more conservative and the pore water concentration selected for molybdenum is based upon the greatest initial measured value of 0.20 mg/L.

6.20 Nickel

Nickel (Ni) concentrations for the Test 1 and 3 measurements are shown on Figure 2. Concentrations decrease with increasing pH. Model derived estimates are significantly greater

than the measured concentrations. Furthermore, all modeled solutions were undersaturated with respect to $Ni(OH)_2$.

The Test 5, 6 and 7 measurements also display a similar pattern (Table 10), with model concentrations significantly greater than measured concentrations. The laboratory testing program indicates approximately 99 percent or better removal of nickel from solution, but the model calculations suggest about 75 percent removal at best. Therefore, it appears that either surface complexation or more likely a coprecipitation process with the precipitating ferrihydrite is controlling the concentrations of Ni^{+2}. The modeled concentrations are several orders of magnitude greater than the measured values, and so a surface complexation process is not likely.

Similar reductions in Ni concentration have been documented at McClean Lake and some possible coprecipitate possibly with ferrihydrite may be responsible for the removal of nickel from these solutions. A reaction path model developed using Geochemist's Workbench selected trevorite ($NiFe_2O_4$) as a possible precipitating phase. This phase has the potential to greatly reduce nickel concentrations. However, this phase is a spinel, and spinels generally form at high temperatures, and so it is probably too stable to precipitate under these low temperature conditions (i.e., any model specifically designed to evaluate nickel behavior in a low temperature neutralization process should probably not include trevorite as a possible precipitating mineral, unless there is compelling evidence to the contrary).

The Test 6 and 7 laboratory results were similar, with values ranging from 0.31 (Test 7) to 0.42 mg/L. The Test 5 result was much lower at 0.01 mg/L. The Test 1 and 3 results showed a range of concentrations, with the non aged lower pH samples showing values of between 0.7 to 0.9 mg/L; upon aging these concentrations decreased. The higher pH samples also showed lower values. In selection of a pore water concentration, the laboratory derived data with the target pH of 7.0 have (Tests 6 and 7) taken priority and the Test 6 result at 0.4 mg/L has been selected as a conservative estimate for nickel.

6.21 Phosphate

Model phosphate (PO_4^{-2}) concentrations (reported as P in Figure 2) are complicated because at a pH 4.0 strengite ($FePO_4{:}2H_2O$) is expected to precipitate. The reason for the complication is because ferrihydrite is also stable and it will tend to take iron away from the strengite. A GWB reaction path model showing the initial formation of strengite followed by its dissolution and the formation of additional ferrihydrite and hydroxyapatite [$Ca_5(PO_4)_3OH$] is plotted on Figure 25. The available phosphate is transferred into hydroxyapatite ($Ca_5(PO_4)_3OH$). The iron originally present in the strengite results in the formation of additional ferrihydrite. Concentrations of selected components are shown on Figure 26. Figures 25 and 26 were prepared using Geochemists Workbench (GWB) (Bethke, 2008, Bethke and Yeakel, 2010). These calculations used the modified version of the Test 1, 3 initial solution (Table 2) (fewer trace metals) as a starting composition. Figure 25 demonstrates how strengite forms initially, but with increasing pH it dissolves as the iron in the strengite is taken up by ferrihydrite [$Fe(OH)_3$]. Eventually the pH increases enough so that hydroxyapatite forms (called hydroxylapatite on Figure 25). Figure 2 shows the effect of this process on the Test 1 and 3 PHREEQC based modeled P concentration. In the near neutral region more hydroxyapatite forms and phosphate concentrations continue to decrease. Among the Test 1 and 3 results the modeled phosphate values are several orders of magnitude greater than the measured concentration.

The Test 5, 6 and 7 results show a similar behavior (Figure 27). This figure shows moles of mineral present, and it should be remembered that hydroxyapatite contains three phosphates per formula unit, while strengite contains only one. Modeled phosphate values are greater than measured concentrations. In selecting the expected pore water concentration, several lines of evidence were used including the alternative GWB simulation. Figure 25 shows selected concentrations for that reaction path model and at a pH of 7 the model reports a concentration of HPO_4^{-2} of 0.1 mg/L. This component has a formula weight of 96 g/mole versus 31 g/mole for just P. Therefore the estimated value is 0.033 mg/L as P, which is comparable to the measured concentrations. Slight differences are noted in the solubility product constants for hydroxyapatite between the two programs.

The expected pore water concentration for P is defined at 0.1 mg/L based upon the highest measured concentration (Test 7), after neutralization (Table 11).

6.22 Selenium

Selenium (Se) has three valence states (Figure 28) including Se(6) which is usually present in water as the selenate ion (SeO_4^{-2}). The Se(4) valence typically forms a selenite ion (SeO_3^{-2}), or biselenite ($HSeO_3^-$) ion, depending upon pH. The third form is zero valent and it commonly is represented by the metal selenium [Se(c)]. Selenate is generally considered to be mobile in groundwater. In these waters, the abundant sulfate will compete for adsorption sites and so surface complexation is expected to have a limited impact on selenate removal. Selenite and biselenite are stable under more moderate redox conditions and so if redox conditions are favorable then some surface complexation can take place on the ferrihydrite surface.

Selenium concentrations for the Test 1 and 3 initial solution were reported at less than 3 mg/L. Consequently the Test 1 and 3 models did not include Se. The Test 5 concentrations decreased from 0.14 (initial) to 0.04 mg/L (neutralized). However, for the Test 6 and 7 measurements, selenium concentrations decreased only slightly from 0.11 mg/L to 0.10 mg/L. The modeling results retain the initial 0.11 mg/L values.

The alternative geochemical model described in section 5.13 (chromium) that represented moderate redox conditions (Eh of approximately 0.37 volts at a pH of 7.0) provided additional insights into the behavior of selenium. Under conditions where selenite is more stable than selenate more selenium (selenite) is adsorbed (compare Figure 7 to Figure 20) and Se concentrations decrease. This may help explain the differences noted particularly in the Test 5 results. In Test 5 laboratory data a decrease in Se is noted, but the Test 6 and 7 results do not show a decrease of the same magnitude as in Test 5. Under moderate reducing conditions it is possible that some adsorption of selenite took place in the Test 5 measurements. These differences are still much less than the model estimates, suggesting that redox conditions may be close to the selenate/selenite boundary line. The Test 6 and 7 results represented a greater oxidation potential where selenate would be the dominant form. Overall the laboratory results suggest that generally selenate is present in these solutions.

Based upon the consistency of the Test 6 and 7 results with the geochemical model and the general understanding of selenium behavior in solution a value of 0.05 mg/L selenium has been selected as representative of the tailings pore water (Table 11). This is considered to be a reasonable compromise between the overly conservative (oxygenated) laboratory experiments and the perhaps overly optimistic (too low) values estimated in the selenite dominant model. If additional evidence indicates a more reducing condition then selenite may become even more stable and some additional attenuation could lower the selected concentration.

6.23 Silver

Silver (Ag) concentrations were below the 0.08 mg/L reporting limit in the Test 1 and 3 initial solution, so a model for Ag was not developed in the Test 1 and 3 experiments. For the Test 5, 6 and 7 experiments, silver concentrations in the initial solutions are low at 0.006 and 0.007 mg/L. At these low initial concentrations silver is not expected to be of environmental concern. The laboratory tests indicate some attenuation. Concentrations in the Test 1 and 3 neutralized solutions were for the most part less than 0.003 mg/L (one aged sample reported a value 0.0287 mg/L, but this is inconsistent with earlier results). For the later experiments, concentrations were 0.001 mg/L or less. The geochemical model showed no significant removal via adsorption and model values remained essentially at their starting concentrations. The reason for the limited sorption of silver in these solutions is related to the fact that silver is considered a soft cation (Railsback, 2003), and it has limited attraction to hard ions such as oxygen. It much prefers complexation reactions with other soft ions such as chloride. A review of the species distribution for these solutions indicated that $AgCl_2^-$ and AgCl° are the dominant silver bearing species. Thus the activity of the Ag^+ ion is lowered and that is the ion (component) that is used to define the surface complexation reactions. Also consistent with the low Ag concentration is the observation that the silver chloride mineral ceragyrite (AgCl) was undersaturated in these samples. Some attenuation is occurring although the exact mechanism has not been identified. With such low starting concentrations various coprecipitates could take up silver with little impact on their stability.

A concentration of 0.001 mg/L silver has been selected as the pore water concentration. This is based primarily upon the results from the laboratory testing program for the Test 5, 6 and 7 measurements.

6.24 Strontium

Strontium (Sr) will be discussed in Section 6 along with a detailed discussion of the radium solid solution calculations. The selected concentration for the pore waters is 3 mg/L based upon the general agreement between the neutralized sample concentrations and the general similarity of the modeled values (Table 11).

6.25 Thallium

Thallium (Tl) concentrations in the untreated barren stream are low, with concentrations of approximately 0.05 mg/L. Thallium is generally considered to be mobile and attenuation mechanisms are limited. Thallium ions tend to be monovalent (Tl^{+1}), consequently they are generally not considered to undergo significant adsorption onto HFO. At high oxidation potentials (Eh) a trivalent form becomes stable (Figure 29). This limited sorption is reflected in the lack of reportable changes to thallium values for the Test 5, 6 and 7 geochemical models. Concentrations of thallium in the neutralized samples do decrease to approximately 0.01 mg/L. Thallium commonly substitutes for potassium (K^{+}) and the neutralized samples do show decreases in potassium concentrations. In the Test 5, 6 and 7 samples, potassium concentrations decrease to about half their initial concentrations. Therefore, it is possible that the reduction in thallium concentration is related to precipitation of potassium bearing phase. Because potassium is not considered an element of concern, potassium bearing phases have not been included in the model, even if K bearing phases were included in the model there is no reasonable means to model coprecipitation of thallium into these phases. However, it is more likely that thallium is involved in the ion exchange reactions that may be operating in these solutions. A pore water concentration of 0.01 mg/L has been selected for thallium in these waters.

6.26 Tin

Tin (Sn) is not usually considered an element of environmental concern and the initial concentrations of tin in the barren streams for the Test 5, 6, and 7 measurements were between 0.04 to 0.05 mg/L. Upon neutralization concentrations decreased to less than 0.001 mg/L. For the Test 1 and 3 measurements the initial solution reported a tin value of less than 2 mg/L. However, the subsequent samples showed very low concentrations with many <0.0001 for the early samples with some increases during aging. Among the Test 1 and 3 samples the maximum reported Sn concentration was 0.00051 mg/L. Tin was not included in the geochemical database used for the modeling; with such variation in neutralized concentrations it is unlikely that a model could be confirmed with these results. Given the low initial concentrations, and even lower concentrations after neutralization, a reasonable pore water concentration for tin is 0.01 mg/L.

6.27 Titanium

Titanium (Ti), in the form of the mineral rutile (TiO_2), is one of most insoluble elements on the surface of the earth; Rutile is extremely stable under near surface conditions. It is commonly a detrital mineral and is often a component of black sand deposits. Preparation of an Eh-pH diagram for titanium indicated that rutile was stable at pH values as low as 1.0 even at a concentration of 0.05 mg/L titanium (1μm). Any model that included titanium and allowed for rutile as a possible phase would produce modeled titanium values far lower than 0.001 mg/L. Because the stability field for rutile was so large it was decided not to include an Eh-pH diagram for this system in this report.

Concentrations of titanium have been measured at concentrations as great as 1.3 mg/L in the Test 1 and 3 barren leach, and concentrations of approximately 1 mg/L have been reported in the other three samples. Upon neutralization, concentrations drop to values often between 0.03 to 0.01 mg/L. Some samples from Test 1 upon aging showed even lower concentrations. Because of the low solubility of this element a precipitation mechanism is not readily identified. It may be that the dissolved titanium concentrations are actually remnant particles from the crushing

operation that are small enough to pass through the filter. Those fine particles are caught up in the flocculated ferrihydrite and other minerals that precipitate upon neutralization. A pore water concentration of 0.01 mg/L is defined.

6.28 Vanadium

The initial concentration of vanadium (V) in the Test 1 and 3 solution was 89 mg/L. The Test 5 starting composition was 80.7 mg/L and the two samples from Tests 6 and 7 had an average concentration of 111.5 mg/l. Significant decreases in vanadium concentrations were noted upon neutralization. At a pH of approximately 4, the two samples from the Test 1 and 3 experiments were found to contain 0.24 and 0.1 mg/L V, respectively. In the Test 1 and 3 Sets, for the higher pH samples, V concentrations dropped to less than 0.01 mg/L although upon aging these concentrations showed a tendency to increase slightly. Vanadium concentrations in the Test 5, 6 and 7 samples displayed higher V concentrations with values of 0.0293, 0.7 and 0.68 mg/L for Total V, respectively. Dissolved concentrations were slightly less than total.

Modeled concentrations showed decreases but there was some variability in the neutralized values, with the Test 5 value coming in at 0.22 mg/L and the Test 6 data had a value of 11.6 mg/L V, Test 7 showed a value of 0.9 mg/L. In these models the primary means of attenuation of vanadium was through surface complexation. Examination of the Test 6 results through a comparison to other constituents indicates that the vanadium adsorption edge (pH at which 50% adsorption occurs) is at a higher pH than the other two test results. Figures 3, 4 and 5 readily explain the differences in vanadium behavior. The Test 6 results show lower percents adsorbed at pH values around 6.95 to 7.0. The figures again demonstrate how differences in initial concentrations and competition for a limited number of adsorption sites can impact the resulting dissolved concentrations. The effect of a slight change in pH is shown in the two results from the Test 7 Model results (Table 10).

Another possibility related to factors that could control vanadium concentrations is the formation of carnotite (KUO_2VO_4) or tyuyamunite [$Ca(UO_2)_2(VO_4)_2$]. Figure 14 shows the Eh-pH diagram for vanadium, potassium and uranium. The diagram indicates a large stability field for carnotite

(KUO_2VO_4). One version of the geochemical model was developed that included carnotite and tyuyamunite as a possible mineral phases. Because of the stability of carnotite, uranium concentrations dropped from the previously modeled values by two to three orders of magnitude, in some situations the difference was even greater. Tyuyamunite was undersaturated. Vanadium concentrations did not change significantly. Uranium acts a limiting reagent in these simulations. Because of the extremely low concentrations for uranium in these models and the disagreement between these modeled and the measured uranium concentrations models that use carnotite as a possible phase have been eliminated from further consideration.

Based upon the measured concentration in the Test 6 and 7 results a value of 0.7 mg/L has been selected as representing the pore water concentration of vanadium in these tailings.

6.29 Zinc

Initial concentrations of zinc in the barren stream ranged from about 48 mg/L to 92 mg/L (Table 10). Upon neutralization the Test 5 results displayed a concentration of approximately 3 mg/L, while the model suggested a value closer to 5 mg/L. The modeled and measured results from the Test 5 experiment are consistent with a surface complexation process. However, the Test 6 and 7 results showed some inconsistencies between the previous results and the model calculations related to the geochemical behavior of zinc in these solutions. Initial concentrations of zinc were nearly twice as great in Test 5. After neutralization the final concentrations were 100 to 1000 times lower; with a value of 0.038 mg/L in the Test 6 result and 0.003 mg/L in the Test 7 sample. The geochemical model calculations, based primarily upon surface complexation, estimated nearly 18 mg/L in the Test 6 sample and a value of about 5 mg/L for the pH 7.33 Test 7 based model.

Tests 1 and 3 had starting zinc concentrations around 40 mg/L and upon neutralization to pH 4 the concentration were less than 1 mg/L. Further neutralization produced concentrations less than 0.3 mg/L, with some values reported at much lower levels (0.005 to 0.007 mg/L). The lower zinc values were consistently noted in the higher pH samples (pH 7.8 to 8.1 group).

The possibility of coprecipitation into calcite was also considered, but there are several problems with that option. Zinc and cadmium are geochemically similar and both elements should form a coprecipitate with calcite. However, cadmium tends to partition more strongly into calcite than zinc and the low concentrations of cadmium noted in the Test 6 and 7 results would support this behavior. Cadmium in the Test 6 sample is reported to be at 0.0007 mg/L and the Test 7 result is greater at 0.003. For a homogenous coprecipitation process the more carrier mineral (calcite) that forms the lower the trace element concentration in the solution. This would suggest that less calcite formed in the Test 7 experiment. However, the zinc data contradict this behavior. Zinc concentrations are lower in the Test 7 solution than in the Test 6 solution. Therefore, an analytical error is suspected and the measured concentrations of the neutralized Test 6 and 7 results have been eliminated from further consideration. Furthermore, because of the inconsistencies between the cadmium and zinc results, as well as the low alkalinities generated in the primary model a secondary model that included a calcite dominant coprecipitate was not considered.

The consistency between the Test 5 measured and modeled concentrations was used as the basis for selection of the pore water concentration. A value of 3 mg/L has been selected based upon the Test 5 neutralized concentration. This is considered to be the most conservative estimate. The expected long term value may be closer to the 0.3 mg/L values noted in Tests 1 and 3. The even lower values noted in some of the higher pH samples from these tests have been eliminated because the target pH is now lower than specified in these tests. Some of the laboratory data (particularly the Test 6 and 7 concentrations) suggest that a much lower value could be obtained but as there were questions related to the reliability of these two values it was decided that the most conservative estimate would be the higher neutralized concentration from Test 5.

7. GEOCHEMICAL MODELING OF RADIUM COPRECIPITATION INTO BARITE

One of the elements of concern at the proposed Kiggavik operation is radium. As part of the tailings treatment operation, barium chloride ($BaCl_2$) will be added to the barren stream to produce additional barium sulfate (barite). Upon precipitation barite can sequester radium in a coprecipitate along with the dominant barium ion. Figure 30 shows a representation of the coprecipitated mineral.

Coprecipitation of radium into barite is the industry standard practice to control radium. In operating uranium mills, barium chloride is commonly added as part of the tailings treatment circuit. The abundant sulfate already in solution precipitates barite and radium is removed by coprecipitation.

The resulting coprecipitation process between barite and radium is well known and numerous researchers have described this process. The earliest discussion is in the now classic paper by Doerner and Hoskins (1925). Recently, a book (Bruno et al., 2007) evaluated the state of the art with respect to this reaction, and other references have been published that provide additional documentation as to the importance of this process (Grandia et al., 2008, and Zhu 2004a,b).

The Doerner and Hoskins process, for a system where a barium mineral is the dominant phase, can be described by the following equation:

$$log\left(\frac{Me_i}{Me_f}\right) = \lambda\, log\left(\frac{Ba_i}{Ba_f}\right)$$

Where:

Me_i = initial quantity of trace metal in solution,

Me_f = final quantity of metal,

Ba_i = initial quantity of barium in solution,

Ba_f = final quantity of barium in solution, and

λ[3] = heterogeneous distribution coefficient (a variant of *D*), where only the precipitating surface is in equilibrium with the solution.

Unlike precipitation of a pure phase such as $CdCO_3$, which has a unit activity, the final concentration of the trace metal in solution is controlled by the amount of barium that precipitates. The greater the amount of precipitate that is formed, the lower the concentration of the trace metal in solution. The resulting precipitated phase is like the layers of an onion where the different layers represent difference concentrations that develop as the reaction proceeds. The inner layers of the solid will have greater concentrations and as the trace metal concentrations decrease in solution so will the concentration in the solid.

Grandia et al (2007) indicated that Doerner and Hoskins (1925) estimated a value for the heterogeneous partition coefficient (λ) for their equation value of 1.8. This is close to the ratio used in the equation described above, where for the log K_{sp} values the ratio of $10^{0.29}$ is about 2.

To demonstrate the importance of barite precipitation in controlling radium concentrations, a coprecipitation model (Mahoney, 1988, 2001) was run using PHREEQC. As part of the evaluation of the tailings treatment process, the geochemical model was expanded to evaluate the coprecipitation reactions to further demonstrate the method that will control radium in the pore water.

7.1 Theory of Solid Solutions

To quantify the extent of the radium partitioning into the dominant barite, a solid solution model based upon thermodynamic principles is applied. In this case, the term solid solution applies to a coprecipitated phase such as $Ba_{(1-x)}Ra_xSO_4$, which can be quantified using a thermodynamic based solid solution model available in PHREEQC. Unlike the heterogeneous Doerner and Hoskins model, the thermodynamic based model as used in PHREEQC produces a homogenous solid.

[3] In the Doerner and Hoskins Equation λ represents a type of distribution coefficient, do not confuse this with the λ_{RaSO4} and λ_{BaSO4} terms shown below which represent rational activity coefficients.

The thermodynamic model requires an estimate of the activities[4] of the two end members in the solid that is formed. The calculation of the end member activities is similar to the method applied to calculate activities in any type of solution. The difference is that these activities are calculated in a solid, rather than in a liquid, hence the term solid solution.

For a pure end member mineral such as barite ($BaSO_4$), the precipitation and dissolution reactions can be represented by the following equation:

$$BaSO_4 \leftrightarrow Ba^{+2} + SO_4^{-2}$$

and quantified by the following relationship:

$$K_{BaSO4} = \frac{\left(Ba^{+2}\right)\left(SO_4^{-2}\right)}{\left(BaSO_4\right)}$$

Where K_{sp} is the solubility product constant, and the items in parentheses represent chemical activities of the barium (Ba^{+2}) and sulfate (SO_4^{-2}) ions. At equilibrium the pure solid phase $BaSO_4$ is present in the solution, and it is assigned an activity of 1.0. In this example, the product $(Ba^{+2})*(SO_4^{-2})$ is commonly called the ion activity product (IAP). Because it is a simple 1:1 product, if the solution is already at equilibrium and if that equilibrium is disturbed by increasing the activity of sulfate, then more barite should precipitate and the activity of the barium ion should decrease by a corresponding amount. The most common way for increasing the activity of an ion in solution is to increase its concentration. For this example, a soluble form of sulfate could be added either by dissolving gypsum, or by adding sulfuric acid.

The K_{sp} for barite is $10^{-9.97}$. As a point of reference, gypsum ($CaSO_4 \cdot 2H_2O$), another divalent sulfate mineral, is much more soluble and has a K_{sp} of $10^{-4.59}$.

Similarly the solubility of $RaSO_4$ can be defined by:

[4] This is the thermodynamic activity of a component, not a measure of a radioactive process.

$$RaSO_4 \leftrightarrow Ra^{+2} + SO_4^{-2}$$

And quantified by the following relationship:

$$K_{RaSO4} = \frac{\left(Ra^{+2}\right)\left(SO_4^{-2}\right)}{\left(RaSO_4\right)}$$

The radium sulfate is slightly less soluble than barite and the solubility product constant selected for these calculations was $10^{-10.26}$, (Langmuir and Riese, 1985). Rearranging the two reactions we can define an exchange reaction:

$$Ra^{+2} + BaSO_4(s) \leftrightarrow RaSO_4(s) + Ba^{+2}$$

Where the terms $BaSO_4(s)$ and $RaSO_4(s)$ represent the activities of the components in the resultant solid solution. Following standard thermodynamic conventions, the equilibrium condition can be defined by:

$$K = \frac{\left(Ba^{+2}\right)\left(RaSO_4(s)\right)}{\left(BaSO_4(s)\right)\left(Ra^{+2}\right)} = \frac{K_{BaSO4}}{K_{RaSO4}} = 10^{0.29}$$

The activities of the end member solids are defined by:

$$\lambda_{RaSO4} X_{RaSO4} = RaSO_4(s)$$

and:

$$\lambda_{BaSO4} X_{BaSO4} = BaSO_4(s)$$

Where λ_{RaSO4} and λ_{BaSO4} represent the rational activity coefficients and X_{RaSO4} and X_{BaSO4} represent their respective mole fractions in the coprecipitate. For an ideal solid solution, the activity coefficients equal one. The assumption about ideality is reasonable in this situation as the amount of Ra is much smaller than the amount of Ba^{+2} available. The mole fraction of Ra in the resultant binary solid solutions was 1.4×10^{-8}. So the ideality assumption is easily satisfied.

Ultimately, a ternary solid solution was applied to this system, where the third component was celesite ($SrSO_4$). This additional component was added because it was thought that it might help explain some of the oversaturated conditions noted for barite in these waters. In PHREEQC ternary solid solutions must be ideal solid solutions.

7.2 Geochemical Model of Radium Coprecipitation into Barite

In the tailings stream neutralization tests, solid $BaCl_2$ was added to the barren stream to raise the concentration of $BaCl_2$ to 150 mg/L, this increase the barium in solution to approximately 90 mg/L. Although initial radium concentrations were not available for these specific samples, other tests performed at AREVA's SEPA laboratory in Bessines suggested that activities of between 40 to 80 Bq/L were reasonable starting values. The measured values for the neutralized solutions based upon the completion of the Test 1 experiment at values of 0.08 Bq/L indicate that the proposed treatment process is capable of removing significant amounts of radium from the pore water. Assuming that the 80 Bq/L was the concentration in the barren stream before treatment the process would be capable of a 99.9% removal of radium from the solution.

The simulation used the major ion composition from the Test 5 barren stream as the starting concentration (Table 4) and allowed it to reach equilibrium with a barite-$RaSO_4$ solid solution (SS), as well as other phases. Measurements of ^{226}Ra in samples from the Test 1 Series (samples from both pH 6.3-to 6.7 range and pH 7.8 to 8.1 range) both were reported to contain concentrations (activities) of 0.08Bq/L. Samples from the Test 3 series experiments after seven days aging time had ^{226}Ra activities of 15 (pH 6.3-to 6.7) and 13 Bq/L (pH 7.8 to 8.1).

As mentioned previously, an initial radium concentration was not provided in any of the tests conducted by SGS. However, ^{226}Ra concentrations were provided from the previously run SEPA samples. A review of these measurements indicated that the maximum reported radium concentration (as ^{226}Ra) was approximately 80 Bq/L. This value was selected as the initial value.

This value was converted to mg/L using the following formula, which was originally written for pCi/L[5].

$$\text{Concentration in mg/L} = 2.8\text{x}10^{-15} * A * t_{1/2} * \text{Concentration in pCi/L}$$

or

$$\text{Concentration in mg/L} = 2.8\text{x}10^{-15} * A * t_{1/2} * \text{Concentration in Bq/L}*27.027$$

Where A is the atomic weight of the isotope (226 g/mole in this case), and $t_{1/2}$ is the half life in years for the specific isotope (1600 years for ^{226}Ra).

In the initial models, a binary solid solution between $BaSO_4$ and $RaSO_4$ was formed, producing a phase with the composition $Ba_{(1-x)}Ra_{(x)}SO_4$. These models also included the $BaSO_4°$ ion pair, and several radium bearing complexes, including $RaSO_4°$, $RaCl^-$, $RaCO_3°$ and $RaOH^+$; constants for the radium bearing aqueous complexes were taken from Langmuir and Riese (1985). The model also included $RaCl_2°$ (Zhu, 2004a, 2004b). Inclusion of these complexes in the model decreases the concentration of available Ba^{+2} and Ra^{+2} ions in solution that may participate in the solid solution reaction, which produces a more conservative final concentration value in the water. For this application, it was assumed that an ideal solid solution would form (Bruno et al., 2007), where the distribution of radium in the solid is controlled by the difference (ratio) between the K_{sp} for $RaSO_4$ (initial calculations used a log K_{sp} of -10.4499 per the LLNL.dat database (Lawrence Livermore National Laboratory database), final calculations used a log K_{sp} of -10.26, based upon Langmuir and Riese, 1985) and barite (log K_{sp} of -9.97, alternative calculations discussed below used a Log K_{sp} of -8.97). Given the low concentrations of radium in this water such an assumption is reasonable. Mole fractions of Ra in the ternary barite solid solution coprecipitate are still $1.4\text{x}10^{-8}$, with less than 5 % as $SrSO_4$, which support the assumptions related to an ideal solid solution.

[5] Equation (originally written using pCi/L) was obtained from http://www.epa.gov/superfund/health/contaminants/radiation/pdfs/tbd-appendix-b-clean.pdf

To convert Becquerels to picocuries, multiply the number of Becquerels by 27.027.

Because of the various issues related to evaluating these reactions (including two different K_{sp} values for $RaSO_4$, and questions about the oversaturated condition of barite in these solutions) it was decided to run a series of models to cover the different conditions and to assess the model sensitivity. Table 12 shows the results of these simulations. One factor that was also assessed was the value of the barite solubility product constant. Because an oversaturated condition was observed in the neutralized Test 5 sample it was decided to decrease the stability of the barite from a log K_{sp} of -9.97 to -8.97. Also there are two different solubility product constants (K_{sp}) for $RaSO_4$, and ultimately the larger value (more soluble) value was selected. Possible precipitated phases include the barite-$RaSO_4$ SS or a ternary solid solution that consisted of barite - $RaSO_4$ and celestite ($SrSO_4$).

Differences among the eight simulations are slight. However to provide the most conservative estimate the ternary model with the less stable $RaSO_4$ (log K_{sp} of -10.26) and a barite assuming a log K_{sp} of -8.97 was used. It should also be mentioned that this model predicts a concentration (activity) of 0.008 Bq/L, which is 10% of the measured value (Table 12) in the Test 1 sample.

Additional models based upon the previously selected ternary SS model were run using the Test 6 and 7 initial solutions, although barium concentrations were not included in the laboratory results, the concentrations are expected to be similar to the values reported in the Test 5 dataset. It was decided that because of the large addition of barium in the form of $BaCl_2$ that the initial Ba concentrations were not required. Those particular simulations resulted in slightly lower ^{226}Ra activities. This is believed related to the greater initial Sr concentrations, which produced slightly more of the ternary solid solution for the sequestration of the radium.

Strontium concentrations are also controlled by the ternary solid solution. The initial concentrations ranged from 4.59 to 9.22 mg/L. The measured concentrations upon neutralization are between 2.7 and 3.2 mg/L. Model concentrations are slightly lower and range between 1.0 to 1.2 mg/L. Differences between the measured and modeled concentrations are not significant. We have selected the average of the measured concentrations at 3.0 mg/L for strontium.

The model tends to over predict the removal of radium by a factor of about ten in the Test 1 results. However, the laboratory results suggest that we are removing 99.9 % of the radium, and the model suggests that we are removing 99.99 %, when considered in that fashion the difference between the model and laboratory derived result becomes less significant.

Removal of radium for those samples that included tailings are not as great as concentrations for samples that included leached residue (solids) are significantly greater. Laboratory analyses for ^{226}Ra are limited six results from four of the tests. The samples include:

- The two results from Test 1 which both were reported to be 0.08 Bq/L,
- two additional results from Test 3, which reported values of 13 and 15 Bq/L, from splits for the low and high pH ranges,
- sample identified as Tails Test 5 Filtrate Diluted with a value of 4.4 Bq/L, and
- a sample identified as Ambient Aging Day 50 sample (Test 6), which had 11 Bq/L.

One possible reason for the differences between the modeled and measured concentrations is the estimate for the initial (pre $BaCl_2$ addition) 226Ra activity (starting concentration) used in the model is in error.

Using the Test 3, 5 and 6 results, a weighted average was prepared by averaging the Test 3 sample results to 14 Bq/L and then calculating an average based upon the Test 3, 5 and 6 results. A value of 10Bq/L (rounded) was estimated to represent the tailings pore water activity for ^{226}Ra. The Test 1 results were not included in the weighted average because the experimental condition in that test did not include solids and therefore were considered to be not representative of the tailings environment. Estimated average ^{226}Ra activities in the JEB pit are reported to be 5 Bq/L (AREVA, 2011). Therefore, the estimated value of 10 Bq/L is consistent with this average value.

8. CONCLUSIONS

This report has examined laboratory testing results at a pilot plant scale of the proposed tailings treatment process for the Kiggavik Project.

Five different tailings neutralization tests were performed and the results have been summarized in this report. Geochemical modeling was also performed to support and better understand the reactions occurring during neutralization. These models, ranging from simple Eh-pH diagrams to full reaction path models, have been used to understand the behavior of these different constituents, and ultimately to support conclusions obtained from the selection process

A concentration of 0.14 mg/L (Test 5 measured concentration after neutralization) has been selected as the pore water concentration for uranium. This value is considered to be a conservative estimate as significantly lower values were measured in the Test 1 and 3 experiments.

Pore water concentrations for the remaining constituents in the neutralized tailings evaluated as part of this report have been selected based primarily upon the laboratory results. These values have been summarized in Table 11.

For most of the constituents evaluated, the proposed neutralization process resulted in significant decreases in concentration. These laboratory tests and the supporting geochemical modeling results demonstrate the efficacy of the proposed treatment process for the Kiggavik Project.

9. REFERENCES

Anderson, G., 2005. Thermodynamics of natural systems. Cambridge University Press. Cambridge. 648 p.

Appelo, C. A. J., Van der Weiden, M. J. J., Tournassat, C., Charlet, L., 2002. Surface complexation of ferrous iron and carbonate on ferrihydrite and the mobilization of arsenic. *Environ. Sci. Technol.*, *36*, 3096–3103.

AREVA Resources Canada, Inc., 2011, McLean Lake Operation - Tailings Optimization and Validation Program, Validation of Long Term Tailings Performance Report (2009). April 26th, 2011.

Bethke, C.M., 2008. Geochemical and Biogeochemical Reaction Modeling, 2nd ed. Cambridge University Press. Cambridge. 543 p.

Bethke, C.M., and Yeakel, S., 2010. The Geochemist's Workbench, Release 8.0 GWB Essentials. Available From Rockware, Golden, CO.

Bruno, J., Bosbach, D., Kulik, D., and Navrotsky, A., 2007. Chemical thermodynamics of solid solutions of interest in nuclear waste management: A state-of-the-art report. OECD Nuclear Energy Agency. 266 p.

Doerner, H.A. and Hoskins, W.M.1925, Co-precipitation of radium and barium sulfates. *J. Am. Chem. Soc.*, 47, 662–675.

Dong, W., and Brooks, S.C., 2006. Determination of the formation constants of ternary complexes of uranyl and carbonate with alkaline earth metals (Mg^{2+}, Ca^{2+}, Sr^{2+}, and Ba^{2+}) using anion exchange method. Environ. Sci. Technol. vol. 40, p. 4689-4695.

Dong, W., and Brooks, S.C., 2008. Formation of aqueous $MgUO_2(CO_3)_3^{2-}$ complex and uranium anion exchange mechanism onto an exchange resin. Environ. Sci. Technol. vol. 42, p. 1979-1983.

Dzombak, D.A., and Morel, F.M.M., 1990, Surface complexation modeling - hydrous ferric oxide: New York, John Wiley and Sons, 393 p.

Grandia, F. Merino, J. and Bruno, J. 2008, Assessment of the radium-barium co-precipitation and its potential influence on the solubility of Ra in the near-field. Technical Report TR-08-07. Svensk Kärnbränslehantering AB, (SKB), Swedish Nuclear Fuel and Waste Management Co. Stockholm. 48 pp.

Guillaumont, R., Fanghanel, T., Neck, V., Fuger, J., Palmer, D., Grenthe, I., Rand, M. H., 2003. Update on the Chemical Thermodynamics of Uranium, Neptunium, Plutonium, Americium and Technetium; Elsevier B.V. Amsterdam. 960 p.

Gustafsson, J.P., 2003, Modeling molybdate and tungstate adsorption to ferrihydrite. Chemical Geology. v. 200, p. 103-115.

Krupka, K. M., and Serne, R.J., 2002. Geochemical factors affecting the behavior of antimony, cobalt, europium, technetium and uranium in vadose sediments. Pacific Northwest National Laboratory, Richland, Washington. PNNL-14126. 95 pages.

Langmuir, D., 1997, Aqueous Environmental Geochemistry: Prentice Hall, Upper Saddle River, NJ, 600 p.

Langmuir, D., Mahoney, J., and Rowson, J., 2006, Solubility products of amorphous ferric arsenate and crystalline scorodite ($FeAsO_4 \cdot 2H_2O$) and their application to arsenic behavior in buried mine tailings: Geochimica et Cosmochimica Acta., vol. 70, p. 2942-2956.

Langmuir, D. and Riese, A.C., 1985, The thermodynamic properties of radium, Geochimica et Cosmochimica Acta, vol. 49, p 1593 -1601.

Mahoney Geochemical Consulting LLC, 2011. Geochemical Evaluation of Uranium in Raffinate and Neutralized Tailings: Kiggavik Project, Prepared For AREVA Resources Canada, Inc., April 2011, 83 pages.

Mahoney, J.J., 1998, Incorporation of coprecipitation reactions in predictive geochemical models: in Proceedings of Tailings and Mine Waste '98, Fort Collins, Colorado, p.689-697.

Mahoney, J.J., 2001, Coprecipitation reactions – verification of computational methods in geochemical models: in Mining Impacted Pit Lakes 2000 Workshop Proceedings: a Multimedia CD Presentation. (Workshop held April 4–6, 2000 Reno, NV) United States Environmental Protection Agency Office of Research and Development. EPA/625/C-00/004. Session 4.

Mahoney, J.J., Cadle, S.A, and Jakubowski, R.T., 2009a, Uranyl adsorption onto hydrous ferric oxide – a re-evaluation for the diffuse layer model database. Environ. Sci. and Technol. vol. 43, no. 24, p. 9260-9266. DOI 10.1021/es901586w.

Mahoney, J.J., Jakubowski, R.T. and Cadle, S.A., 2009b, Corrections to the diffuse layer model database for uranyl adsorption onto hydrous ferric oxide - Ramifications for solute transport modeling. (Poster presented at U2009 Global Uranium Symposium, May 2009 Keystone, CO.)

Mahoney, J., Slaughter, M., Langmuir, D., and Rowson, J., 2007, Control of As and Ni releases from a uranium mill tailings neutralization circuit: Solution chemistry, mineralogy, and

geochemical modeling of laboratory study results. Applied Geochemistry, Vol. 22, (12) p. 2758 – 2776.

Merkel, B. J., and Planer-Friedrich, B. 2008, Groundwater Geochemistry, a practical guide to modeling of natural and contaminated aquatic systems. 2nd Edition. Edited by Nordstrom, D.K., Springer, Berlin, 230 p.

Pabalan, R.T., Turner, D.R., Bertetti, P., and Prikryl, J.D., 1998, Uranium VI sorption onto selected mineral surfaces. in Adsorption of Metals by Geomedia variables, Mechanisms, and Model Applications. E. Jenne, Editor, Academic Press, San Diego, pp. 99-130.

Parkhurst, D.L., and Appelo, C.A.J., 1999, User's guide to *PHREEQE* (version 2) - a computer program for speciation, batch-reaction, one-dimensional transport, and inverse geochemical calculations. U.S. Geological Survey Water Resources Investigation Report 99-4259, 312 p.

Puigdomenech, I., 2009. MEDUSA – Make Equilibrium Diagrams Using Sophisticated Algorithms. Inorganic Chemistry, Royal Institute of Technology (KTH), Stockholm. http://www.kemi.kth.se/medusa

Railsback, L.B., 2003. An earth scientist's periodic table of the elements and their ions. Geology, v.31, no. 9, p. 737-740.

Tokunaga, T.K., Kim, Y., and Wan, J., 2009. Potential remediation approach for uranium-contaminated groundwaters through potassium uranyl vanadate precipitation. Environ. Sci. and Technol. vol. 43, p. 5467-5471.

Wollenberg, P. , 2010. AREVA's Kiggavik Project Exploration Update 2010. Igaluit Nunavut Mining Symposium.

Zhu, C., 2004a, Coprecipitation in the barite isostructural family: 1 Binary mixing properties. Geochimica et Cosmochimica Acta, vol. 68, p. 3327 -3337.

Zhu, C., 2004b, Coprecipitation in the barite isostructural family: 2 Numerical simulations of reactions and mass transport. Geochimica et Cosmochimica Acta, vol. 68, p. 3338 - 3349.

TABLES

Table 1. Tailings Neutralization Procedure (Details for the Test 5 samples)

	INITIAL PREPARATION
1.	The Composite #2 RIP pulp was agitated such that all solids were off the bottom.
2.	8 L of pulp was transferred into a 20 L pail. The pulp was weighed.
3.	The pulp was agitated with a Teflon rushton impellor using a caframo mixer.
4.	A volume of the Resin U ppt Bulk Barren was measured out equivalent to 10% v/v of the RIP Pulp, weighed and added.
5.	A mass of the OC Test 6 Resin Gypsum ppt Bulk Solids was measured out equivalent to 25 g/L of the RIP pulp and added.
6.	The pH meter was calibrated and the probes inserted into the solution and the initial pH and ORP are measured.
7.	The solution was agitated until the pH and ORP readings stabilized, approximately 30 minutes.
8.	A sample of approximately 700 g was taken, weighed and filtered.
9.	The filtrate was collected and the pH, ORP and SG readings were taken. The sample was then submitted for assay.
10.	The residue was displacement washed three times with deionized water. The wet residue was weighed.
11.	The filter cake was then dried, weighed and submitted for assay.
12.	150 mg/L $BaCl_2$ was then added to the mixture (calculated below).
13.	Fresh 20% w/w Calcium Hydroxide slurry was prepared.
14.	A stir bar was placed in the lime slurry and it was weighed prior to starting test.
15.	The lime slurry was placed on a stir plate and agitated.
	STAGE 1 Neutralize to pH 4
16.	Lime slurry was then added slowly - drop wise using a disposable pipette - to a pH of 4 and held for 2 hours.
17.	The weight of Lime slurry was recorded throughout the test as was the pH and temperature.
	STAGE 2 Neutralize to pH 7
18.	Lime slurry was then added slowly - drop wise using a disposable pipette to a pH of 7 and held for 2 hours.
19.	The weight of lime slurry was recorded throughout the test as was the pH and temperature.
20.	The final pulp (neutralized tailings) was weighed.
21.	Approximately half the pulp was filtered using a Buchner funnel/Erlenmeyer flask set up.
22.	The filtrate was collected and the pH, ORP and SG readings were taken. A small sample (~50 mL) was submitted for assay and the remainder was set aside for further testwork.
23.	The residue was displacement washed three times with deionized water. The wet residue was weighed.
24.	The filter cake was then dried, weighed and submitted for assay.

Table 2. Summary of Tailings Neutralization Test 1 - No solids, No Added Ferric Sulphate. Results for total concentrations reported.

Parameter	Units	Tail Test 1 pH 4 - 2 Hour Pls	Tail Test 1 pH 6.3-6.7 - 2 Hour Pls	Tail Test 1 pH 7.8-8.1 - 2 Hour Pls	Tail Test 1 pH 6.3-6.7 48 Hour Pls	Tail Test 1 pH 7.8-8.1 48 Hour Pls	Tail Test 1 pH 6.3-6.7 - 7 Day PLS	Tail Test 1 pH 7.8-8.1 - 7 Day PLS
Temp Upon Receipt	°C	18	18	18	22	22	20	20
pH		3.98	7.15	7.81	6.92	7.46	6.84	7.73
pe		8.8265	8.9787	8.5729	9.3676	9.4183	6.1211	6.9665
Fe2	mg/L	< 0.5	< 0.5	< 0.5	< 0.5	< 0.5	< 0.5	< 0.5
Fe3	mg/L	452	< 0.5	< 0.5	< 0.5	< 0.5	< 0.5	< 0.5
Alkalinity	mg/L as CaCO3	< 2	58	104	93	153	64	189
SO4	mg/L	24000	14000	10000	14000	9800	16000	9300
NH3+NH4	as N mg/L	2.9	2.1	1.8	2.8	2.7	1.9	1.4
Ag (tot)	mg/L	0.0008	0.0024	0.0029	0.0001	0.0004	0.00023	0.00002
Al (tot)	mg/L	1810	0.95	0.62	0.54	0.36	0.06	0.12
As (tot)	mg/L	0.09	0.005	0.007	0.0067	0.0103	0.0052	0.0061
Ba (tot)	mg/L	0.215	0.119	0.112	0.0671	0.0608	0.051	0.0515
Be (tot)	mg/L	0.336	0.0003	< 0.0002	0.00007	0.00003	0.00004	< 0.00002
B (tot)	mg/L	11.3	5.48	2.66	3.02	1.99	4.59	3.35
Bi (tot)	mg/L	0.0047	0.0002	0.0001	0.00002	< 0.00001	0.00002	< 0.00001
Ca (tot)	mg/L	407	437	418	441	443	452	443
Cd (tot)	mg/L	0.0756	0.0112	0.00028	0.00879	0.00996	0.00284	0.000659
Co (tot)	mg/L	3.95	0.24	0.01	0.165	0.00451	0.0415	0.0028
Cr (tot)	mg/L	2.86	0.006	0.005	0.005	0.0035	0.0029	0.0026
Cu (tot)	mg/L	251	0.357	0.047	0.117	0.0427	0.0574	0.0238
Fe (tot)	mg/L	452	0.327	0.067	0.331	0.092	0.081	0.012
K (tot)	mg/L	1840	1660	1560	1490	1450	1540	1390
Li (tot)	mg/L	26.6	23.7	18.9	11.6	0.776	1.28	0.414
Mg (tot)	mg/L	3640	3180	2190	2240	1830	1970	1500
Mn (tot)	mg/L	47.8	23.6	3.12	24.6	3.26	25.8	4.73
Mo (tot)	mg/L	0.0077	0.0079	0.0297	0.0139	0.0387	0.0138	0.0397
Na (tot)	mg/L	225	198	185	199	193	188	172
Ni (tot)	mg/L	24.5	0.861	0.033	0.181	0.0116	0.0295	0.0049
P (tot)	mg/L	3.89	0.031	0.039	0.013	0.021	0.012	0.022
Pb (tot)	mg/L	0.123	0.0026	0.0013	0.00678	0.00457	0.00293	0.00057
Sb (tot)	mg/L	0.022	< 0.002	< 0.002	< 0.0002	< 0.0002	< 0.0002	< 0.0002
Se (tot)	mg/L	0.1	0.03	0.03	0.032	0.029	0.033	0.03
Si (tot)	mg/L	21.3	0.76	0.62	1.84	0.96	1.33	1.01
Sn (tot)	mg/L	< 0.0001	0.0001	< 0.0001	0.00041	0.00048	0.00051	0.0005
Sr (tot)	mg/L	2.36	2.16	1.67	2.67	1.95	2.8	1.77
Ti (tot)	mg/L	0.032	0.014	0.012	0.0081	0.0025	0.0023	0.0017
Tl (tot)	mg/L	0.028	0.018	0.011	0.0158	0.0109	0.0152	0.011
U (tot)	mg/L	1.92	0.0126	0.017	0.00658	0.0222	0.0078	0.0217
U (diss)	mg/L	1.99	0.00934	0.018	0.00622	0.0218	0.0079	0.021
V (tot)	mg/L	0.242	0.0063	0.0087	0.0144	0.0126	0.00792	0.0149
Zn (tot)	mg/L	44.7	0.756	0.005	0.278	0.015	0.177	0.007

Table 3 Summary of Tailings Neutralization Test 3 – Solids Included, No Added Ferric Sulphate. Results for total concentrations reported.

Parameter	Units	Tail Test 3 pH 4 - 2 Hour Pls	Tail Test 3 pH 6.3-6.7 - 2 Hour Pls	Tail Test 3 pH 7.8-8.1 - 2 Hour Pls	Tail Test 3 pH 6.3-6.7 48 Hour Pls	Tail Test 3 pH 7.8-8.1 48 Hour Pls	Tail Test 3 pH 6.3-6.7 - 7 Day PLS	Tail Test 3 pH 7.8-8.1 - 7 Day PLS
Temp Upon Receipt	°C	18	18	18	22	22	20	20
pH		4	7.25	7.5	7.41	7.78	7.41	7.84
pe		8.8772	8.4376	7.5414	9.114	8.184	6.8651	6.1887
Fe2	mg/L	< 0.5	< 0.5	< 0.5	< 0.5	< 0.5	< 0.5	< 0.5
Fe3	mg/L	471	0.8	< 0.5	< 0.5	1.1	< 0.5	< 0.5
Alkalinity	mg/L as CaCO3	< 2	102	96	201	159	211	204
SO4	mg/L	19000	10000	7100	11000	7200	10000	7800
NH3+NH4	as N mg/L	2.5	1.6	1.1	1.7	1.2	1.3	1
Ag (tot)	mg/L	0.0022	0.0001	0.0001	0.00006	0.00679	0.0287	0.00063
Al (tot)	mg/L	898	1.62	0.6	0.22	0.47	0.08	0.08
As (tot)	mg/L	0.074	< 0.002	0.004	0.0036	0.0045	0.0038	0.0056
Ba (tot)	mg/L	0.239	0.177	0.205	0.102	0.107	0.0941	0.0589
Be (tot)	mg/L	0.161	< 0.0002	< 0.0002	0.00004	0.00015	0.00005	< 0.00002
B (tot)	mg/L	9.82	3.25	1.58	2.14	1.27	2.74	1.97
Bi (tot)	mg/L	0.0023	0.0001	< 0.0001	0.00002	0.00001	< 0.00001	< 0.00001
Ca (tot)	mg/L	372	412	444	453	442	440	469
Cd (tot)	mg/L	0.0671	0.00098	0.00018	0.00856	0.00343	0.000933	0.00175
Co (tot)	mg/L	3.81	0.208	0.00471	0.0961	0.00311	0.0421	0.00272
Cr (tot)	mg/L	1.09	< 0.005	< 0.005	0.0031	0.0028	0.0012	0.0011
Cu (tot)	mg/L	202	0.168	0.041	0.0722	0.0268	0.0513	0.0226
Fe (tot)	mg/L	471	0.86	0.15	0.109	1.09	0.168	0.026
K (tot)	mg/L	1640	1100	870	1000	817	850	704
Li (tot)	mg/L	27.4	17.6	8.43	2.63	0.514	0.85	0.413
Mg (tot)	mg/L	3020	2720	1470	2060	1400	1750	1240
Mn (tot)	mg/L	48.2	18.6	1.29	18.9	1.6	19.3	2.25
Mo (tot)	mg/L	0.0296	0.0369	0.15	0.0734	0.251	0.102	0.35
Na (tot)	mg/L	257	208	200	206	180	191	176
Ni (tot)	mg/L	22.5	0.726	0.02	0.0786	0.0099	0.0341	0.0053
P (tot)	mg/L	0.928	0.051	0.087	0.024	0.196	0.065	0.046
Pb (tot)	mg/L	0.283	0.0144	0.0043	0.0074	0.00478	0.00369	0.00109
Sb (tot)	mg/L	0.009	< 0.002	< 0.002	< 0.0002	< 0.0002	0.0002	0.0003
Se (tot)	mg/L	0.09	0.03	0.03	0.042	0.036	0.047	0.042
Si (tot)	mg/L	18.8	1.38	0.65	4.78	2.01	4.73	2.27
Sn (tot)	mg/L	< 0.0001	< 0.0001	< 0.0001	0.00039	0.00045	0.00032	0.0004
Sr (tot)	mg/L	2.37	2.84	2.36	3.61	2.9	3.36	2.82
Ti (tot)	mg/L	0.048	0.011	0.01	0.0044	0.0338	0.018	0.0024
Tl (tot)	mg/L	0.02	0.007	0.003	0.0052	0.0022	0.0043	0.0019
U (tot)	mg/L	0.484	0.00881	0.0172	0.0207	0.0258	0.0205	0.0281
U (diss)	mg/L	0.501	0.0121	0.0204	0.0242	0.0245	0.0223	0.0282
V (tot)	mg/L	0.106	0.0078	0.0084	0.0134	0.0171	0.0141	0.0241
Zn (tot)	mg/L	37.9	0.283	0.006	0.217	0.006	0.132	0.007

Table 4. Summary of Test 5 Results

Parameter	unit	Tails Test 5 Initial Pulp Filtrate	Tails Test 5 Neutralized Tailings Filtrate	**Parameter**	unit	Tails Test 5 Initial Pulp Filtrate	Tails Test 5 Neutralized Tailings Filtrate
Fe2	mg/L	13.8	< 0.5	Li (tot)	mg/L	29.9	1.33
Fe3	mg/L	4470	4.5	Li (diss)	mg/L	30	1.39
Alkalinity	mg/L as CaCO3	< 2	231	Mg (tot)	mg/L	4210	2650
CO3	mg/L as CaCO3	< 2	< 2	Mg (diss)	mg/L	4370	2620
HCO3	mg/L as CaCO3	< 2	231	Mn (tot)	mg/L	41.2	8.91
SO4	mg/L	69000	15000	Mn (diss)	mg/L	39.9	9.23
NO3	as N mg/L	< 1.5	< 0.5	Mo (tot)	mg/L	0.181	0.173
Tot.Reactive P	mg/L	195	0.08	Mo (diss)	mg/L	0.183	0.178
NH3+NH4	as N mg/L	3.2	1.5	Na (tot)	mg/L	262	215
Ag (tot)	mg/L	0.00546	0.0002	Na (diss)	mg/L	275	193
Ag (diss)	mg/L	0.00528	0.00004	Ni (tot)	mg/L	28.3	0.0098
Al (tot)	mg/L	8940	6.57	Ni (diss)	mg/L	28.1	0.0094
Al (diss)	mg/L	9260	0.35	P (tot)	mg/L	139	0.059
As (tot)	mg/L	0.992	0.0176	P (diss)	mg/L	136	0.054
As (diss)	mg/L	1.07	0.014	Pb (tot)	mg/L	2.56	0.0167
Ba (tot)	mg/L	0.138	0.134	Pb (diss)	mg/L	2.53	0.00493
Ba (diss)	mg/L	0.128	0.136	Sb (tot)	mg/L	0.0022	0.0002
Be (tot)	mg/L	0.911	0.00006	Sb (diss)	mg/L	0.0019	0.0015
Be (diss)	mg/L	0.912	0.00006	Se (tot)	mg/L	0.131	0.035
B (tot)	mg/L	11	3.59	Se (diss)	mg/L	0.124	0.035
B (diss)	mg/L	9.59	3.56	Si (tot)	mg/L	242	3.51
Bi (tot)	mg/L	0.299	0.00015	Si (diss)	mg/L	241	3.32
Bi (diss)	mg/L	0.287	0.00009	Sn (tot)	mg/L	0.0712	0.00026
Ca (tot)	mg/L	355	411	Sn (diss)	mg/L	0.0681	0.00025
Ca (diss)	mg/L	352	411	Sr (tot)	mg/L	4.17	2.64
Cd (tot)	mg/L	0.0482	0.0598	Sr (diss)	mg/L	4.16	2.66
Cd (diss)	mg/L	0.0491	0.0605	Ti (tot)	mg/L	0.987	0.0024
Co (tot)	mg/L	3.71	0.0207	Ti (diss)	mg/L	0.962	0.0022
Co (diss)	mg/L	3.7	0.0205	Tl (tot)	mg/L	0.0415	0.0047
Cr (tot)	mg/L	41.5	0.0039	Tl (diss)	mg/L	0.0426	0.0048
Cr (diss)	mg/L	41.1	0.0032	U (tot)	mg/L	8.65	0.138
Cu (tot)	mg/L	297	0.187	U (diss)	mg/L	8.44	0.14
Cu (diss)	mg/L	301	0.132	V (tot)	mg/L	80.7	0.0293
Fe (tot)	mg/L	4480	4.59	V (diss)	mg/L	79.8	0.0254
Fe (diss)	mg/L	4620	0.155	Zn (tot)	mg/L	43.5	3.01
K (tot)	mg/L	2030	1130	Zn (diss)	mg/L	43.4	2.93
K (diss)	mg/L	2130	1400	pH	s.u.	1.5	6.95

Table 5. Summary of Test 6 Results

Parameter	unit	Tails Test 6 Initial Filtrate	Tails Test 6 Neutralized Filtrate	**Parameter**	unit	Tails Test 6 Initial Filtrate	Tails Test 6 Neutralized Filtrate
Alkalinity	mg/L as CaCO3	< 2	219	Li (tot)	mg/L	42.6	21
CO3	mg/L as CaCO3	< 2	< 2	Li (diss)	mg/L	41.8	20.9
HCO3	mg/L as CaCO3	< 2	219	Mg (tot)	mg/L	4170	2690
Fe2	mg/L	17.4	0.61	Mg (diss)	mg/L	4160	2590
Fe3	mg/L	***	***	Mn (tot)	mg/L	56	9.8
Tot.Reactive P	mg/L	277	< 0.09	Mn (diss)	mg/L	53.3	9.41
SO4	mg/L	80000	11000	Mo (tot)	mg/L	0.148	0.1
Cl	mg/L	530	460	Mo (diss)	mg/L	0.144	0.094
NH3+NH4	as N mg/L	12.8	2.6	Na (tot)	mg/L	83.7	66
Ag (tot)	mg/L	0.006	< 0.001	Na (diss)	mg/L	80.5	63.3
Ag (diss)	mg/L	0.006	< 0.001	Ni (tot)	mg/L	40.8	0.41
Al (tot)	mg/L	9100	0.49	Ni (diss)	mg/L	32.8	0.42
Al (diss)	mg/L	9130	0.36	P (tot)	mg/L	241	0.052
As (tot)	mg/L	1.62	< 0.02	P (diss)	mg/L	241	0.044
As (diss)	mg/L	1	< 0.02	Pb (tot)	mg/L	2.78	0.035
Ba (tot)	mg/L	***	***	Pb (diss)	mg/L	2.8	0.016
Ba (diss)	mg/L	***	***	Sb (tot)	mg/L	< 0.02	< 0.02
Be (tot)	mg/L	1.4	0.008	Sb (diss)	mg/L	< 0.02	< 0.02
Be (diss)	mg/L	1.17	0.007	Se (tot)	mg/L	< 0.1	< 0.1
B (tot)	mg/L	17.2	4.36	Se (diss)	mg/L	< 0.1	< 0.1
B (diss)	mg/L	15.4	3.72	Si (tot)	mg/L	96.3	1.19
Bi (tot)	mg/L	***	***	Si (diss)	mg/L	89.7	0.96
Bi (diss)	mg/L	***	***	Sn (tot)	mg/L	0.049	< 0.001
Ca (tot)	mg/L	639	522	Sn (diss)	mg/L	0.048	< 0.001
Ca (diss)	mg/L	637	501	Sr (tot)	mg/L	8.28	2.91
Cd (tot)	mg/L	0.0466	0.0007	Sr (diss)	mg/L	7.99	3.03
Cd (diss)	mg/L	0.0456	0.0005	Ti (tot)	mg/L	1.05	0.03
Co (tot)	mg/L	5.86	0.11	Ti (diss)	mg/L	0.96	0.02
Co (diss)	mg/L	5.72	0.109	Tl (tot)	mg/L	0.05	0.009
Cr (tot)	mg/L	63.3	0.32	Tl (diss)	mg/L	0.051	0.009
Cr (diss)	mg/L	61.6	0.35	U (tot)	mg/L	5.91	0.112
Cu (tot)	mg/L	415	2.76	U (diss)	mg/L	5.89	0.109
Cu (diss)	mg/L	418	2.46	V (tot)	mg/L	112	0.7
Fe (tot)	mg/L	4370	1.49	V (diss)	mg/L	111	0.614
Fe (diss)	mg/L	4400	0.11	Zn (tot)	mg/L	82.6	0.037
K (tot)	mg/L	2120	1140	Zn (diss)	mg/L	80.3	0.02
K (diss)	mg/L	2120	1100	pH	s.u.	1.68	6.95

Table 6. Summary of Test 7 Results

Parameter	unit	Tails Test 7 Initial Filtrate	Tails Test 7 Neutralized Filtrate	**Parameter**	unit	Tails Test 7 Initial Filtrate	Tails Test 7 Neutralized Filtrate
Alkalinity	mg/L as CaCO3	< 2	161	Li (tot)	mg/L	42.2	14.1
CO3	mg/L as CaCO3	< 2	< 2	Li (diss)	mg/L	41.4	13.6
HCO3	mg/L as CaCO3	< 2	161	Mg (tot)	mg/L	4440	2300
Fe2	mg/L	17.4	0.86	Mg (diss)	mg/L	3990	2320
Fe3	mg/L	***	***	Mn (tot)	mg/L	170	5.75
Tot.Reactive P	mg/L	279	< 0.09	Mn (diss)	mg/L	165	5.4
SO4	mg/L	78000	11000	Mo (tot)	mg/L	0.159	0.141
Cl	mg/L	610	390	Mo (diss)	mg/L	0.153	0.136
NH3+NH4	as N mg/L	12.4	2.3	Na (tot)	mg/L	107	63.5
Ag (tot)	mg/L	0.006	0.001	Na (diss)	mg/L	106	60.5
Ag (diss)	mg/L	0.006	< 0.001	Ni (tot)	mg/L	33.3	0.31
Al (tot)	mg/L	9690	0.39	Ni (diss)	mg/L	32.4	0.28
Al (diss)	mg/L	8750	0.36	P (tot)	mg/L	258	0.112
As (tot)	mg/L	0.99	< 0.02	P (diss)	mg/L	232	0.085
As (diss)	mg/L	0.97	< 0.02	Pb (tot)	mg/L	2.31	0.016
Ba (tot)	mg/L	***	***	Pb (diss)	mg/L	2.44	< 0.002
Ba (diss)	mg/L	***	***	Sb (tot)	mg/L	< 0.02	< 0.02
Be (tot)	mg/L	1.2	0.009	Sb (diss)	mg/L	< 0.02	< 0.02
Be (diss)	mg/L	1.16	0.008	Se (tot)	mg/L	< 0.1	< 0.1
B (tot)	mg/L	16	3.14	Se (diss)	mg/L	< 0.1	< 0.1
B (diss)	mg/L	15.3	2.8	Si (tot)	mg/L	106	1.32
Bi (tot)	mg/L	***	***	Si (diss)	mg/L	91	1.13
Bi (diss)	mg/L	***	***	Sn (tot)	mg/L	0.045	< 0.001
Ca (tot)	mg/L	689	512	Sn (diss)	mg/L	0.044	< 0.001
Ca (diss)	mg/L	614	514	Sr (tot)	mg/L	6.11	3.16
Cd (tot)	mg/L	0.0317	0.003	Sr (diss)	mg/L	6.11	3.05
Cd (diss)	mg/L	0.0301	0.0022	Ti (tot)	mg/L	1.39	0.03
Co (tot)	mg/L	5.79	0.0556	Ti (diss)	mg/L	1.39	0.02
Co (diss)	mg/L	4.74	0.0491	Tl (tot)	mg/L	0.051	0.008
Cr (tot)	mg/L	63.2	0.34	Tl (diss)	mg/L	0.049	0.007
Cr (diss)	mg/L	61.4	0.3	U (tot)	mg/L	5.94	0.109
Cu (tot)	mg/L	443	2.52	U (diss)	mg/L	5.77	0.106
Cu (diss)	mg/L	433	2.56	V (tot)	mg/L	111	0.682
Fe (tot)	mg/L	4660	0.198	V (diss)	mg/L	109	0.602
Fe (diss)	mg/L	4220	0.066	Zn (tot)	mg/L	79.5	0.003
K (tot)	mg/L	2290	1060	Zn (diss)	mg/L	80	< 0.002
K (diss)	mg/L	2020	1070	pH	s.u.	1.59	7.33

Table 7. Initial concentrations used in PHREEQC based geochemical models. Concentrations are in mg/L, unless specified.

Parameter	Test 1, 3 initial soln.	Test 5 initial soln.	Test 6 initial soln.	Test 7 initial soln.
Temp °C	25	25	25	25
pH (s.u.)	1.2	1.55	1.68	1.59
pe (s.u.)	NA	13	12	12
Fe(2)	NA	13.8	NA	NA
Fe(3)	NA	4470	NA	NA
Fe	3970	--	4370	4660
Alkalinity	0.0	0.0	0.0	0.0
S(6)	68000	69000	80000	78000
N(-3)	--	3.2	12.8	12.4
Ag	--	0.00546	0.006	0.006
Al	7130	8940	9100	9690
As	--	0.992	1.62	0.99
Ba	0.22	0.138	0.000001	0.000001
Be	--	0.911	1.4	1.2
B	--	11	17.2	16
Ca	582	355	639	689
Cd	0.14	0.0482	0.0466	0.0317
Co	4.6	3.71	5.86	5.79
Cr	47.1	41.5	63.3	63.2
Cu	434	297	415	443
K	1580	2030	2120	2290
Li	33	29.9	42.6	42.2
Mg	3270	4210	4170	4440
Mn	48.6	41.2	56	170
Mo	--	0.181	0.148	0.159
Na	62	262	83.7	107
Ni	33.4	28.3	40.8	33.3
P	228	139	241	258
Pb	--	2.56	2.78	2.31
Sb	--	0.0022	0.02	0.02
Se	--	0.131	0.1	0.1
Si	--	242	96.3	106
Sr	10.6	4.17	8.28	6.11
Tl	--	0.0415	0.05	0.051
U	3	8.65	5.91	5.94
V	89	80.7	112	111
Zn	75	43.5	82.6	79.5
Ra	--	2.19E-06	2.19E-06	2.19E-06
^{226}Ra (Bq/L)		80	80	80
Cl	383	500	530	610

Note: Laboratory analyses report ^{226}Ra in units of Bq/L, however PHREEQC model inputs were in terms of mg/L. Both types of unit are included here to provide traceability.

Table 8. PHREEQC derived uranium concentrations for Tests 5, 6 and 7.

Description	pH	ALKALINITY	U mg/L
Test 5 Initial	1.55	NA	9.51
Test 5 Neutralized	6.95	235.40	0.14
Test 5 Neutralized Modeled	6.95	12.74	0.009
Test 6 Initial	1.68	NA	6.58
Test 6 Neutralized	6.95	222.37	0.11
Test 6 Neutralized Modeled	6.95	14.71	0.0042
Test 7 Initial	1.59	NA	6.61
Test 7 Neutralized	7.33	163.37	0.11
Test 7 Neutralized Modeled	7.33	26.40	0.036
Test 7 Neutralized Modeled	6.95	15.30	0.0053

Table 9. Comparison of Model Calculated Uranium Concentrations as a Function of the Partial Pressure of Carbon Dioxide. Calculations Used Initial Conditions From Test 5.

pH	Pressure CO2(g) (log atms)	Uranium (mg/L)	Comment
1.55	NA	9.507	Initial measured
6.95	-1.7729	0.141	Measured after neutralization
6.95	-3.4	0.009	Model calculation
6.95	-3	0.059	Model calculation
6.95	-2.75	0.166	Model calculation
6.95	-2.5	0.420	Model calculation

Table 10. Summary and Comparison of Neutralized and Modeled Concentrations for Tests 5, 6, and 7.

Parameter (units in mg/L) unless specified	Barren Stream Laboratory Measured Concentrations Test 5	Neutralized Solution Laboratory Measured Concentrations Test 5	Modeled Value after Neutralization Test 5	Barren Stream Laboratory Measured Concentrations Test 6	Neutralized Solution Laboratory Measured Concentrations Test 6	Modeled Value after Neutralization Test 6	Barren Stream Laboratory Measured Concentrations Test 7	Neutralized Solution Laboratory Measured Concentrations Test 7	Modeled Value after Neutralization Test 7 pH 6.95	Modeled Value after Neutralization Test 7 pH 7.33
pH	1.55	6.95	6.95	1.68	6.95	6.95	1.59	7.33	6.95	7.33
ALKALINITY		235.40	16.24		222.37	18.28		163.37	18.87	34.60
Sulfate	75841	15291	6716	89053	11173	16718	86791	11166	10077	9561
U	9.51	0.14	0.008	6.58	0.11	0.004	6.61	0.11	0.005	0.036 (0.024)
Ra226 (Bq/L)	88		0.008	90		0.005	89		0.006	0.007
Ag	0.006	0.0002	0.006	0.007	0.001	0.007	0.007	0.001	0.007	0.007
Al	9839	6.71	0.47	10143	0.50	0.49	10796	0.40	0.49	1.10
As	1.09	0.0180	0.0011	1.80	0.0203	0.0209	1.10	0.0203	0.0038	0.0005
Ba	0.15	0.14	0.16	NA	NA	0.09	NA	NA	0.13	0.13
Be	1.00	6.11E-05	6.72E-06	1.56	0.008	1.37E-05	1.33	0.01	1.15E-05	1.13E-05
B	12.09	3.66	12.3	19.1	4.43	19.6	17.80	3.19	18.2	18.2
Ca	390	418	1141	710	530	452	766	519	751	775
Cd	0.053	0.061	0.048	0.052	0.0007	0.037	0.035	0.003	0.022	0.013
Co	4.08	0.021	4.16	6.53	0.11	6.68	6.45	0.06	6.60	6.61
Cr	45.6	0.0040	5.07	70.5	0.33	27.0	70.4	0.35	15.5	18.1
Cr(III) reduced Eh			0.64			0.72			0.67	0.36
Cu	327	0.19	0.13	462	2.81	0.27	493	2.56	0.22	0.08
Fe	4900	5.07	0.002	4836	1.50	0.003	5155	0.20	0.003	0.002
K	2232	1152	2286	2361	1158	2421	2549	1076	2618	2618
Li	33	1.36	34	47	21	49	47	14	48	48
Mg	4628	2702	4633	4643	2733	4705	4941	2335	4994	4882
Mn	45.3	9.1	35.7	62.4	10.0	53.6	189.3	5.8	86.3	14.9
Mo	0.20	0.18	0.018	0.16	0.10	0.049	0.18	0.14	0.032	0.029
Na	288.3	219.4	295.3	93.3	67.1	95.7	119.2	64.5	122.4	122.4
Ni	31.1	0.010	8.59	45.44	0.42	17.22	37.07	0.31	11.87	6.46
P	152.9	0.06	0.25	268.4	0.05	1.43	287.2	0.11	0.55	0.15
Pb	2.8	0.02	0.0015	3.10	0.04	0.0017	2.57	0.02	0.0009	0.0003
Sb	0.0017	0.00014	0.0017	0.0157	0.0143	0.0161	0.0157	0.0143	0.0161	0.0161
Se	0.14	0.04	0.14	0.11	0.10	0.11	0.11	0.10	0.11	0.11
Se(IV) reduced Eh			0.001			0.007			0.002	0.001
Si	242.0	3.51	(242)	96.0	1.19	(96)	106.0	1.32	(106)	(106)
Sr	4.59	2.69	1.14	9.22	2.96	1.00	6.80	3.21	1.18	1.22
Tl	0.05	0.005	0.047	0.056	0.009	0.057	0.057	0.008	0.058	0.058
V	88.9	0.03	0.22	125	0.71	11.72	124	0.69	0.91	0.05
Zn	47.9	3.07	4.87	92	0.038	17.59	89	0.0030	11.77	4.99
Silicon not modeled using PHREEQC										

Table 11. Selection of Pore Water Concentrations for Neutralized Tailings based upon Initial, Neutralized and Modeled Concentrations for Tests 5, 6, and 7.

Parameter	Selected Value or Range (units in mg/L) unless specified	Comments on Selected Value(s)
pH (s.u.)	**6.9 to 7.3**	To be specified in operation plan
U	**0.14**	Based upon highest Uranium concentration in Test 5, 6 and 7 neutralized solutions
Ag	**0.001**	Alternative mechanism may explain lower Ag concentration, As the starting concentration is very low the small amount of Ag could easily be accomodated into a coprecipitate Selected highest measured concentration from the three tests
Al	**0.50**	Based upon consistency between measured concentration and modelled values for Tests 6 and 7
As	**0.02**	Selected greatest value from measured concentration Low initial arsenic concentration and very high dissolved iron expected to produce low As value in final solution
Ba	**0.15**	Tests 6 and 7 did not include Ba Concentrations In reaction path model BaCl2 added at 150 mg/L for a concentration of 99 mg/L Ba See text for discussion of solid solution model
Be	**0.01**	As the model has a tendency to over estimate surface complexation in some cases the larger of the two values (Measured concentration) has been selected.
Bi	**0.00015**	Based upon Test 5 neutralized concentration
B	**4.50**	Selected measured concentration Test 6 rounded up
Cd	**0.003**	Cadmium concentrations not signifcantly reduced in Test 5 samples, actually increase, therefore Test 5 result eliminated, nor do models show significant decreases in Cd, Tests 6 and 7, Coprecipitation with precipitating Calcite likely process. Selected greater of two neutralized values from Test 6 and 7
Co	**0.10**	Selected greater value for Co from model result, although low measured concentration indicates possible coprecipitate with HFO A model of ferric hydroxide coprecipitation was not included Retained initial concentrations because a mechanism to attenuate cobalt was not defined
Cr	**0.35**	Selected greater value for Cr from model result the low measured concentration indicates possible coprecipitate with HFO Selected partial pressure of O2 prevents reduction to CrO3 phases in model
Cu	**0.40**	Close agreement noted between measured concentration and modeled result for Test 5 but increases in Cu show a nonlinear adsorption
Fe	**5.0 to 0.1**	measured concentration signficantly greater than modeled value. Likely kinetic inhibition for oxdiation of ferrous to ferric conversion in measured concentration expect lower concentrations over time, also given potential coprecipitate stability of ferrihydrite may be impacted
Li	**20**	Selected greatest measured concentration (rounded) after neutralization Test 6, Mechanism for reduction in concentration not identified, however ion exchange may play a role
Mn	**10 to less than 1.0 mg/L**	Neutralized test solutions are probably saturated with respect to a Rhodochrosite of intermediate stability, Saturation indices for crystalline and more amorphous rhodochrosite phases bracket model calculated value Because of low alkalinities Rhodochrosite could not precipitate in Model Evaluated Hausmannite as alternative oxide but too stable
Mo	**0.20**	Selected greates initial measured value Tests show only slight removal fo Mo Model appears to overpredict surface complexation
Ni	**0.40**	Selected measured value possible coprecipitate, similarly lower Ni Concentration observed in McClean Lake operation
P	**0.10**	Selected greatest modeled value Neutralized concentrations similar enough to model values
Pb	**0.04**	Selected measured concentration because greater than modeled value
^{226}Ra (Bq/L)	**10.0**	Weighted average of Result from Tests 3, 5 and 6.
Sb	**0.016**	Attenuation of Sb in these models expected to be minimal Selected highest initial measured concentration
Se	**0.05**	Minimum surface complexation observed in model for selenate. Selenite dominant model values were much lower (0.007 mg/L), Models show the importance of redox on final value. The 0.05 mg/L represents reasonable and conservative compromise between two models.
Si	**5**	Selected measured value low concentration suggests low solubility Si Al phase is probably controlling Si concentration
Sr	**3.0**	Based upon concurrence of laboratory measured concentration and modeled result
Sn	**0.01**	laboratory results
Ti	**0.01**	laboratory results
Tl	**0.01**	Selected greatest measured concentration(s) after neutralizaiton
V	**0.70**	Additional model run with Carnotite precipitating did not change modeled V value significantly in Test 5 simulation, selected average of the two greater values Tests 6 and 7
Zn	**3.0**	Based upon Test 5 measured concentrations in neutralized solution Adsorption mechanism most likely Test 6 and 7 Zn values too low for conservative estimate possible errors in analytical results

Table 12. Comparison of Solid Solution Model Results

		Radium Solubility Product	
		Log Ksp = -10.4499	Log Ksp = -10.26
	Initial ^{226}Ra Bq/L	88.4	88.4
Barite log Ksp = -9.97 $BaSO_4$ and $RaSO_4$	^{226}Ra Bq/L	0.0058	0.009
	Percent ^{226}Ra Removed	99.993	99.990
Barite log Ksp = -8.97 $BaSO_4$ and $RaSO_4$	^{226}Ra Bq/L	0.0058	0.009
	Percent ^{226}Ra Removed	99.993	99.990
Barite log Ksp = -9.97 $BaSO_4$, $SrSO_4$ and $RaSO_4$	^{226}Ra Bq/L	0.0055	0.0085
	Percent ^{226}Ra Removed	99.994	99.990
Barite log Ksp = -8.97 $BaSO_4$, $SrSO_4$ and $RaSO_4$	^{226}Ra Bq/L	0.0055	0.0085
	Percent ^{226}Ra Removed	99.994	99.990

FIGURES

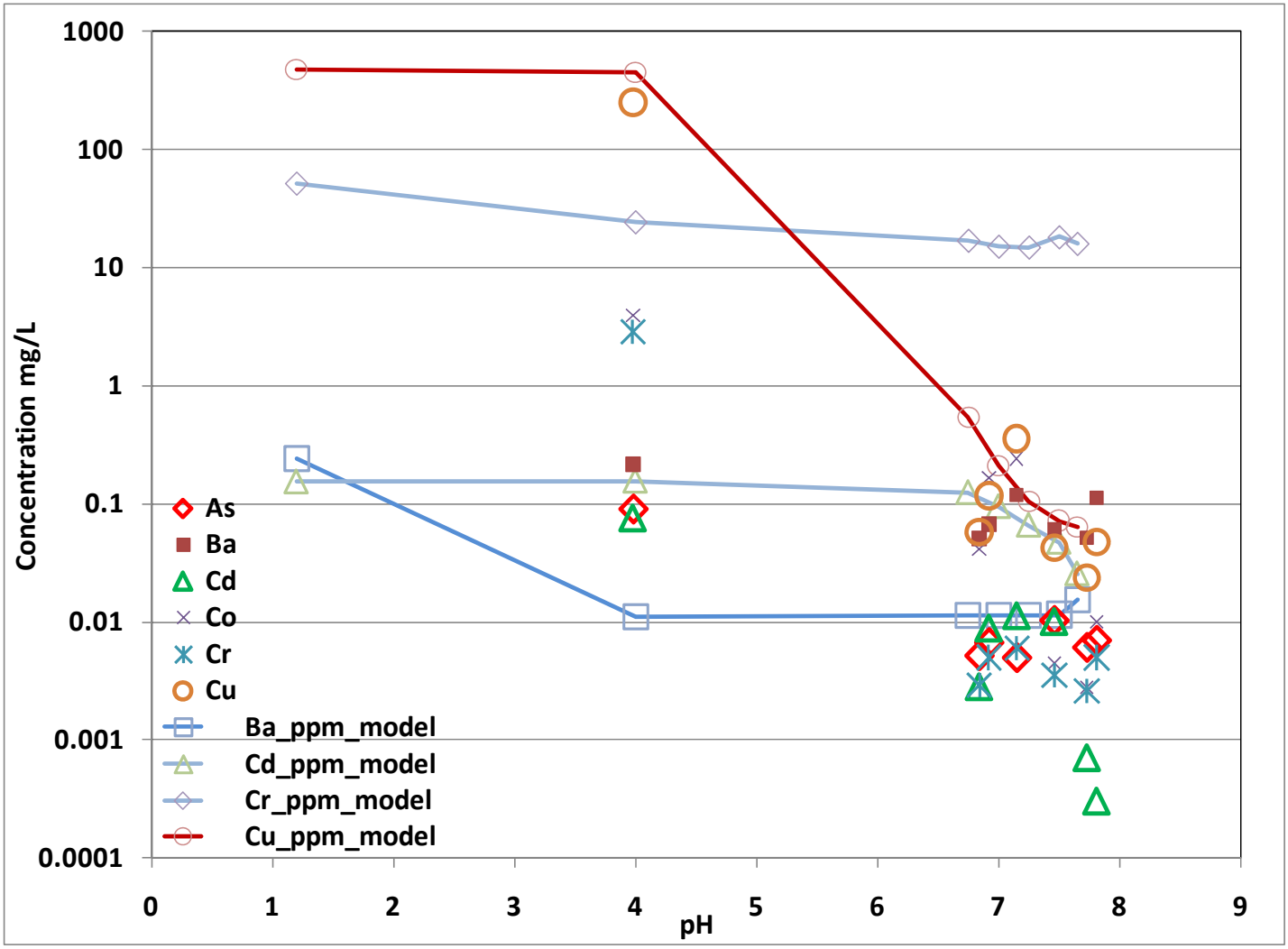

Figure 1. Summary of trace metal results As, Ba, Cd, Co, Cr, and Cu for Tests 1 and 3, initial model.

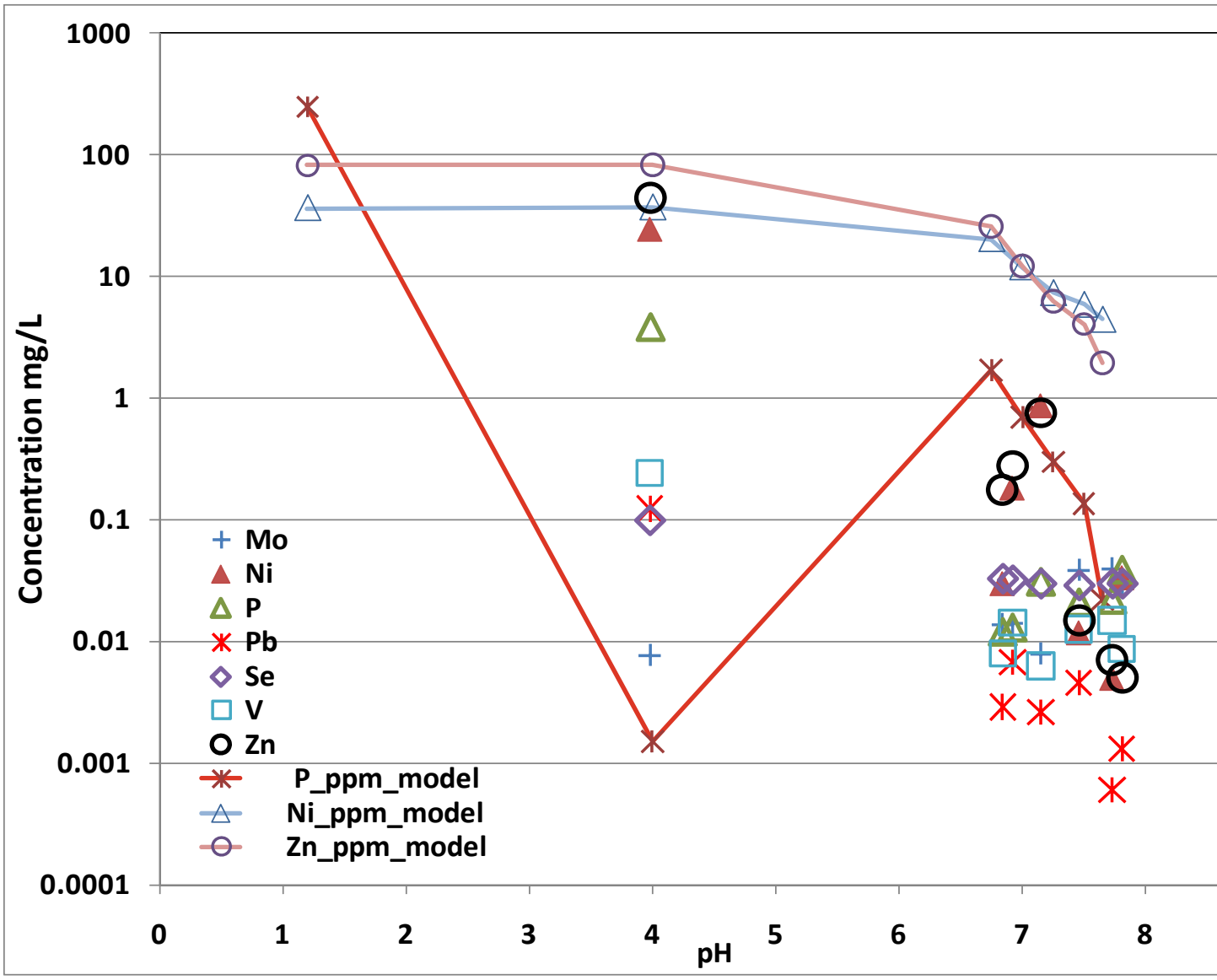

Figure 2. Summary of trace metal results Mo, Ni, P, Pb, Se, V and Zn for Tests 1 and 3, initial model.

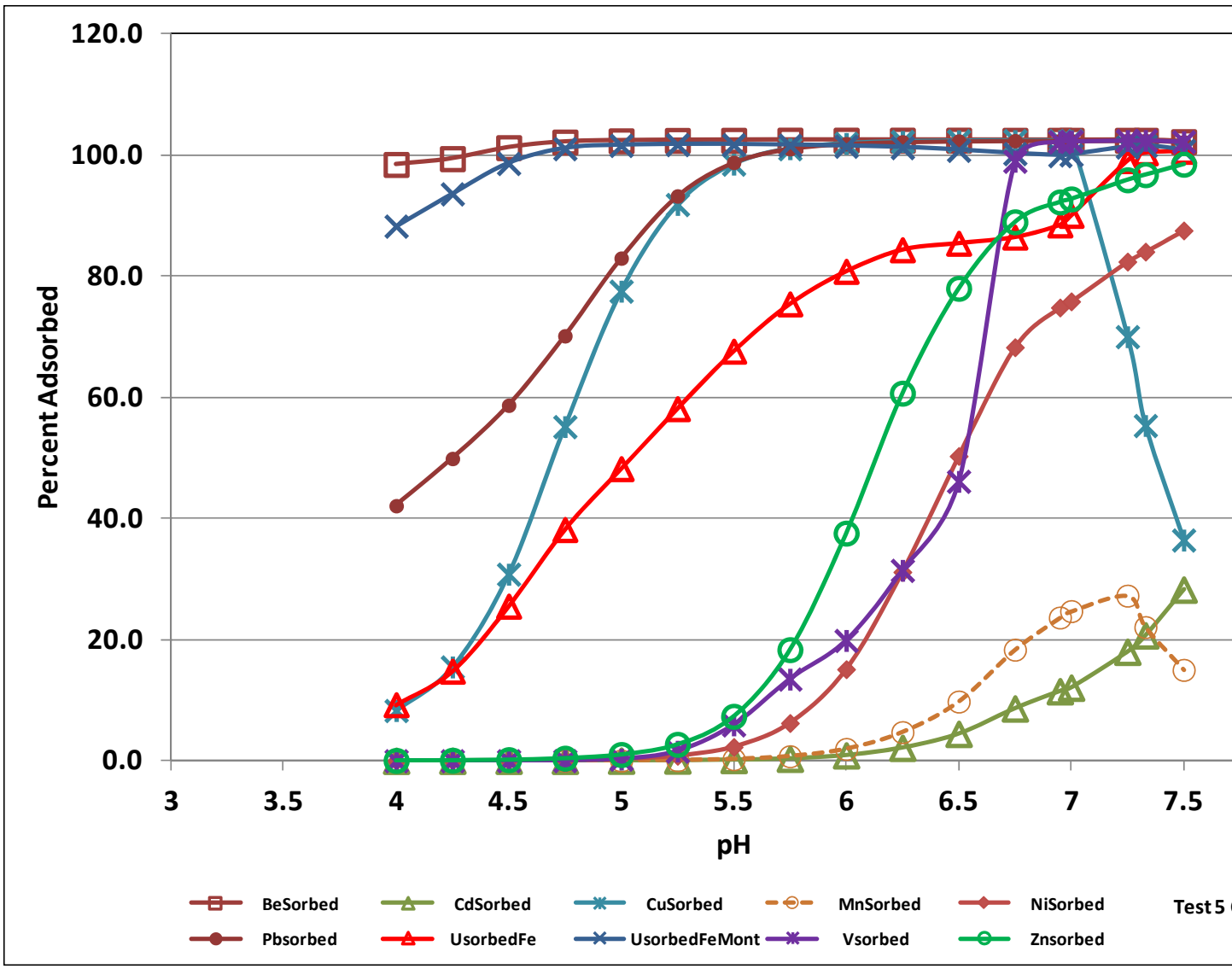

Figure 3. Selected Cations Percent Adsorbed onto HFO as a Function of pH, for the Test 5 Geochemical Model. Figure also includes Uranium Adsorption onto HFO and Montmorillonite.

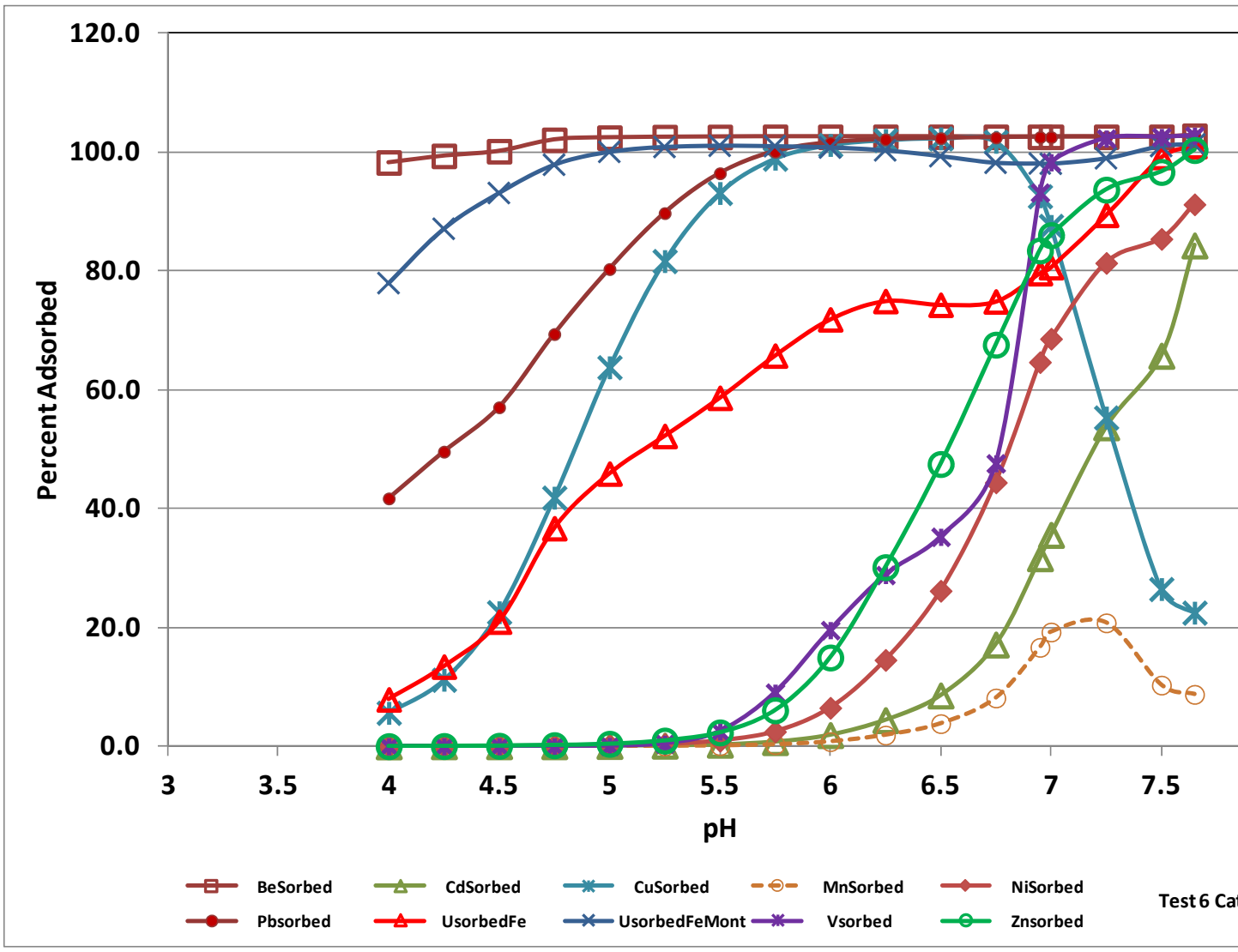

Figure 4. Selected Cations Percent Adsorbed onto HFO as a Function of pH, for the Test 6 Geochemical Model. Figure also includes Uranium Adsorption onto HFO and Montmorillonite.

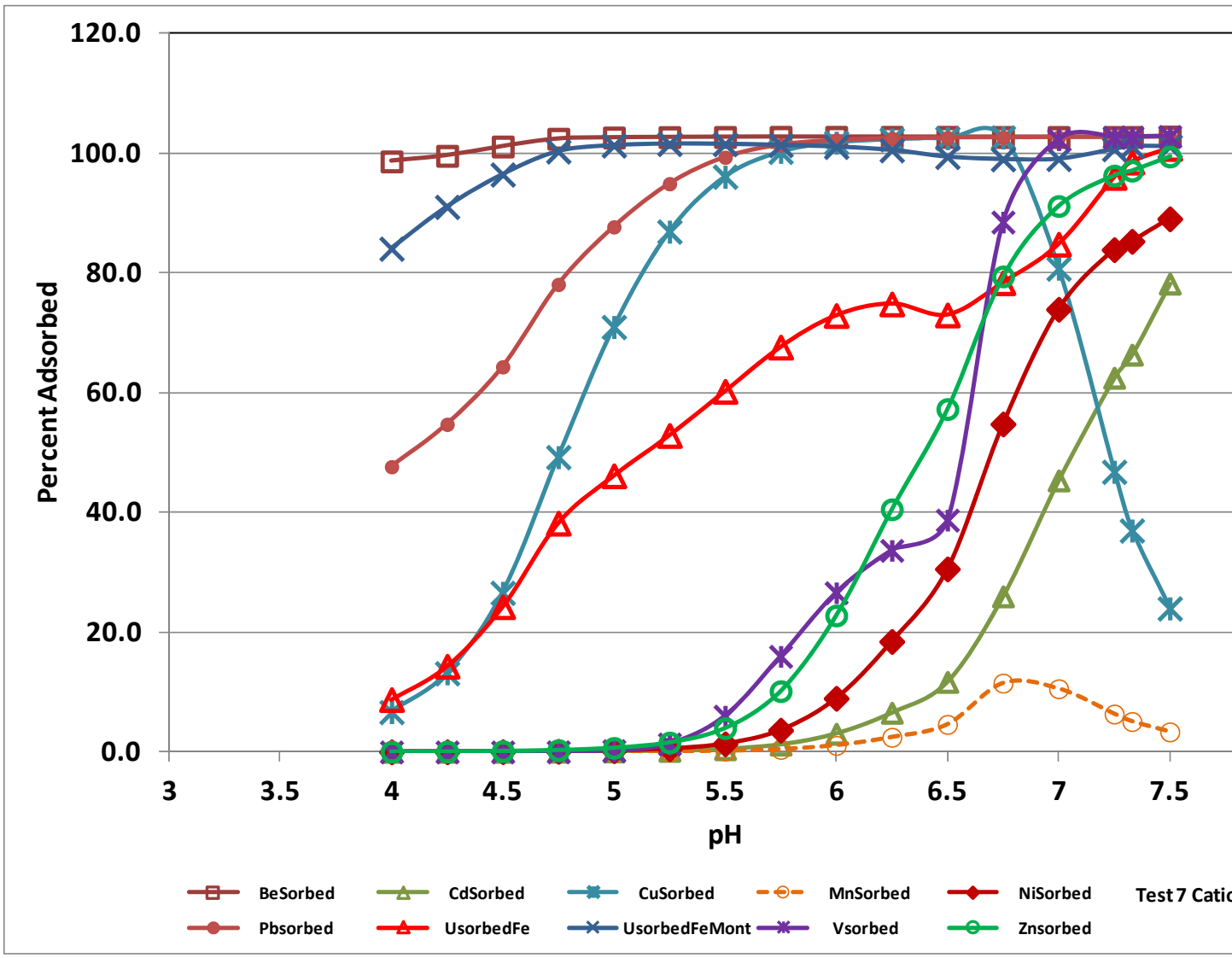

Figure 5. Selected Cations Percent Adsorbed onto HFO as a Function of pH, for the Test 7 Geochemical Model. Figure also includes Uranium Adsorption onto HFO and Montmorillonite.

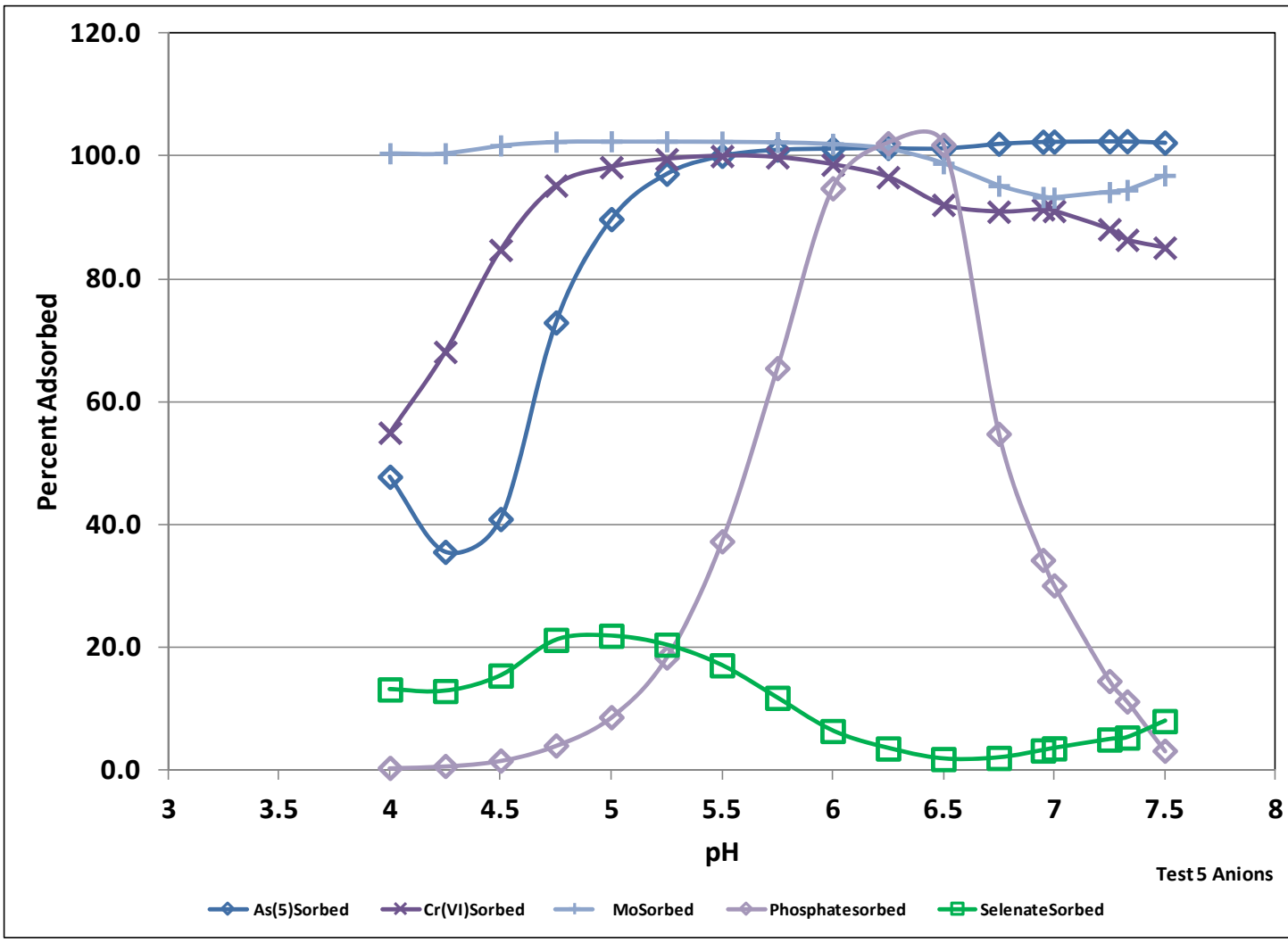

Figure 6. Selected Anions Percent Adsorbed onto HFO as a Function of pH, for the Test 5 Geochemical Model.

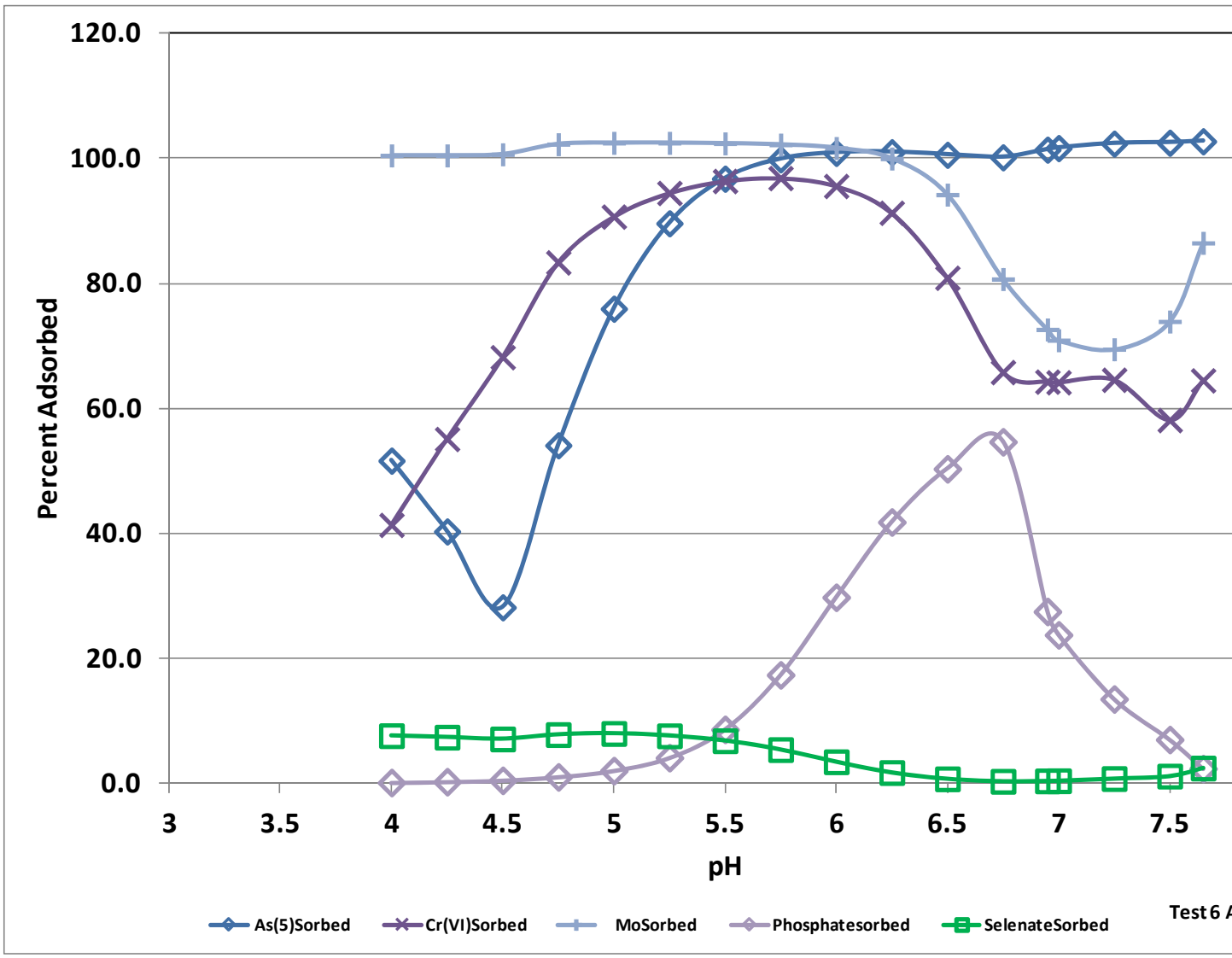

Figure 7. Selected Anions Percent Adsorbed onto HFO as a Function of pH, for the Test 6 Geochemical Model.

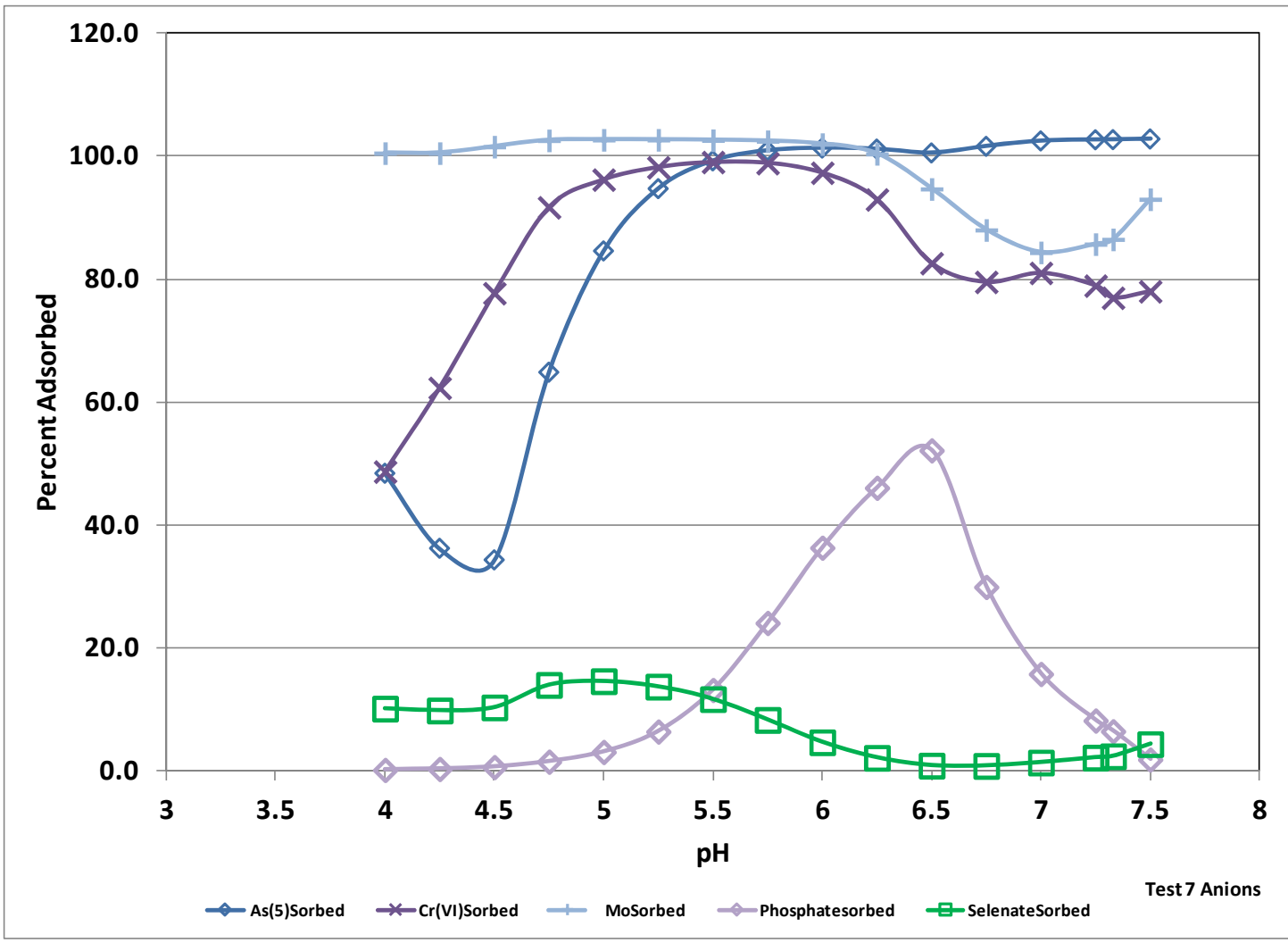

Figure 8. Selected Anions Percent Adsorbed onto HFO as a Function of pH, for the Test 7 Geochemical Model.

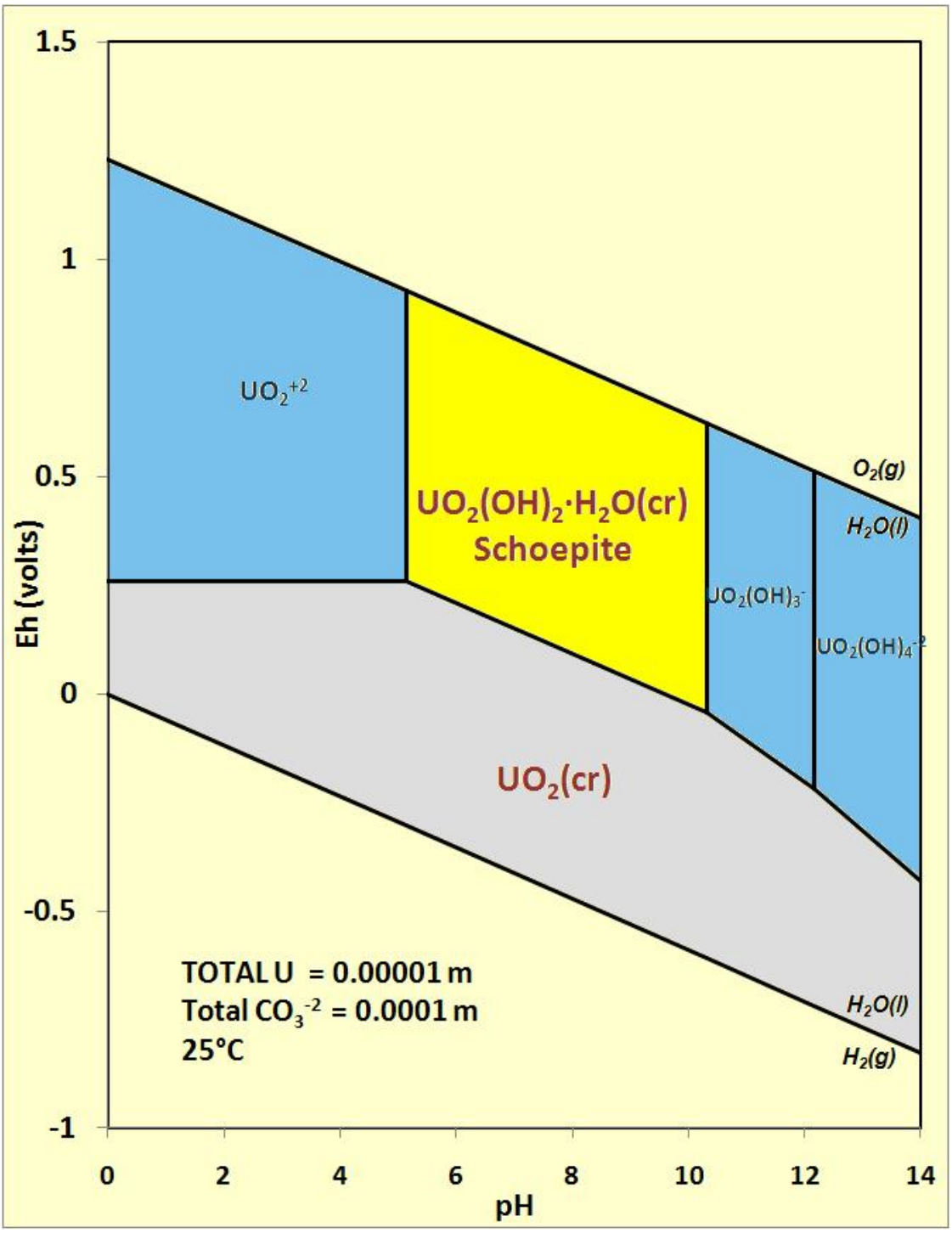

Figure 9a. Eh-pH diagram for the system U, C, H and O at 25°C – Total U 2.4 mg/L.

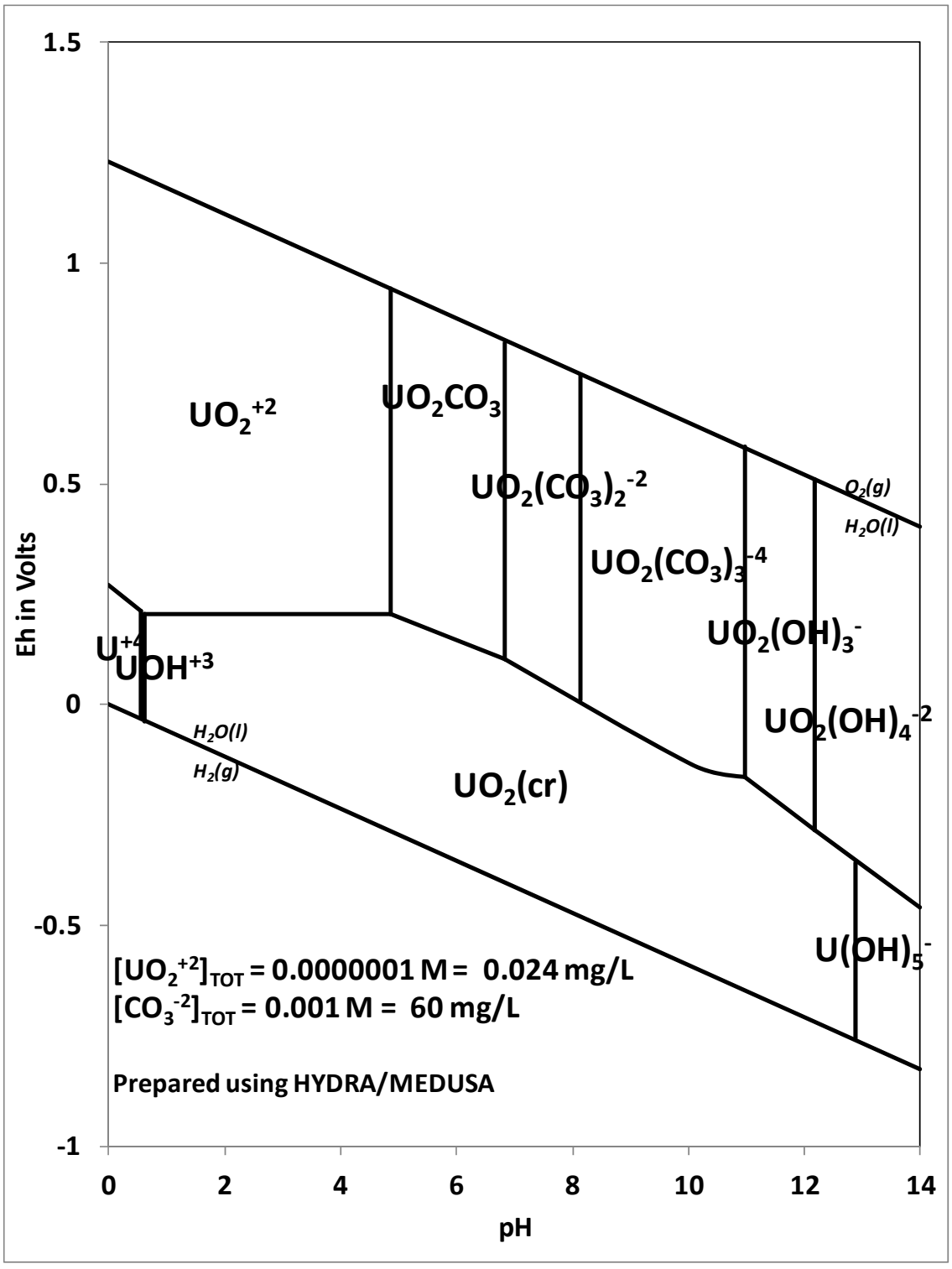

Figure 9b. Eh-pH diagram for the system U, C, H and O at 25°C – Total U 0.024 mg/L

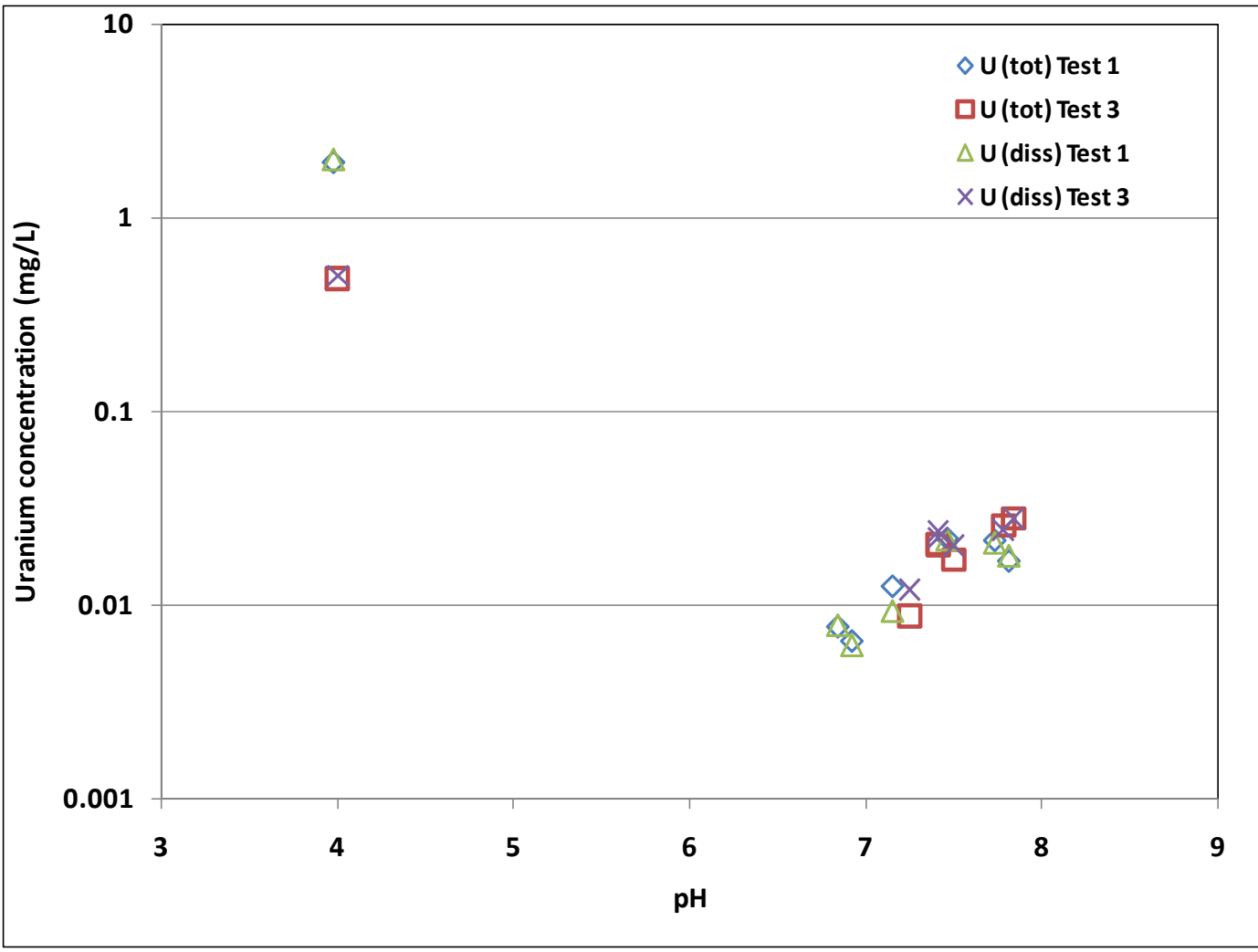

Figure 10. Uranium concentrations for Tests 1 and 3. Total and dissolved concentrations shown. Concentrations in mg/L.

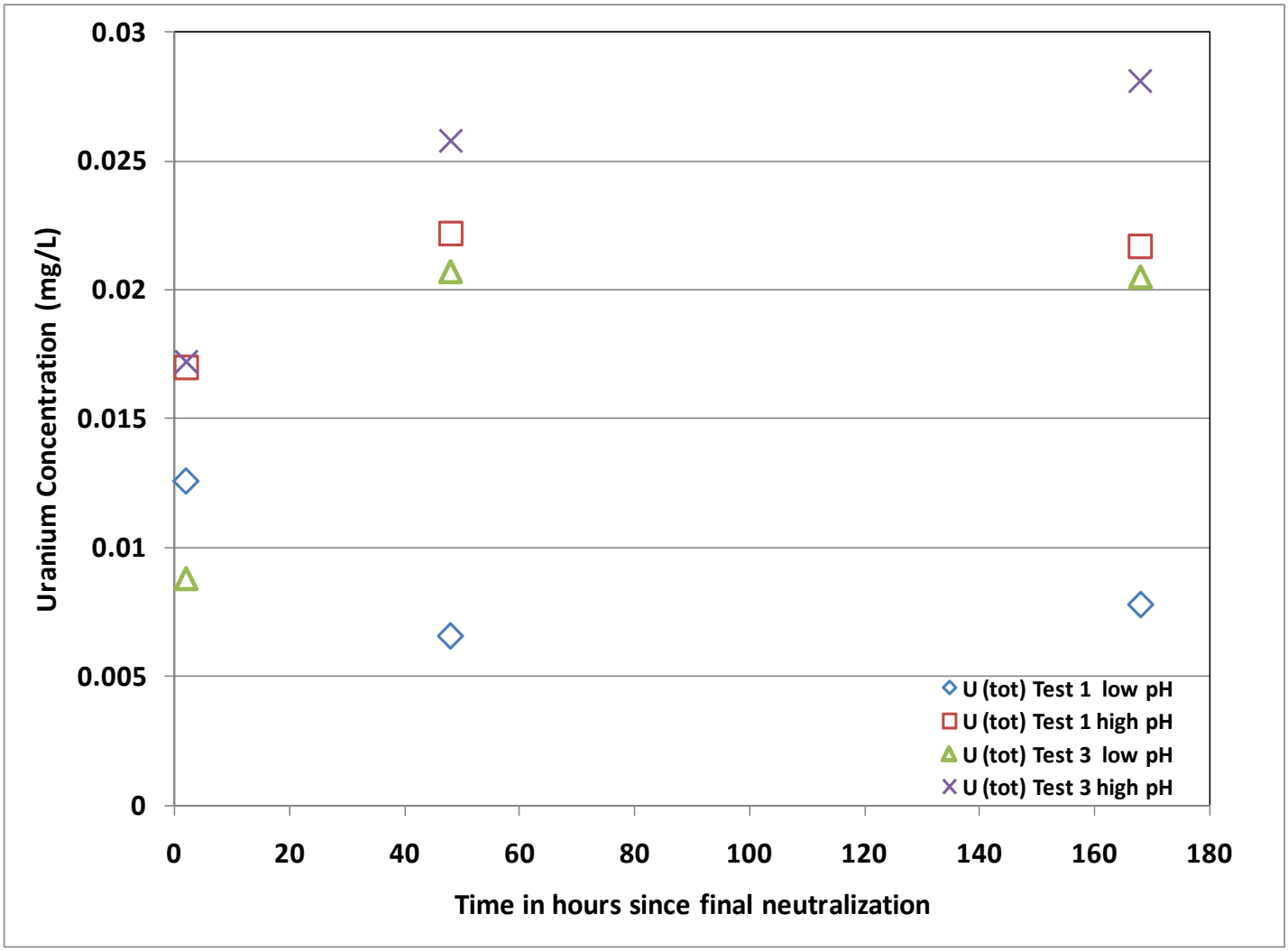

Figure 11. Aging test results for Tests 1 and 3. Uranium total concentrations in mg/L.

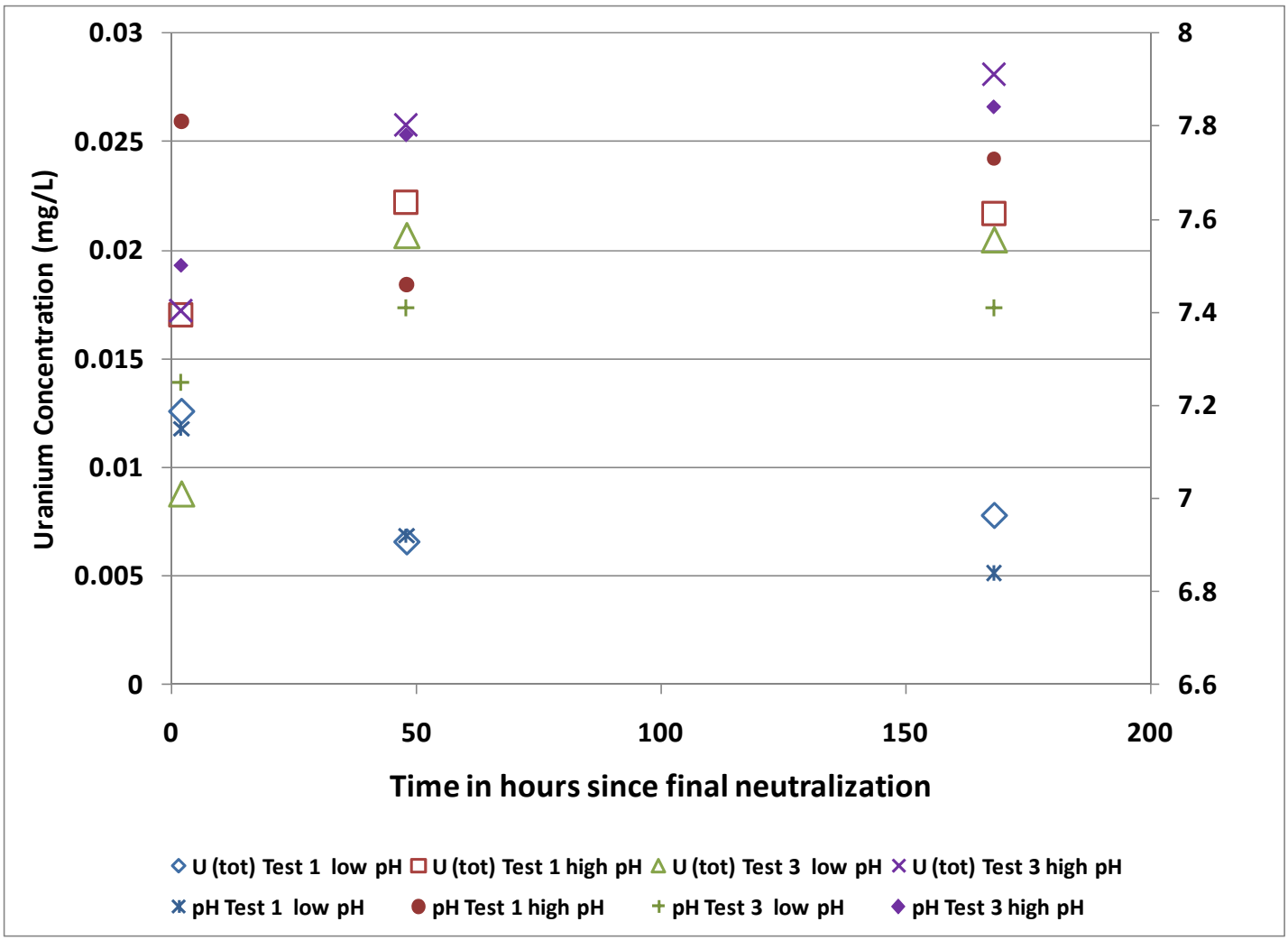

Figure 12. Aging test results for Tests 1 and 3, Uranium and pH values plotted as a function of time

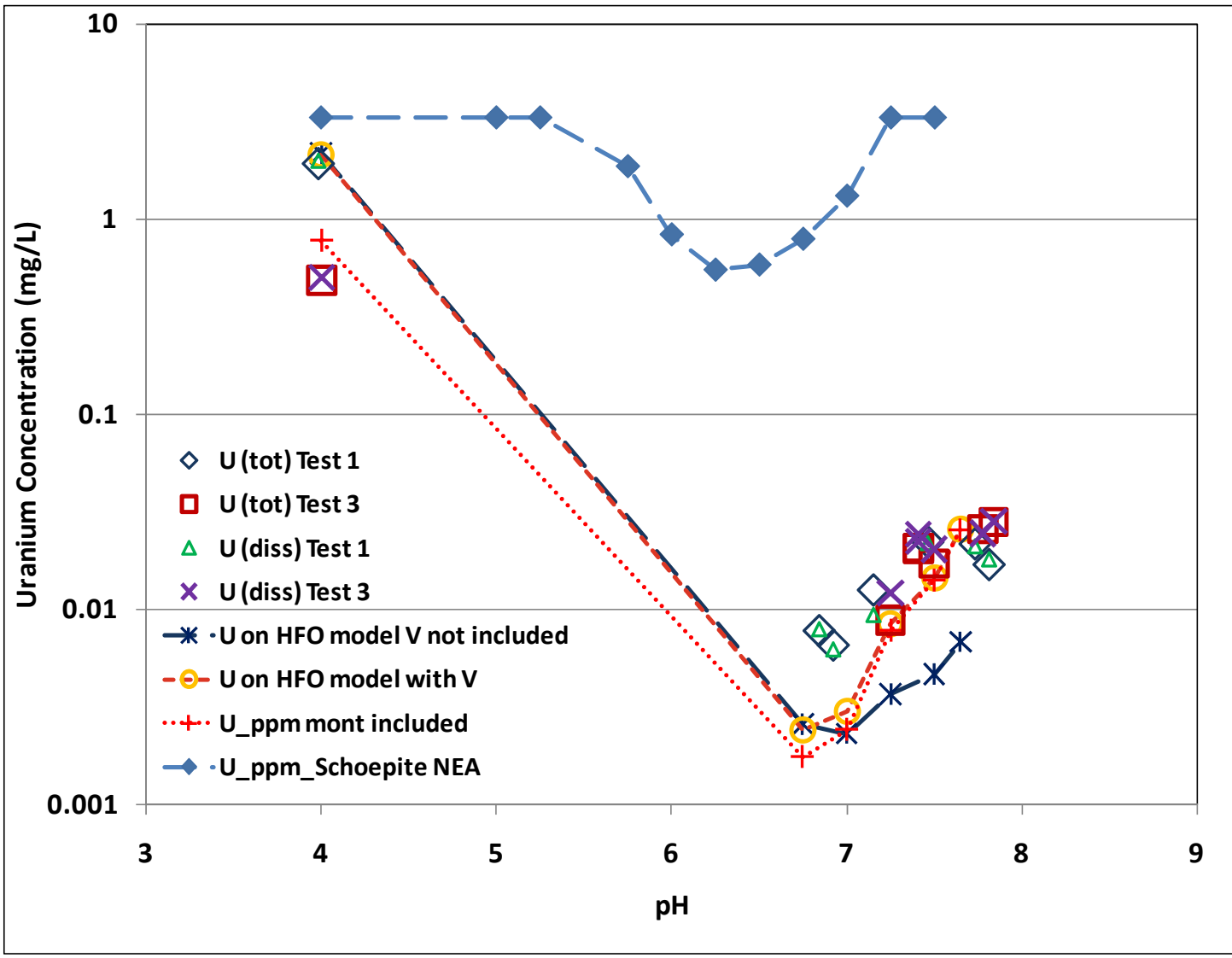

Figure 13. Comparison of measured uranium concentrations and model calculated results. (Tests 1 and 3)

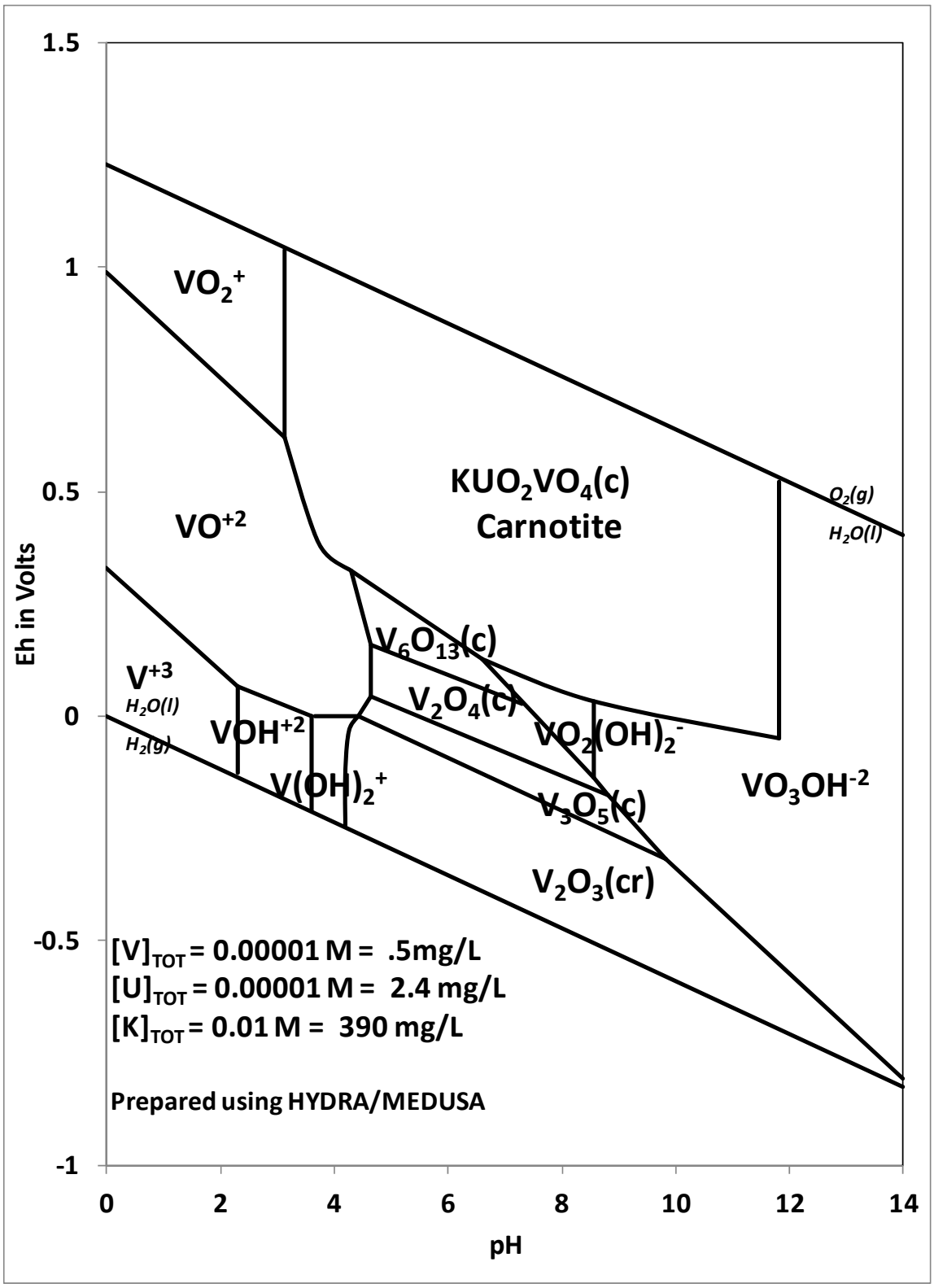

Figure 14. Eh-pH diagram for the system V-K-U-O-H at 25°

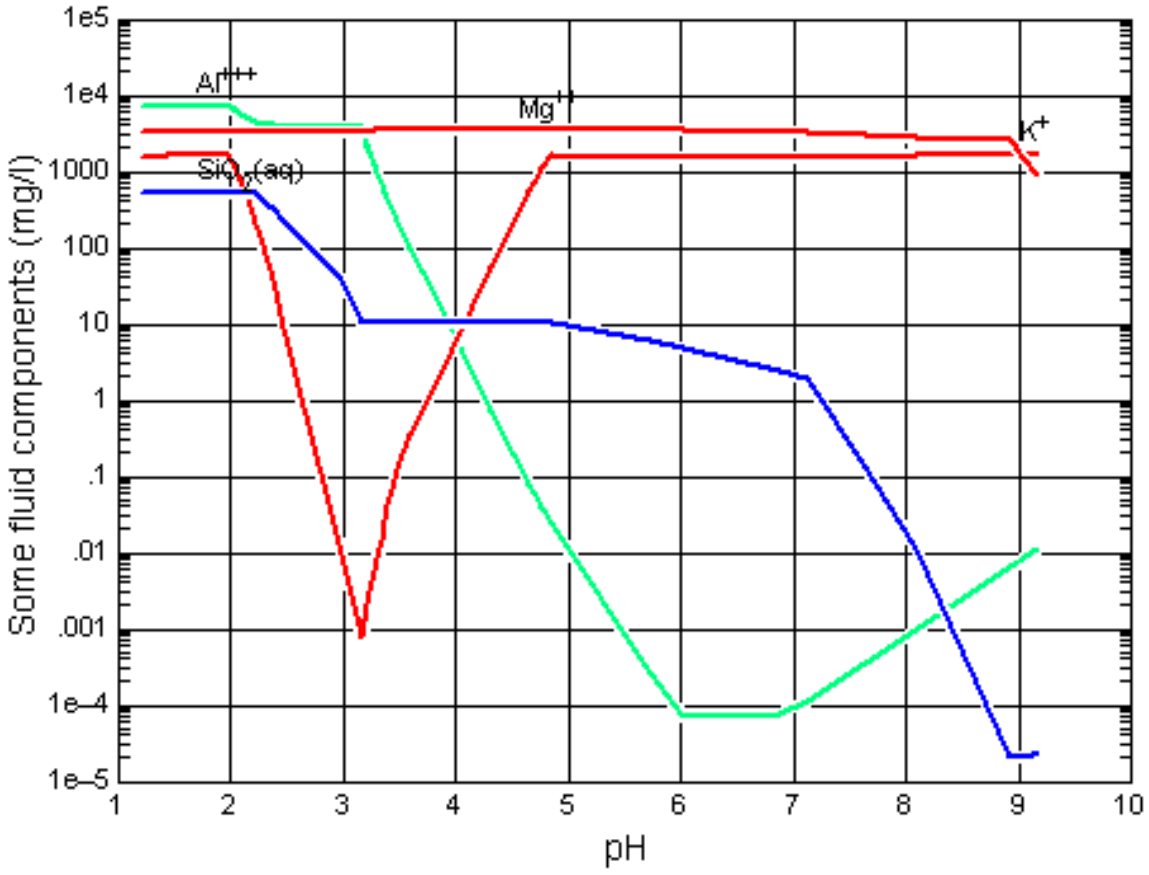

Figure 15 GWB reaction path model showing changes in concentration for Silicon (as Silica) and aluminum.

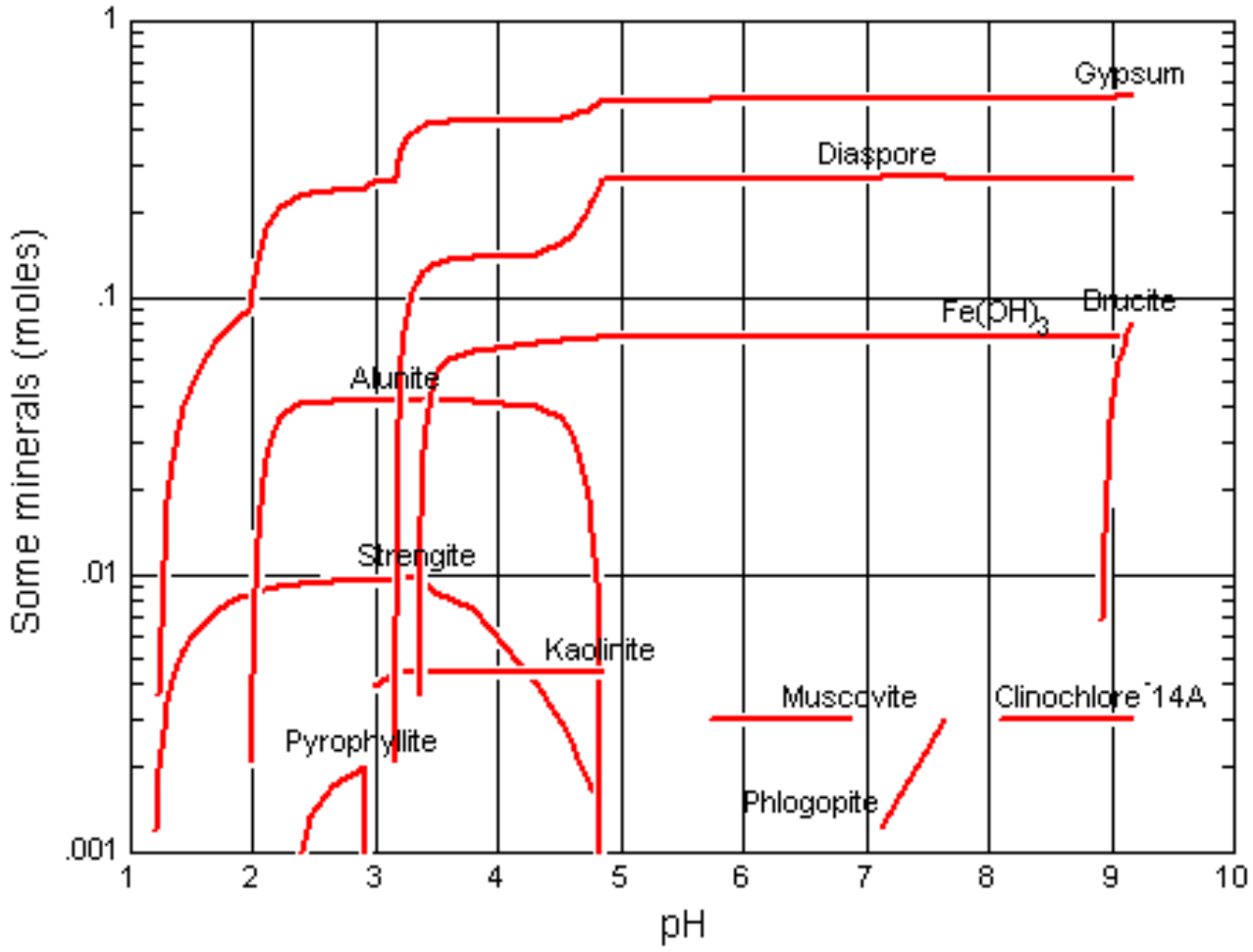

Figure 16. GWB reaction path model showing mineral precipitation and dissolution reactions.

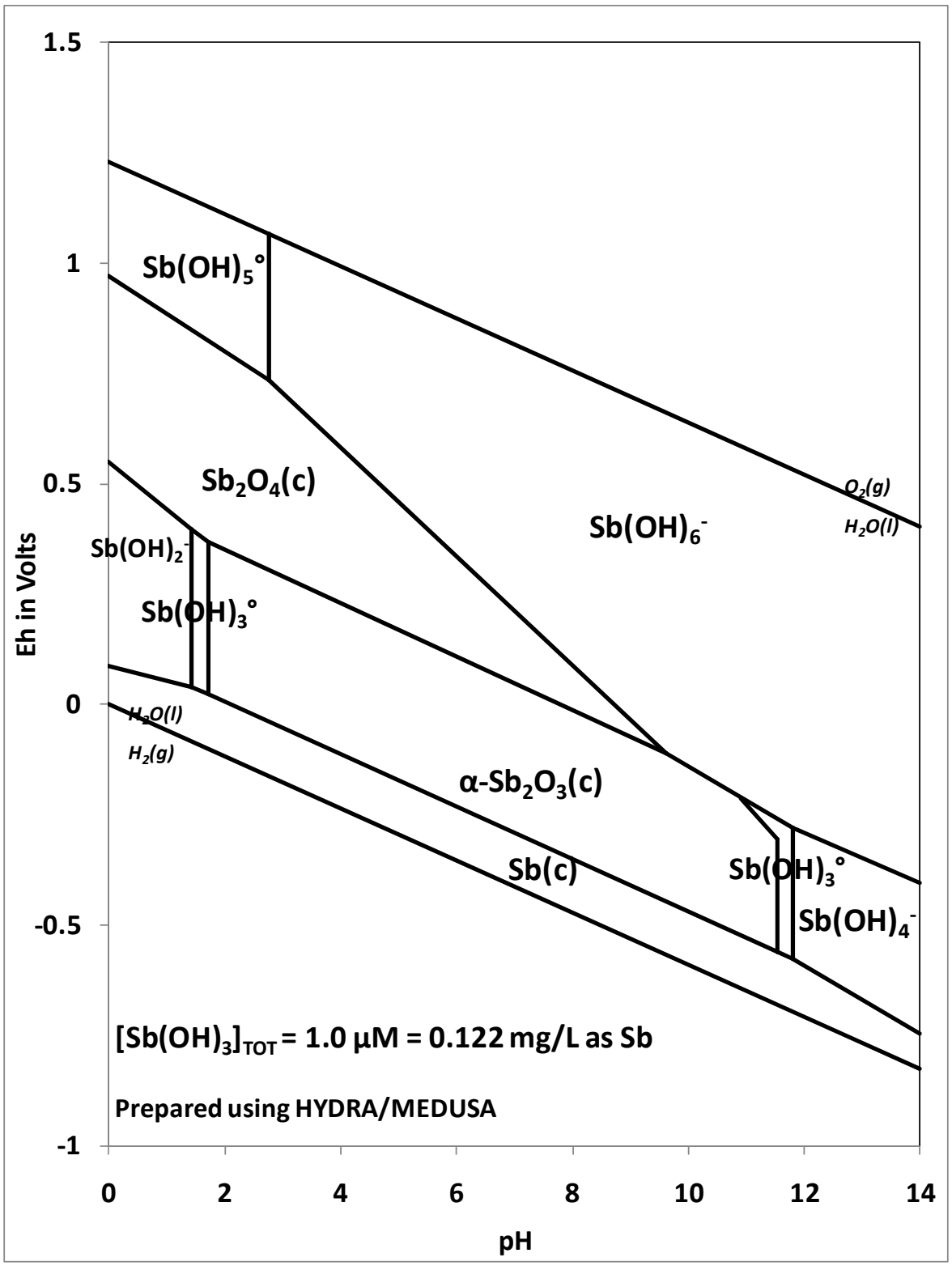

Figure 17. Eh-pH diagram for the system Sb-O-H at 25°C.

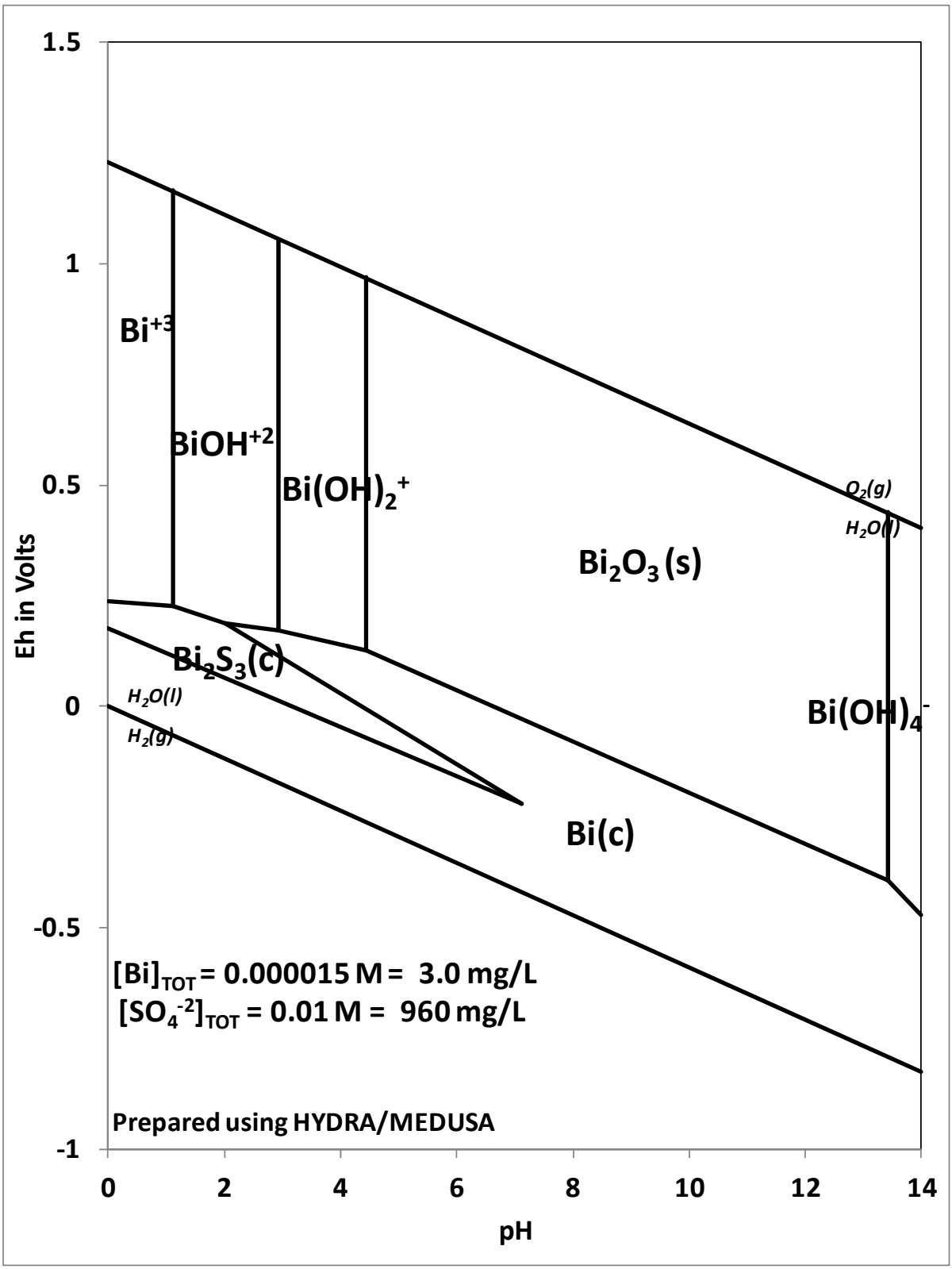

Figure 18a. Eh-pH diagram for system Bi-S-O-H at 25 °C. (note: higher concentration of Bi).

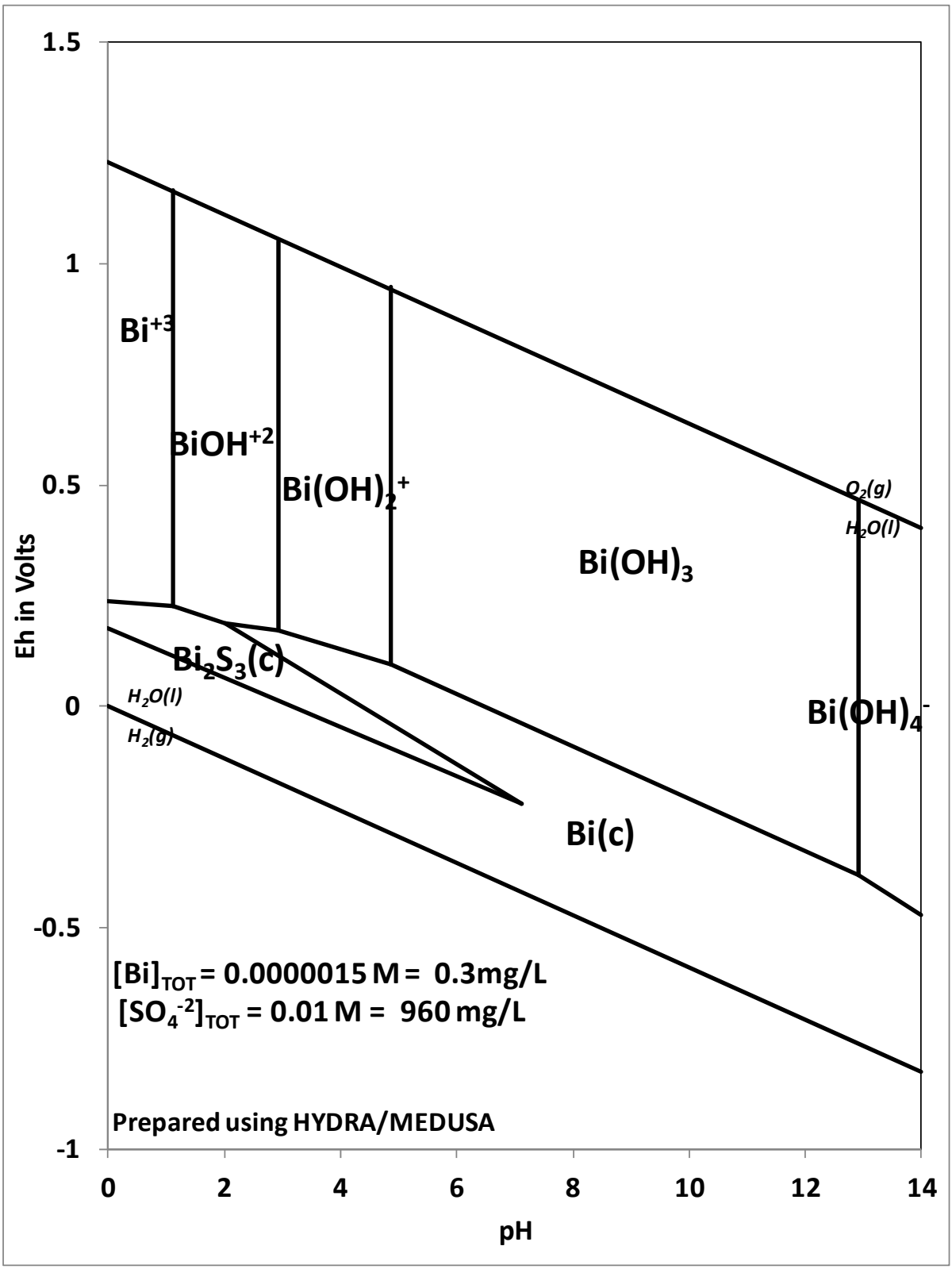

Figure 18b. Eh-pH diagram for system Bi-S-O-H at 25 °C (note: lower concentration of Bi).

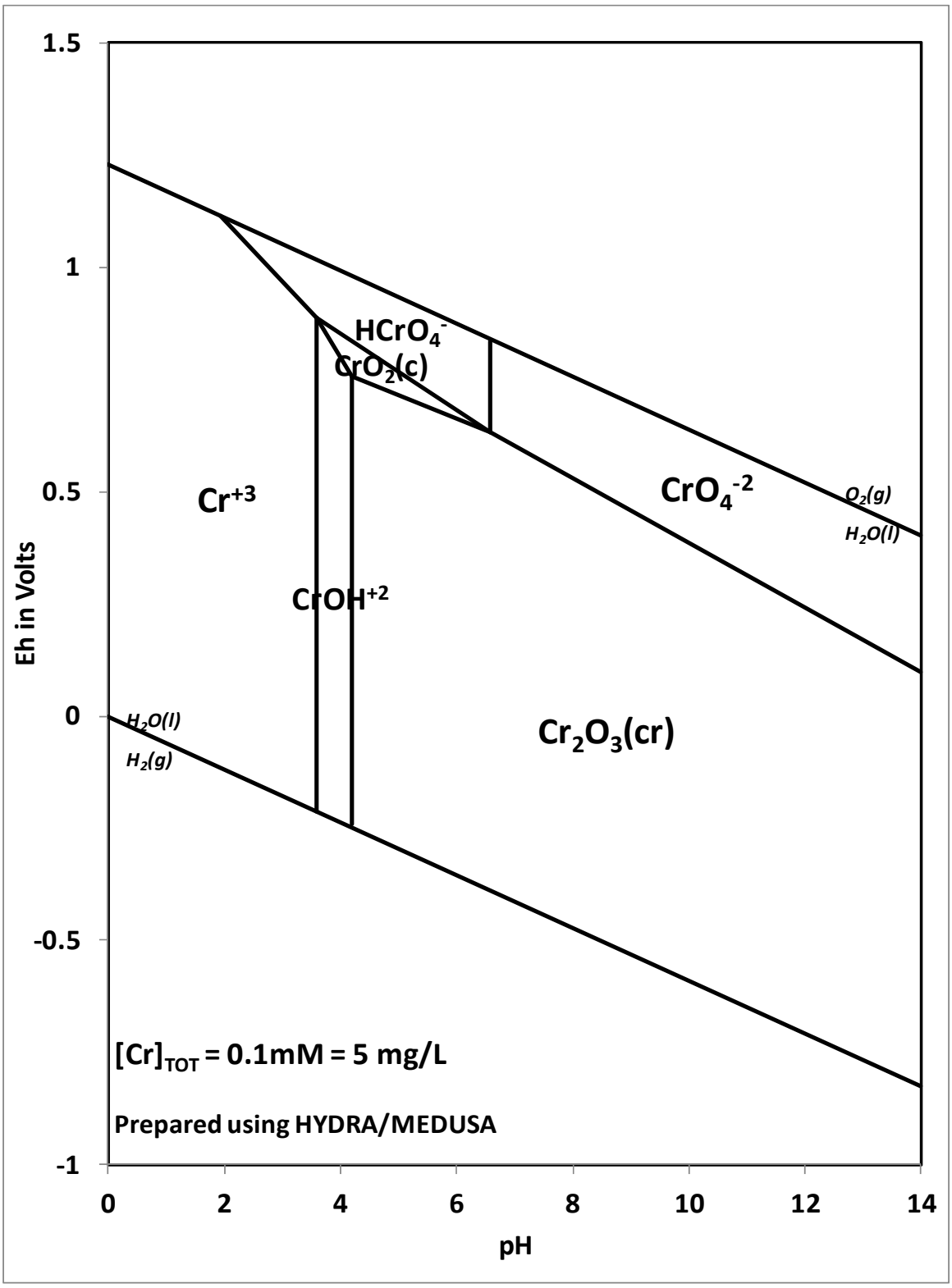

Figure 19a. Eh-pH diagram for the system Cr-O-H at 25°C. Figure shows most stable solids.

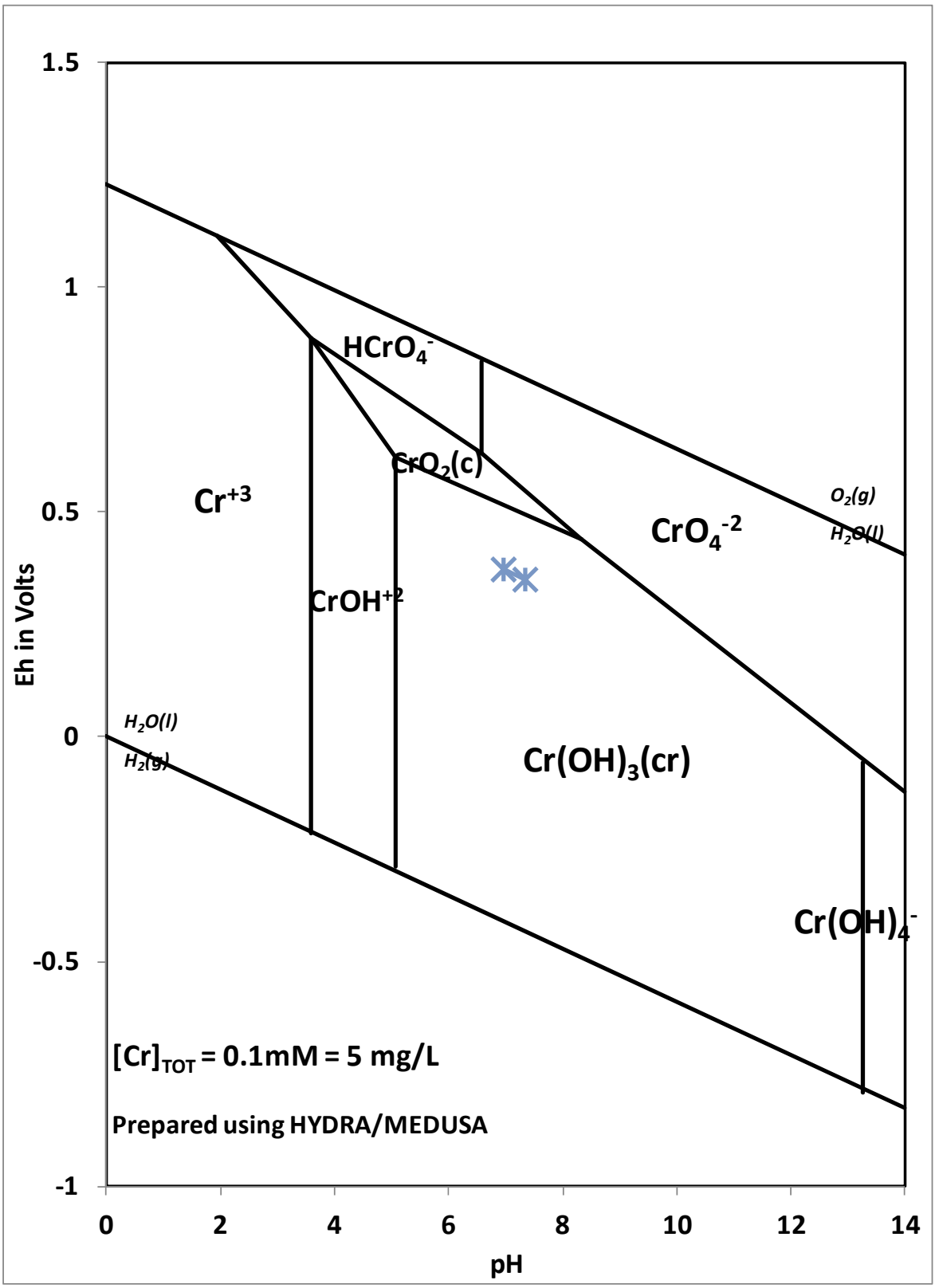

Figure 19b. Eh-pH diagram for the system Cr-O-H at 25°C. Figure replaces Cr_2O_3(cr) with chromium hydroxide [$Cr(OH)_3$(cr)].

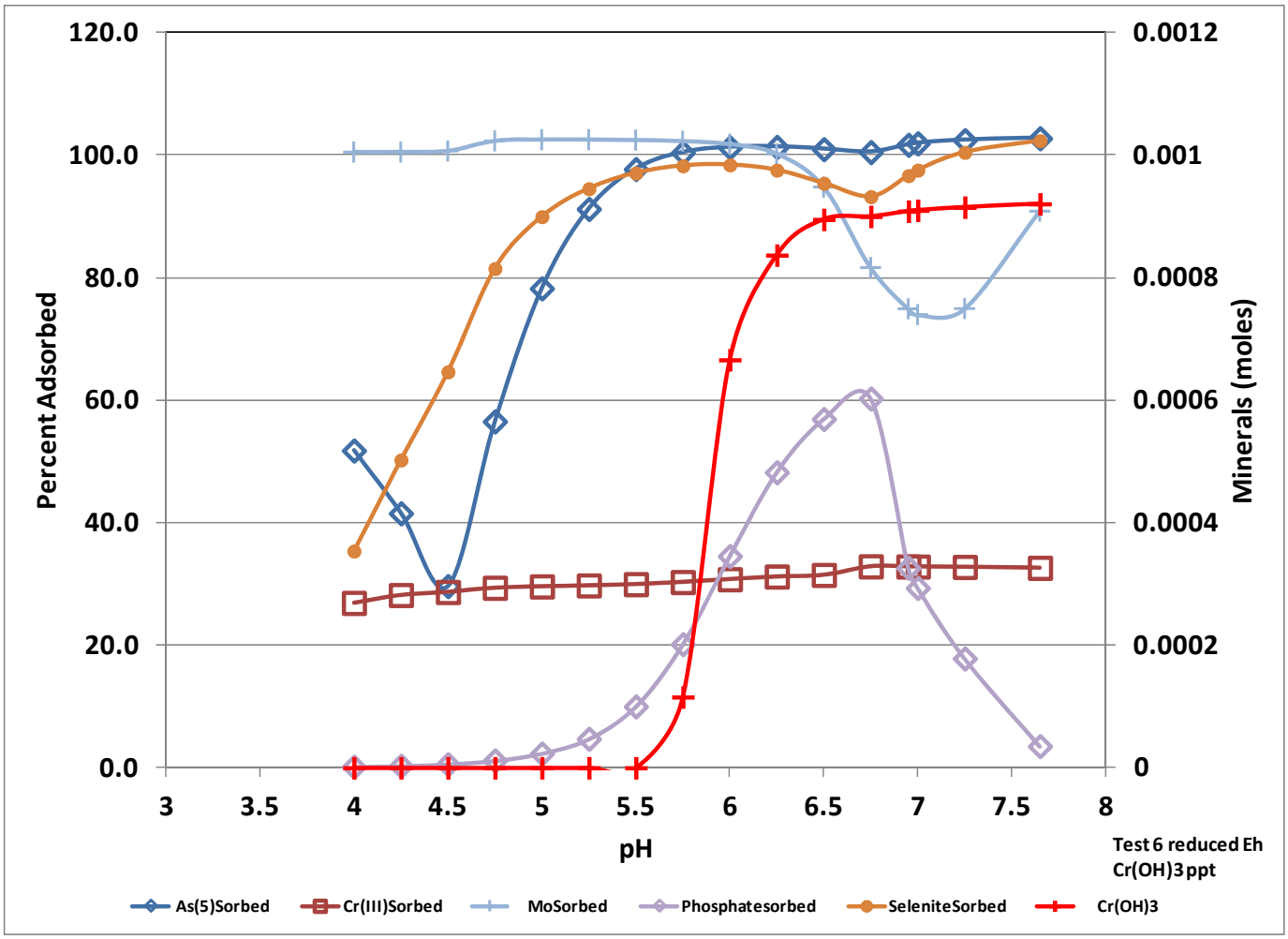

Figure 20. Results from alternative geochemical model for chromium lowered Eh. Partial pressure of $O_2(g)$ equals 10^{-30} atmospheres. $Cr(OH)_3$ allowed to precipitate.

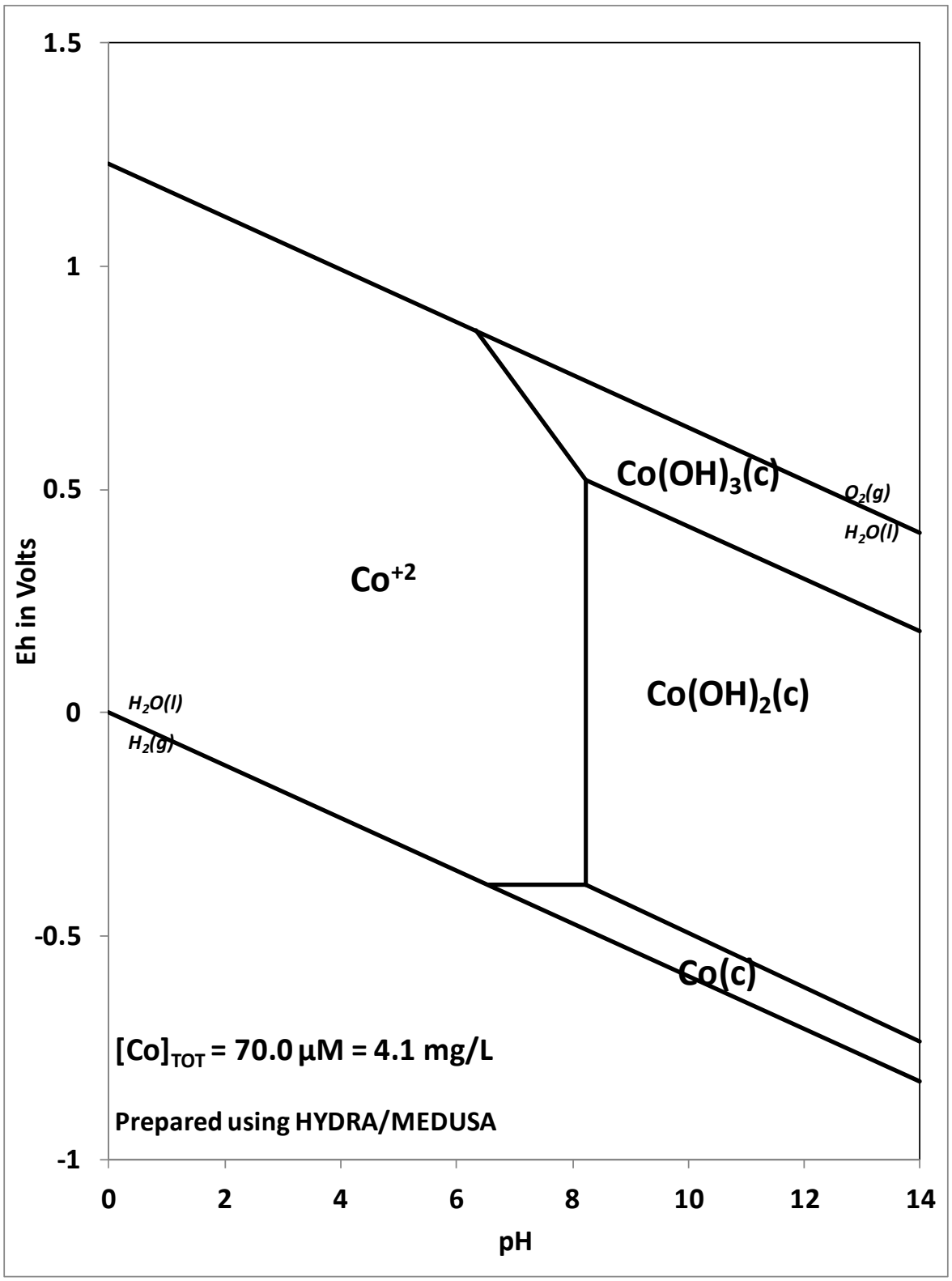

Figure 21. Eh-pH diagram for the system Co-O-H at 25°C. Cobalt at ~ 4 mg/L.

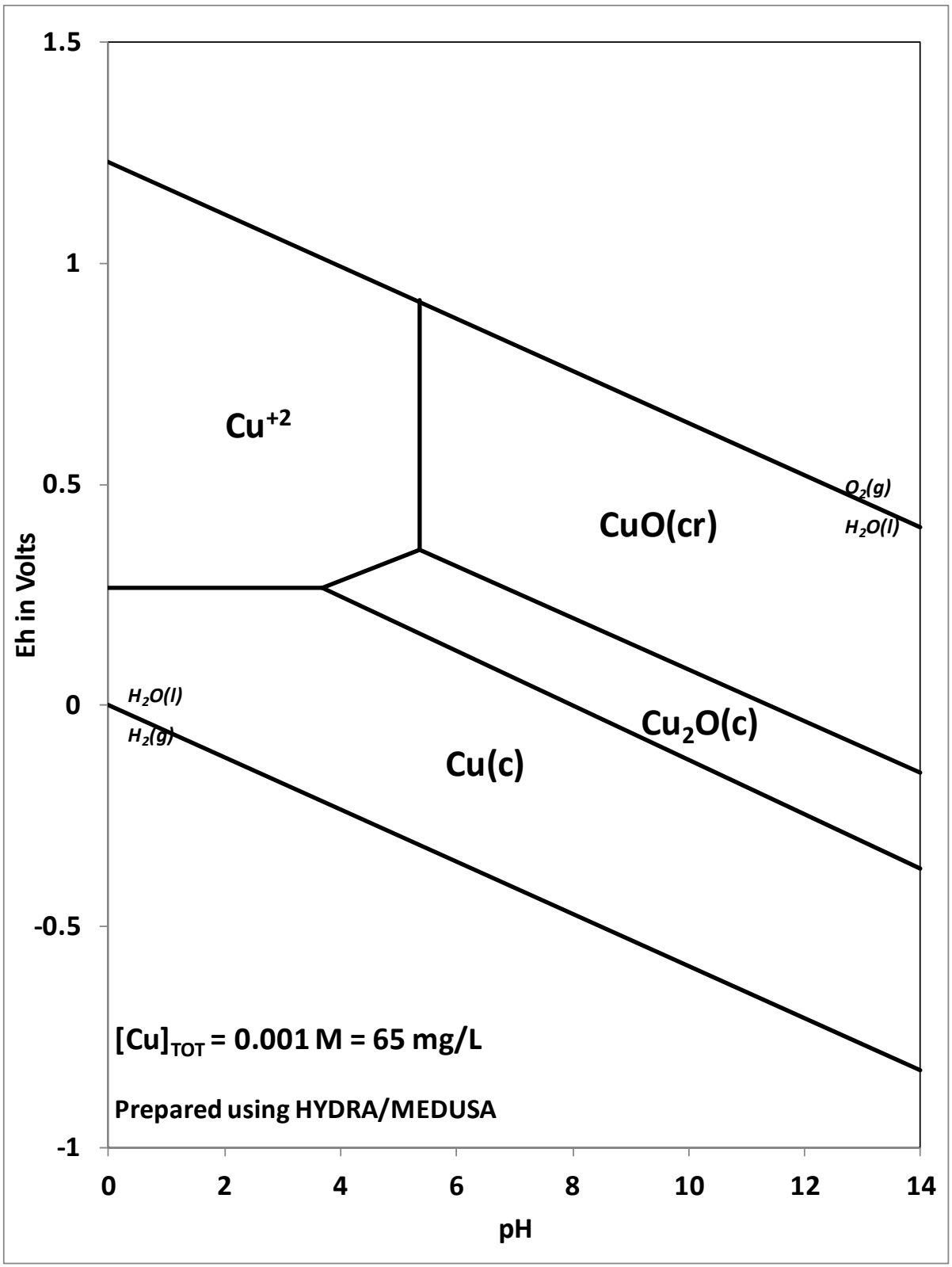

Figure 22. Eh-pH diagram for the system Cu-O-H at 25°C.

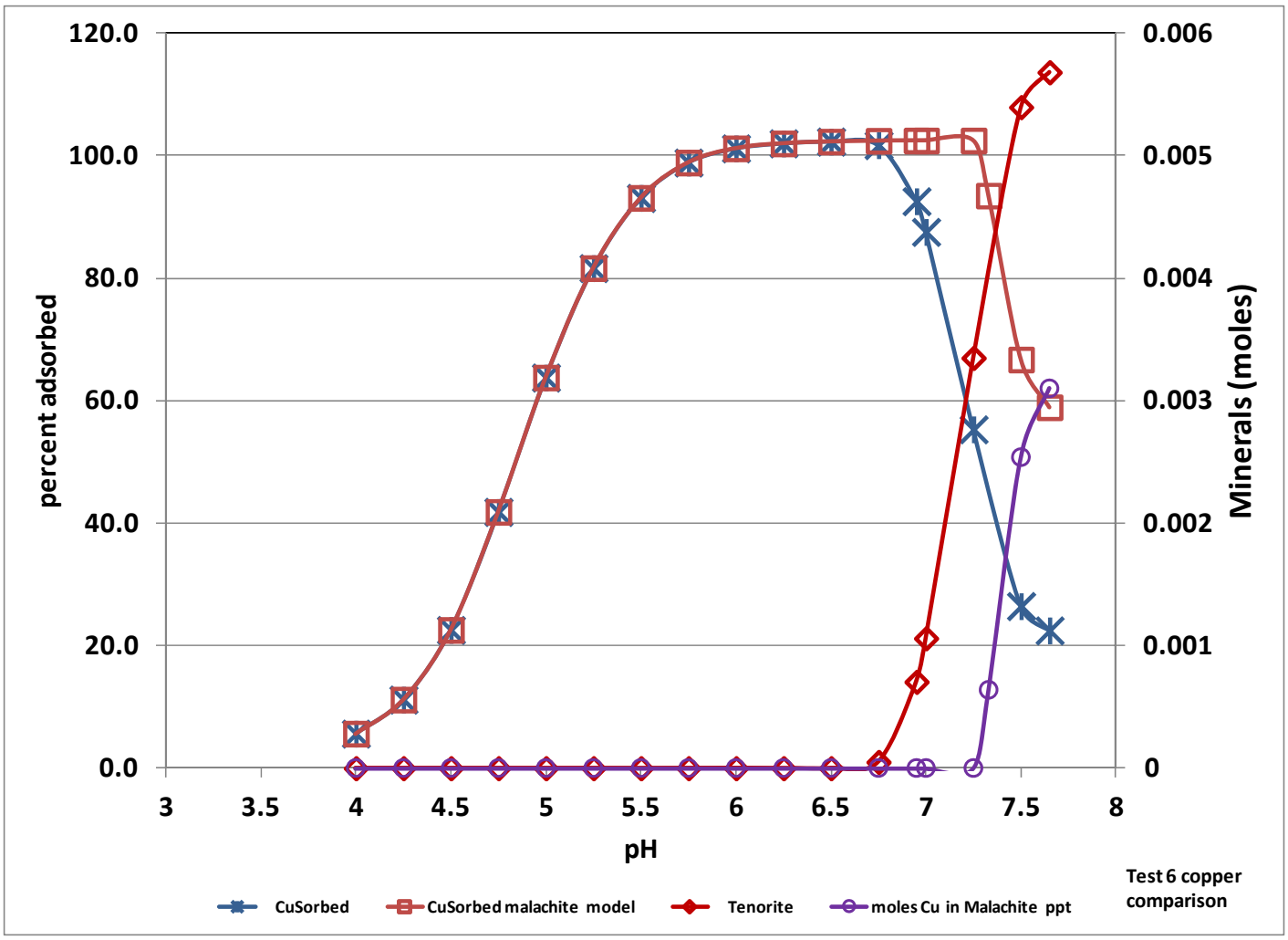

Figure 23. Distribution of copper (adsorbed and mineral phases) in geochemical model simulations. Comparison of tenorite and malachite precipitated phases.

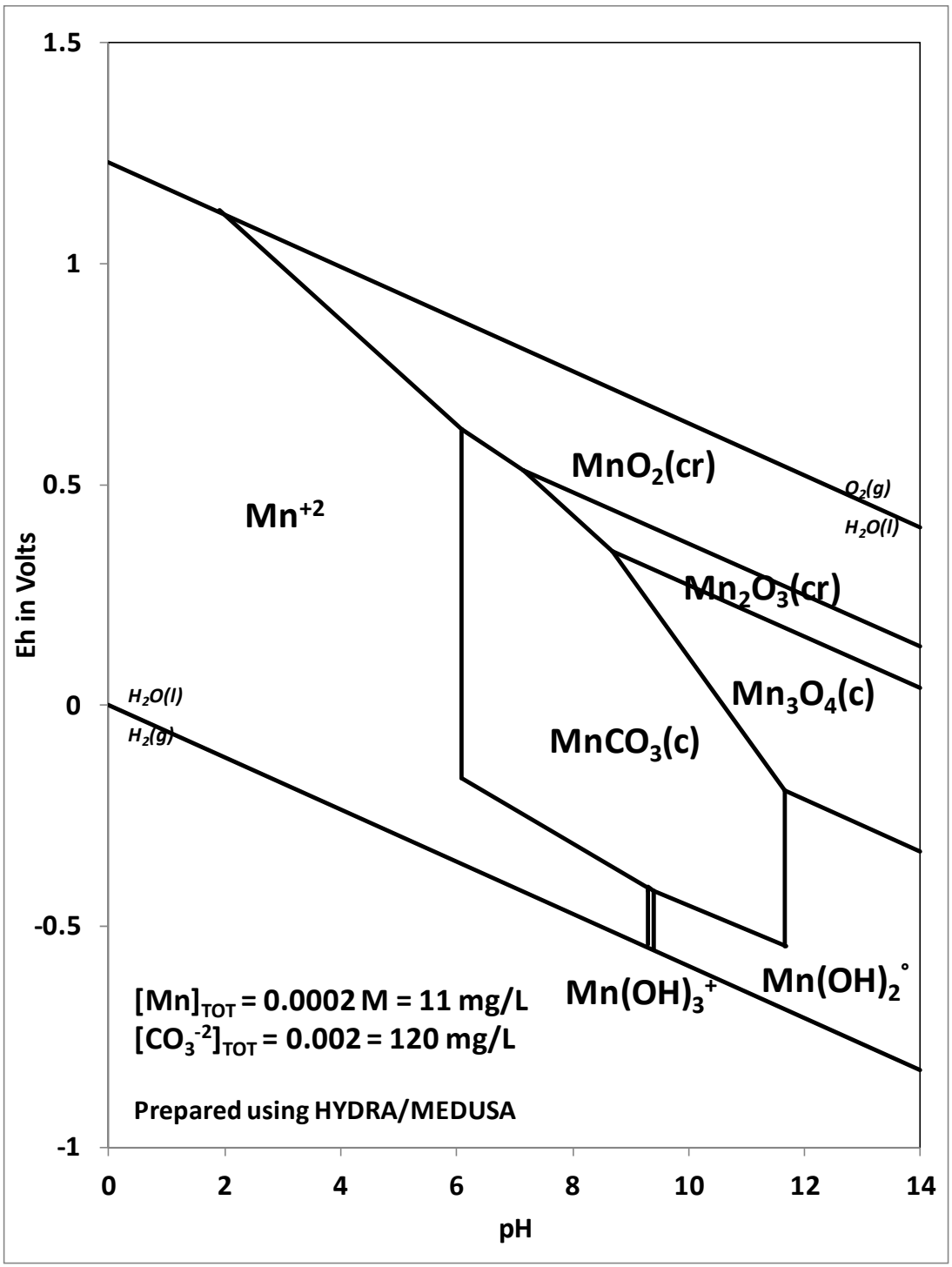

Figure 24. Eh-pH diagram for the system Mn-C-O-H at 25°C.

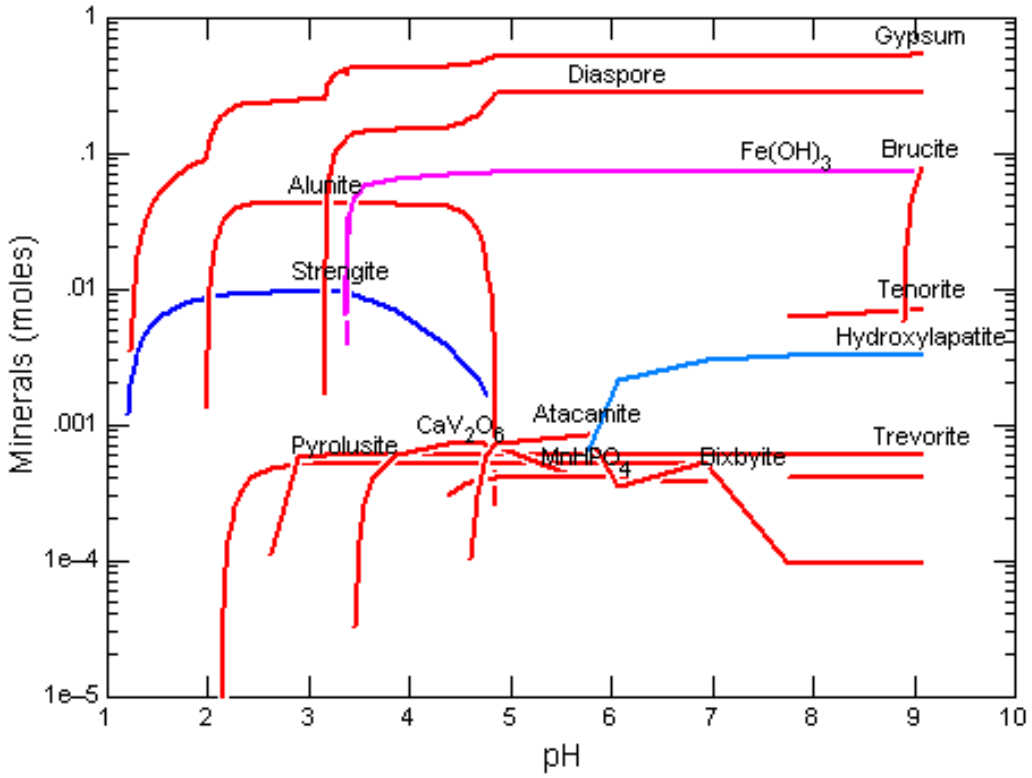

Figure 25. GWB based reaction path model showing the formation and subsequent dissolution of Strengite.

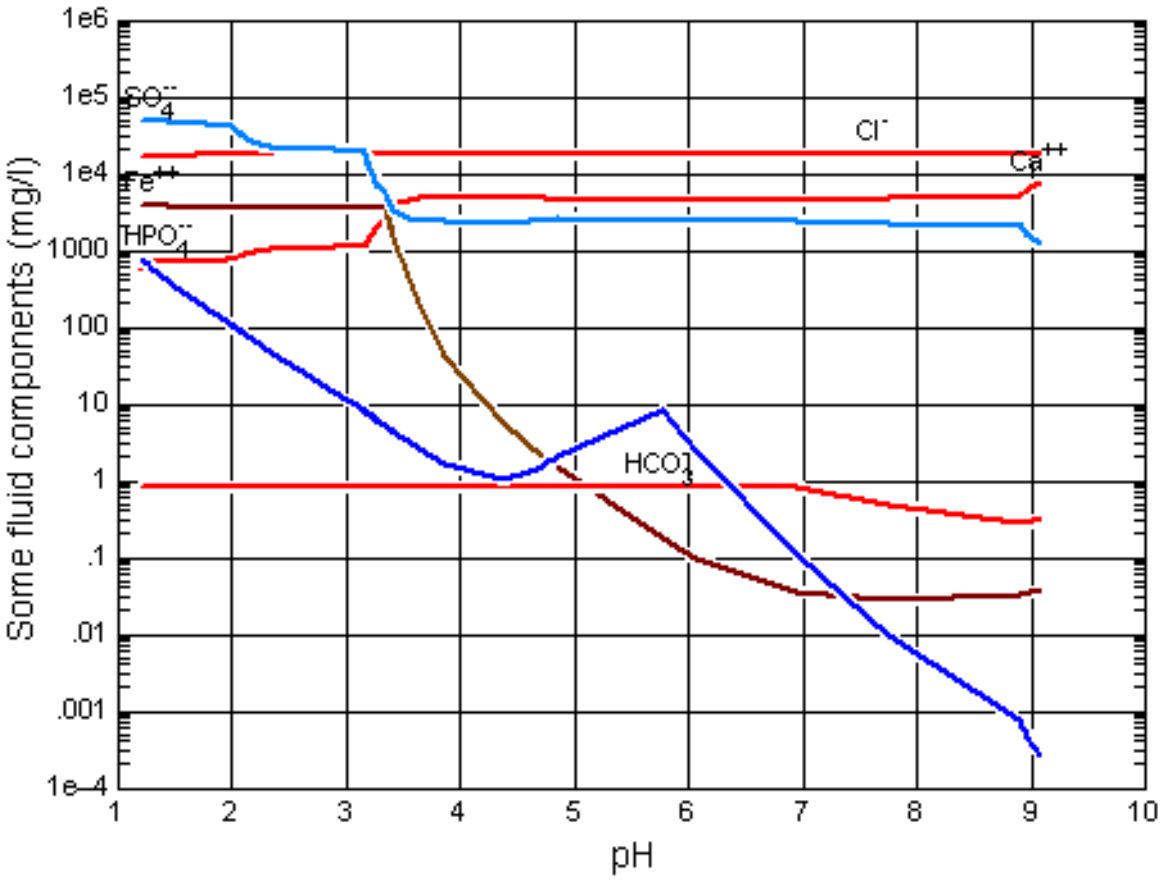

Figure 26. Concentrations of selected parameters for GWB reaction path model shown on Figure 19.

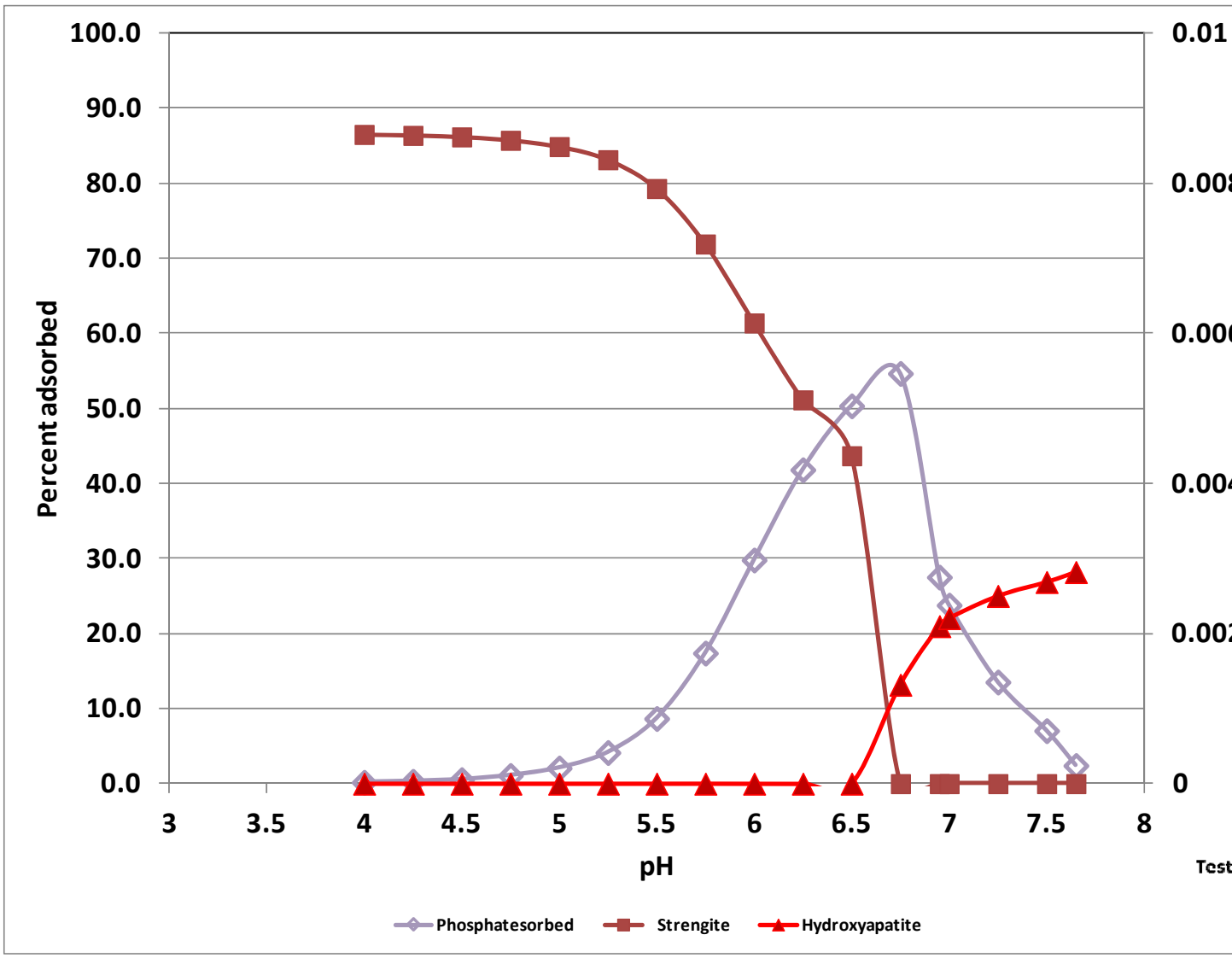

Figure 27. Results from geochemical model (sweep) showing dissolution of strengite and formation of hydroxyapatite and intermediate adsorption of phosphate.

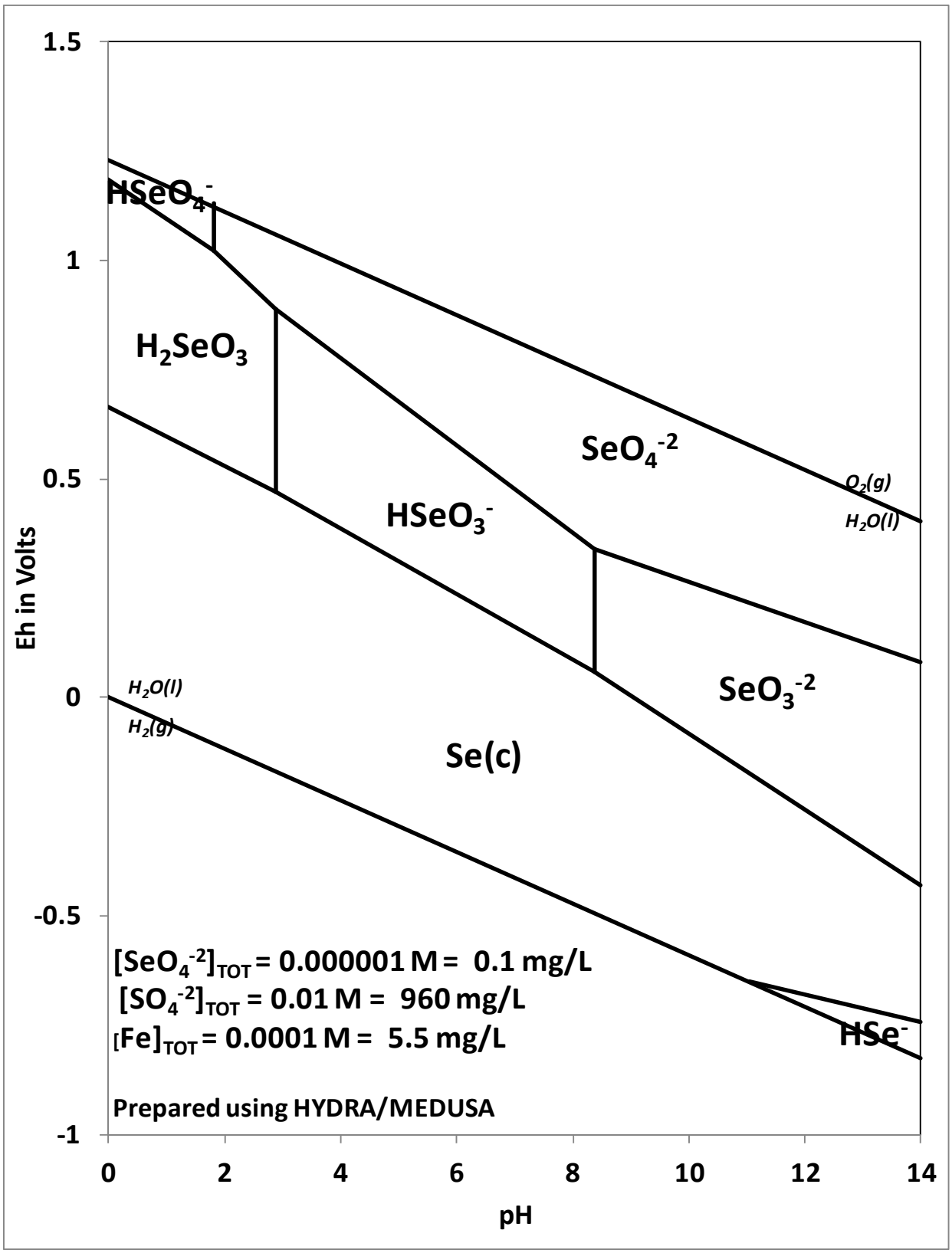

Figure 28. Eh-pH diagram for the system Se-S-Fe-O-H at 25°C.

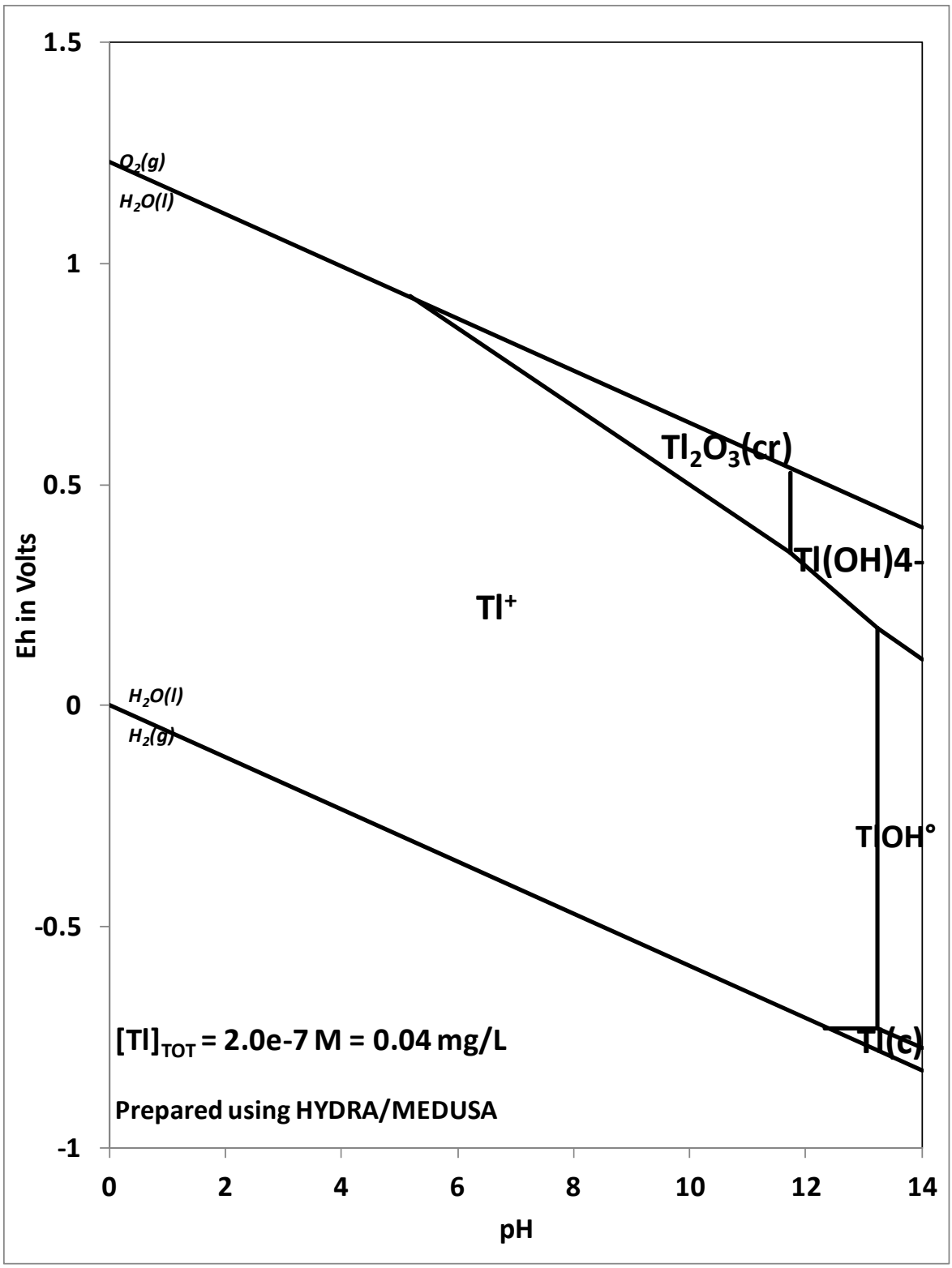

Figure 29. Eh-pH diagram for the system Tl-O-H at 25°C, Tl concentration of 0.04 mg/L. -U-O-H at 25°C.

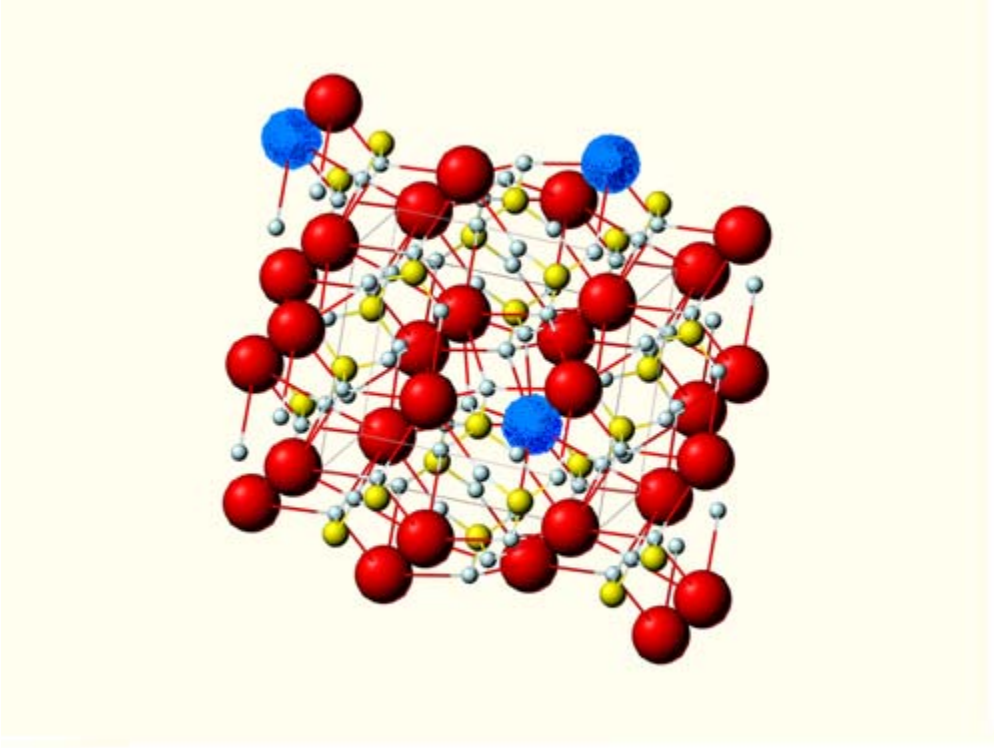

Figure 30. Barite ($BaSO_4$) crystal structure showing replace of barium ions (red spheres) with radium (blue spheres) sulfur – yellow spheres, oxygen - white sphere.